Assessing Electrical Conductivity and Total Alkalinity for Carbon Accounting in Enhanced Rock Weathering Applications

Dissertation

with the aim of achieving a doctoral degree

at the Faculty of Mathematics, Informatics and Natural Sciences
Department of Earth System Sciences
at University of Hamburg

submitted by

Lukas Rieder

Hamburg, 2026

Department of Earth System Sciences

Date of Oral Defence:	30.06.2026
Reviewers:	Prof. Dr. Jens Hartmann Dr. Mathilde Hagens
Panel Chair:	Prof. Dr. Felix Ament
Members of the examination commission:	Prof. Dr. Jens Hartmann Dr. Mathilde Hagens Prof. Dr. Florian Scholz Prof. Dr. Felix Ament Dr. Janine Börker
Chair of the Subject Doctoral Committee Earth System Sciences:	Prof. Dr. Dirk Notz
Dean of Faculty MIN:	Prof. Dr.-Ing. Norbert Ritter

Eidesstattliche Versicherung | Declaration on Oath

I hereby declare and affirm that this doctoral dissertation is my own work and that I have not used any aids and sources other than those indicated.

If electronic resources based on generative artificial intelligence (gAI) were used in the course of writing this dissertation, I confirm that my own work was the main and value-adding contribution and that complete documentation of all resources used is available in accordance with good scientific practice. I am responsible for any erroneous or distorted content, incorrect references, violations of data protection and copyright law or plagiarism that may have been generated by the gAI.

Hamburg 12.03.2026

Ort, den | City, date

Unterschrift | Signature

Abstract

Enhanced rock weathering (ERW) is an emerging carbon dioxide removal (CDR) strategy that has attracted increasing attention, with a growing number of publications since 2020. The approach aims to accelerate the natural weathering of silicate rocks to enhance alkalinity generation and thereby remove atmospheric carbon dioxide (CO_2). ERW is considered a promising CDR approach because it is scalable, cost-effective, and compatible with existing agricultural practices, enabling its deployment on croplands without direct competition for land use. However, a major challenge for the broader implementation of ERW remains the reliable quantification of CO_2 removal.

This thesis aims to improve the understanding of how CO_2 removal by ERW can be quantified across different environmental and experimental settings. In particular, it investigates the interpretation of total alkalinity (TA) and its individual components, with a focus on the contribution of non-carbonate alkalinity (A_{NC}) in different aqueous systems. Furthermore, the thesis examines the influence of microorganisms on mineral weathering and evaluates whether the electrical conductivity (EC) of bulk soil or aqueous solutions can serve as a proxy for TA across different environments.

To address these questions, data from several experimental setups were analyzed, including controlled soil reaction experiments, crushed rock column experiments, and controlled flow-through rock weathering reactors. The soil experiments investigated whether bulk soil electrical conductivity (EC_b) can be used to predict TA in soil pore water. The crushed rock column experiments with organic amendments were used to quantify the contribution of non-carbonate alkalinity (A_{NC}) to TA in relation to dissolved organic carbon (DOC) and to assess the impact of microorganisms and organic matter additions on TA generation. Finally, a flow-through reactor experiment was conducted to test whether the EC of leachate water can be used as a predictor for its TA and the corresponding CO_2 uptake. While this reactor system differs from cropland-based ERW applications, it enables the isolation and investigation of the EC–TA relationship generated solely by rock feedstock dissolution under controlled conditions. Analyzing these fundamental relationships in isolated experiments provides a reference framework that can support the interpretation and quantification of ERW processes in more complex soil environments.

This thesis demonstrates that bulk soil electrical conductivity (EC_b) is not a reliable predictor of pore water total alkalinity (TA). Even pore water EC alone is insufficient, as numerous processes in soils introduce additional ions that affect EC without contributing to TA. The presence of such non-alkalinity-contributing anions would require extensive corrections, limiting the applicability of EC-based TA estimates in ERW field systems. The crushed-rock column experiment further showed that organic amendments can contribute to measured TA through the release of organic alkalinity, i.e., the conjugate bases of low-molecular-weight organic acids (e.g., acetate, oxalate, citrate) that can contribute to the TA. In DOC-rich

systems, this fraction may represent a substantial component of the TA signal. In contrast, the isolated rock dissolution reactor experiment demonstrated a successful use case for rapid and non-destructive EC measurements as a predictor of TA. The reactor experiment demonstrated that, under controlled soil-free conditions with a forsterite-rich rock substrate, EC measurements can provide a robust predictor of TA through a well-defined EC–TA calibration.

For ERW applications in croplands, EC-based prediction of TA may be possible if, after an initial calibration phase, only ions released from the applied rock feedstock contribute to the soil pore water EC. Under such conditions, increases in EC would primarily reflect feedstock dissolution and associated TA generation. However, plant activity and common agricultural practices such as organic or mineral fertilization or mulching introduce additional ions that influence EC but alter TA independently of the EC–TA relationship associated with rock feedstock dissolution. As a result, the EC–TA relationship would require repeated recalibration, which again needs direct TA measurements. This requirement represents a major obstacle for the practical application of EC-based TA prediction in ERW cropland systems.

Zusammenfassung

Die beschleunigte Verwitterung (Enhanced Rock Weathering, ERW) ist ein neues Verfahren zur Kohlendioxid (CO_2) Entnahme (Carbon Dioxide Removal, CDR), das in den letzten sechs Jahren mit zunehmender Zahl an Veröffentlichungen zunehmend Aufmerksamkeit erlangt hat. Der Ansatz zielt darauf ab, die natürliche Verwitterung von Silikatgestein zu beschleunigen, um die Alkalinitätsbildung zu fördern und dadurch CO_2 aus der Atmosphäre zu entfernen. ERW gilt als vielversprechender CDR-Ansatz, da er skalierbar, kostengünstig und mit bestehenden landwirtschaftlichen Praktiken kompatibel ist, sodass er auf Ackerflächen eingesetzt werden kann, ohne dass es zu einer direkten Konkurrenz um die Landnutzung kommt. Eine große Herausforderung für die breitere Umsetzung von ERW bleibt jedoch die zuverlässige Quantifizierung der CO_2-Entfernung.

Diese Arbeit zielt darauf ab, das Verständnis dafür zu verbessern, wie die CO_2-Entfernung durch ERW unter verschiedenen Umwelt- und Versuchsbedingungen quantifiziert werden kann. Insbesondere untersucht sie die Interpretation der Gesamtalkalinität (TA) und ihrer Komponenten, wobei der Schwerpunkt auf dem Beitrag der Nicht-Karbonat-Alkalinität (A_{NC}) in verschiedenen wässrigen Systemen liegt. Darüber hinaus untersucht die Arbeit den Einfluss von Mikroorganismen auf die Verwitterung und bewertet, ob die elektrische Leitfähigkeit (EC) des gesamten Bodens oder des Boden-Porenwassers als Ersatz für die TA in verschiedenen Umgebungen dienen kann.

Um diese Fragen zu beantworten, wurden Daten aus mehreren Versuchsanordnungen analysiert. Dazu gehören kontrollierte Bodenreaktionsexperimente, Säulenexperimente mit zerkleinertem Gestein sowie kontrollierte Reaktoren zur Untersuchung der Gesteinsverwitterung. In den Bodenexperimenten wurde untersucht, ob die elektrische Leitfähigkeit des Bodens (EC_b) zur Vorhersage der TA im Bodenporenwasser herangezogen werden kann. Die Gesteinssäulenexperimente mit organischen Zusätzen dienten dazu, den Beitrag der A_{NC} zur TA in Bezug auf gelösten organischen Kohlenstoff (DOC) zu quantifizieren und den Einfluss von Mikroorganismen und organischer Substanz auf die Alkalinitätsbildung zu bewerten. Schließlich wurden Reaktor-Experimente durchgeführt, um zu testen, ob die elektrische Leitfähigkeit von Sickerwasser als Prädiktor für dessen TA und die entsprechende CO_2-Aufnahme verwendet werden kann. Obwohl dieses Reaktorsystem von typischen ERW-Anwendungen auf Ackerflächen abweicht, ermöglicht es die Isolierung und Untersuchung der EC–TA Beziehung, ausschließlich für das Gesteinssubstrat. Die Untersuchung dieser grundlegenden Beziehungen liefert ein wichtiges Verständnis, das die Interpretation und Quantifizierung von ERW-Prozessen in komplexeren Bodenumgebungen unterstützen kann.

Diese Arbeit zeigt, dass die elektrische Leitfähigkeit des Bodens (EC_b) kein zuverlässiger Prädiktor für die TA des Porenwassers ist. Selbst die elektrische Leitfähigkeit des Porenwassers allein ist unzureichend, da zahlreiche relevante Prozesse im Boden zusätzliche Ionen einbringen, die die elektrische Leitfähigkeit erhöhen, ohne zur TA beizutragen. Das

Vorhandensein solcher Anionen, die nicht zur Alkalinität beitragen, würde umfangreiche Korrekturen erfordern und damit die Anwendbarkeit EC-basierter Vorhersagen der TA in ERW-Feldsystemen einschränken. Das Säulenexperiment zeigte ferner, dass organische Zusätze durch die Freisetzung organischer Alkalinität, d. h. der konjugierten Basen organischer Säuren (z. B. Acetat, Oxalat, Citrat), die zur gemessenen TA beitragen können. In DOC-reichen Systemen kann dieser Anteil einen wesentlichen Bestandteil des gesamten Alkalinitätssignals ausmachen. Im Gegensatz dazu zeigte das kontrollierte Reaktorexperiment einen erfolgreichen Anwendungsfall für schnelle und zerstörungsfreie EC-Messungen als Prädiktor für TA. Das kontrollierte Reaktorexperiment zeigte, dass unter kontrollierten bodenfreien Bedingungen mit einem Forsterit-reichen Gesteinssubstrat EC-Messungen durch eine genau definierte EC–TA-Kalibrierung einen robusten Prädiktor für TA liefern können.

Für ERW-Anwendungen auf Ackerflächen ist eine auf der EC basierende Vorhersage der TA möglich, wenn nach einer anfänglichen Kalibrierungsphase nur Ionen, die aus dem ausgebrachten Gestein freigesetzt werden, zur elektrischen Leitfähigkeit des Bodenporenwassers beitragen. Unter solchen Bedingungen würde ein Anstieg der EC die Auflösung des Gesteins sowie die damit verbundene TA-Bildung widerspiegeln. Pflanzenaktivität und gängige landwirtschaftliche Praktiken wie organische oder mineralische Düngung oder Mulchen führen jedoch zu zusätzlichen Ionen, die die EC beeinflussen, die TA jedoch unabhängig von der Beziehung zwischen EC und TA des Gesteins verändern. Infolgedessen würde die Beziehung zwischen EC und TA eine wiederholte Neukalibrierung erfordern, was wiederum direkte TA-Messungen erforderlich machen würde. Diese Anforderung stellt ein großes Hindernis für die praktische Anwendung der EC-basierten TA-Vorhersage in ERW-Ackerböden dar.

Contents

Abstract ii

Zusammenfassung iv

Nomenclature ix

List of Publications x

1 Introduction 1
- 1.1 Motivation . . . 1
- 1.2 Research Objectives . . . 3

2 Soil electrical conductivity as a proxy for enhanced weathering in soils 5
- 2.1 Introduction . . . 5
- 2.2 Methods . . . 8
  - 2.2.1 Testing soils . . . 8
  - 2.2.2 Soil analysis . . . 9
  - 2.2.3 Testing solutions . . . 9
  - 2.2.4 Setup EC_b experiment . . . 10
  - 2.2.5 Setup soil reaction experiment . . . 12
- 2.3 Results . . . 13
  - 2.3.1 Bulk soil electrical conductivity (EC_b) . . . 13
  - 2.3.2 Brown earth reaction experiment . . . 16
- 2.4 Discussion . . . 19
  - 2.4.1 Bulk soil electrical conductivity response . . . 20
  - 2.4.2 Soil + $NaHCO_3$ solution reaction experiment . . . 21
  - 2.4.3 Source of errors in the experiments . . . 25
- 2.5 Conclusion . . . 26

3 Contribution of dissolved organic carbon to total alkalinity in Enhanced Weathering experiments 27
- 3.1 Introduction . . . 28
- 3.2 Methods . . . 30
  - 3.2.1 Experimental Setup . . . 30
  - 3.2.2 Materials . . . 33
  - 3.2.3 Microorganisms and earthworm types . . . 33
  - 3.2.4 Measurements in the leachate water . . . 34
  - 3.2.5 Calculations . . . 36
- 3.3 Results and discussion . . . 38
  - 3.3.1 Non-carbonate alkalinity (A_{NC})determination . . . 38
  - 3.3.2 Charge balance error (CBE) analysis . . . 42
  - 3.3.3 Analysis of LMWOAs . . . 44

3.3.4 Improved titration for organic alkalinity . . . 45
3.3.5 DOC source and dilution effect . . . 47
3.3.6 Comparison with other water samples from EW experiments and natural environments . . . 48
3.4 Conclusion . . . 53

4 Testing the bio-additionality hypothesis for enhancing the alkalinity production via Enhanced Weathering 55
4.1 Introduction . . . 56
4.2 Materials and methods . . . 58
4.2.1 Experimental setup . . . 58
4.2.2 Materials . . . 61
4.2.3 Biota Preparations . . . 65
4.2.4 Measurements . . . 66
4.2.5 Data analysis . . . 67
4.3 Results . . . 68
4.3.1 Biota effect on TA . . . 68
4.3.2 Overall leachate water analysis . . . 70
4.3.3 Biological Indications . . . 78
4.4 Discussion . . . 78
4.4.1 (Additional) biotic weathering effect . . . 79
4.4.2 Wheat straw effect . . . 80
4.5 Conclusion . . . 83

5 Using Electrical Conductivity as a predictor for Total Alkalinity in controlled ERW systems 84
5.1 Introduction . . . 85
5.2 Materials and Methods . . . 87
5.2.1 Experimental setup . . . 87
5.2.2 Rock type . . . 88
5.2.3 Measurements . . . 90
5.2.4 Data treatment . . . 91
5.2.5 Calculation of CO_2 removal . . . 91
5.3 Results . . . 92
5.3.1 Time series of chemical parameters . . . 92
5.3.2 EC-TA calibration . . . 94
5.3.3 CO_2 removal . . . 97
5.4 Discussion . . . 98
5.4.1 TA prediction from EC . . . 98
5.4.2 CO_2 removal assessment . . . 102
5.5 Conclusion . . . 103

6 Synthesis 105

A Appendix for Chapter 2 109
A.1 Used reagent $NaHCO_3$ . . . 109

B Appendix for Chapter 3 **111**
B.1 Total alkalinity determination . . . 111
B.2 Dissolved organic and inorganic carbon determination . . . 112
B.3 Carbonate alkalinity models comparison . . . 112
B.4 Charge balance determination . . . 114
B.5 Irrigation rate impact . . . 115
B.6 Organic-rich soil . . . 116
B.7 Brown earth soil . . . 117
B.8 Experimental setup for both soils . . . 118
B.9 Rock powder pictures . . . 120
B.10 Rock Classification . . . 124

C Appendix for Chapter 4 **126**
C.1 Tephrite rock substrate . . . 127
C.2 Experimental setup . . . 128
C.3 Tukey-Kramer test . . . 129
C.4 Factorial linear model results . . . 130
C.5 Leachate water analysis . . . 131
C.5.1 Charge balance error (CBE) . . . 131
C.5.2 Molar ratio . . . 132
C.6 Microbial community in wheat straw . . . 133

D Appendix for Chapter 5 **135**
D.1 Calibration for Mg . . . 138
D.2 Apparent dissolution rate . . . 139

Acknowledgements **143**

References **145**

Nomenclature

Abbreviations

Abbreviation	Definition
ERW	Enhanced Rock Weathering
EW	Enhanced Weathering
CDR	Carbon Dioxide Removal

Variable Names

Symbol	Definition	Unit
TA	Total alkalinity	[eq L^{-1}]
A_C	Carbonate alkalinity	[eq L^{-1}]
A_{NC}	Non-carbonate alkalinity	[eq L^{-1}]
CBE	Charge balance error	[%]
DIC	Dissolved inorganic carbon	[mmol L^{-1}]
DOC	Dissolved organic carbon	[mmol L^{-1}]
EC	Electrical conductivity	[µS cm^{-1}]
EC_b	Bulk (soil) electrical conductivity	[µS cm^{-1}]
EC_w	Electrical conductivity of soil solution (water)	[µS cm^{-1}]
θ	Volumetric water content (of soil)	[vol%]

List of publications

Calogiuri, Tullia, Hagens, Mathilde, Van Groenigen, Jan Willem, Wichern, Florian, Poetra, Reinaldy P.**, Rieder, Lukas**, Janssens, Ivan A., Hartmann, Jens, Neubeck, Anna, Niron, Harun, Singh, Abhijeet, Vlaeminck, Siegfried E., Vicca, Sara, and Vidal, Alix (Nov. 2025). "Alive and Dead Earthworms Capture Carbon during Mineral Weathering through Different Pathways". In: *Communications Earth & Environment* 6.1, p. 851. ISSN: 2662-4435. DOI: 10.1038/s43247-025-02766-4. (Visited on 11/11/2025).

Calogiuri, Tullia, Janssens, Iris, Vidal, Alix, Van Groenigen, Jan Willem, Verdonck, Tim, Corbett, Thomas, Hartmann, Jens, Neubeck, Anna, Niron, Harun, Poetra, Reinaldy P.**, Rieder, Lukas**, Servotte, Thomas, Singh, Abhijeet, Van Tendeloo, Michiel, Vlaeminck, Siegfried E., Vicca, Sara, and Hagens, Mathilde (Feb. 2025). "How Earthworms Thrive and Drive Silicate Rock Weathering in an Artificial Organo-Mineral System". In: *Applied Geochemistry* 180, p. 106271. ISSN: 08832927. DOI: 10.1016/j.apgeochem.2024.106271. (Visited on 03/24/2025).

Calogiuri, Tullia, Hagens, Mathilde, Van Groenigen, Jan Willem, Corbett, Thomas, Hartmann, Jens, Hendriksen, Rick, Janssens, Iris, Janssens, Ivan A., Ledesma Dominguez, Guillermo, Loescher, Grant, Mortier, Steven, Neubeck, Anna, Niron, Harun, Poetra, Reinaldy P.**, Rieder, Lukas**, Struyf, Eric, Van Tendeloo, Michiel, De Schepper, Tom, Verdonck, Tim, Vlaeminck, Siegfried E., Vicca, Sara, and Vidal, Alix (Nov. 2023). "Design and Construction of an Experimental Setup to Enhance Mineral Weathering through the Activity of Soil Organisms". In: *Journal of Visualized Experiments* 201, p. 65563. ISSN: 1940-087X. DOI: 10.3791/65563. (Visited on 03/27/2024).

Corbett, Thomas D. W., Westholm, Marcus, Rosling, Anna, Calogiuri, Tullia, Poetra, Reinaldy, Niron, Harun, Hagens, Mathilde, Vidal, Alix, Van Groenigen, Jan Willem, Hartmann, Jens, Janssens, Ivan A.**, Rieder, Lukas**, Struyf, Eric, Van Tendeloo, Michiel, Vlaeminck, Siegfried E., Vicca, Sara, and Neubeck, Anna (Apr. 2024). "Organic Carbon Source Controlled Microbial Olivine Dissolution in Small-Scale Flow-through Bioreactors, for CO2 Removal". In: *npj Materials Degradation* 8.1, p. 34. ISSN: 2397-2106. DOI: 10.1038/s41529-024-00454-w. (Visited on 11/17/2025).

Janssens, Iris, Servotte, Thomas, Calogiuri, Tullia, Mortier, Steven, Niron, Harun, Corbett, Thomas, Poetra, Reinaldy P.**, Rieder, Lukas**, Van Tendeloo, Michiel, Singh, Abhijeet, Latré, Steven, Vlaminck, Siegfried E., Hartmann, Jens, Van Groenigen, Jan Willem, Neubeck, Anna, Vidal, Alix, Janssens, Ivan A., Hagens, Mathilde, Vicca, Sara, and Verdonck, Tim (Sept. 2025). "Machine Learning-Based Identification of Key Biotic and Abiotic Drivers of Mineral Weathering Rate in a Complex Enhanced Weathering Experiment". In: *Open Research Europe* 5, p. 71. ISSN: 2732-5121. DOI: 10.12688/openreseurope.19252.3. (Visited on 10/14/2025).

Rieder, Lukas, Amann, Thorben, and Hartmann, Jens (Jan. 2024). "Soil Electrical Conductivity as a Proxy for Enhanced Weathering in Soils". In: *Frontiers in Climate* 5. (Chapter 2 of dissertation), p. 1283107. ISSN: 2624-9553. DOI: 10.3389/fclim.2023.1283107. (Visited on 11/17/2025).

Rieder, Lukas, Hagens, Mathilde, Poetra, Reinaldy, Hartmann, Jens, Vicca, Sara, Niron, Harun, Vlaeminck, Siegfried E., Neubeck, Anna, Singh, Abhijeet, and Calogiuri, Tullia (2026). "Testing the Bio-Additionality Hypothesis for Enhancing the Alkalinity Production via Enhanced Weathering". In: *Applied Geochemistry*. Manuscript under review.

Rieder, Lukas, Hagens, Mathilde, Poetra, Reinaldy, Vidal, Alix, Calogiuri, Tullia, Neubeck, Anna, Singh, Abhijeet, Corbett, Thomas, Niron, Harun, Vicca, Sara, Vlaeminck, Siegfried E., Janssens, Iris, Verdonck, Tim, Janssens, Ivan, Li, Xuming, Hammes, Jens S., and Hartmann, Jens (Feb. 2026). "Contribution of Dissolved Organic Carbon to Total Alkalinity in Enhanced Weathering Experiments". In: *Applied Geochemistry* 198. (Chapter 3 of dissertation), p. 106685. ISSN: 08832927. DOI: 10.1016/j.apgeochem.2026.106685. (Visited on 01/23/2026).

Manuscripts in preparation

Rieder, Lukas, Hagens, Mathilde, Poetra, Reinaldy, Hartmann, Jens, Vicca, Sara, Niron, Harun, Vlaeminck, Siegfried E., Neubeck, Anna, Singh, Abhijeet, and Calogiuri, Tullia (2026). "Testing the Bio-Additionality Hypothesis for Enhancing the Alkalinity Production via Enhanced Weathering". In: *Applied Geochemistry*. Manuscript under review (Chapter 4 of dissertation).

Rieder, Lukas, Hagens, Mathilde, Poetra, Reinaldy, and Hartmann, Jens (n.d.). "Using Electrical Conductivity as a predictor for Total Alkalinity in controlled ERW systems". (Chapter 5 of the dissertation).

Author contributions

Introduction

Lukas Rieder: Writing — original draft.

Soil electrical conductivity as a proxy for enhanced weathering in soils

Lukas Rieder: Writing — original draft, Conceptualization, Data curation, Formal analysis, Investigation, Methodology, Software, Validation, Visualization. **Thorben Amann:** Data curation, Investigation, Supervision, Validation, Visualization, Writing — review & editing. **Jens Hartmann:** Conceptualization, Funding acquisition, Investigation, Methodology, Project administration, Resources, Supervision, Writing — review & editing.

Contribution of dissolved organic carbon to total alkalinity in Enhanced Weathering experiments

Lukas Rieder: Writing — original draft, Visualization, Validation, Software, Methodology, Investigation, Formal analysis, Data curation, Conceptualization. **Mathilde Hagens:** Writing — review & editing, Supervision, Funding acquisition. **Reinaldy Poetra:** Writing — review & editing, Methodology, Investigation, Data curation. **Alix Vidal:** Writing — review & editing. **Tullia Calogiuri:** Writing — review & editing, Investigation, Data curation. **Anna Neubeck:** Writing — review & editing, Funding acquisition. **Abhijeet Singh:** Writing — review & editing, Investigation, Data curation. **Thomas Corbett:** Investigation, Data curation. **Harun Niron:** Investigation, Data curation. **Sara Vicca:** Writing — review & editing, Project administration, Funding acquisition. **Siegfried E. Vlaeminck:** Writing — review & editing, Funding acquisition. **Iris Janssens:** Writing — review & editing, Software, Data curation. **Tim Verdonck:** Funding acquisition, Data curation. **Ivan Janssens:** Writing — review & editing, Funding acquisition. **Xuming Li:** Investigation, Data curation. **Jens S. Hammes:** Writing — review & editing, Investigation, Data curation. **Jens Hartmann:** Writing — review & editing, Supervision, Funding acquisition, Conceptualization.

Testing the bio-additionality hypothesis for enhancing the alkalinity production via Enhanced Weathering

Lukas Rieder: Writing — original draft, Visualization, Methodology, Conceptualization, Investigation, Formal analysis, Validation, Data curation, Software. **Mathilde Hagens:** Writing — review & editing, Funding acquisition, Supervision. **Tullia Calogiuri:** Writing —

review & editing. **Reinaldy Poetra:** Writing — review & editing, Investigation, Data curation, Methodology. **Anna Neubeck:** Writing — review & editing. **Abhijeet Singh:** Writing — review & editing, Investigation, Formal analysis. **Harun Niron:** Writing — review & editing. **Sara Vicca:** Writing — review & editing, Funding acquisition. **Siegfried E. Vlaeminck:** Writing — review & editing. **Jens Hartmann:** Writing — review & editing, Conceptualization, Funding acquisition, Supervision.

Using Electrical Conductivity as a predictor for Total Alkalinity in controlled ERW systems

Lukas Rieder: Writing — original draft, Visualization, Methodology, Conceptualization, Investigation, Formal analysis, Validation, Data curation, Software. **Mathilde Hagens:** Writing — review & editing, Funding acquisition, Supervision. **Reinaldy Poetra:** Writing — review & editing, Methodology. **Jens Hartmann:** Writing — review & editing, Supervision, Funding acquisition, Conceptualization.

Synthesis

Lukas Rieder: Writing — original draft.

1 Introduction

1.1. Motivation

The global increase in mean surface temperature is one of the most pressing environmental issues of the 21st century. To limit this human-caused global warming to a specific temperature, the worldwide cumulative emissions of carbon dioxide (CO_2) and other greenhouse gases, such as methane (CH_4) and nitrous oxide (N_2O), must be significantly and urgently reduced (IPCC, 2023).

However, mitigation through emission reductions alone is insufficient to restrict global temperature rise to 2 °C or below by 2100. Most mitigation pathways consistent with this target, therefore, combine strong emission reductions with large-scale deployment of carbon dioxide removal (CDR) technologies (IPCC, 2022b; IPCC, 2022a; Steve Smith et al., 2024). This requirement is reflected in the IPCC's modelled Shared Socioeconomic Pathways (SSPs) that achieve temperature stabilization at 2 °C or lower.

The growing relevance of CDR is further underscored by the IPCC's planned *2027 Methodology Report on Carbon Dioxide Removal Technologies, Carbon Capture, Utilization and Storage* (IPCC, 2025). The development of a dedicated methodology report underscores the growing importance of robust accounting frameworks and scientifically rigorous assessment methods for CDR technologies. The report will be important for the possible integration of CDR into national greenhouse gas (GHG) inventories and climate action plans.

Geden, Steve Smith, and Cowie (2024) split CDR methods into conventional and novel methods. The conventional methods are those already deployed at scale, such as afforestation, reforestation, agroforestry, soil carbon sequestration, peatland and coastal wetland restoration, and durable wood products. Novel CDR methods, as defined by Geden, Steve Smith, and Cowie (2024), generally have lower readiness and are currently deployed at a small scale. Examples of such methods include bioenergy with carbon capture and storage (BECCS), direct air carbon capture and storage (DACCS), enhanced rock weathering (ERW), biochar, mineral products, and ocean alkalinity enhancement (OAE).

The current CO_2 removal rates of novel CDR in the year 2023 were analyzed by Pongratz

et al. (2024). Their analysis shows that biochar currently provides $-0.79\,\mathrm{MtCO_2/yr}$, and BECCS $-0.51\,\mathrm{MtCO_2}$ per year. DACCS contributes $-0.004\,\mathrm{MtCO_2/yr}$, and ERW approximately $-0.03\,\mathrm{MtCO_2/yr}$.

This thesis focuses on ERW, also known as enhanced weathering (EW), as a carbon dioxide removal (CDR) strategy. The current CO_2 removal rates of ERW remain far below the estimated potential of the method, which has been projected to remove 0.5 to $2\,\mathrm{GtCO_2/yr}$ by 2050 (Beerling et al., 2025).

ERW aims to accelerate the dissolution of rock and increase alkalinity fluxes to the oceans (Beerling et al., 2020; Goll et al., 2021; Hartmann et al., 2013; Schuiling and Krijgsman, 2006; Seifritz, 1990). Dissolution of silicate minerals is a natural process that regulates the global carbon cycle on geological timescales. At the same time, the weathering of carbonates provides a CO_2 sink on shorter time scales due to carbonate formation in the ocean and following CO_2 degassing (Berner, 2003; Walker, Hays, and Kasting, 1981). As an illustrative example of silicate weathering, the dissolution of wollastonite ($CaSiO_3$) by carbonic acid H_2CO_3 is shown in Equation 1.1.

$$CaSiO_3(s) + 2\,CO_2(g) + 3\,H_2O \longrightarrow Ca^{2+} + 2\,HCO_3^- + H_4SiO_4(aq) \tag{1.1}$$

There are substantial uncertainties associated with the quantification and large-scale deployment of ERW, as comprehensively outlined by Schiedung et al. (2026). These uncertainties span socio-economic considerations, feedstock availability and composition, biogeochemical impacts on plant–soil systems, and the ultimate fate of weathering products within the global carbon cycle.

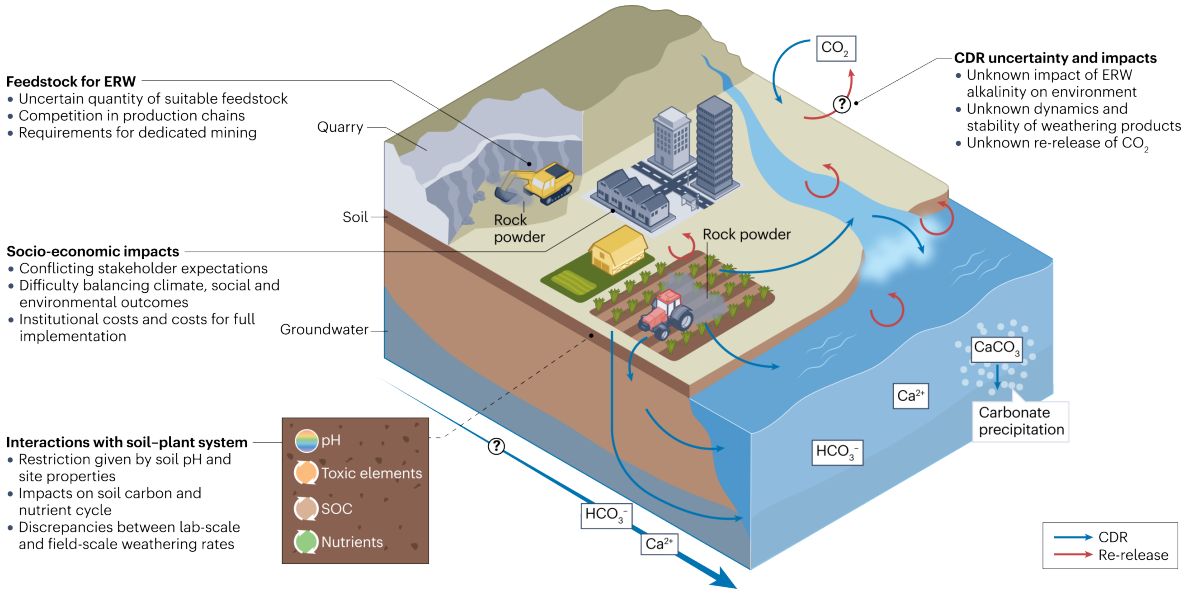


Figure 1.1: Constraints on ERW as a climate-change mitigation measure. Adapted from Schiedung et al. (2026)

While these broader constraints (Figure 1.1) challenge the overall feasibility of ERW as a climate change mitigation strategy, this thesis focuses on small-scale experimental systems and field-scale systems, including agricultural cropland soils and controlled reactor-based ERW setups. The emphasis of the thesis is placed on the quantification of CO_2 removal in soil-based experiments under more controlled conditions.

Among the identified uncertainties in Figure 1.1, the development of robust Measurement, Reporting, and Verification (MRV) frameworks represents the central challenge for large-scale implementation of ERW. Within MRV, reliable measurement (M) is particularly important. Accurate quantification of CO_2 removal is essential to build confidence in ERW as a carbon dioxide removal strategy. This will enable the development of a transparent carbon market for negative emission certificates from ERW (Power et al., 2025).

Various approaches have been proposed to quantify ERW, which can broadly be categorized into solid-phase, liquid-phase, and gas-phase measurements (Clarkson et al., 2024). Solid-phase approaches in soils aim to determine the extent of mineral dissolution by measuring changes in base cation inventories and residual mineral fractions within the soil profile. This soil-based mass balance approach has been applied in multiple studies (Vienne et al., 2025; Suhrhoff et al., 2024; Suhrhoff et al., 2025; Reershemius et al., 2023). An advantage of this method is that soil sampling aligns well with established agronomic monitoring practices (Clarkson et al., 2024).

However, carbon accounting based solely on base cation release may overestimate actual CO_2 removal if the released cations are not balanced by carbonate alkalinity derived from carbonic acid weathering (Power et al., 2025). Consequently, cation-based approaches require careful correction to ensure that only carbon-consistent weathering fluxes are attributed to durable CDR. In addition, the formation of secondary clay minerals must be considered, as incorporation of base cations into newly formed solid phases can decouple cation fluxes from alkalinity generation and thereby affect carbon accounting (Bijma et al., 2026).

This thesis focuses on liquid-phase measurements as a basis for ERW quantification. Soil porewater and reactor leachates can be analyzed for major cations and anions, total alkalinity (TA), dissolved organic carbon (DOC), dissolved inorganic carbon (DIC), pH, temperature (T), electrical conductivity (EC), and isotope composition of $\delta^{13}C$, $\delta^{18}O$, or novel isotope tracers (Clarkson et al., 2024).

The objective of this work is to evaluate both the limitations and the potential of these aqueous parameters for reliably quantifying CO_2 removal through enhanced rock weathering. A key parameter to be tested is EC, as it is very inexpensive to measure and its measurement is non-destructive.

1.2. Research Objectives

This dissertation investigates methods to quantify enhanced rock weathering (ERW) rates and their implications for TA generation and CO_2 removal. Two overarching research questions

are addressed here. The first examines whether EC can serve as a reliable proxy for TA. The second explores how the individual constituents of TA should be interpreted in the context of CO_2 removal, with particular emphasis on the role of non-carbonate alkalinity. Non-carbonate alkalinity is not directly linked to inorganic CO_2 removal, which represents the primary mechanism of CO_2 removal considered in most ERW studies. Therefore, its contribution was analyzed in detail, particularly with respect to its relationship with DOC. The individual chapters address the following research objectives:

- **Chapter 2** investigates how different soils and sands respond to the addition of alkaline $NaHCO_3$ solutions. Particular focus is placed on how bulk soil electrical conductivity (EC_b) responds to variations in volumetric water content (θ) and different concentrations of $NaHCO_3$/TA addition.
- **Chapter 3** analyzes the composition of total alkalinity (TA) in a crushed-rock column experiment with organic amendments. The study evaluates the contribution of different alkalinity components and their implications for dissolved CO_2 storage. Results are further compared with water samples from natural analogue systems, with particular emphasis on the formation of organic alkalinity.
- **Chapter 4** examines how microorganisms and earthworms influence rock weathering rates using column experiments with crushed rock substrate and organic amendments.
- **Chapter 5** evaluates the potential of using electrical conductivity (EC) measurements of leachate water to predict total alkalinity (TA). A calibration relationship is developed for a rock substrate rich in forsterite (Mg_2SiO_4). This can be a beneficial proxy for low-cost assessment of CO_2 removal in controlled setups.

2

Soil electrical conductivity as a proxy for enhanced weathering in soils

Abstract

To effectively monitor and verify carbon dioxide removal through enhanced weathering (EW), this study investigates the use of soil electrical conductivity (EC) and volumetric water content (θ) as proxies for alkalinity and dissolved inorganic carbon (DIC) in soil water. EC-θ sensors offer a cost-effective and straightforward alternative to traditional soil and water sampling methods. In a lab experiment, three different substrates were treated with $NaHCO_3$ solutions to increase the alkalinity of the soil water and analyze the response. The combination of EC and θ to track the increase in carbonate alkalinity due to EW, and therefore CO_2 consumption, is applicable for low cation exchange capacity (CEC) soil-substrates like the used quartz sand. However, the presence of organic material and pH-dependent CEC complicates the detection of clear weathering signals in soils. In organic-rich and clay-rich soils, only a high alkalinity addition has created a clear EC signal that could be distinguished from a non-alkaline baseline with purified water. Cation exchange experiments revealed that the used soil buffered alkalinity input and thereby might consume freshly generated alkalinity, initially mitigating CO_2 uptake effects from EW application. Effective CEC changes with pH and pH buffering capacity by other pathways need to be considered when quantifying the CO_2 sequestration potential by EW in soils. This should be estimated before the application of EW and should be part of the monitoring reporting and verification (MRV) strategy. Once the soil-effective CEC is raised, the weathering process might work differently in the long term.

2.1. Introduction

The problem of climate change has been known for decades, and the need for CO_2 removal (CDR) from the atmosphere has been highlighted in recent years (IPCC, 2023). The recent AR6 IPCC synthesis report states that CDR is a crucial element in all future emission scenarios that limit global warming to 2 °C (Babiker et al., 2022; IPCC, 2023). The use of negative emission technologies (NETs) will likely play a considerable role in climate change mitigation by removing $\approx$10 $GtCO_2$/yr globally by midcentury and 20 $GtCO_2$/yr needed by the end of the century (NASEM National Academies of Sciences, Engineering, and Medicine, 2019).

Chemical weathering of minerals is a natural process that has regulated the global carbon cycle on geological timescales (Walker, Hays, and Kasting, 1981; Berner, 2003). Enhanced weathering (EW) is understood as the acceleration of this natural chemical weathering process by the application of powdered rock to either the land surface or the ocean surface, thereby speeding up the reaction between minerals, water and CO_2 (Schuiling and Krijgsman, 2006; Hartmann et al., 2013; Beerling et al., 2020).

Enhanced Weathering (EW) is a promising method that might be able to contribute significantly to the CDR goals (Schuiling and Krijgsman, 2006; Hartmann et al., 2013; Beerling et al., 2020; Goll et al., 2021), with estimated costs ranging from 50 to 200 USD/tCO_2 globally (Fuss et al., 2018) and 45 to 472 USD/tCO_2 in the Midwestern U.S (B. Zhang et al., 2023). The global potential of EW has been described by multiple studies (Renforth, 2012; Hartmann et al., 2013; Goll et al., 2021). First terrestrial EW field trials at smaller scales quantify the in-situ weathering rates and amounts of sequestered CO_2 (Haque, Santos, and Chiang, 2020; Larkin et al., 2022).

However, the reliable quantification of carbon dioxide (CO_2) sequestration is the most crucial building block for any CDR method to facilitate a CO_2 certificate trading scheme. Like for most nature-based solutions, the measurement of CO_2 removal by enhanced weathering in soils is relatively complex compared to technical approaches like direct air capture (DAC).

The small number of extensive local field-scale experiments conducted worldwide poses a significant obstacle to obtain a comprehensive evaluation of the EW effectiveness on a global scale. This limitation arises from the diversity of soils worldwide, each with its unique chemical and physical properties, which inhibits the extrapolation of findings from one local experiment to another. To measure the efficacy of this technology for terrestrial experiments, reliable and cost-effective measurements are necessary to facilitate more field trials. Similar to other nature-based NETs, CO_2 sequestration quantification, also known as carbon accounting, is manifold (Brander et al., 2021).

In terrestrial EW experiments, finely crushed silicate rock powder is spread on arable land, where it is left to react under elevated pCO_2 conditions in the soil (Brook, Folkoff, and Box, 1983; Romero-Mujalli et al., 2019), amplifying the chemical weathering reaction.

The Equation 2.1 shows the chemical weathering reaction of wollastonite ($CaSiO_3$) with carbonic acid (H_2CO_3). Wollastonite is a simple silicate mineral used here as an example of silicate weathering reactions in general.

$$\text{Silicate weathering} \quad CaSiO_3 + 2\,CO_2 + H_2O \longrightarrow Ca^{2+} + 2\,HCO_3^- + SiO_2 \tag{2.1}$$

$$\text{Carbonate precipitation} \quad Ca^{2+} + 2\,HCO_3^- \longrightarrow CaCO_3 + CO_2 + H_2O \tag{2.2}$$

The second part (bold) of Equation 2.1 shows the weathering products. This idealized

equation gives us the upper limit for CO_2 sequestration by the weathering process. The released bicarbonate (HCO_3^-) is contributing to the total alkalinity (TA) of the water. The direct measurement of the TA usually involves acid titration of the water.

As a cheaper measurement to assess TA in natural waters for known environmental conditions, EC was suggested to track sequestered CO_2 in the water (Amann and Hartmann, 2022). The amount of dissolved ions drives the EC of an aqueous solution. Those carry charge through the water and thereby conduct electric current.

As EC works as a predictor of TA for some natural waters (surface water or spring water from draining volcanic rock or loess catchment), it is tested to see if this relationship could be useful for alkalinity change detection in bulk soils with unsaturated water conditions. If and how soil bulk electrical conductivity (EC_b) changes with added silicate minerals and released weathering products for EW field trials is unknown. The contribution of individual ions to the EC of the water (EC_w) can be calculated (McCleskey et al., 2012). The EC_w will increase with the released TA in a unique pattern depending on the composition of the dissolved mineral (Amann and Hartmann, 2022). When a specific mineral is added to the soil and chemically weathered by carbonic acid, it will gradually increase the DIC and TA in the soil water, thereby increasing the amount of ions in the soil water and the EC_W. An increase in EC_w must affect the EC_b as well. However, the behavior of a bulk soil is complex because of chemical interactions between the solid and the liquid phase (Merkel and Planer-Friedrich, 2008). The EC_b is driven by multiple pathways for electrical conduction, making a model for the contribution of dissolved species to the EC_b more sophisticated (J. D. Rhoades et al., 1989; Hendrickx et al., 2002).

Different agricultural soil samples were treated with alkaline $NaHCO_3$ solutions to simulate the release of weathering products after EW application to test whether EC_b could be used to track the additional weathering signal and, thereby, the conversion of CO_2 into TA. It is investigated how the EC_b reacts to the added weathering products in the form of Na^+ and TA, predominantly in the form of HCO_3^-. Soil water samples were collected after the soils were treated with $NaHCO_3$ solutions to examine how the chemical composition of the soil water changed.

This study aims to improve the understanding of relevant soil properties for EW experiments and processes that must be considered for quantifying CO_2 removal and interpreting EC_b data. For example, the CEC and pH buffering capacity of soils have yet to be considered for the assessment of CO_2 sequestration. The weathering of non-carbonic soil acids must be accounted for (Dietzen and Rosing, 2023). A better understanding of the cation exchange processes in different soils, soil acidity and bulk soil EC_b could facilitate the use of simpler low-cost measurements for carbon accounting of EW.

2.2. Methods

2.2.1. Testing soils

Three different substrates were used in this experiment to test the EC_b response on the alkaline solution for different soil types. The two soil samples originate from arable land in Bramstedt in Northern Germany and Fürth in Southern Germany. Those sites are being used for long-term EW field trials, and the soil samples have been taken before applying the silicate mineral powder on those sites. The soil samples were collected from the upper 30 cm of the soil, representing a typical deeper plowing depth (Baumhardt, O. R. Jones, and Schwartz, 2008).

The Bramstedt test site is situated within a fen, an area characterized by wetlands. The field was initially used as grassland and cropland the years before the soil sampling took place. The soil in this location has some peat and a considerable organic matter content, resulting in a dark color. The soil is a strong loamy sand with a clay content of 12 to 17 %, as determined according to *DIN 19682-2* (2023).

The Fürth test site was previously used for agriculture. It has a low inorganic carbon content and much lower organic carbon content than the soil from Bramstedt (Table 2.1). The soil type is identified as brown earth, which is also known as Cambisol or, for sandy soils, Brunic Arenosol (Amelung et al., 2018). Both types are characterized by little or no soil profile differentiation (IUSS Working Group WRB, 2022). The brown earth can be found in Europe, North- and South America, and southern parts of Siberia (Pehamberger and Gerzabek, 2009), making the findings comparable to other European agricultural sites.

Table 2.1: Soil properties including carbon content, clay mineralogy, and cation exchange capacity (CEC).

Material	Total inorganic carbon [wt. %]	Total organic carbon [wt. %]	Clay content [wt. %]	effective CEC (at ambient pH) [cmol kg^{-1}]
Pool filter quartz sand (0.4 to 0.8 mm grain size)	-	-	-	in theory ≈ 0[a]
Brown earth (soil sample from Fuerth)	0.04	1.4	2:1 layer silicates: 8.3 Chlorite: 0.95	5.6
Organic-rich soil (soil sample from Bramstedt)	0.36	7.22	2:1 Layer silicates 4.8 Chlorite: 1.5	8.5

a = Not measured value. When the quartz sand does not contain any impurities its CEC is 0 cmol kg^{-1}.

To mimic non-reactive soil with minimal nutrients as well as low organic matter and clay content, resulting in low effective CEC, plain quartz sand (commercially available pool filter

sand) was used (Table 2.1).

Soil samples were air-dried and sieved to 2 mm to break down the soil clods, remove bigger stones, and get a homogeneous mass, destroying any natural soil horizons. Therefore, the following experiments will treat the upper 30 cm soil sample as one homogeneous material.

2.2.2. Soil analysis

The soil samples for the mineralogical analysis were dried at 40 °C and wet-milled. The bulk composition of the soil was measured by X-ray diffraction quantitative phase analysis (QPA, Bruker D8 Advance system).

The total organic carbon (TOC) and total inorganic carbon (TIC) were measured by splitting the soil sample into two representative parts. One part was treated with HCl to remove all TIC from the total carbon content (TC). Both samples were fused by open-system pyrolysis at 1 600 to 1 800 °C, in which the amount of CO_2/TC produced was measured by chromatography with the Carlo Erba EA1108 elemental analyzer. The TIC was then determined by subtracting the total organic carbon from the total carbon (TIC = TC − TOC).

The soil samples for the cation exchange capacity (CEC) measurement were dried at 110 °C to lose adsorbed water and ground to < 500 µm. The CEC analysis is based on the exchange of the sample with Co-hexamine trichloride $[Co(NH_3)_6]Cl_3$ (Co-Hex) (Orsini and Remy, 1976; Ciesielski et al., 1997) solution and the subsequent spectrophotometric analysis of the exchanged liquid using a Shimadzu UV-1280.

The Co-Hex solution is added to the dried soil sample. After the exchange reaction, the suspension is centrifuged and filtered, and absorption is measured at a wavelength of 475 nm to determine the concentration of the left Co-Hex ions. The calibration set is composed of different Co-Hex concentrations and blanks. The result gives the effective CEC at ambient pH.

For the pool filter quartz sand as a non-reactive soil example, the parameters were not measured. As the Bramstedt soil sample contains more organic carbon than the Fuerth soil, it is referred to as organic-rich in the following text. It also contains more clay minerals (Table 2.1), making the soil overall more reactive (Churchman, 2018).

All experiments were conducted in a controlled lab environment at T = 20 °C and pCO_2 = 450 ppm, slightly higher than the average global mean atmospheric pCO_2 of 418 ppm (Lan et al., 2023). The samples of each site were dug and mixed, then dried and sieved to 2 mm; thus, there will no longer be high pCO_2 in the soil pore space.

2.2.3. Testing solutions

All the different soils were watered with sodium bicarbonate solutions ($NaHCO_3$) with ≥ 99 % purity. This compound was chosen for carbonate alkalinity creation because of its high

solubility [96 g L^{-1} at 20 °C, (Haynes, 2015)]. One mole of HCO_3^- increases the TA of the solution by one acid equivalent (eq) that can be buffered; thus, 1 mol $NaHCO_3$ L^{-1} equals 1 eq L^{-1}. The concentrations of the different solutions were chosen based on previous column EW experiments conducted using the same organic-rich soil (Li et al., unpublished data). They observed TA up to 10 meq/L in the percolating soil water of soil columns treated with silicate minerals. $NaHCO_3$ should simulate the released weathering products to avoid the long weathering reaction times when applying silicate rock powder to soils. In this study, the kinetics of the weathering process are not analyzed. Instead, the solutions already contain the weathering products. The solutions were produced volumetrically by weighing in $NaHCO_3$ powder, dissolving, and filling up to the target volume. The solutions used in the experiment have $NaHCO_3$ concentrations of 0, 2.5, 5, 10, and 50 mmol L^{-1}

2.2.4. Setup EC_b experiment

The EC_b sensor (Dragino LSE01) used in this study is composed of a conductivity meter to get the bulk soil electrical conductivity EC_b, a resistance temperature detector (RTD) to measure the soil temperature, and a frequency domain reflectometry (FDR) probe to measure the volumetric water content (θ) with the compensation from soil temperature and electrical conductivity. It is designed to measure θ of saline-alkali soil and loamy soil (mineral soils) and is made for outdoor agricultural use (Dragino, 2022). The sensor is not strictly research-grade because there is just a single internal calibration for θ that could not be adjusted. Still, it was used because the same sensors were used on the test sites in the Carbdown project (Carbdown, 2022) to test them for the assessment of carbon sequestration. The sensor was calibrated for a mineral soil type and not organic-rich soils. Hence, the exact θ values might be biased, and θ will not be interpreted in-depth in this study. The EC_b and θ value pairs are not compared for different soils. Nevertheless, sensors should show differences in EC_b at constant volumetric water content θ for different $NaHCO_3$ treatments for the same soil.

The sensor converts the measured EC_b values to the reference temperature at 25 °C, suppressing the measured values' temperature dependence. It uses the same reference temperature as the EC_w measurement of the solutions and soil water, which increases with temperature by about 1 to 3 % $°C^{-1}$(Robinson and Stokes, 2002).

To determine how the EC_b reacts to the released weathering products in the soil water (Na^+ and HCO_3^-, air-dried soil samples were watered with different $NaHCO_3$ concentrations and purified water as a non-alkaline reference (Figure 2.1). The EC_b, θ and the soil temperature were measured with the Dragino LSE01 probe. In addition, the EC_w and the pH of the input solution were measured with the WTW Multimeter 3630 IDS. For further details about the used probes, see Table 2.2.

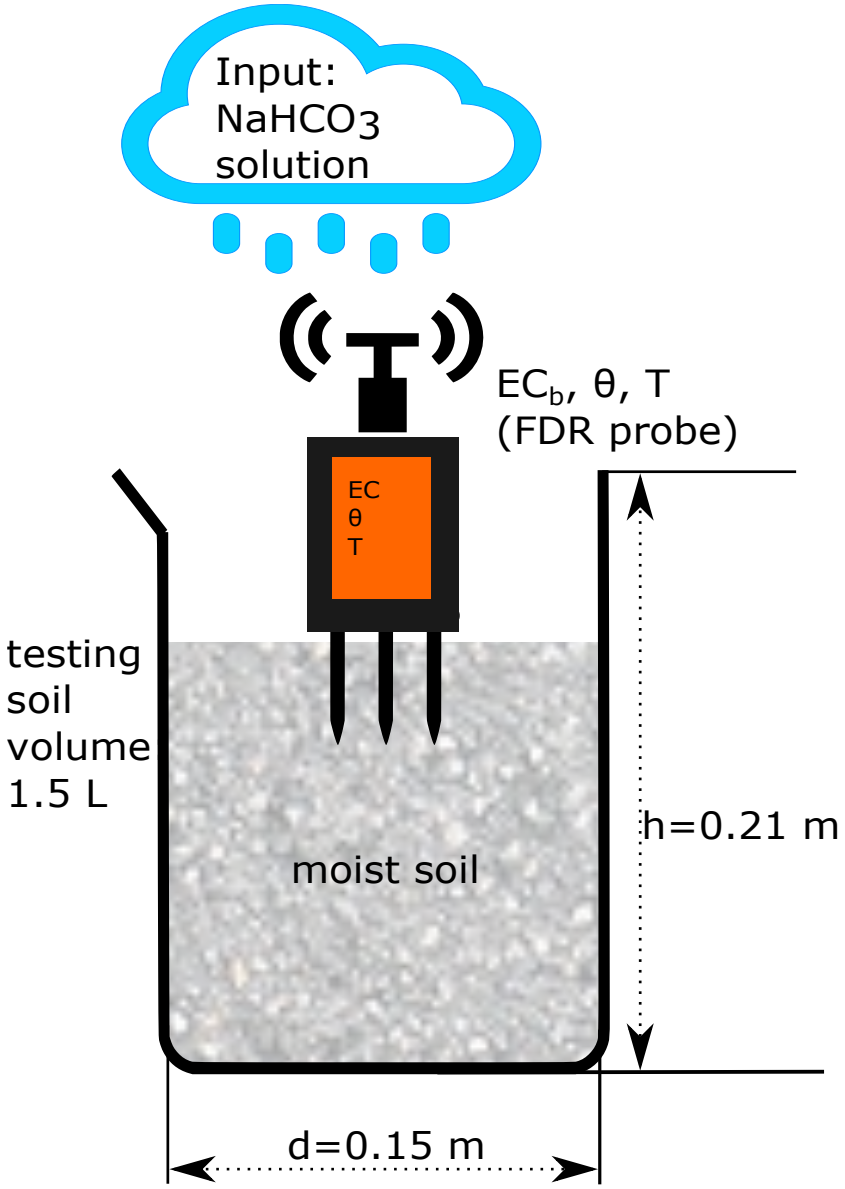


Figure 2.1: Setup to test soil bulk electrical conductivity EC_b for different θ.

For each concentration/experimental run, a container (Figure 2.1) was filled with 1.5 L (around 1 700 g) of sieved air-dry soil to ensure a large enough volume for the sensor's electrical field penetration depth and physical size. This sensitive measurement volume of the sensor can be approximated by a cylinder with a height of 10 cm and a 7 cm diameter around the central probe (Dragino, 2022).

The containers were then filled with the $NaHCO_3$ solution in 75 g steps until reaching the soil saturation point, starting from 500 g of added solution for the used soils. After each irrigation step, the soil was mixed manually with a spatula to homogenize the soil water mix. Ten measurements in different sensor positions were taken to minimize the effects of soil heterogeneity and sensor-soil coupling.

Table 2.2: Measurements in the soil water samples.

Parameter	Explanation	Device
pH	to track pH buffering effects from the soil	WTW Multimeter 3630 IDS with Sentix 940
EC_w	Electrical conductivity of the aqueous solution (EC25)	WTW Multimeter 3630 IDS with TetraCon 925
Cations	Major cations measured by ion chromatography	Metrohm 881 Compact IC Pro system with Metrosep A Supp 17–150/4.0
Anions	Major anions measured by ion chromatography	Metrohm 881 Compact IC Pro system with Metrosep C4–100/4.0
TA	Total alkalinity measurement with automated Gran titration to find equivalence point	Metrohm Titrando with Aquatrode plus

2.2.5. Setup soil reaction experiment

The brown earth from the Fuerth test site was chosen to investigate the reactions of the alkaline $NaHCO_3$ solutions with the soil more closely. It is the soil with a much lower organic matter content; therefore, one would expect a weaker pH buffering reaction. The water of the saturated paste was extracted from this soil. The chemical analysis of the soil water extracts gives a better understanding of the observed EC_b signal, as the EC_b is mainly a function of the dissolved ions in the soil water (Hendrickx et al., 2002; D. Corwin and Lesch, 2005). Air-dried soil samples were saturated with the different $NaHCO_3$ solutions. The method used closely follows the method presented by D. L. Corwin and Yemoto (2020) for measuring soil salinity.

For each reaction setup, 1 700 g of air-dried soil was mixed with 485 mL of $NaHCO_3$ solution. This ratio was kept constant for all treatments. Therefore, the brown earth was watered with the produced $NaHCO_3$ solution until it reached the saturation point. Following Corwin and Yemoto (2020), it is the point where the soil water mix: (i) surface sparkles, (ii) can flow, (iii) slides freely off a spatula, (iv) is malleable so that when running a spatula through the mix the channel will hold shape and (v) when shaking the container the channel collapses. The soil water mix is called the saturated paste at this saturation point.

Even though it is faster and more effective to extract the soil water at higher water content like 1:1, 1:2, and 1:5 (soil to water ratio) in this experiment, the low saturation level extraction will be used. It is the standard for EC studies as it provides the lowest but sufficient water volume to be analyzed for its chemical composition (D. L. Corwin and Yemoto, 2020). It is closer to the natural moisture processes in actual soil. In our case, it represents the actual conditions in the soil of the (θ, EC_b) measurements of the EC_b experiment setup.

To measure the range of responses the brown earth was irrigated with the same solutions as in the previous experiment of 0, 2.5, 5, 10, and 50 mmol L^{-1} of $NaHCO_3$. There are three duplicates to capture the variability and get more reliable results for each $NaHCO_3$

treatment. In total, 15 saturated paste samples (5 $NaHCO_3$ solutions times 3 duplicates) except a third one for the high concentration of 50 mmol L^{-1} due to the lack of further extraction equipment. After saturating the samples with the solutions, they were stored for 24 h in the fridge inside containers covered with snap-tight lids to avoid evaporation from the sample. In this period, the soil and the solution have time to react, and dissoluble compounds can dissolve in the soil water. After the time had passed, the saturated paste was placed outside the fridge until it reached room temperature again. Then, the soil water of the saturated paste, called saturation extract, was pumped out with vacuum pumps (see Figure 2.2). The extraction took 1 day, as the soil holds very little free water at the saturation point, and it takes longer to pump it out. After applying the vacuum for 1 day, the saturation extract was directly analyzed for the chemical composition; see Table 2.2 for further details.

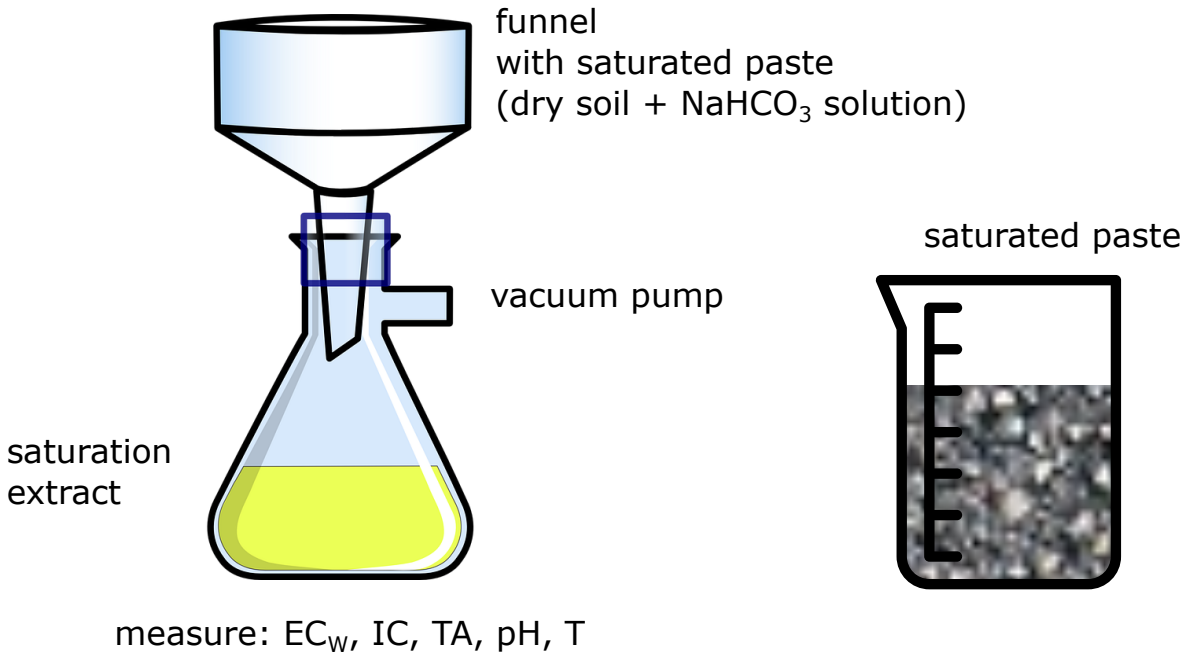


Figure 2.2: Soil water extraction setup (extraction of saturation extract from saturated paste).

All the soil water samples were filtered with 0.45 µm cellulose acetate (CA) dead-end filtration. All measurements except the EC_w and pH were measured in the filtered samples. The EC_w probe applies an internal linear temperature compensation to 25 °C. All shown EC_w values thus are normalized to 25 °C.

2.3. Results

2.3.1. Bulk soil electrical conductivity (EC_b)

Pure quartz sand (non-reactive soil example)
In the quartz sand experiment, the different $NaHCO_3$ treatments are distinguishable (Figure 2.3). The purified water treatment shows a very low EC_b signal for the whole range of θ. This low EC_b reflects a low concentration of soluble salts in the quartz sand. The data points have a weak spread and follow the trend lines well.

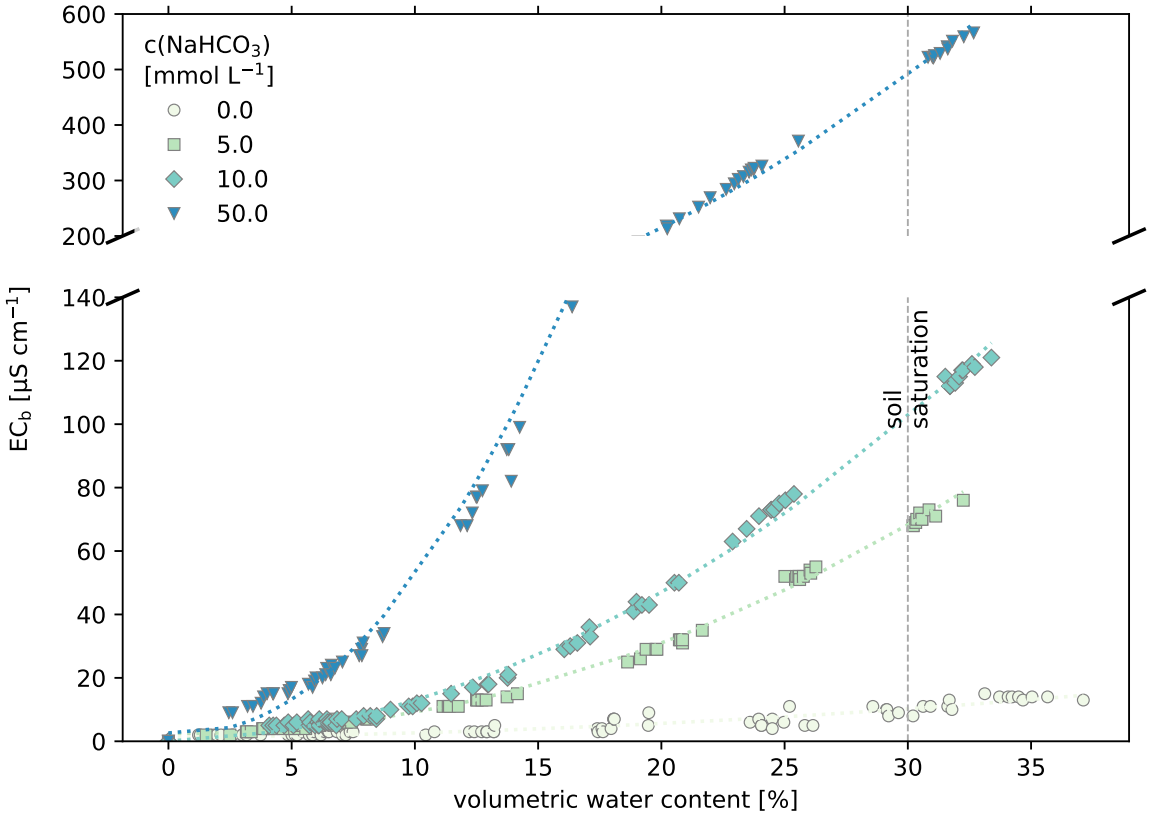


Figure 2.3: Electrical conductivity measured in the bulk soil (EC_b) against the volumetric water content of the soil (θ) using pure quartz sand as the substrate. The quartz sand was watered stepwise with $NaHCO_3$ solution to raise the water content until reaching the saturation point at 30 %. The quartz sand mimics a non-reactive, sandy and low effective-CEC soil.

Brown earth

In the brown earth soil (Figure 2.4), EC_b values are not distinguishable for up to 15 % volumetric water content. Only the high 50 mmol L^{-1} $NaHCO_3$ concentration is visible and distinct from the other low-concentration treatments.

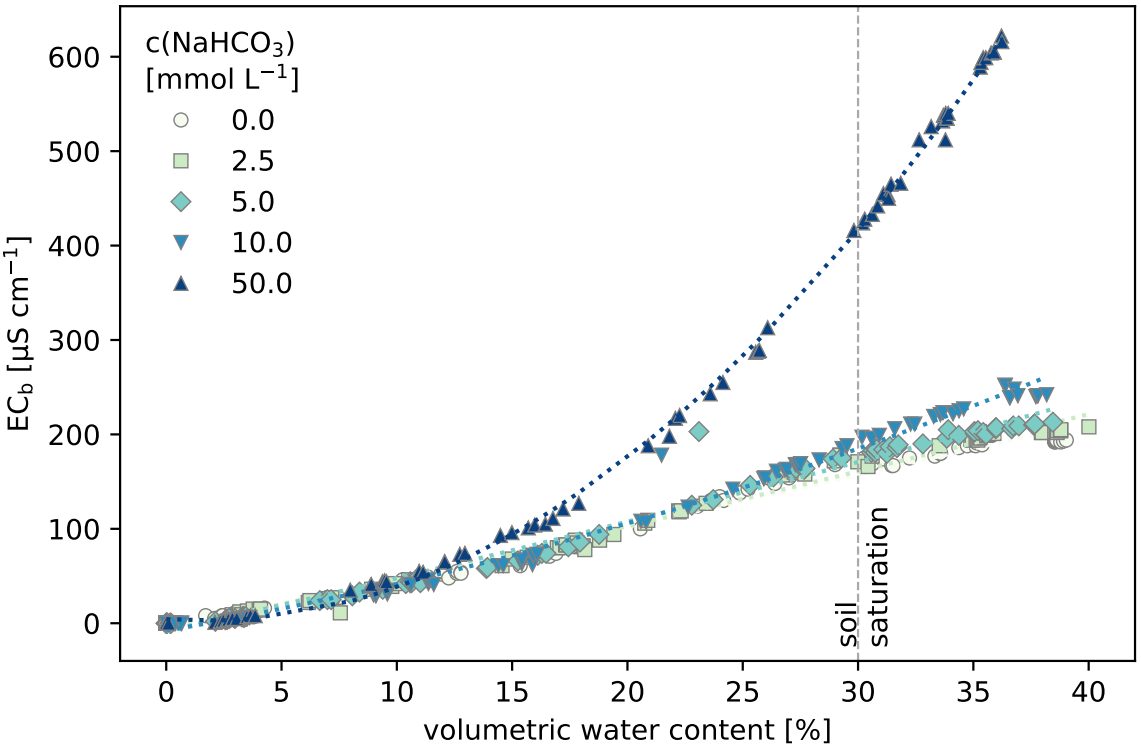


Figure 2.4: Electrical conductivity measured in the bulk soil (EC_b) against the volumetric water content of the soil (θ) using brown earth as the substrate. The brown earth was watered stepwise with $NaHCO_3$ solution to raise the volumetric water content until reaching the saturation point at 30 %.

Organic-rich soil

The organic-rich soil (Figure 2.5) mostly suppressed the whole signal. All different treatments have the same trend until 20 % volumetric water content. Above 20 % volumetric water content, the high 50 mmol L^{-1} $NaHCO_3$ concentration can be distinguished from the others. Treatments until 10 mmol L^{-1} all show the same trend, including some noise.

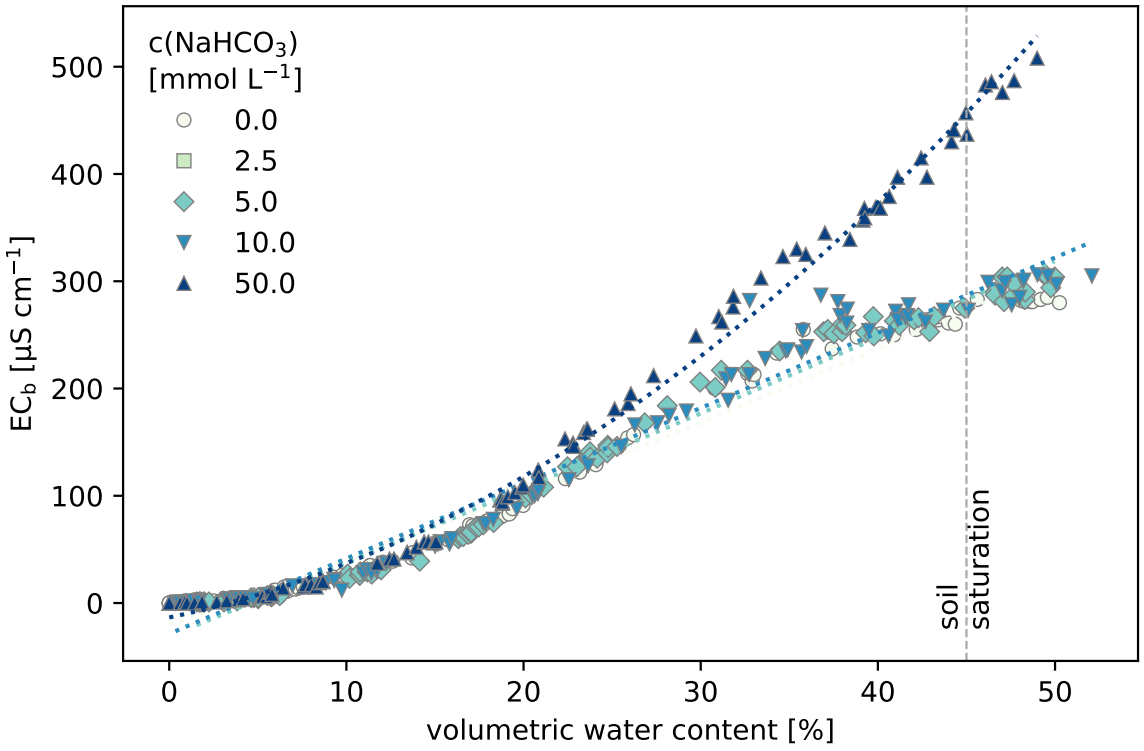


Figure 2.5: Electrical conductivity measured in the bulk soil (EC_b) and the volumetric water content of the soil (θ) using the organic-rich soil as the substrate. The organic-rich soil was watered stepwise with $NaHCO_3$ solution to raise the volumetric water content until reaching saturation point at 45 %. This soil is rich in soluble salts and has a high effective CEC.

2.3.2. Brown earth reaction experiment

Electrical conductivity of the soil water (EC_b)

The saturation extract experiment results (see Figure 2.6) reflect the observed EC_b response from the first experiment (see Figure 2.4). Despite the significantly different EC_w of the initial $NaHCO_3$ solutions, see orange bars in Figure 2.6, the saturation extracts for the range of 0 to 5 mmol L^{-1} $NaHCO_3$, see blue bars, show a very similar EC_w. In the next higher concentration of 10 mmol L^{-1}, there is a slight difference in the EC_w, but the standard deviation is huge and overlaps with the other error bars; thus, it is insignificant. Only in the high 50 mmol L^{-1} treatment a significant difference in the EC_w of the soil extract compared to the others is visible. It is also interesting to note that compared to the input, the EC dropped significantly for this treatment, whereas for the other treatments, it increased.

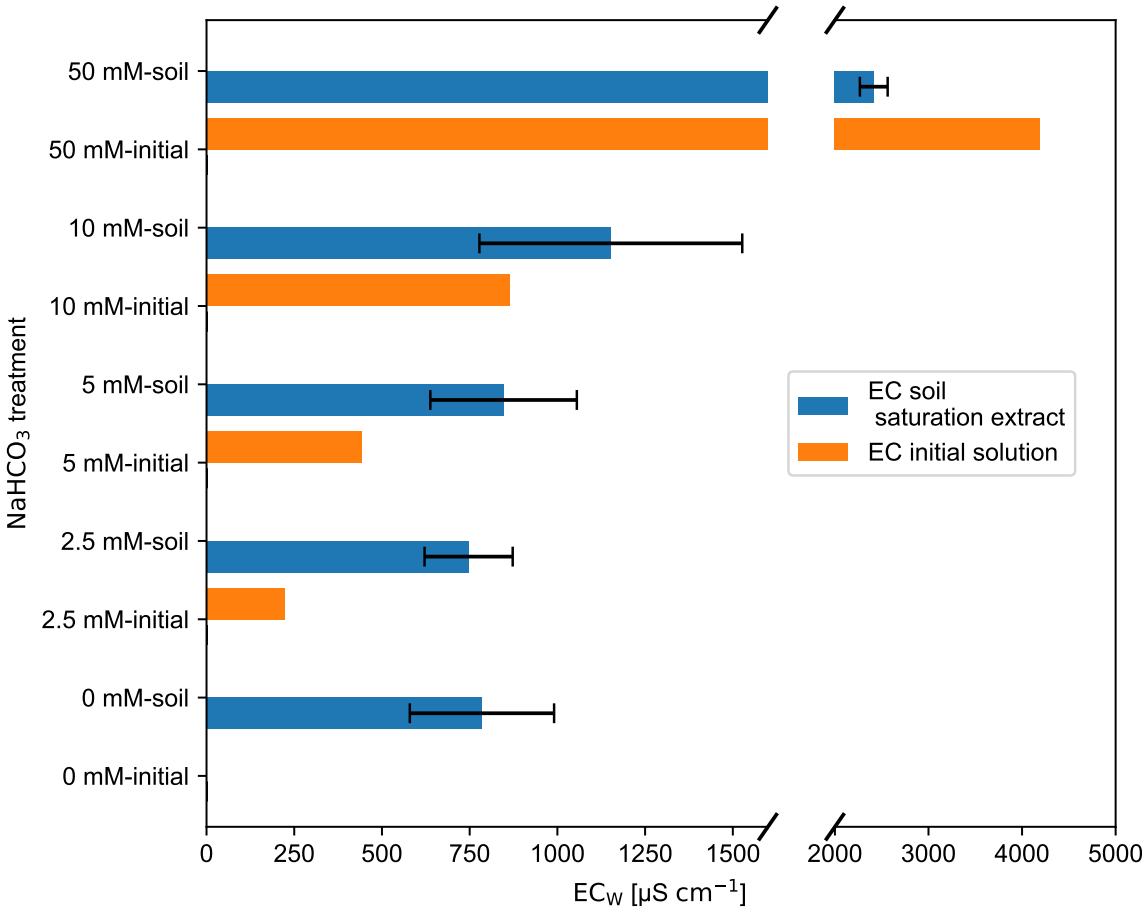


Figure 2.6: The mean value of the solution electrical conductivity (EC_w), measured in the saturation extracts from the brown earth, is presented in this bar chart. This mean value and the black error bars, showing the ±1 standard deviation, were calculated from the three duplicate saturation extract samples for each $NaHCO_3$ solution treatment.

Electrical conductivity is a collective measure of all dissolved ions in the solution. One might expect that the electrical conductivity of the 0 mmol L^{-1} soil extract (pure water soil extract) just adds up to the initial conductivity. However, as observable in the further plots, the $NaHCO_3$ solution reacts with the soil solids and partly disappears from the soil water. Thus, the reduction in the Na^+ and HCO_3^- concentrations leads to a decrease in the EC_w.

Cations

The major cations (see Figure 2.7) reveal an interesting pattern that follows the EC_w and TA signals. In all treatments, a similar amount of calcium ions Ca^{2+}, potassium ions K^+, and magnesium ions Mg^{2+} is dissolved. The cations dissolved contributed to the EC_w. However, the initially added Na^+ concentration was reduced in all cases. As Na^+ is the most dominant cation in the $NaHCO_3$ solutions, it will force a reaction of the soil solids with the Na+ cations and lead to cation exchange reactions. Especially in the 50 mmol L^{-1} $NaHCO_3$ treatment, the Na^+ concentration was even halved.

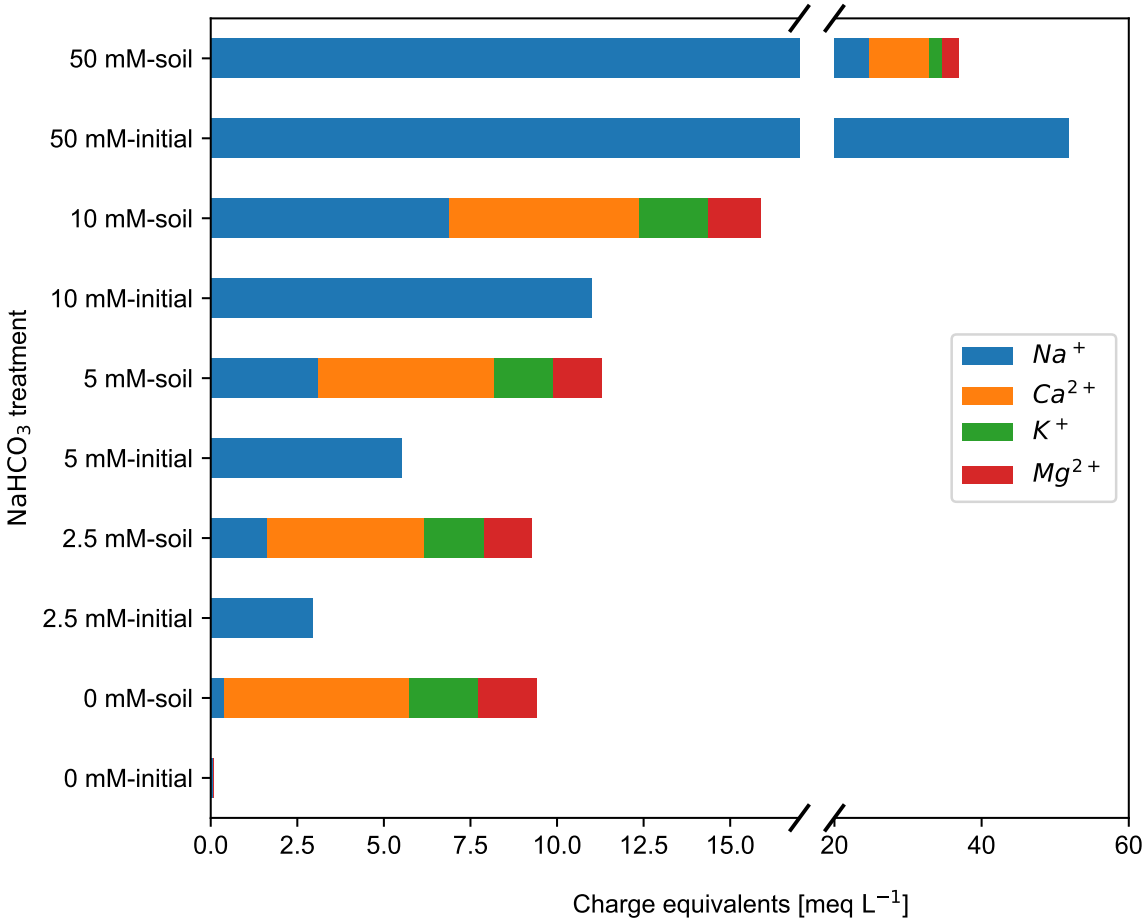


Figure 2.7: Mean major cations charge equivalent concentrations measured in brown earth saturation extracts. Each parameter was calculated using three duplicate samples for each $NaHCO_3$ solution treatment.

Anions

While there are interesting trends in the EC_w, TA, and cations, the concentrations of measured anions without the TA do not reveal such a trend (see Figure 2.8). The dissolution of these anions is unaffected by the different introduced alkaline $NaHCO_3$ solutions. All soil treatments from 0 to 50 mmol L^{-1} show a similar behavior by releasing a comparable number of anions to the soil water.

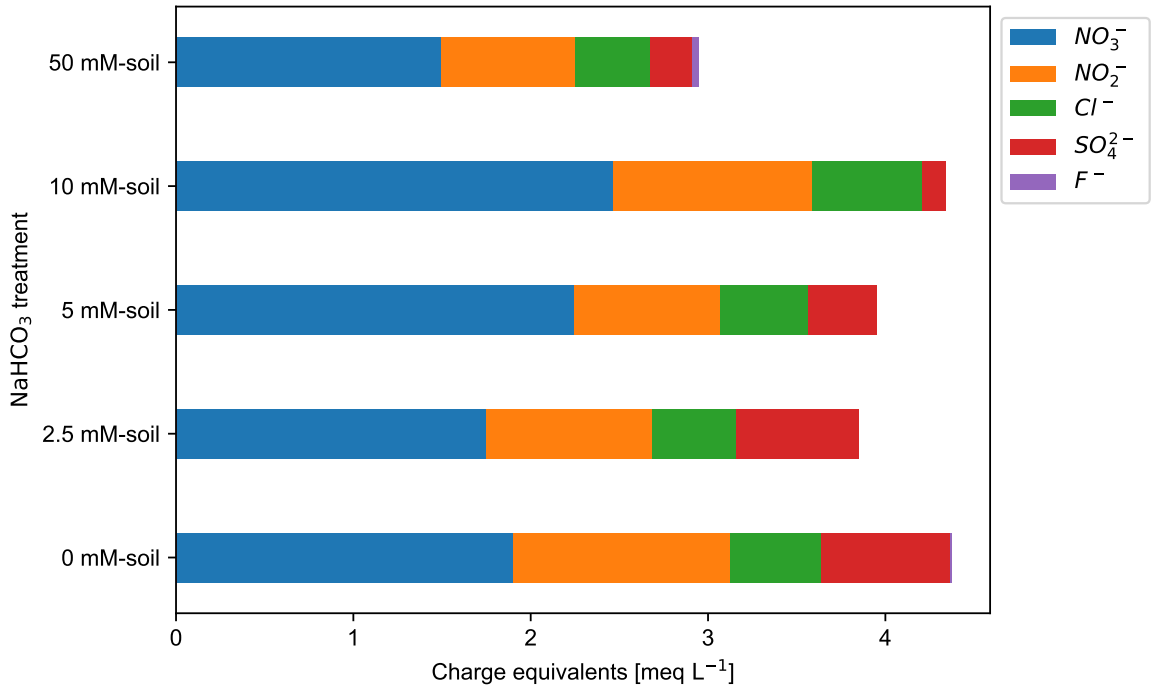


Figure 2.8: Anion charge equivalent concentrations (without TA) measured in the saturation extract. Values are based on three duplicate samples for each $NaHCO_3$ solution treatment. The liquid extract from the brown earth shows dominance of nitrogen species when excluding TA.

Except for the purified water treatment, the TA in the initial solutions was always reduced after the reaction with the soil. For the 5, 10 and 50 mmol L^{-1} treatments, even less than half of the initial TA was left after the $NaHCO_3$ solution passed through the brown earth.

2.4. Discussion

Using EC_b and θ to predict soil water TA might work for non-reactive or low-reactive substrates, like the used quartz sand, with low effective CEC. A distinguishable EC_b response for different $NaHCO_3$ treatments was visible in the pool filter quartz sand in this experiment. However, the brown earth with organic matter and clay minerals buffered the introduced TA proportional to the TA concentration that was added to the soil. Due to this buffering effect, no clear EC_b signal is detectable for both analyzed soils (subsection 2.4.1).

The following discussion (subsection 2.4.2) describes two potential pathways that could have neutralized the added TA input and led to the observed result. Either the growth in effective CEC has buffered the TA or the precipitation of carbonates inside the soil. When the soil effective CEC grows and the soil releases H^+ from acid sources other than carbonic acid, it also shrinks the CO_2 removal potential. Understanding this initial buffering effect is crucial for parties searching for a cheap and suitable MRV tool to track the sequestered CO_2 (transformed into TA) for EW experiments.

2.4.1. Bulk soil electrical conductivity response

All three different substrates have in common that the EC_b increases with θ (Figure 2.3 to Figure 2.5). Most $EC_b(\theta)$ plots have a curvilinear shape with the slope changing with θ. Considering the purified water treatments [$NaHCO_3$] = 0 mmol L^{-1} together with the [$NaHCO_3$] = 50 mmol L^{-1}. The slope $\frac{dEC}{d\theta}$ is increasing with higher solution concentrations since this also increases the electrical conductivity of the soil water (EC_w). All the characteristics mentioned above can be described with the EC_b equation from J. Rhoades, Raats, and Prather (1976):

$$EC_b = \left(a\,\theta^2 + b\,\theta\right) EC_w + EC_s. \tag{2.3}$$

With a and b as empirical fitting constants for the soil, surface electrical conductivity (EC_s), and the soil water electrical conductivity (EC_w).

When considering plausible TA levels of up to 10 meq L^{-1}, based on leachate water from soil EW experiments by Li (unpublished data) for the same organic-rich soil (see Figure 2.5), a reliable separation of EC_b, in terms of the different $NaHCO_3$ treatments, is not possible. The initial concentration of the $NaHCO_3$ inputs cannot be derived anymore because the resulting $EC_b(\theta)$ curves are almost equal for low-concentrated $NaHCO_3$ solution additions. Additionally, the considered high-water contents θ are rare in natural soils and are probably just present after heavy rainfall. Outdoors, the soil moisture is mostly at field capacity (FC) (McCauley, C. Jones, and Jacobsen, 2005). That implies typically smaller θ, so a regression analysis's determination of the different $NaHCO_3$ treatments is even more limited. However, this experiment also showed distinguishable $EC_b(\theta)$ curves when using pure pool filter quartz sand as substrate (see Figure 2.3), as the sand conserves the water's chemical properties.

The brown earth and the organic-rich soil buffered a considerable part of the introduced TA (see Figure 2.9) as the soil reacted with the $NaHCO_3$ solution. The EC_b represents how the soil reduced the introduced TA, thereby lowering the EC_b signal. Apart from the initially different EC_w of the $NaHCO_3$ solutions, the $EC_b(\theta)$ curves look very similar. However, when the $NaHCO_3$ addition and thus the concentration in the soil water is big enough, it can be detectable with EC_b and θ.

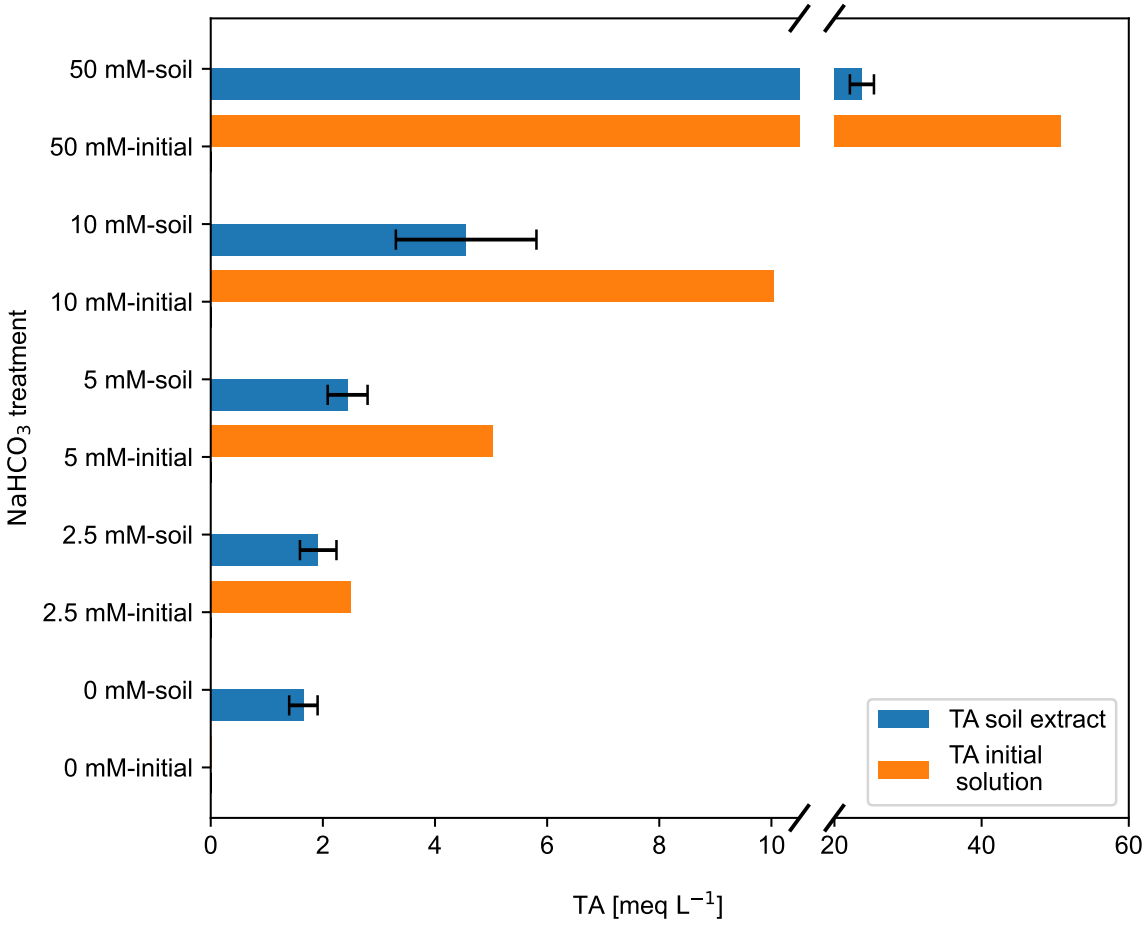


Figure 2.9: Total alkalinity of the initial produced $NaHCO_3$ sol(orange bars) and the total alkalinity measured in the brown earth saturation extract (after the $NaHCO_3$ solution passed the soil). The TA values are calculated from three duplicate samples for each $NaHCO_3$ solution treatment. The error bars indicate ±1 standard deviation.

2.4.2. Soil + $NaHCO_3$ solution reaction experiment

EC_w of the soil extracts

An interesting pattern is shown for the high concentration of 50 mmol L^{-1} $NaHCO_3$ (see Figure 2.6). EC of the soil water dropped significantly after interacting with the soil. This drop is reflected in the composition of the soil water, in which the Na^+ and TA decreased significantly (Figure 2.7 and Figure 2.9). For the other $NaHCO_3$ treatments, the EC_w increased, most likely due to the dissolution of any available soluble salts, which wasn't a big enough share in the 50 mmol L^{-1} $NaHCO_3$ treatment to be visible.

Anions in the saturation extract

While there are trends in EC_w, TA, and cations, the concentrations of anions without TA do not depend on the different treatments (Figure 2.8). The concentrations of anions without TA measured in the extracted soil water were in the range of extracted TA, except for the 50 mmol L^{-1} $NaHCO_3$ treatment (compare Figure 2.8 and Figure 2.9). The concentrations of anions without TA were unaffected by the different $NaHCO_3$ solution treatments (Figure 2.8).

All $NaHCO_3$ soil treatments from 0 to 50 mmol L^{-1} show a similar pattern, indicating that the analyzed anions (mainly NO_3^-, NO_2^-, and Cl^-) do not react or interact much with the introduced $NaHCO_3$ solution.

During the rewetting of the soil with the $NaHCO_3$ solutions, there was an accumulation of CO_2 bubbles on the surface of the wet soil, especially for the 50 mmol L^{-1} $NaHCO_3$ treatment. It has been qualitatively measured with air CO_2 meters; thus, no quantitative assessment is presented here. This strong CO_2 outgassing during the mixing indicates that part of the introduced HCO_3^- was neutralized by H^+ rather than adsorbed and exchanged with another anion in the soil. The TA measurement also reflects this HCO_3^- drop/neutralization (see Figure 2.9).

For most soils, the cation exchange capacity (CEC) is bigger than the anion exchange capacity (AEC) (Havlin, 2005). Thus, the measured anions in the soil water are most likely a result of the dissolution of the soil's soluble salts. The different $NaHCO_3$ treatments do not impact the availability of those soluble salts.

In contrast, the soil water's pH value and TA affect the release of cations bound by organic functional groups and clay minerals. The AEC tends to be relevant mainly in soils like spodosols, ultisols, oxisols (Sposito, 2008) and very acidic, heavy-weathered ferralsols present in the tropics as well as volcanic soils (e.g., andosols) (Amelung et al., 2018). Whereas in mildly to moderately weathered soils, as the used brown earth is, the negative surface charge dominates the soil system. This negative surface charge results from the permanent negative surface charge of the 2:1 layer silicates and the organic functional group's pH-dependent negative surface charge (Amelung et al., 2018). This is why the AEC will be neglected in the discussion of the used soils. The further discussion focuses on the concentration changes of cations and TA.

Major cations and TA in the saturation extract

The Na^+ and the TA have dropped to a comparable extent (Figure 2.10). In parallel, strong CO_2 outgassing was observed while mixing the dry soil with the $NaHCO_3$ solution. Three possible processes in the soil that can lead to the mentioned results are described in the following text.

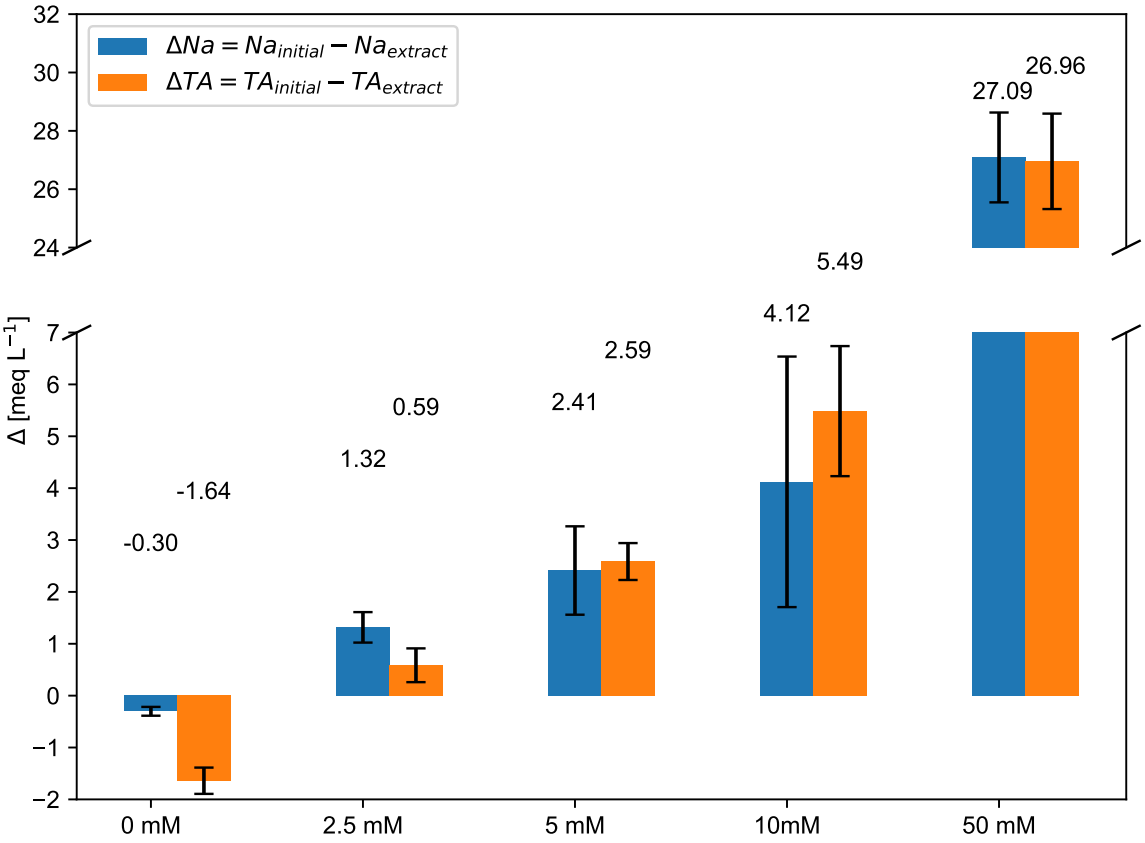


Figure 2.10: Total alkalinity (TA) and Na^+ equivalent concentration difference ($\Delta X = X_{\text{initial solution}} - X_{\text{soil extract}}$).

Biotic CO_2 respiration

The soil solution extraction experiment involves time-dependent chemical reactions. Some reactions, like cation exchange and neutralization of acid and base in extreme ranges, occur quickly, while others involving life are slower. However, the observed CO_2 outgassing response origin upon rewetting soil might be both abiotic and biotic. It is known that rewetting of dry soil can produce a fast CO_2 pulse generated by biotic respiration (Barnard, Blazewicz, and Firestone, 2020), also known as the Birch effect (Birch, 1958). However, the observed decrease in the introduced TA (mainly carbonate alkalinity) must also have caused CO_2 outgassing. Thus, the cation exchange reaction must have also contributed to the observed CO_2 pulse. The observed CO_2 outgassing is unlikely of a pure biotic nature.

Growth of pH-dependent effective CEC releasing H^+

The negative surface charge sites, produced by pH-dependent clay minerals and deprotonation of weakly acidic chemical functional groups on soil solids, bind exchangeable cations (Helling, Chesters, and Corey, 1964; Curtin, Campbell, and Messer, 1996; Bloom and Skyllberg, 2011). Soil organic matter contributes much to soil pH-dependent CEC (Baldock and Broos, 2011; Bloom and Skyllberg, 2011). The carboxyl and phenolic structural groups can donate protons when the pH in the soil water is raised and act as a buffer (García-Gil et al., 2004; Thomas and Hargrove, 2015). Furthermore, the increase in the soil's pH can lead to a substantial loss in organic carbon (OC) by leaching (Te Pas, Hagens, and Comans, 2023), but OC was not

measured in this study.

The higher the initial solution TA ($NaHCO_3$ concentration), the more organic acid structures and clay minerals will deprotonate and neutralize the TA in the soil water (see Figure 2.9). This is in line with the theory that the effective CEC increases with the pH (De Villiers and Jackson, 1967; Curtin, Campbell, and Messer, 1996). Consequently, the soil particles release H^+, and one negative charge site is produced where one cation can be adsorbed (Helling, Chesters, and Corey, 1964; Sims, 2018).

In this study, the loss of TA in soil water is directly proportional to the quantity of introduced TA. As the soil water pH is elevated, more organic functional groups and pH-dependent clays actively buffered the rising pH levels. For organics, the ionization of carboxyl groups is generally complete at pH 8, and the ionization of phenolic groups is complete at pH 11 (Bloom and Skyllberg, 2011). The clay minerals, especially vermiculite and smectite, will also contribute to pH buffering (Bourg and Sposito, 2011). Curtin, Campbell, and Messer (1996) provide a regression equation to describe the pH buffering capacity of some Canadian soils (titratable acidity until pH = 8) just by two variables. It shows the relative impact of organic carbon and clay content.

$$Y = 0.02 + 59 \cdot \mathrm{OC} \cdot \Delta\mathrm{pH} + 3 \cdot \mathrm{clay} \cdot \Delta\mathrm{pH} \tag{2.4}$$

Where Y is the titratable acidity to pH 8 [$\mathrm{cmol\,kg^{-1}}$], OC is the organic carbon content, and clay the clay fraction of the material (both in [$\mathrm{kg\,kg^{-1}}$]), and ΔpH the pH difference from initial acidic soil to pH = 8 ($\Delta\mathrm{pH} = 8 - \mathrm{pH_{initial}}$).

The pH buffer strength of the OC is one order of magnitude higher than that of the clay. Even though the organic carbon content in the brown earth was just 1.4 % (Table 2.1), its contribution to buffer strength might be bigger than the one of the cumulative 9.25 % (Table 2.1) clay content if the contributions from each fraction are comparable to Equation 2.4.

The soil particles must absorb one positive charge for every released H^+ ion to maintain charge neutrality in the soil system. Thus, the decrease in TA directly corresponds to changes in the concentration of Na+ ions (see Figure 2.10). Since Na^+ ions are present in the highest concentrations within the $NaHCO_3$ solutions, they have the highest tendency to be bound by the negative charge sites. As the H^+ ions were released into the soil water, they neutralized the carbonate alkalinity (HCO_3^-), which in turn caused visible CO_2 outgassing during the mixing experiments. This underlying process can be exemplified by a reaction involving an organic carboxylic acid structure (X–COOH).

$$X\text{–}COOH + Na^+ + HCO_3^- \rightarrow X\text{–}COO^- + Na^+ + HCO_3^- + H^+ \quad \rightarrow X\text{–}COONa + CO_2 + H_2O \tag{2.5}$$

The strength of the acid is defined by the X–COO^- anion. The product X–COONa will either stay solid in the soil or might form a complex X–$COONa^0$(aq). The 0.45 µm filters might also capture this complex and suppress the contribution to the TA in the final measurement.

However, for real terrestrial EW applications involving silicate minerals, there might be no

abiotic CO_2 outgassing in this initial phase as the H^+ released by soil particles might directly attack the silicate minerals without the carbonic acid weathering step in between producing the carbonate alkalinity first.

The high TA of the 50 mmol L^{-1} $NaHCO_3$ solution resulted in the deprotonation of more acid structures in the soil. It is yet to be determined which organic functional groups or clays were involved in the chemical reaction Equation 2.5 and where all reaction products remain afterwards. The observed decrease in TA, coupled with the drop in Na^+ concentration, represents this CEC pH dependence well. The effective CEC grows with the soil pH (De Villiers and Jackson, 1967).

Formation of carbonate minerals

The soil humic substance and clay minerals can hold exchangeable Ca^{2+} cations. These cations are part of the effective CEC of the soil. When the Ca^{2+} was exchanged with the abundant Na^+ cations, the high TA, and the Ca^{2+} ion concentration in the soil water might have caused rapid precipitation of carbonate minerals. It is called a heterovalent exchange reaction because Na^+ and Ca^{2+} have different valence. Assuming that half of the added Na^+ was exchanged with Ca^{2+}, the soil water likely became supersaturated with respect to calcite for all $NaHCO_3$ treatments. In this study, the carbonate content of the soil sample was not measured after the treatment with alkaline solutions. It might have increased, and part of the TA loss was due to the precipitation reaction of carbonate minerals, as the soil exchanged part of the Na^+ ions with Ca^{2+} and Mg^{2+} ions. This process also leads to CO_2 outgassing and removal of TA in the soil water. The process is exemplified in the following reaction equation:

$$2Na^+ + 2\,HCO_3^- + X_2Ca \rightarrow 2\,XNa + Ca^{2+} + 2\,HCO_3^- \quad \rightarrow 2\,XNa + CO_2 + H_2O + CaCO_3 \tag{2.6}$$

X = clay mineral or organic molecule with a negative surface charge.

2.4.3. Source of errors in the experiments

The Dragino LSE01 sensors are not calibrated precisely enough to accurately measure soil volumetric water content θ) for all soil types. A specific calibration needs to be done for each soil type to achieve a more precise θ reading. It's important to note that the mineral soil type calibration used may not be suitable for organic-rich soil samples.

Different soils and materials have varying abilities to absorb water. Coarse sand, for example, consists mainly of macropores, while other soils contain finely textured micropores. Additionally, saturation levels and dissolution reactions may change over time, so one needs to consider the time dynamic component for similar experiments. The soil needs sufficient time to absorb the added solution.

The biggest driver of fluctuations in the chemical composition of the soil solution samples is the low water content of the soil. The extracted soil solution sample volume can vary significantly. Therefore, it is recommended to use a different method for ongoing experiments. One approach involves increasing the water content significantly (1:1, 1:2, or 1:5 soil: water ratios) to homogenize everything. A centrifuge can then be used to extract the solution with

better efficiency. The vacuum pumps in this experiment might have allowed for preferential pathways and led to different extraction sample volumes. Nevertheless, the low water content was chosen in this experiment to keep it close to the electrical conductivity observed outdoors in the field.

2.5. Conclusion

The combination of EC_b and volumetric water content θ as a proxy for soil water TA to track CO_2 sequestration by EW was successfully shown for low CEC quartz sand. However, in organic-rich and clay-rich soils, abundant CEC places and weakly acidic functional groups cause the exchange of ions between water and solids after adding ions simulating EW.

Using EC_b and θ as a predictor for any changes in soil water chemical properties requires the initial amount of soil water ions to be known to compensate for its contribution to the EC_b. Particularly, the dynamic pH buffering effects and pH-dependent cation exchange processes of the soil need to be quantitatively known to interpret the EC_b-θ measurement. An input of an alkaline solution will shift the soil to a higher pH, thereby potentially increasing the CEC, precipitating carbonates and altering the soil system (Figure 2.10).

As the here used brown earth buffered half of the added TA input, it was not possible with the equipment used to observe significant EC_b changes for added solutions with TA concentrations below 10 meq L^{-1}. A significant change in EC_b was detectable only for a higher TA concentration input of 50 meq L^{-1} at high volumetric water content. The alkaline input solution raises the pH of the soil water, leading to the deprotonation of soil acid structures that buffer the pH change and react with HCO_3^- to produce CO_2 and H_2O. This study has shown a significant pH buffering effect, even in soil with a low total organic carbon (TOC) content of 1.4 %. One would expect an even much greater neutralization of alkalinity for soils with higher organic matter content. As long as H^+ is deprotonized from the solid phase into the liquid phase, added TA will be neutralized. This behavior should be the case specifically in acidic soils. When the effective CEC increases, and the soil releases H^+ from acid sources other than carbonic acid, the full CO_2 removal potential of such soils cannot be archived. An initial amount of added TA is consumed to raise the soil pH, also known as the lime requirement (Mclean, 2015). However, once effective CEC is raised and remains at this higher level, CO_2 sequestration by weathering silicate minerals and creating carbonate alkalinity might be more effective. Long-term application studies are crucial for future MRV and CO_2 sequestration potential calculation. Given the possible combination of soils, climate, and rock powder quality and application rates and frequency, large combinations of tests will be required if the true potential of EW as a CO_2 sink should be adequately evaluated.

3

Contribution of dissolved organic carbon to total alkalinity in Enhanced Weathering experiments

Abstract

Total Alkalinity (TA) is widely used as a proxy for captured CO_2 in enhanced weathering (EW) applications. However, organic anions can also contribute to TA. To improve carbon accounting in EW, which is often simplified to that TA equals carbonate alkalinity, their contribution should be taken into account.

In this study, we tested how dissolved organic carbon (DOC) contributes to non-carbonate alkalinity (A_{NC}) using microcosm experiments with artificial organo-mineral mixtures. We used different combinations of rock powder with straw, microbes and earthworm additions, under ambient air conditions. The microcosms were flow-through columns placed in a climate chamber at 25 °C, which were irrigated with groundwater at rates between 1 200 to 3 600 mm yr^{-1}. The concentrations of several low-molecular-weight organic acids (oxalate, citrate,acetate, gluconate) were quantified to assess which conjugate base anions impact the measured TA.

Results revealed a ratio of 3.5 mol DOC per A_{NC} equivalent. In the overall experiment the median contribution of A_{NC} to TA was around 5.5 %. A positive correlation between DOC and charge-balance error suggests that some organic acid anions remained deprotonated during TA titration. Acetate anions found in DOC-rich water samples further support a substantial contribution of organic anions to TA. To investigate the relevance of A_{NC} for natural EW systems, we also quantified A_{NC} contributions in natural waters and leachates from soil EW experiment mesocosms. Because DOC levels were lower, A_{NC} contributions were smaller, ranging from a median of 4.1 % in soil mesocosm leachates down to 0.9 % in Elbe estuary water samples. This A_{NC} contribution, despite seeming small, is relevant for carbon accounting in terrestrial EW practices, where TA is often assumed to be solely carbonate alkalinity

Graphical Abstract

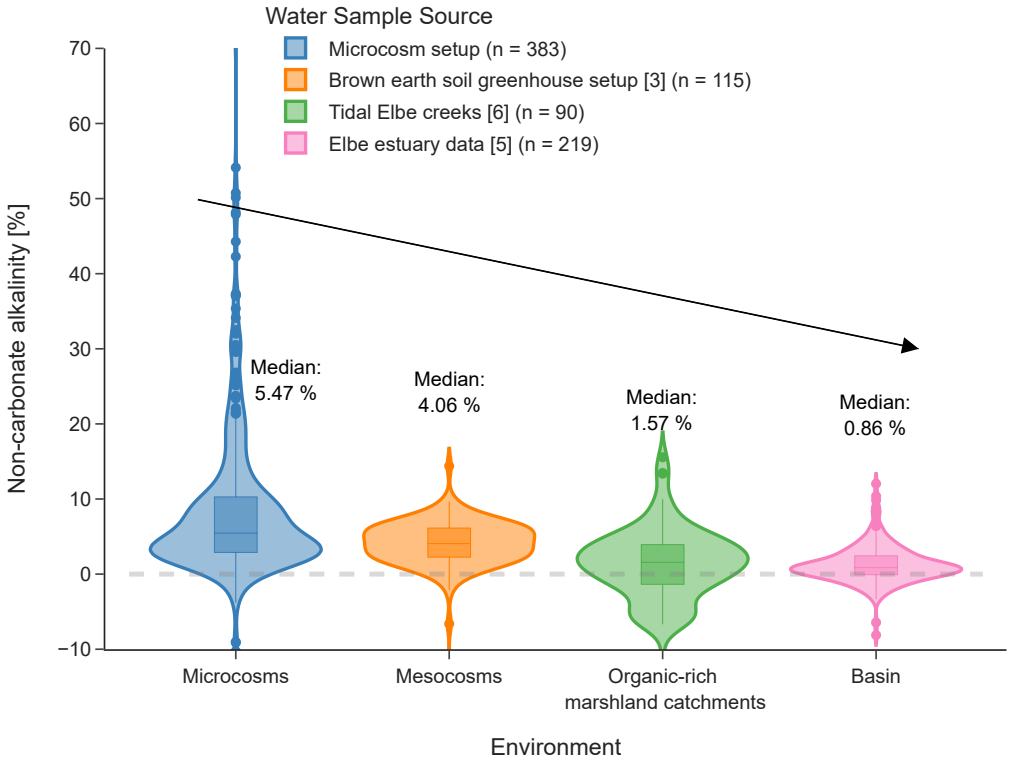


Figure 3.1: Contribution of non-carbonate alkalinity for different systems

3.1. Introduction

Climate change is one of the most urgent environmental problems of the 21st century. To limit anthropogenic global warming to 2 °C or lower by 2100, all IPCC emission scenarios require not only substantial emission reductions but also the deployment of carbon dioxide removal (CDR) approaches (IPCC, 2022b; IPCC, 2022a; Steve Smith et al., 2024). One CDR approach receiving growing scientific and practical interest is enhanced weathering (EW), a novel, nature-based CDR method.

EW aims to accelerate the dissolution of rock and increase alkalinity fluxes to the oceans (Beerling et al., 2020; Goll et al., 2021; Hartmann et al., 2013; Schuiling and Krijgsman, 2006; Seifritz, 1990). Dissolution of silicate minerals is a natural process that has regulated the global carbon cycle on geological timescales, while the weathering of carbonates provides a CO_2 sink on shorter time scales due to carbonate formation in the ocean and following CO_2 degassing (Berner, 2003; Walker, Hays, and Kasting, 1981).

Due to their global abundance and rapid weathering rates, mafic and ultramafic silicate rocks

are the main focus of EW application studies (Hartmann et al., 2013). Mafic and ultramafic rocks are mainly composed of low-silica silicate minerals, including olivine, pyroxene, and plagioclase. Mineral dissolution rates vary between minerals by several orders of magnitude for constant environmental conditions (Lasaga et al., 1994). Compared to terrestrial carbonate weathering, silicate weathering and transfer of bound CO_2 in the form of alkalinity into the ocean are assumed to represent a longer removal pattern. When dissolved carbonate species (HCO_3^-, CO_3^{2-}) reprecipitate as carbonate minerals (in the ocean or in soils) CO_2 is released (see Equation 3.2 and Equation 3.3). As an illustrative example, the weathering reactions of wollastonite ($CaSiO_3$) and calcite ($CaCO_3$) with carbonic acid are shown below (see Equation 3.1 and Equation 3.2).

$$\text{Silicate dissolution} \quad CaSiO_{3(s)} + 2\,CO_{2(g)} + 3\,H_2O \longrightarrow Ca^{2+} + 2\,HCO_3^- + H_4SiO_{4(aq)} \tag{3.1}$$

$$\text{Carbonate dissolution} \quad CaCO_{3(s)} + CO_{2(g)} + H_2O \longrightarrow Ca^{2+} + 2\,HCO_3^- \tag{3.2}$$

$$\text{Mineral carbonation} \quad Ca^{2+} + 2\,HCO_3^- \longrightarrow CaCO_{3(s)} + CO_{2(g)} + H_2O \tag{3.3}$$

After the dissolution reaction, the previously gaseous CO_2 is bound as aqueous carbonate species (HCO_3^-, CO_3^{2-}), which at a pH of around 7 to 8 are mostly HCO_3^- ions. The carbonate species act as buffers to added acid in the water. To measure this buffering capacity, also called the total/titrated alkalinity (TA), water is titrated with a strong acid to a given endpoint based on the carbonate system, typically around pH = 4.3. If, in addition to the carbonate alkalinity, other species such as organic molecules add to TA, these molecules counterbalance released cations from the dissolution reaction (Equation 3.1 and Equation 3.2), and reduce the captured CO_2 in the form of DIC.

The importance of the contribution of organic molecules to TA (organic alkalinity) was studied for natural freshwaters by (S. Liu, Butman, and Raymond, 2020; Lozovik, 2005) and in estuarine and coastal waters by (Cai, Wang, and Hodson, 1998; Hu, 2020; Kerr et al., 2021; Muller and Bleie, 2008; S. Song et al., 2020). Also, it was closely studied in the Baltic Sea (Hammer et al., 2017; Kuliński et al., 2014) and for seawater (Kim and K. Lee, 2009; Ko et al., 2016; C.-H. Lee et al., 2024; Lukawska-Matuszewska, 2016; Lukawska-Matuszewska et al., 2018; Sharp and Byrne, 2020). A comprehensive review on ocean alkalinity emphasizes the distinction between titration and charge balance alkalinity (Middelburg, Soetaert, and Hagens, 2020). To generate organic alkalinity, an organic acid needs to react with an alkaline substance so that the conjugate base of the organic acid is left in the solution. An example of mineral dissolution for wollastonite with an organic acid would be:

$$CaSiO_{3(s)} + 2\,R{-}COOH + H_2O \longrightarrow Ca^{2+} + 2\,R{-}COO^- + H_4SiO_{4(aq)}. \tag{3.4}$$

Organic acids in natural waters originate from microbial organic matter decomposition and direct exudation by living organisms such as plants, algae, and microbes. They are weak acids and donate H^+ to the water, lowering pH. Deprotonation of functional groups on organic acids typically happens in the pH range of 3–10, depending on the overall chemical composition and structure of the respective organic acid (Pittman and Lewan, 1994). Organic acids affect

mineral dissolution rates through several processes. First, they can lower the pH of the solution and thereby impact mineral dissolution (Drever, 1997). Second, the deprotonated organic acid conjugate base anions can form complexes with cations in the solution, also known as chelation (Pittman and Lewan, 1994). This chelation reaction can further enhance mineral dissolution rates in addition to the effect of pH alone (S. A. Welch, Taunton, and Banfield, 2002; Susan A Welch and Ullman, 1993). Furthermore, the conjugate base anions can also act on the mineral surfaces and form surface complexes (Adeleke, Nwangburuka, and Oboirien, 2017; Pittman and Lewan, 1994). Organic acids also have indirect effects on mineral dissolution through microorganisms, serving as a food source for them. In turn, these microorganisms release microbial metabolic byproducts that can then contribute to mineral dissolution (de los Ríos and Souza-Egipsy, 2021; Wiesenbauer et al., 2025). A specific environmentally relevant subgroup of organic acids comprises low-molecular-weight organic acids (LMWOAs). They are widespread on the earth's surface, play central roles in the Krebs cycle (M. Xiao and Wu, 2014), and occur widely in soils (Tani et al., 2001). LMWOAs are also generated during the early stages of plant litter decomposition, making them common constituents of fresh litter leachates (Küsel and Drake, 1998; Lv et al., 2023). LMWOAs typically are composed of 1–6 carbon atoms and 1–3 carboxylic functional groups (M. Xiao and Wu, 2014). Due to their high density of ionizable functional groups relative to their molecular size, they are more water-soluble than highmolecular-weight organic acids (Perminova et al., 2003), which makes them particularly relevant for studies of natural water chemistry. In order to quantify the contribution of dissolved organic carbon (DOC) to released TA, reducing the potential to transfer CO_2 into carbonate alkalinity, a flow-through microcosm experiment with an artificial organo-mineral mixture was set up. In addition, the concentrations of LMWOAs were measured, and their contribution to TA was discussed. To verify the validity in non-artificial systems, we compare our results with data from other EW soil column experiments and natural water samples from estuaries. This helps to define typical DOC-to noncarbonate alkalinity ratios and the large-scale impact of DOC on TA. Understanding the importance of DOC in this context has important implications for estimating the realized CDR potential of rock weathering and contributes to knowledge of monitoring, reporting, and verification (MRV) efforts for EW-based CDR.

3.2. Methods

3.2.1. Experimental Setup

The experimental setup was designed to investigate the impact of diverse biological, chemical, and physical factors on mineral dissolution by utilizing microcosms filled with artificial organo-mineral mixtures that included various soil biota under ambient conditions. By putting together the various ingredients of natural soils in different combinations, the goal was to enhance mineral dissolution rates and TA through the interactions of different organic and inorganic components. The setup included various silicate-rich rock types and organic matter types (subsection 3.2.2) alongside a diverse array of bacteria, fungi, and earthworms (subsection 3.2.2) to mimic the complex interactions found in natural soil environments.

The microcosms were placed in a climate chamber at a constant temperature of 25 °C. They were watered daily with natural groundwater (Table 3.1) from the top with automated

sprinklers. The added water could flow through the microcosm/column and drain at the bottom, where it was collected and stored in a fridge below the microcosms. Experiments lasted for 56 d, during which the irrigation rates were adjusted to be between 50 and 150 mL per day. These rates correspond to 1 200 to 3 600 mm yr^{-1} of precipitation, comparable to rainfall in tropical regions. After 56 d, leachate samples were taken to analyze the dissolved compounds. This experiment was a subset of a bigger experiment comprising 203 columns in the microcosm system. Overall, the experiment included 4 rounds of filling the 203 columns. The bigger experiment also used extremely alkaline steel slag, which was excluded from this analysis as it impacted the TA not with carbonates but hydroxides. Excluding those steel slag combinations, as well as those where required data were missing and thus prevented calculations, led to a subset of 383 microcosm combinations that were used for this study, allowing for a comprehensive analysis of the role of organic acids in mineral dissolution.

Table 3.1: Composition of the natural groundwater used for irrigation of the microcosms (mean ± s.d., n = 10). The values below the detection limit (bdl) have the detection limit in brackets.

Parameter	unit	Mean ± standard dev
pH	-	7.99 ± 0.10
Water Temperature	°C	14.87 ± 1.56
Electrical Conductivity (normalized to 25 °C)	µS cm^{-1}	194.30 ± 6.60
Measured total alkalinity (TA)	µeq kgw^{-1}	1 551.01 ± 65.32
Total Carbon		1 460.11 ± 0.08
Dissolved inorganic carbon (DIC)		1 409.54 ± 8.03
Dissolved organic carbon (DOC)		44.69 ± 6.57
dissolved silica		220.58 ± 9.08
Ca^{2+}		714.72 ± 14.60
K^{+}		23.59 ± 9.02
Mg^{2+}		105.42 ± 17.68
P (total P)	µmol L^{-1}	0.29 ± 0.25
Na^{+}		283.22 ± 11.60
F^{-}		6.19 ± 3.38
Cl^{-}		237.89 ± 23.65
NO_2^{-}		bdl (0.01)
SO_4^{2-}		98.09 ± 11.32
PO_4^{3-}		bdl (0.01)
Br^{-}		bdl (0.005)
Charge balance error (CBE) (see Equation 3.9)	%	−1.09 ± 0.79

This study focuses on the dissolved compounds in the leachate water of the microcosms. TA, DIC, pH, and temperature are used to calculate non-carbonate alkalinity, which is then compared to the DOC. Anions and cations were also measured to calculate the charge balance error (CBE) of the leachate water samples and compare it with DOC. Two different approaches were used to understand the contribution of organic acids to mineral dissolution. The first comparison was between the modeled carbonate alkalinity and the measured total alkalinity

(subsection 3.2.5). The second test determined whether the DOC affects the CBE of the water (Equation 3.2.5). The analyzed dataset comprised a total of $n = 383$ leachate water samples (Section 2.5.1); however, not all measurements were taken for each water sample. This resulted in smaller subsets of samples for the performed CBE analysis, with $n = 135$ (Section 2.5.2).

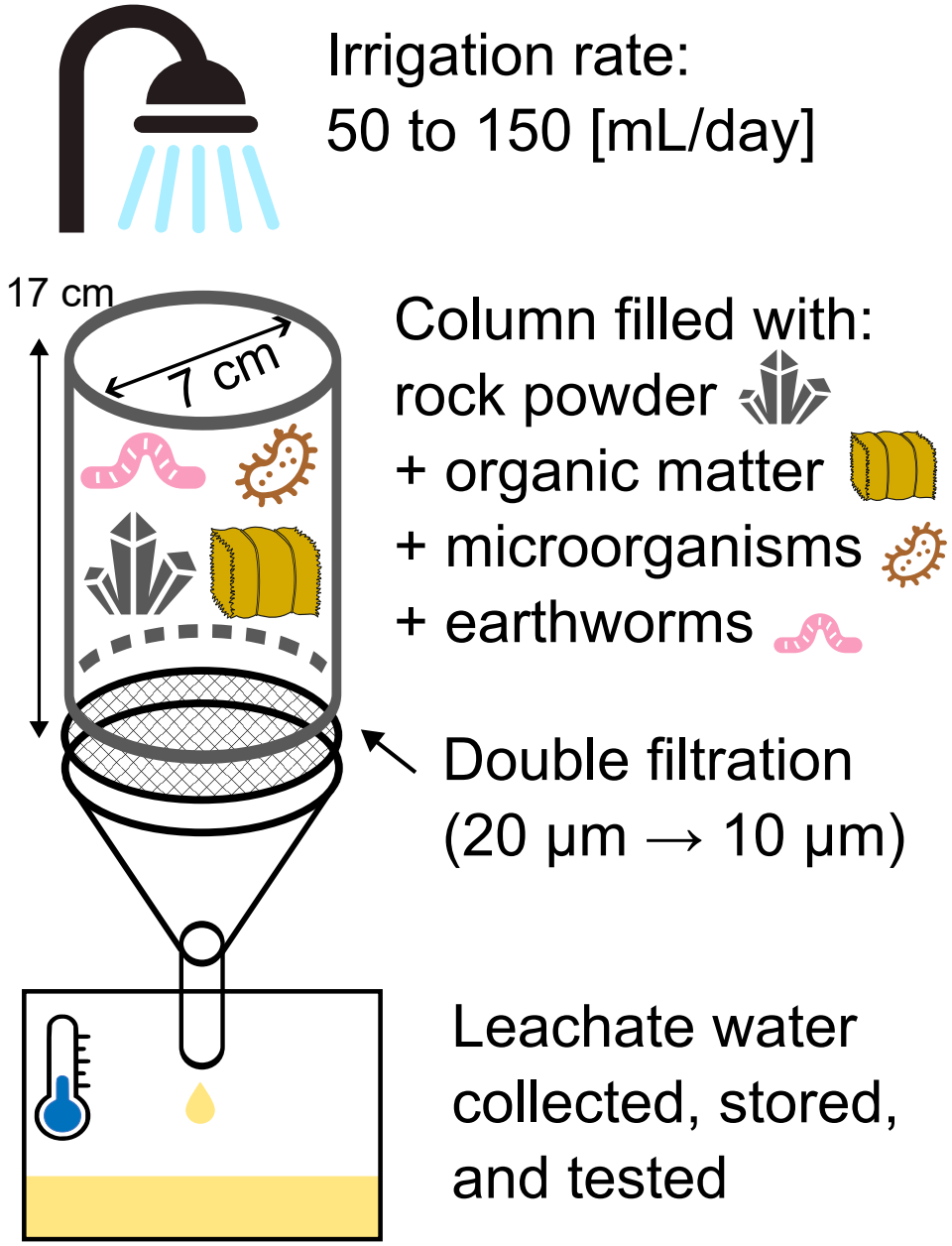


Figure 3.2: Sketch of the flow-through microcosm.

3.2.2. Materials

The microcosm system is explained in detail in (Calogiuri et al., 2023). The columns were made from PVC tubes cut into 15 cm pieces with a double filter mesh at the bottom (Figure 3.2) and are filled with organo-mineral substrates. Each column received 400 g of rock powder as the primary component of the organo-mineral mix. Additionally, 10 g of organic matter as feedstock for the biota was added to each column. The experimental design aimed to enhance the dissolution of the rock powder by adding organic matter, microorganisms, and earthworms. To this aim, four different rock types were selected: two volcanic rocks with different compositions, dunite, and diabase (compositions see Table 3.2). The two volcanic rocks, mined in the Eifel region, Germany, were obtained from RPBL Basalt & Lava aus der Eifel. The supplier refers to them as *Basaltgestein* and *Lavagestein*, respectively. *Basaltgestein* is a dense, grey variant, while *Lavagestein* is porous and reddish-brown. According to the TAS classification, they are defined as Basalt and Basanite/Tephrite (see Appendix Figure B.11 and Figure B.12). In the following text, they are referred to as Basalt (*Basaltgestein*) and Basanite/Tephrite (*Lavagestein*), respectively. The dunite (about 90 % olivine) was mined in Åheim, Norway, and supplied by Sibelco. The carbonate-rich, light grey diabase rock powder was sourced from Schicker Mineral, Germany. Its high $CaCO_3$ content is unusual, as this rock type typically contains little to no carbonate. This suggests that it has undergone natural alteration through interaction with CO_2 and water, leading to the formation of carbonates. The initial elemental composition of all rock powders was measured with X-ray fluorescence (XRF; Panalytical Magix Pro; Table 3.2). For more details on the method, see (Calogiuri et al., 2024). To serve as a blank material, quartz sand was included, obtained from Stonewish Sand, Netherlands.

In addition to the rock materials, the study included organic amendments to feed the microorganisms and earthworms inside the microcosms. A co-digestate, a novel solid fraction of pig manure with low phosphorus content, was selected for its potential as a soil improver. This biobased fertilizer, derived from a biogas power plant, was sourced from Groene Mineralen Centrale, Netherlands. Finally, wheat straw, commonly used as bedding material for pets, was obtained from Pets Place, Netherlands. The elemental composition of the wheat straw and co-digestate was analyzed with ICP-MS after digestion with nitric and hydrochloric acid and heating in a microwave, adapted from the method described by Novozamsky et al. (1996). Their total carbon (C) and nitrogen (N) levels were measured using an elemental analyzer (FlashSmart, Thermo Fisher Scientific, USA). The elemental composition is shown in Table 3.3.

To enhance the applicability and scalability of the mineral dissolution experiments, locally sourced groundwater was used to water the microcosms. The water was pumped from a borewell on the Wageningen University campus and underwent only a single filtration step without further treatment. The composition of the input irrigation water can be found in Table 3.1.

3.2.3. Microorganisms and earthworm types

The bacteria and fungi used in this study were selected for their known capacity to enhance mineral dissolution (see references below). We inoculated the organo-mineral mixture with

a selection of fungi, including Knufia petricola (Breitenbach et al., 2022; Gerrits et al., 2020; Pokharel et al., 2019), Aureobasidium pullulans (Rensink et al., 2024; Schoeman and Dickinson, 1996) and Suillus variegatus (Rosenstock et al., 2019; Szubstarska, Jarzyńska, and Falandysz, 2012), as well as bacteria such as Bacillus subtilis (H. Liu et al., 2021; W. Song et al., 2007) and Cupriavidus metallidurans (Bryce et al., 2016; Byloos et al., 2018). The cell densities varied between 1.5×10^9 and 4.8×10^{10} cells per column for bacteria and between 5.5×10^7 and 5.5×10^8 cells per column for fungi. This work does not aim to isolate the specific contributions of inoculated fungi and bacteria to mineral dissolution, but we rather examine the overall bulk production of organic acids, which result from multiple factors, including microbial activity. Earthworms were also tested in some microcosms. Two endogeic earthworm species, *Aporrectodea caliginosa* [Savigny] and *Allolobophora chlorotica* [Savigny], were used in the microcosms. These earthworm species were selected for this experiment due to their high abundance in the Netherlands, where the experiment took place, and their feeding habits, which primarily involve soil particles and associated organic matter (Bouché, 1977). Their effect on mineral dissolution rates in the context of this work is explained in (Calogiuri et al., 2024). In short, these effects are physical by increasing available reactive surface area (Suzuki, Matsubara, and Hoshino, 2003) as well as chemical by increasing decomposition and releasing CO_2 (Lubbers et al., 2013; Schwartzman, 2015), and release of organic compounds from microbes living in the earthworm gut (Georgiadis et al., 2019).

3.2.4. Measurements in the leachate water

All leachate water samples were filtered using 0.45 µm polyether sulfone dead-end syringe filters before measurements were taken. The pH was measured using a WTW Multimeter 3430 IDS equipped with a SenTix 940 probe to assess the equilibrium stage of the carbonate system, which is essential for calculating carbonate alkalinity (subsection 3.2.5). Electrical conductivity (EC) was determined with non-linear temperature compensation at a reference temperature of 25 °C, following *DIN EN 27888* (1993), using the same multimeter fitted with a TetraCon® 925 probe. Total alkalinity (TA) was analyzed using an automated Gran potentiometric titration with 4 pH endpoints at [4.5, 4.3, 4.0, 3.7], based on Koenig (2005). The titration was performed using a Metrohm 888 Titrando, equipped with a 10/20 mL cylinder volume and an Aquatrode plus pH electrode.

Elemental concentrations, including Ca, Mg, K, P, Fe, Ni, Cr, Sr, Cu, Al, Li, Mn, and Zn, were determined using either ICP-MS or ICP-OES, depending on concentration levels. ICP-MS measurements were conducted with a Thermo Scientific™ Element2™, while ICP-OES measurements were performed using a Thermo Scientific™ iCAP 6500 duo. Anions, including fluoride (F^-), chloride (Cl^-), nitrite (NO_2^-), nitrate (NO_3^-), and sulfate (SO_4^{2-}), were analyzed using ion chromatography with a Metrohm 881 Compact IC Pro system and a Metrosep A Supp 17–150/4.0 column. For selected samples organic anions were tested. Specifically, low-molecular-weight organic acid anions, including citrate, oxalate, acetate, and gluconate, were analyzed using a Metrohm 883 Basic IC Plus ion chromatography system with a Metrosep A Supp 5 (250 mm × 4.0 mm) column.

Furthermore, dissolved silica (DSi) was quantified photometrically at a wavelength of 810 nm using the molybdate-blue method, as described by Hansen and Koroleff (1999).

The analysis was conducted with a Hach Lange spectrophotometer DR3800 (Type: LPG 424.99.00001). To solve the carbonate system and check the relationship of A_{NC}, the dissolved inorganic carbon (DIC) and dissolved organic carbon (DOC) were measured using a catalytic combustion-based TOC analyzer (FormacsHT TOC analyzer, Skalar, NLD). DIC detection was achieved by acidifying the sample with 4 % H_3PO_4.

Table 3.2: Elemental composition of the rock types was measured using X-ray fluorescence (XRF) measurements. (nd = below detection limit, LOI = loss of ignition, i.e., heating the sample to 1 000 °C to gas out all carbon).

Elements	Dunite mass percent (%)	Basalt mass percent (%)	Basanite/Tephrite mass percent (%)	Diabase mass percent (%)
SiO_2	41.55 ± 0.23	43.87 ± 0.55	43.44 ± 0.27	35.93 ± 0.73
TiO_2	0.02 ± 0.01	2.15 ± 0.06	2.58 ± 0.33	2.77 ± 0.09
Al_2O_3	0.78 ± 0.01	12.13 ± 0.18	13.79 ± 0.25	11.83 ± 0.13
Fe_2O_3	7.26	11.66 ± 0.18	11.19 ± 0.26	13.31 ± 0.13
MnO	0.09	0.17	0.17 ± 0.01	0.14 ± 0.01
MgO	47.87 ± 0.24	11.40 ± 0.31	8.68 ± 0.12	4.86 ± 0.12
CaO	0.35 ± 0.19	10.41 ± 0.02	12.60 ± 0.10	14.29 ± 0.20
Na_2O	0.03	2.26 ± 0.01	2.99 ± 0.08	1.81 ± 0.03
K_2O	0.03 ± 0.01	1.01 ± 0.06	3.29 ± 0.09	1.61 ± 0.11
P_2O_5	0.01	0.62	0.53 ± 0.07	0.41 ± 0.01
SO_3	nd ± nd	0.01 ± 1.00	0.03 ± 0.01	0.29 ± 0.18
LOI	1.80 ± 0.13	4.2 ± 2.0	0.62 ± 0.08	13.06 ± 1.10
Sum	99.78 ± 0.12	99.91 ± 0.07	99.91 ± 0.44	100.31 ± 0.23

Table 3.3: Elemental composition of the organic matter used in the microcosms, presented as mean ± s.d. (n = 4).

Parameter	unit	Wheat straw	Co-digestate
C:N ratio	[g:g]	85.98 ± 16.27	50.48 ± 3.15
C	$mg\,g^{-1}$	443.64 ± 9.83	442.24 ± 6.90
N		5.16 ± 0.97	8.76 ± 0.53
K		8.00 ± 0.08	2.75 ± 0.06
Na		0.019 ± 0.002	0.914 ± 0.012
Ca		2.92 ± 0.07	12.38 ± 0.91
Mg		0.46 ± 0.01	1.31 ± 0.01
P		0.47 ± 0.01	4.72 ± 0.38
Zn		0.004 ± 0.001	0.140 ± 0.006
Fe		0.112 ± 0.016	1.176 ± 0.092
Mn		0.051 ± 0.001	0.120 ± 0.005

3.2.5. Calculations

Modelling of the non-carbonate alkalinity contribution
To model the non-carbonate alkalinity (A_{NC}), first, the carbonate alkalinity (A_C) was calculated and then subtracted from the measured TA ($TA_{measured}$) similar to previous studies (Hammer et al., 2017; Ko et al., 2016; S. Song et al., 2020; Yang, Byrne, and Lindemuth, 2015). To calculate A_C (Equation 3.5), we applied a simplified model using only the dissolved inorganic carbon (DIC), pH, and temperature (T) observed in the leachate water right after sampling. Based on this set of variables, A_C was calculated using phreeqpython (Heinsbroek, 2021), assuming a closed system (DIC = const) (see Appendix Figure B.1). One might correctly assume that this set of variables is insufficient and too simple to model A_C. Considering that all cations and anions impact the ionic strength (I) of the water sample, these should be included as well to accurately calculate A_C. With the lack of including all ions in the A_C model, the I will be underestimated (Solomon, 2001). When the ionic strength of the aqueous solution is underestimated, the stoichiometric first and second dissociation constants of carbonic acid are overestimated (Harned and Davis Jr, 1943; Hastings and Sendroy Jr, 1925; Wolf-Gladrow et al., 2007). This overestimation will lead to a lower modeled A_C than the A_C modeled from the full set of ions. To check whether this simplified model is sufficient, both models are compared. For 211 water samples, it was checked how the full A_C model (cations, anions, T, pH, DIC) compares to the simple A_C model (T, pH, DIC). They do match to a sufficient extent for our analysis (see Appendix Figure B.2). This allowed us to use all 383 samples for the calculation of A_C. In the following text the squared brackets imply the concentration of the compound is meant, i.e. $c(CO_3^{2-}) = [CO_3^{2-}]$ [mol kgw^{-1}]:

$$A_C = [HCO_3^-] + 2 \cdot [CO_3^{2-}]. \tag{3.5}$$

The modeled A_C was then subtracted from the $TA_{measured}$. The difference between the two terms is A_{NC}. Any conjugate base of a (weak) acid that can accept protons until the endpoint of the modified Gran titration (see Appendix section B.1) will contribute to the measured total alkalinity. Assuming that other inorganic compounds able to buffer will be minor contributors, $TA_{measured}$ can be described in the following way:

$$TA_{\text{measured}} = A_C + A_{\text{org}} + \text{minor} \tag{3.6}$$

$$A_{NC} = TA_{\text{measured}} - A_C = A_{\text{org}} + \text{minor} \approx A_{\text{org}}. \tag{3.7}$$

In addition, we also calculate the fraction of non-carbonate alkalinity as ($A_{NC}/TA_{measured}$). This is highly relevant in the context of CDR, where the non-carbonate fraction should ideally be as small as possible. Because $TA_{measured}$ is often used as a direct measure for the captured CO_2 in inorganic form, large concentrations of A_{NC} will complicate the overall assessment of CO_2 capture and shift the focus to the generation and decomposition pathways of the involved organic molecules.

Calculating the charge balance of the water
The charge balance error (CBE) is a quality check in aquatic geochemistry that assesses the consistency of measured cation and anion concentrations in a water sample. It is calculated as the relative difference between the total equivalent concentrations of cations and anions

and is used to identify potential analytical errors, missing ions, or inconsistencies in water chemistry data. Part of the involved anions are conjugate bases of organic acids, which have a wide range of pK values (Schwarzenbach, Imboden, and Gschwend, 2003) and thereby impact CBE. In aquatic geochemistry anions are divided into two fractions: the conservative anions and the alkalinity contributors (Stumm and Morgan, 1996). The conservative anions are conjugate base anions from strong acids. The other anions are the conjugate base anions of weak acids to a given reference level, which is defined by the titration endpoints. The presence of a conjugate base of an organic acid with a low pK, i.e., lower than or inside the titration endpoint pH window of 4.5 to 3.7 , leads to un-neutralized organic anions that are left in the water after the alkalinity titration. Thus, these conjugate base anions are missing in the TAmeasured. When these are not quantified in another way and included in the calculation (Equation 3.8), it will lead to an excess of cations over anions and thus a positive CBE. For this study, this missing alkalinity is called Alow-pH.

In the case of accurate measurements, the CBE values should form a distribution with a median value of CBE = 0 % and a variance as small as possible. Any systematic positive trends show that a negative charge is missing in the determination.

$$TA_{\text{measured}} = \sum \text{cations} - \sum \text{anions} \tag{3.8}$$

In this study:

Cations:
Na^+, K^+, Mg^{2+}, Ca^{2+}

Anions:
Anions that do not buffer pH in the range of alkalinity titration (conservative anions):
Cl^-, F^-, NO_2^-, NO_3^-, SO_4^{2-}

Based on Equation 3.8 the charge balance error (CBE) for water samples can be defined as:

$$\text{CBE}\,[\%] = \frac{\sum \text{cations} - (\sum \text{anions} + TA_{\text{measured}})}{\sum \text{cations} + (\sum \text{anions} + TA_{\text{measured}})} \cdot 100. \tag{3.9}$$

For seawater with high ionic strength and low DOC content, this definition (Equation 3.9) usually fits well with the commonly accepted charge balance error (CBE) of below 5 % (DIN 38402-62, 2014; Fritz, 1994). However, in low ionic strength, high DOC freshwaters, such as the tested leachate water, CBEs are usually larger than 5 %. One must therefore know the organic anion concentrations and other alkalinity contributions and include them in the definition to lower the calculated CBE. For the tested leachate water samples the hypothesis is that the organic anions can describe the missing part, therefore this simple equation will be expanded by adding the unprotonated part ($A_{\text{low-pH}}$) that does not buffer to the given pH endpoints of the alkalinity titration:

$$TA_{\text{measured}} + A_{\text{low-pH}} = \sum \text{cations} - \sum \text{anions}. \tag{3.10}$$

Moving TA_{measured} to the right-hand side we get the following definition:

$$A_{\text{low-pH}} = \sum \text{cations} - \left(\sum \text{anions} + TA_{\text{measured}}\right). \tag{3.11}$$

The CBE [%] (Equation 3.9) will be calculated and plotted against the DOC concentration for the analyzed water samples. When organic compounds are driving the charge balance error, the DOC must correlate with a positive charge balance error. Therefore, a linear regression is performed with x = CBE and y = DOC.

Determination of LMWOAs
Based on the large values for A_{NC} and CBE of the previous calculations, it was decided to also monitor the concentrations of certain LMWOAs. A water sample with large A_{NC} must contain more organic alkalinity and thus detectable organic acid conjugate base anions.

To determine which organic acid anions are present in the water samples, a subset of the samples $A_{NC} \geq 3\,\mathrm{meq\,kgw^{-1}}$) was analyzed for acetate, oxalate, gluconate, and citrate. These samples with high A_{NC} are potentially have higher concentrations of the conjugate bases of LMWOAs compared to the samples with low A_{NC}. Table 3.4 shows the dissociation constants of selected acids, including the LMWOAs tested in the setup.

In case of abundant LMWOAs, their speciation was modeled with phreeqpython (Heinsbroek, 2021) using the *minteq.v4.dat* database for the organic acid constants that were derived from (US EPA, 2013).

Table 3.4: Acid constants of selected organic and inorganic acids. All shown acid constants are for $T = 25\,^{\circ}\mathrm{C}$ and $I = 0$ taken from NIST46 (2013).

Compound (trivial name)	**Preferred IUPAC name**	**Formula**	**pK_{a1}**	**pK_{a2}**	**pK_{a3}**	**Ratio [$\frac{\text{Catoms}}{\text{charge}}$]**
Acetic acid	Acetic acid	$C_2H_4O_2$	4.757			2
Lactic acid	2-Hydroxypropanoic acid	$C_3H_6O_3$	3.860			3
Malic acid	2-Hydroxybutanedioic acid	$C_4H_6O_5$	3.459	5.097		4, 2
Oxalic acid	Oxalic acid	$C_2H_2O_4$	1.250	4.266		2, 1
Citric acid	2-Hydroxypropane-1,2,3-tricarboxylic acid	$C_6H_8O_6$	3.128	4.761	6.396	6, 3, 2
Carbonic acid	Carbonic acid	H_2CO_3	6.325	10.329		1, 0.5
Gluconic acid	D-gluco-Pentahydroxy-hexanoic acid (D-Gluconic acid)	$C_6H_{12}O_7$	3.46			6

3.3. Results and discussion

3.3.1. Non-carbonate alkalinity (A_{NC})determination

First the A_C is plotted against the $TA_{measured}$ to give a first impression of non-carbonate alkalinity (Figure 3.3). In the diagram we can divide the datapoints by the 1:1 line into two areas. One

is the area above the 1:1 line where the calculations imply that A_C is bigger than $TA_{measured}$. This is conceptually impossible, given that A_C is a part of $TA_{measured}$. One can see very few datapoints above this line, which is also a good indication of the data quality. An A_C larger than $TA_{measured}$ usually indicates that DIC or pH has been overestimated (Dickson et al., 2007).

More interesting is the area below the 1:1 line where the $TA_{measured}$ exceeds A_C. This results in the calculated A_{NC} to be positive. The uncertainty in A_{NC} was propagated from the standard deviation of $TA_{measured}$ input water replicates and the error in A_C for each sample using standard error propagation rules. The resulting mean propagated uncertainty across all samples was 0.066 meq kgw^{-1}. Out of the 383 samples 350 had an A_{NC} bigger than the error in the A_{NC} determination. The A_{NC} varied from −0.357 to 8.466 meq kgw^{-1}.

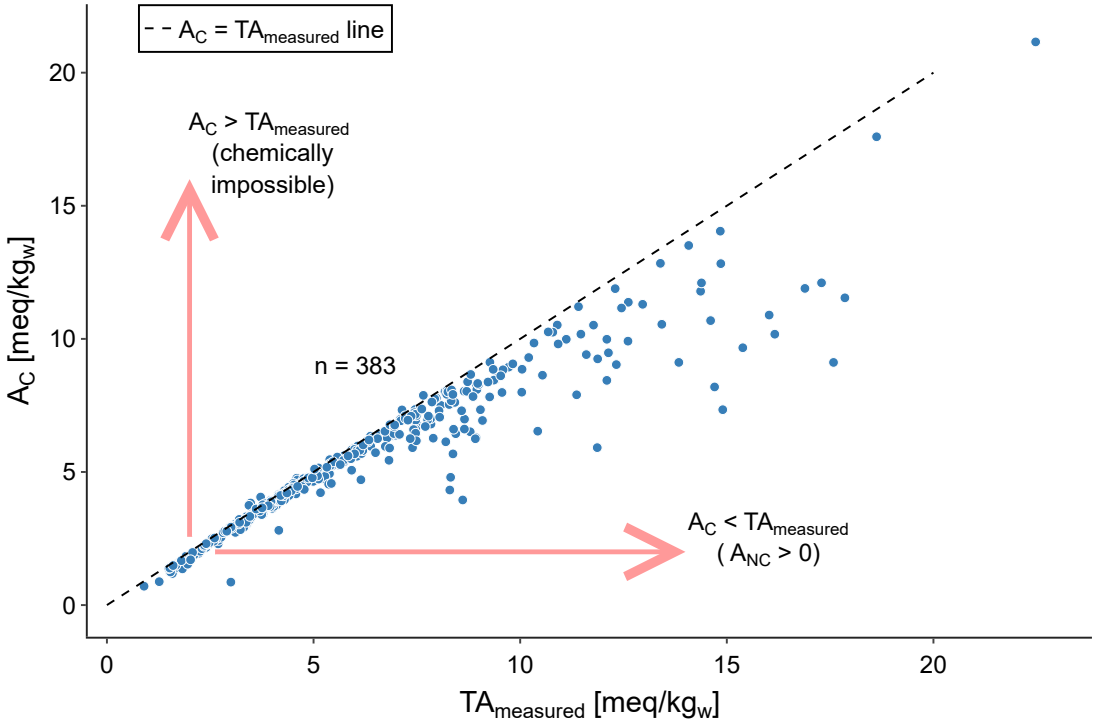


Figure 3.3: Calculated carbonate alkalinity (A_C) vs. measured total alkalinity ($TA_{measured}$).

In the next diagram (Figure 3.4), the calculated A_{NC} is plotted against $TA_{measured}$. Most of the data points are spread close to the $A_{NC} = 0$ line. This implies that the produced alkalinity must be close to the carbonate alkalinity ($TA_{measured} \approx A_C$). From Figure 3.4 it is also possible to observe, that A_{NC} also grows with $TA_{measured}$ for DOC-rich samples. As the alkalinity in the microcosm environment was increased also the release of DOC was increased due to the higher pH. This trend in DOC concentrations is also visible in the plot. Low DOC samples also show low A_{NC}.

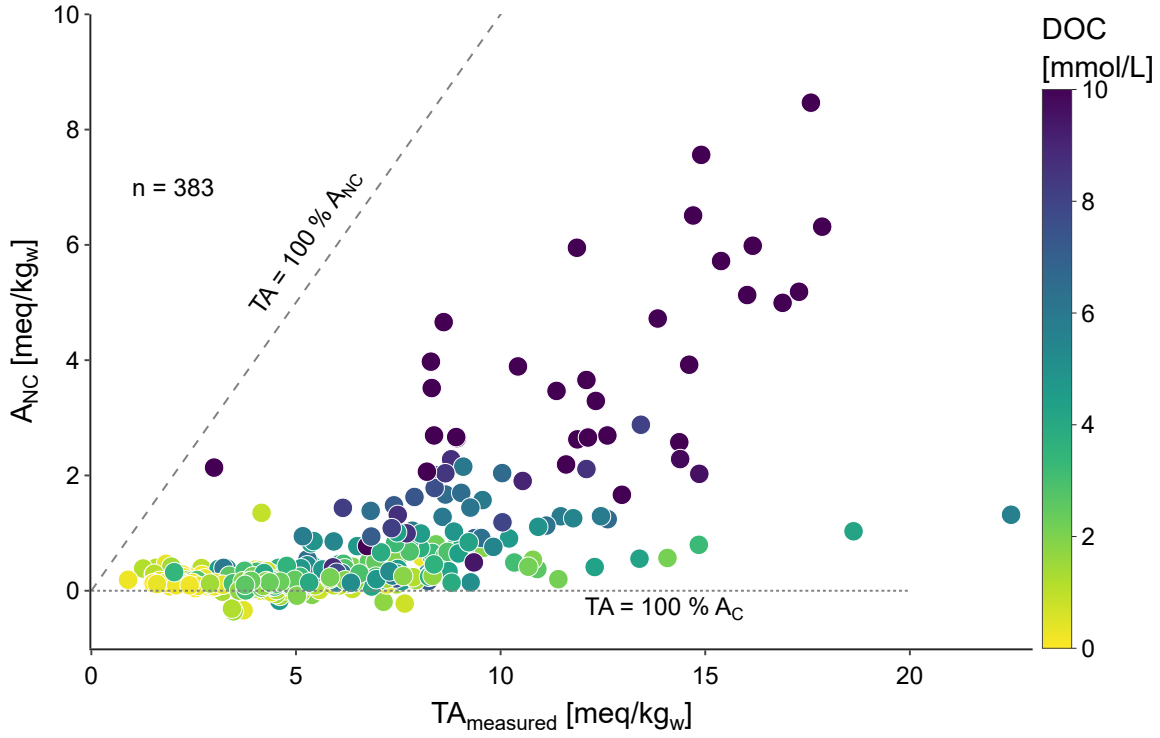


Figure 3.4: Non-carbonate alkalinity (A_{NC}) versus measured alkalinity, with dissolved organic carbon (DOC) concentration represented by color. The dashed and dotted lines show the cases of pure (A_{NC})and pure (A_C), respectively.

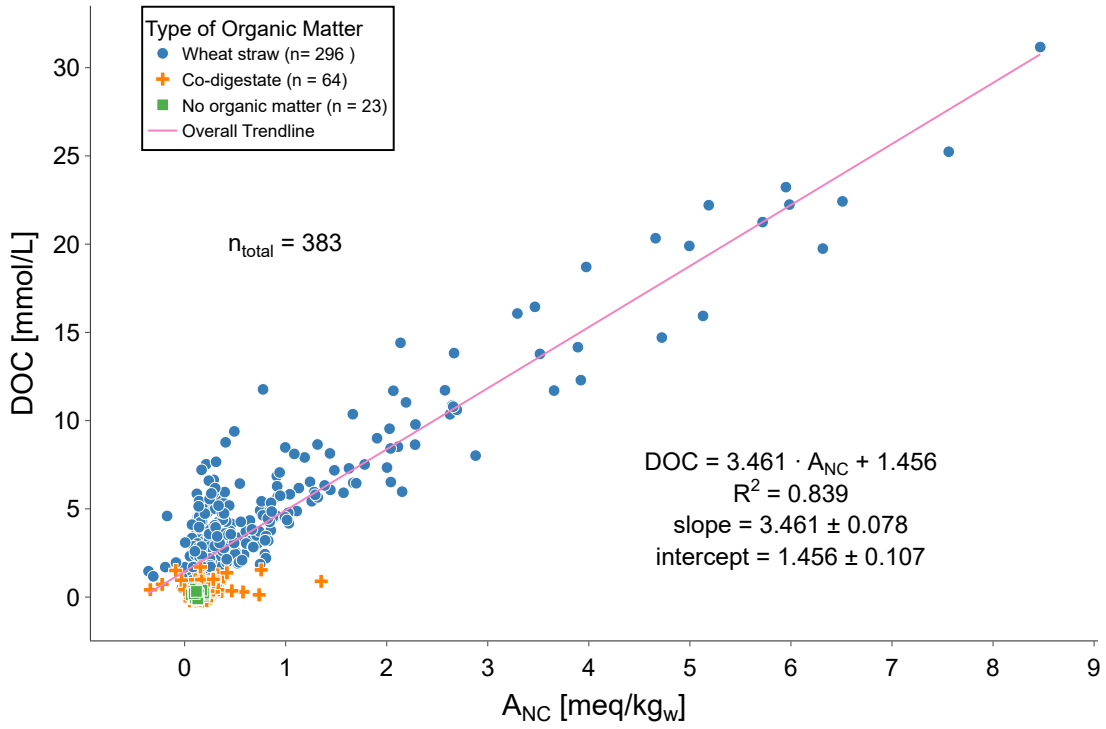


Figure 3.5: Relationship between dissolved organic carbon (DOC) concentration and non-carbonate alkalinity (A_{NC}) for all selected samples (n = 383).Different organic matter sources used in the microcosms are distinguished by color. The plot includes an ordinary least squares (OLS) regression, with A_{NC} meq kgw^{-1} on the x-axis and DOC mmol L^{-1} on the y-axis. Standard errors are indicated by the ± symbol in the regression equation.

To better understand the relationship between DOC and A_{NC}, we display the DOC concentration against A_{NC} (Figure 3.5). All points as a bulk show the pattern of an increasing DOC with A_{NC}, but some small variations are visible. We observe an accumulation of datapoints with low DOC concentrations and low A_{NC} in the bottom-left corner.

From the relationship between DOC and A_{NC}, we can learn something about the nature of the organic molecules that make up the DOC. The trendline in Figure 3.5 illustrates the relationship between the number of organic carbon atoms and alkalinity equivalents. Because of the theoretical proportional relationship of conjugate base anions and $TA_{measured}$ a linear relationship was used to describe the pattern and the data seem to fit this relationship.

From the ratio of DOC to A_{NC}, one can infer the characteristics of the organic molecules that have contributed to the observed alkalinity. The relationship shows how much DOC is needed to impact the alkalinity. In theory, a huge intercept and huge slope would tell us that there is a lot of uncharged DOC present with only a few deprotonation sites per organic carbon atom. A small intercept and slope would tell us there is a big charge density and more deprotonation sites per carbon atom. Two factors might drive this intercept and slope. First, the measurement uncertainty in DOC and A_{NC} will lead to variation in the regression

parameters. Second, the quality of DOC, as the involved organic molecules have a varying amount of carbon atoms and functional groups that act as deprotonation sites (Boyer, Singer, and Aiken, 2008; Mostofa et al., 2013; Vogt et al., 2024).

For the analyzed water samples, the ratio of DOC to A_{NC} is roughly 3.5, indicating that 3.5 mol of organic carbon correspond to 1 equivalent of alkalinity. This factor gives an insight into the nature of the dissolved organic molecules. LMWOAs would fulfill this criterion. Their molecules generally comprise 1–6 carbon atoms and have 1–3 carboxylic groups (M. Xiao and Wu, 2014), which can either donate or accept protons (see Table 3.4). In an alkaline solution (pH > 7) as observed in all microcosms leachate waters, the organic acids primarily consist of their deprotonated conjugate bases. Like the carbonate species, those conjugate bases will buffer acid input, contributing to the titrated alkalinity.

3.3.2. Charge balance error (CBE) analysis

Additionally, in the CBE-DOC diagram (Figure 3.6), the impact of organic alkalinity is demonstrated. A positive CBE either indicates that the measurements of major cations and anions are inaccurate or reveals inconsistency with the TA determination. For our dataset, the latter is the case for the DOC-rich samples.

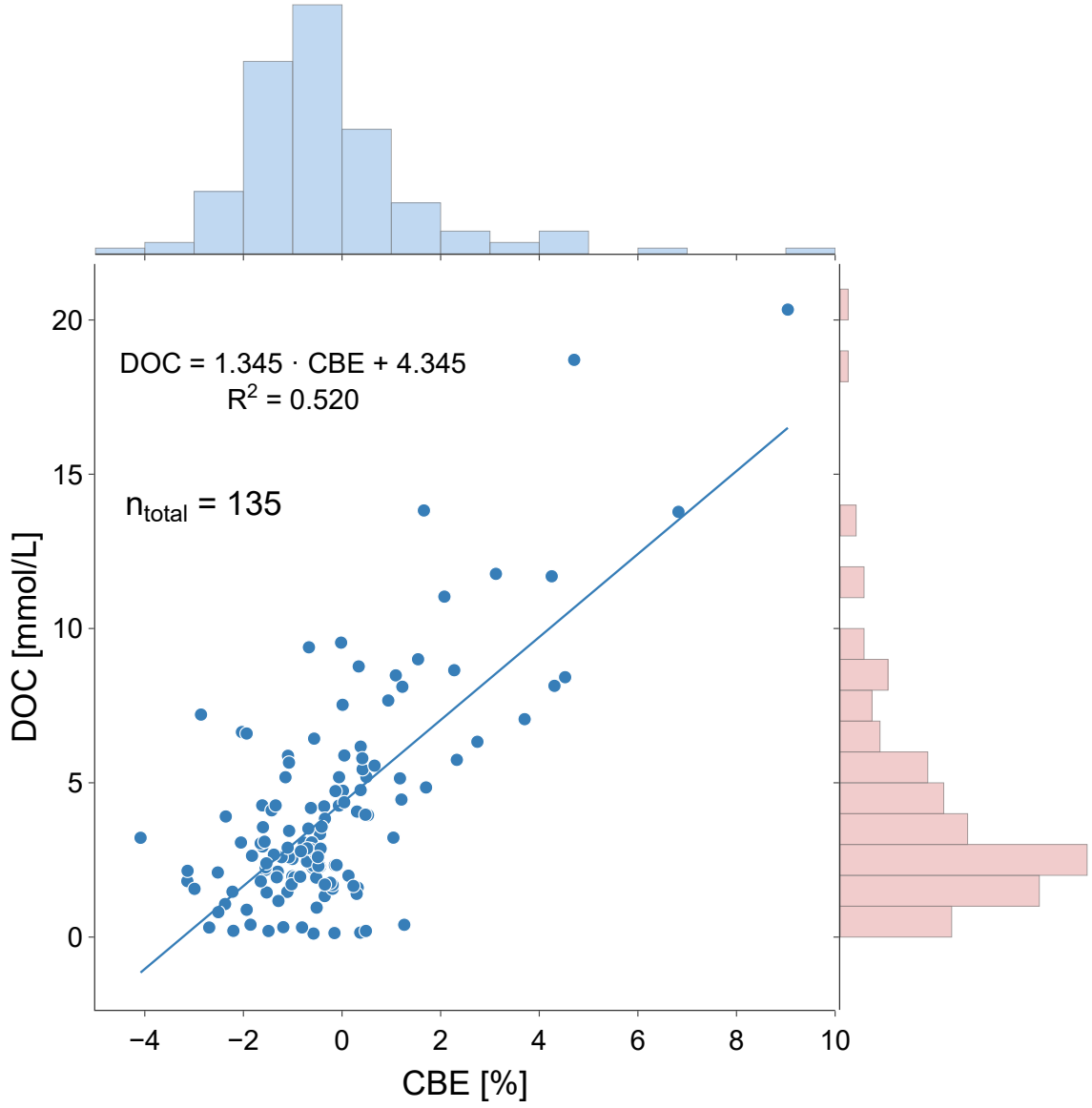


Figure 3.6: DOC against the charge balance error (CBE). The CBE was calculated following Equation 3.9 using $TA_{measured}$, ICP cation data and IC inorganic anions.

Most CBE values for leachate samples with a DOC below 5 mmol L^{-1} range from −4 to 4 % (Figure 3.6). There is no clear positive trend in CBE for such low DOC samples. For leachate water samples with DOC < 5 mmol L^{-1}, the overall mean CBE is −1.53 ± 4.32 %. That is why the overall distribution yields a comparably weak coefficient of determination of 0.52 (52.05 %). More leachate water samples with higher DOC concentrations would strengthen the relationship.

When examining the samples with higher DOC concentrations, the systematic relationship between the incomplete CBE and DOC becomes more visible. For samples with DOC concentrations of at least 5 mmol L^{-1}, the overall mean CBE is 1.84 ± 5.65 %. For samples

with DOC concentrations of at least 10 mmol L^{-1}, the overall mean CBE is 4.37 ± 5.28 %. The standard deviation remains large due to the heterogeneous nature of the leachate water samples included.

The CBE-DOC plot demonstrates how the CBE (positively) grows with the DOC. This positive trend indicates that the unprotonated organic anions remaining in the solution represent a portion of the actual alkalinity that is not accounted for. Capturing also these missing anions can be done by selecting lower endpoints for the alkalinity titration. As A_C remains constant a lower titration endpoint will potentially increase $TA_{measured}$ and thereby A_{NC}. Then the aforementioned factor of DOC to A_{NC} of 3.5 will slightly decrease. How the titration procedure could be improved is described in Section subsection 3.3.4.

3.3.3. Analysis of LMWOAs

To see which organic acids anions drive the A_{NC} and CBE, we selected water samples with $A_{NC} \geq 3$ meq kgw^{-1}. Due to the high A_{NC} and high DOC, these samples have the greatest potential for detecting LMWOAs. From the tested species, only acetate was found; citrate, gluconate, and oxalate were not detected in the leachate water (Figure 3.7). The lack of citrate and oxalate can be explained because they are polydentate ligands, also known as chelates, while acetate is a monodentate ligand in solution (Miessler, Fischer, and Tarr, 2014). Oxalate and citrate anions can form stable chelate rings together with metal cations. These can precipitate and leave the aqueous phase and form solids. Some examples are calcium oxalate monohydrate with a solubility of 0.006 1 g kg^{-1} (20 °C) (David R. Lide, 2005) also known as kidney stones, iron(II) oxalate dihydrate with solubility of 0.78 g kg^{-1} (25 °C) (David R. Lide, 2005) known as humboldtine mineral (Müller, Bourcet, and Hanfland, 2021) and tricalcium dicitrate tetrahydrate with solubility of 3.081 g L^{-1} (25 °C) (Vavrusova and Skibsted, 2016) also known as the earlandite mineral (Herdtweck et al., 2011). Thus, the oxalate and citrate anions might have formed complexes with metal cations and precipitated at some point in the setup or were removed by the 0.45 µm filters before analyzing the leachate water. Gluconate, in contrast, is known to form stable complexes with high solubility (Kutus et al., 2020), so it might have simply not been generated inside the microcosms. In contrast, acetate's monodentate binding and monovalent charge result in weaker complexes that remain soluble under most conditions and are less prone to form precipitates (Van Der Sluys, 2001). However, only the acetate concentration is not enough to explain the whole A_{NC}. Also, decomposition into other organic anions or complete remineralization into CO_2 and A_C (Hu, 2020) might have occurred in the time between the measurement of main variables and the organic anion measurements. Moreover a wide variety of untested low molecular weight organic acids, each present in low concentrations, and with properties similar to acetate, such as formate and lactate (Lazo, Dyer, and Alorro, 2017; Neaman, 2005), could collectively account for the observed bulk signal in A_{NC}.

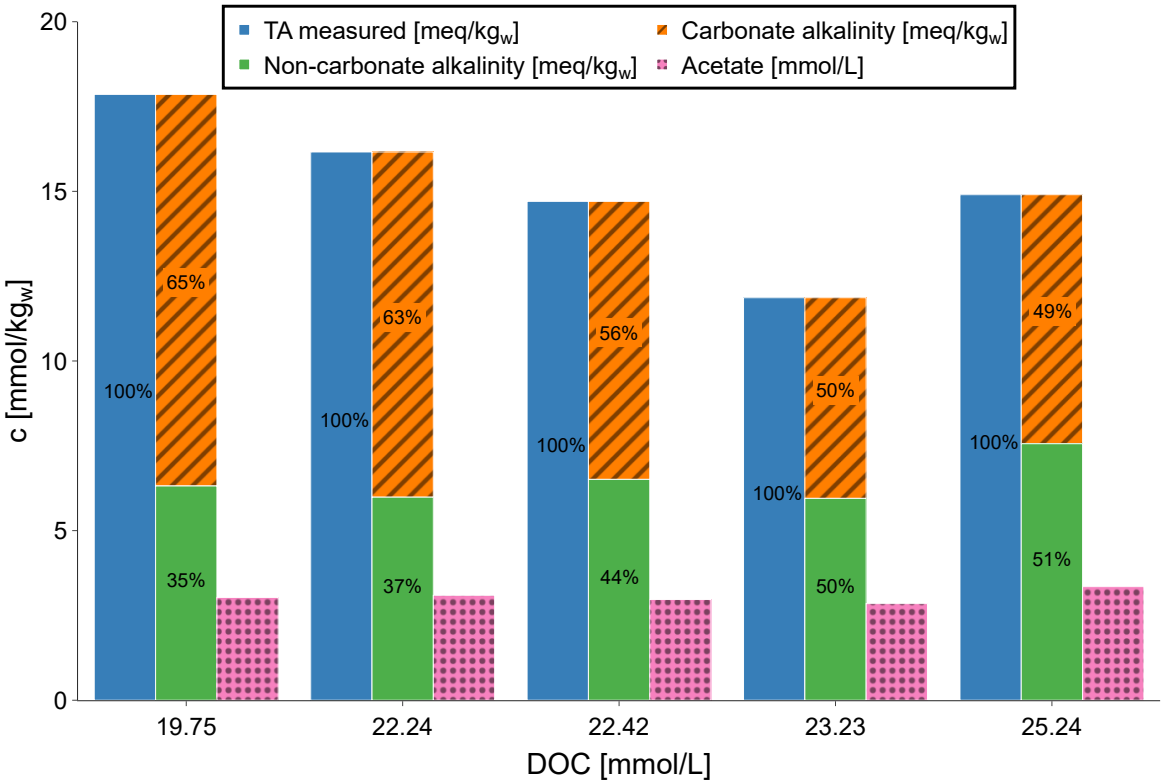


Figure 3.7: Organic anions tested in the leachate water in selected DOC-rich leachate samples with $A_{NC} \geq 3\,\text{meq}\,\text{kgw}^{-1}$. Oxalate, citrate, and gluconate were not detected in the tested leachate water.

For the tested DOC-rich samples,A_{NC} contributes between 30 % and 50 % of the $TA_{measured}$ (Figure 3.7). Acetate was abundant in the water samples tested. Its theoretical contribution to the acid buffering capacity of water is such that 1 mol L^{-1} of acetate corresponds to 1 equivalent of alkalinity. However, when testing the $TA_{measured}$, one selects certain endpoints to calculate the TA from. For this study, an automated gran potentiometric titration with the endpoints [4.5, 4.3, 4.0, 3.7] was used to measure TA based on (Koenig, 2005). For that pH range, the acetate anions ($pK = 4.757$ see Table 3.4) will not be entirely protonated, which will lead to an underestimation of the TA (see grey lines in Figure 3.8). That is why acetate in Figure 3.7 is presented solely as concentration without percentage.

3.3.4. Improved titration for organic alkalinity

To capture the full contribution of acetate and other organic acids, it is necessary to select lower pH endpoints. For the DOC-rich samples, the actual TA will thus be larger. The actual A_{NC} will also be larger because the carbonate alkalinity (A_C) will not change as it was modeled from DIC.

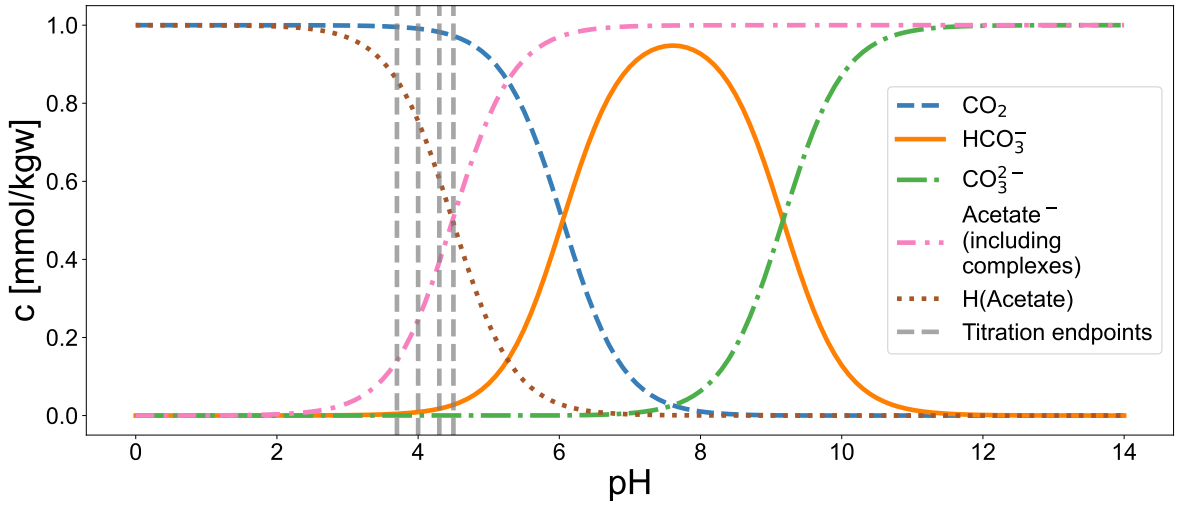


Figure 3.8: Acetate (1 mmol NaAcetate) and carbonate (1 mmol $NaHCO_3$) system speciation at T = 25 °C. Modeled with phreeqpython (Heinsbroek, 2021) using the 'minteq.v4.dat' database (US EPA, 2013) (closed system DIC = 0.001 mol kgw^{-1}). NaOH is added to the solution to raise the pH, and HCl is added to lower it. The vertical lines indicate the endpoints used for the alkalinity titration [4.5; 4.3, 4.0; 3.7] after (Koenig, 2005).

A part of the organic acid conjugate base anions, for example acetate, is not measured due to the selected titration endpoints (Figure 3.8). This not captured part is then missing in the $TA_{measured}$ and leads to an imbalance towards the positive CBE, because there is more total positive charge than negative charge put into the calculation (see Equation 3.11). To close this gap, one needs to know what organic anions are expected in the leachate water sample to select the pH endpoints of the alkalinity titration to it. For any weak acids, the titration endpoint should be selected following the Henderson-Hasselbach equation (Po and Senozan, 2001):

$$\mathrm{pH} = \mathrm{p}K_{\mathrm{a1}} + \log_{10}\left(\frac{[\mathrm{A}^-]}{[\mathrm{HA}]}\right). \tag{3.12}$$

In the buffering range of the weak acid, it can be described with the degree of titration τ:

$$\mathrm{pH} = \mathrm{p}K_{\mathrm{a1}} + \log_{10}\left(\frac{\tau}{1-\tau}\right). \tag{3.13}$$

Targeting that 99 % of the weak acid should be in HA form and just 1 % of unprotonated A^- left it will lead to $\tau = 0.01$ and thus $\log_{10}(\frac{0.01}{1-0.01}) \approx -2$. Putting it into the equation, we get the appropriate pH endpoint that should be selected: $\mathrm{pH} = \mathrm{p}K_{a1} - 2$.

However, lowering the endpoint of the titration will also protonate more of the inorganic proton acceptors that need to be accounted for. In the tested water samples from the microcosms, those other inorganic species were considered negligible. In seawater, for example, this cannot be neglected for a precise assessment. The contribution of other inorganic proton acceptors is explained by Wolf-Gladrow et al. (2007).

In general, for all water sample types, to isolate the organic alkalinity, the best practice is to perform a regular titration to remove all A_C, then bubble N_2 gas the sample to strip

away all CO_2 while performing the back titration with NaOH and incorporating it into the calculation as presented in multiple studies (Cai, Wang, and Hodson, 1998; Hunt, Salisbury, and Vandemark, 2011; Kerr et al., 2021; Ko et al., 2016; Yang, Byrne, and Lindemuth, 2015).

3.3.5. DOC source and dilution effect

Having discussed how the generated DOC affects the water chemistry, we can now examine the source of the DOC. For most microcosms (n = 296), wheat straw was used (see Figure 3.5). Wheat straw is generally composed of 34 to 40 % cellulose, 20 to 25 % hemicellulose, and 20 % lignin (Rodriguez-Gomez et al., 2012). Those complex carbohydrates are broken down into soluble compounds and increase the DOC concentration in the leachate water. The microorganisms attached to the wheat straw begin to break it down once the straw becomes moist. The co-digestate substrate does not leach much DOC as it is already processed material from a biogas power plant, and the most labile parts of the OM have already been lost during the processing (Karki et al., 2021).

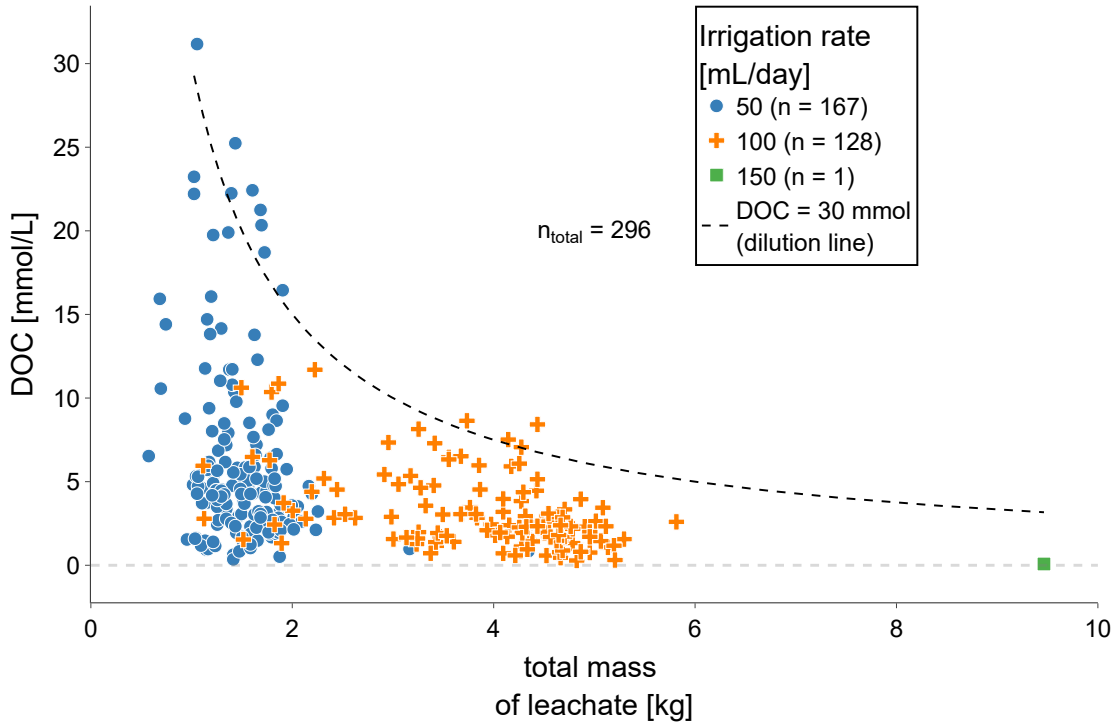


Figure 3.9: Relationship between dissolved organic carbon (DOC) concentration and the total mass of leachate for microcosms containing straw. The colors represent different irrigation rates used in the microcosms. The dashed line represents a theoretical dilution line for a constant dissolved organic carbon (DOC) concentration of 30 mmol L^{-1}.

However, the presence of wheat straw alone cannot account for the huge variation in DOC concentrations, which ranges from nearly 0 to 31 mmol L^{-1} (Figure 3.9). This pattern was due to multiple reasons, which are elaborated below.

The main driver for the diverse DOC concentrations was the different irrigation rates that varied from 50 to 150 mL d^{-1}. The wheat straw mass was always set to 10 g in the microcosms. Thus, the more water is flushed through the microcosms, the higher the dilution of produced DOC in the leachate water containers. Only wheat straw mixed with rock powder microcosms were selected for Figure 3.9 to eliminate the variability caused by different organic matter sources. The dilution effect for the water samples is displayed in Figure 3.9, indicated by the dashed line. The path follows a constant DOC amount of 30 mmol, which was chosen arbitrarily to illustrate the pattern. For more diagrams illustrating the impact of irrigation rates on the dilution of DOC, see Appendix Figure B.4 and Figure B.5.

When examining microcosms containing wheat straw and a constant irrigation rate category alone, a significant spread in leached DOC is still evident (see Figure 3.9). This spread is a result of the diverse composition of the microcosms. They contain different rock types in various grain sizes and combinations of biota additions, including fungi, bacteria, and earthworms. Of the 296 microcosms containing wheat straw, the biota composition is shown in the Table 3.5.

Table 3.5: Number of different microcosm categories containing rock powder and wheat straw.

Category	**Count**
rock powder + organic matter + bacteria + fungi	130
rock powder + organic matter + earthworms	86
rock powder + organic matter + bacteria +fungi + earthworms	58
rock powder + organic matter	22
Total	296

All those components supply DOC in varying amounts. For the experiment microorganisms were grown in a DOC-rich nutrient medium. This nutrient medium was added together with the microorganisms and can also contribute to the DOC itself. Furthermore, different microorganisms were added to the microcosms. The different species could not reveal a strong impact on the $TA_{measured}$ and other weathering indicators, but they were all grown in different nutrient media optimized for the given bacteria or fungi species to grow. Those different nutrient media can also impact the DOC concentrations.

Additionally, the different rock types and grain sizes impact the size of the pH, thereby affecting the release of DOC (Evans, Monteith, and Cooper, 2005; Kalbitz et al., 2000). Generally, the highest $TA_{measured}$ and thus also pH was usually reached with microcosms containing dunite rock powder.

3.3.6. Comparison with other water samples from EW experiments and natural environments

To assess whether similarly high DOC concentrations occur in other EW experiments and how they impact the measured TA, the same calculations for A_C were applied to additional datasets of various environments (Table 3.6).

Table 3.6: Datasets used for comparison.

Dataset number	Short description
[1]	Leachate water samples from an organic-rich soil column EW experiment, excluding plants (setup in Appendix section B.6).
[2]	Leachate water samples from a brown earth soil column EW experiment, excluding plants (setup in Appendix section B.7).
[3]	Leachate water samples from mesocosms filled with brown earth soil comparable with [2] from an EW experiment inside a greenhouse, including grass plants from the Carbon Drawdown Initiative (Paessler et al., 2024).
[4]	Leachate water samples from a natural salt marsh soil column experiment with no rock addition (Tutiyasarn, 2024).
[5]	Water samples from the Elbe estuary along the salinity gradient, including samples with high organic mineralization rates due to prolonged residence time (Amann, 2013).
[6]	Water samples from creek outlets besides the Elbe estuary, draining organic-rich tidal marsh land soils, partly affected by sediment deposition with carbonate content (Weiss, 2013).

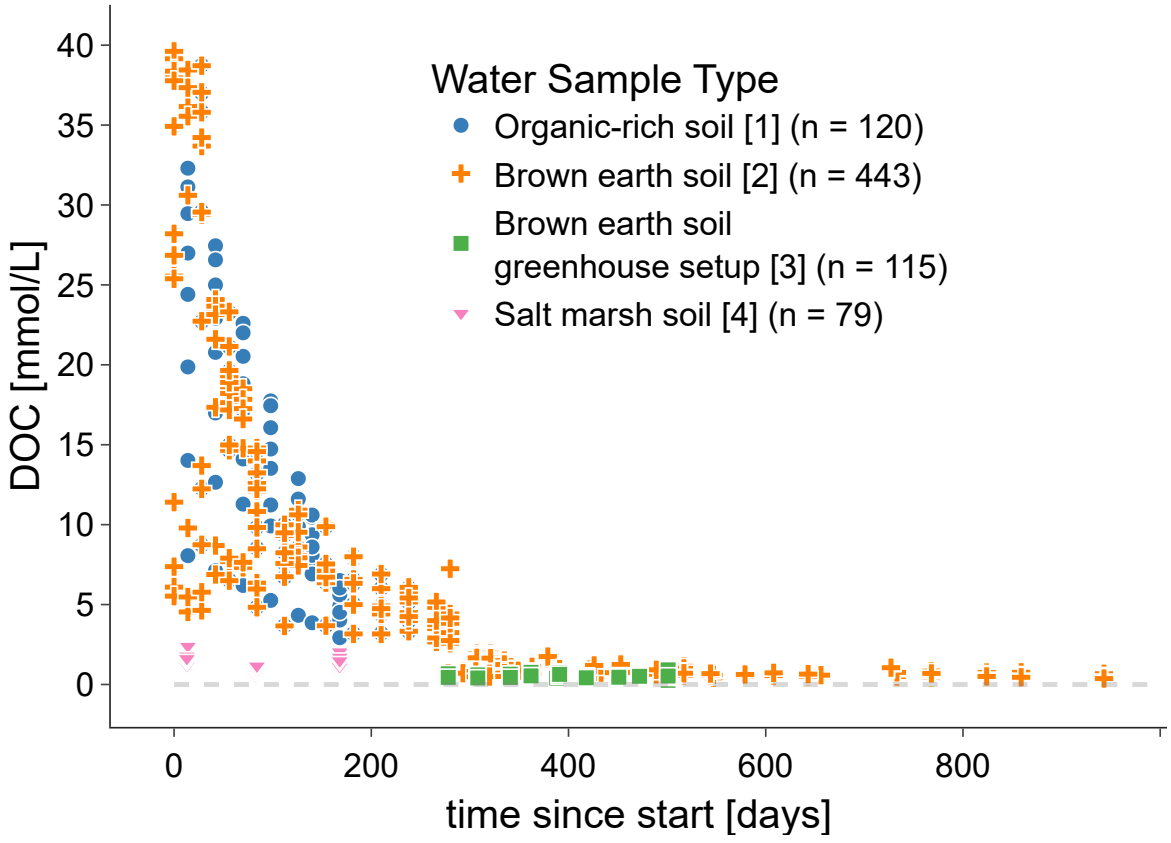


Figure 3.10: DOC time series for different EW soil column experiments.

In Figure 3.10, water samples from 4 different soil leaching experiments are shown, as well as water samples from the Elbe estuary region for a general DOC level comparison. A key factor is the time dependency in DOC concentrations. For the datasets [1] and [2] (Figure 3.10), initially high DOC concentrations are leached from the soil, and after around 400 d, the DOC levels remain constant at a low level. In the dataset [3], one cannot see any temporal trend in DOC concentration. We attribute this to the late sampling start, such that the major DOC loss had already occurred. In dataset [4], no temporal trend in DOC concentrations was observed.

After an initial phase of high leaching, the DOC concentrations in soil EW experiments are expected to decline until stabilization after some time. How long it takes to stabilize the DOC levels is likely a function of multiple factors. First, the initial soil pH, which controls how quickly the added rock powder will dissolve and then elevate the soil pH (Dupla et al., 2025). Second, the initial SOC content and quality, which also controls how acidic the soil reacts when increasing pH (Curtin, Campbell, and Messer, 1996). Third, the total water volume that flowed through the soil, which transports the DOC out of the soil. Fourth, the alkalinity released to the soil by the used rock powder or alkaline material, where more alkaline materials will cause a bigger soil pH increase and thereby more DOC release.

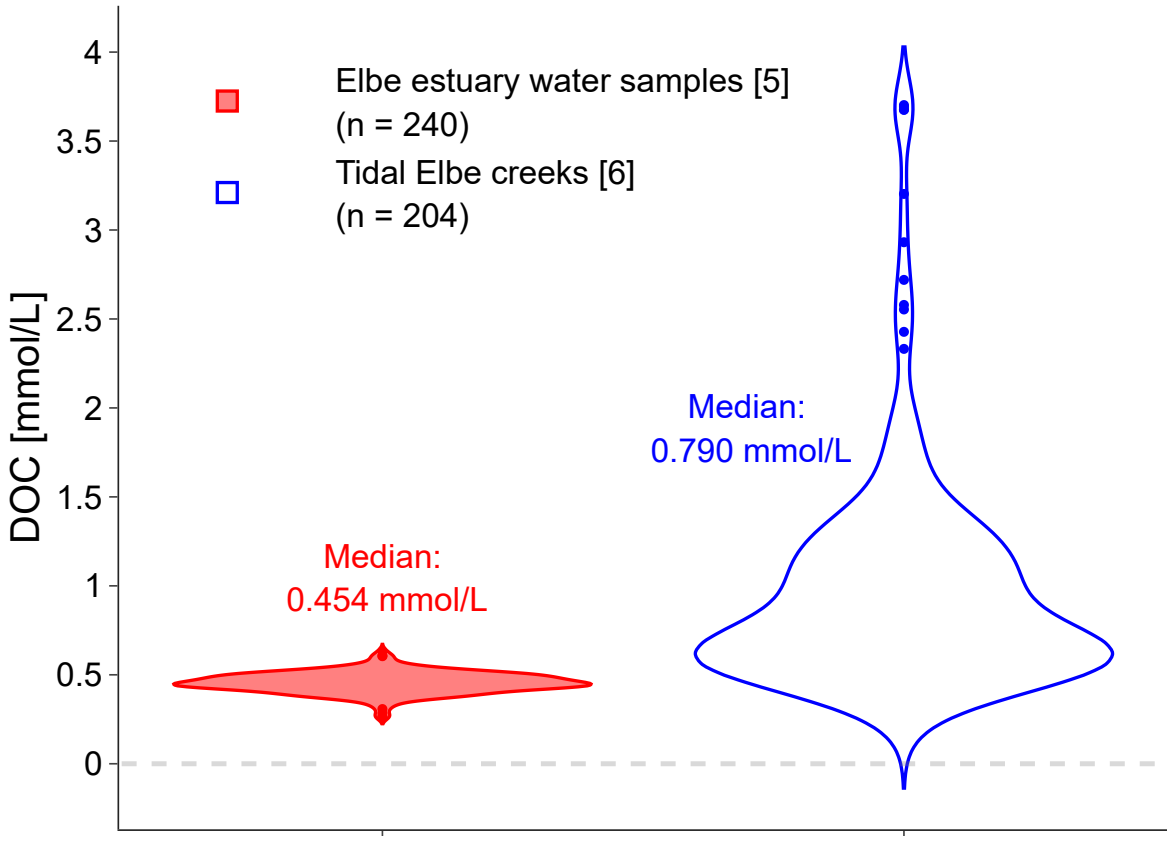


Figure 3.11: DOC concentrations in Elbe estuary water samples, used as a natural baseline for a comparison for the experimental data.

The A_C was calculated for mesocosm experiments in the greenhouse [3] and for the Elbe

estuary [5], covering different zones (Amann, Weiss, and Hartmann, 2015) from the freshwater river part, to the organic matter decomposition zones, the oxygen minimum zone, to the outlet, as well as for tidal creeks draining organic-rich marshland soil [6]. From each dataset only a subset of the water samples was tested for $TA_{measured}$, pH, T, DIC, this led to fewer samples compared to Figure 3.10 and Figure 3.11. On those subsets the A_C was calculated and plotted against $TA_{measured}$ (Figure 3.12). The A_C matches well with the $TA_{measured}$. This can be explained by their relatively low DOC concentrations compared to the early period of the soil column experiments (first 300 d). As a result, the calculated A_{NC} is small (Figure 3.13). Only for the water samples coming from the organic-rich tidal soils, there might be some impact of A_{NC} with large uncertainty reflected by the patterns in the A_C and $TA_{measured}$ space (Figure 3.13). However, the tested samples from all three datasets in Figure 3.13 have no clear relationship with DOC concentration. The A_{NC} is mostly dispersed around 0 meq kgw^{-1} with just a slight positive trend.

Based on this, it can be concluded that most EW soil column experiments might exhibit an initial DOC leaching phase characterized by high DOC concentrations (Figure 3.10). During this phase, the A_{NC} can likely not be neglected, and organic alkalinity may play a role in influencing the $TA_{measured}$. With lower DOC concentrations, the impact of organic alkalinity will also decline. After this initial leaching phase, the A_C will be close to the $TA_{measured}$.

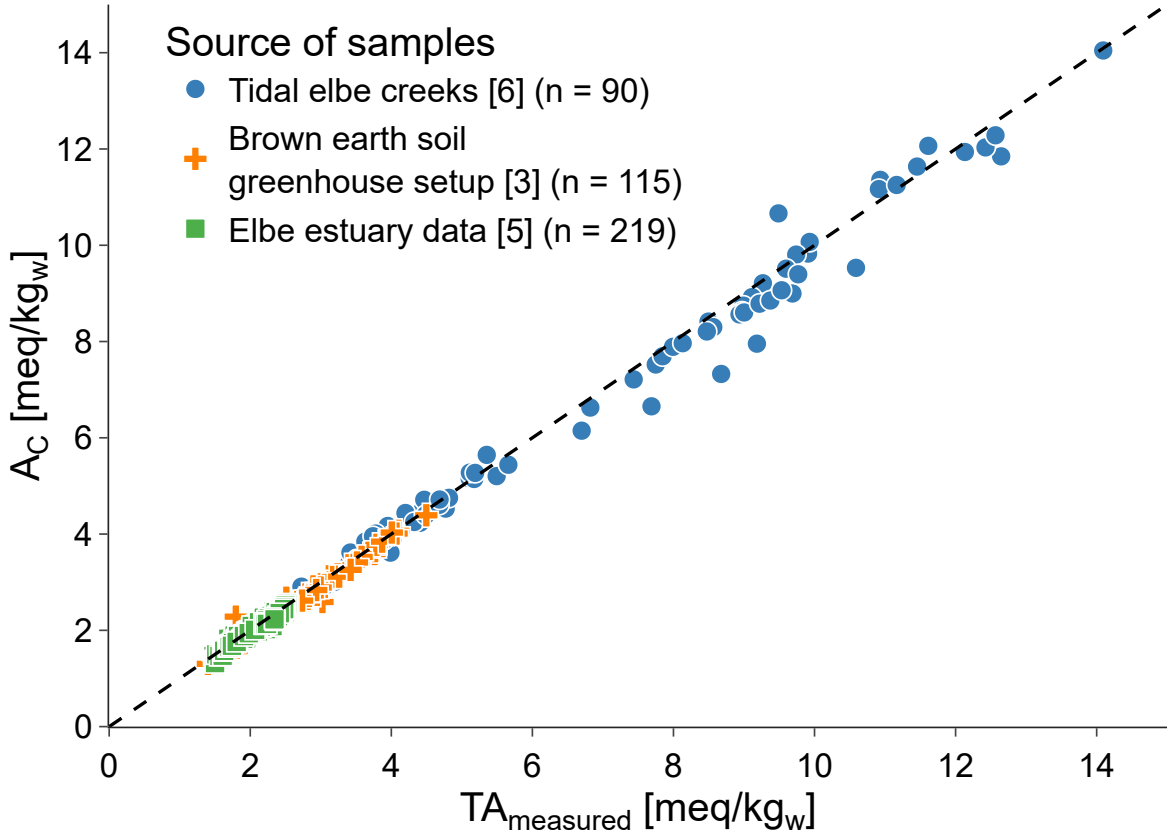


Figure 3.12: Carbonate alkalinity (A_C) versus measured TA for different datasets. The dashed line represents the 1:1 line.

From Figure 3.13 one can infer that other non-organic species likely contributed to the A_{NC}. The water samples from the Elbe estuary region (datasets [3] and [6]) might have more dominant contributions from other inorganic proton acceptors (Wolf-Gladrow et al., 2007). This leads to a weak correlation of A_{NC} with the DOC concentration (Figure 3.13). Only in the microcosm experiment where the organic contributions to A_{NC} outweigh other inorganic proton acceptors the DOC will correlate well with the A_{NC} (Figure 3.5).

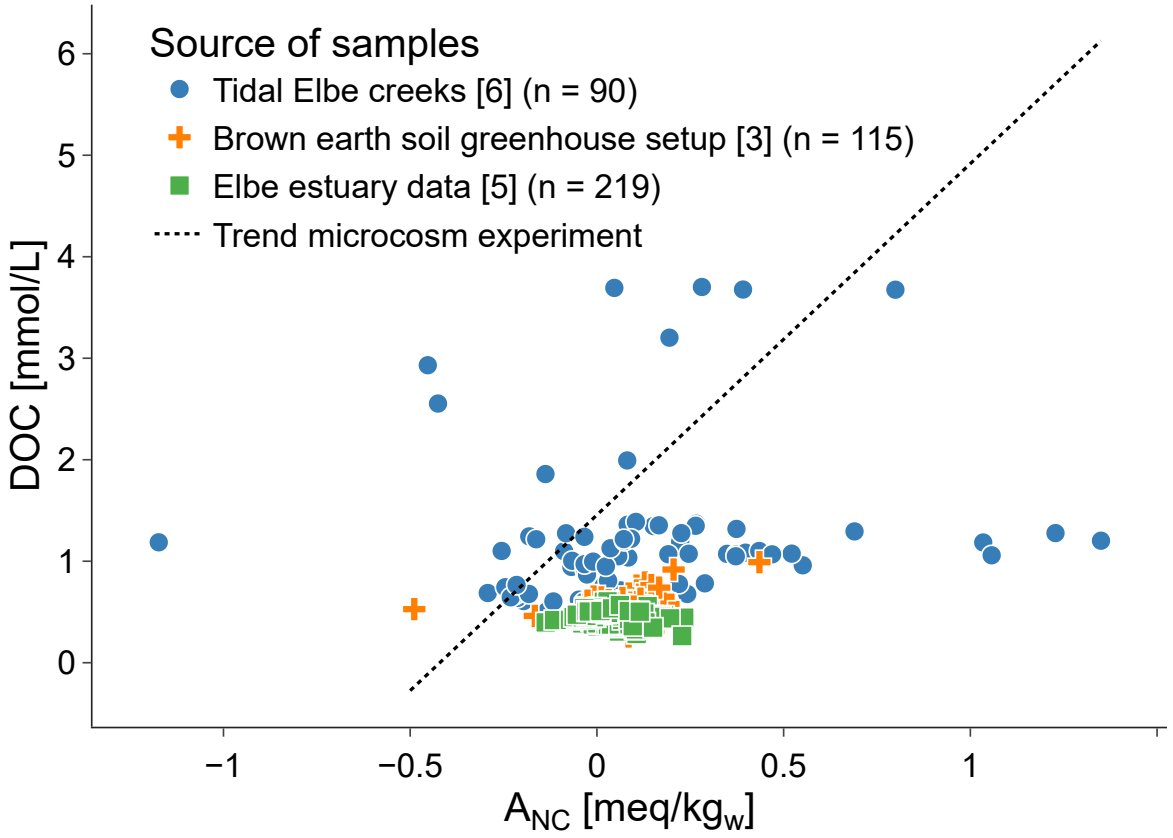


Figure 3.13: DOC versus non-carbonate alkalinity (A_{NC}) for different datasets. The dashed line shows the DOC A_{NC} relationship from the microcosm leachate water samples.

Overall, the contribution of A_{NC} decreases from the microcosm leachate water scale to the mesocosms and drainage creeks from marshland soils to the Elbe estuary area (Figure 3.14). While the decomposition of fresh organic matter in the microcosms provided high DOC concentrations that elevated the A_{NC} contribution, it is decreasing on larger scales. In the soil mesocosm data, the impact of DOC on A_{NC} will also be different as the available organic carbon pool is qualitatively distinct (Ukalska-Jaruga et al., 2021). In contrast to fresh organic inputs such as wheat straw, the stabilized soil organic carbon pool consists of decomposed and microbially processed material that is more resistant to further degradation. However, to analyze this quality of leached DOC in depth, samples from the initial 300 d (see Figure 3.10) with high DOC concentrations would be beneficial.

Overall, in the tested microcosm leachate waters, the median A_{NC} contribution was around

5 %, while in the Elbe estuary, it is just around 1 % (Figure 3.14). The water in the basin is more diluted and mineralization of DOC already occurred on the way which will convert the organic acid anions contribution to A_{NC} into A_C. The water in the basin is more diluted, and mineralization of dissolved organic carbon (DOC) has already occurred along its flow path, progressively converting the organic acid anions that contribute to A_{NC} into A_C (Hu, 2020; Xinping Hu, 2020), as it is exposed to a range of bio-geochemical processes from soils to the estuarine region.

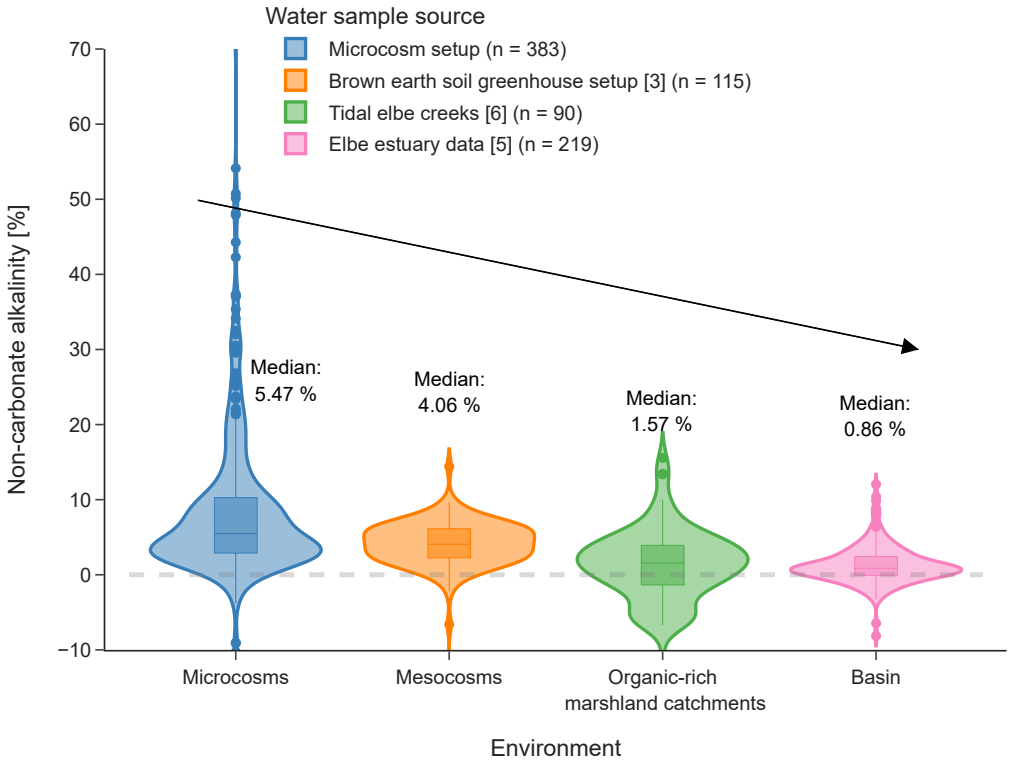


Figure 3.14: Relative non-carbonate alkalinity contribution ($A_{NC}/TA_{measured}$). From left to the microcosm scale down to the Elbe River basin.

3.4. Conclusion

In our tested leachate water samples of a rock weathering microcosm experiment with artificial organo-mineral mixtures, the relationship between dissolved organic carbon (DOC) and non-carbonate alkalinity (A_{NC}) was quantified as $DOC = 3.461 \cdot A_{NC} + 1.462$. This indicates that approximately 3.5 DOC equivalents contribute to one total alkalinity (TA) equivalent. The relatively low factor of 3.5 suggests that not much long-chained organic acids were present, but rather the conjugate base anions of low-molecular-weight organic acids (LMWOAs). This was also verified by the abundance of acetate in DOC-rich samples. In addition, increasing DOC levels also amplified the charge balance error, as accurate TA measurements require titration to a pH below the point where organic conjugate base anions are fully protonated. In

this experimental design, the initial goal was to increase carbonate alkalinity; thus, a titration with endpoints [4.5; 4.3; 4.0; 3.7] was used. In this range the observed acetate was not fully protonated. This suggests that the endpoint for titration should be adjusted to a value lower than in the definition of TA commonly used (Wolf-Gladrow et al., 2007), ensuring proper measurement for organic-rich water samples.

Organic alkalinity, comprising the conjugate base anions of organic acids, has an uncertain long-term fate. It is expected to eventually convert into CO_2 and carbonate alkalinity by anerobic pathways and photodegradation (S. Song et al., 2020) while maintaining charge balance of the water. A critical question for future CDR assessments using EW is determining how much additional DOC and its quality is mobilized by alkaline material application compared to its stability without EW interventions.

The organic alkalinity can be a non-neglectable part of the measured alkalinity depending on the environmental conditions and the composition of the organo-mineral substrate. In this experimental setup, organic acids were produced by decomposition of wheat straw. From the tested LMWOAs, only acetate was detected. The acetate anions could not explain all the detected non-carbonate alkalinity, but there are far more organic acids that can have an impact than the tested oxalate, citrate, and acetate. All dissolved organic matter with charged functional groups will impact the measured alkalinity.

This study demonstrates that organic alkalinity can contribute substantially to total alkalinity in short-term experiments involving fresh organic inputs, such as cropland soil incubations or artificial systems enriched with easily degradable organic matter. However, its influence diminishes over time: in long-term cropland experiments, the contribution of non-carbonate alkalinity typically falls below 5 %. This suggests that organic alkalinity is most relevant under conditions where fresh, readily deprotonatable organic compounds are actively produced or added. In soils, where most organic matter is older and more resistant to degradation, its contribution likely becomes negligible once pH stabilizes following rock powder application. Nevertheless, in cropland soil settings, it remains essential to consider this initial phase and account for the SOC loss when assessing the overall CO_2 budget. It is suggested that this aspect should be considered in publicly available databases aggregating knowledge from experiments like those conducted here, to provide a knowledge database for MRV-protocols. With this it could be possible to identify conditions where the aspect of organic alkalinity should be addressed in MRV-schemes.

4

Testing the bio-additionality hypothesis for enhancing the alkalinity production via Enhanced Weathering

Abstract

Natural silicate weathering is considered one of the most important natural CO_2 sinks on geological time scales. Accelerating this natural process to capture more CO_2 also on human timescales is known as enhanced weathering. This can be done, for example, by spreading crushed rock on agricultural soils, where it can sequester CO_2 and have beneficial effects as a mineral nutrient fertilizer. Previous studies have shown that specific bacteria, fungi, and earthworms enhance mineral dissolution. The interaction of all these biotic components and whether this can be optimized through specific species mixtures is not yet well understood.

In this study, we investigate how the addition of biota, including bacteria (*Bacillus subtilis*), the endogeic earthworm *Aporrectodea caliginosa* [Savigny], and the fungus *Aureobasidium pullulans*, to a wheat-straw and crushed-tephrite substrate affects rock dissolution. The action of biota on a low-inorganic-carbon tephrite-straw mixture was studied in a flow-through column setup lasting 56 d. Groundwater was used to irrigate these columns daily. Leachate water was collected and analyzed for total alkalinity (TA), dissolved inorganic and organic carbon, pH, electrical conductivity (EC), major anions, and major cations to assess the impact of biota on these parameters.

The addition of biota to the straw–tephrite rock mixture did not increase the equivalent amount of TA, cations, or anions over the 56-day experimental period. The addition of straw itself might have increased the dissolution of the tephrite. It is likely that the CO_2 generated during straw decomposition increased the local CO_2 partial pressure, thereby lowering the pH and promoting the dissolution of minerals. The added microbes were unable to colonize the substrate, and earthworm survival was low (36 ± 24 %), with small activity (38 ± 42 %) observed. Although inoculated biota did not enhance weathering in this case, the addition of wheat straw helped increase the leached amounts of K and Na.

Graphical Abstract

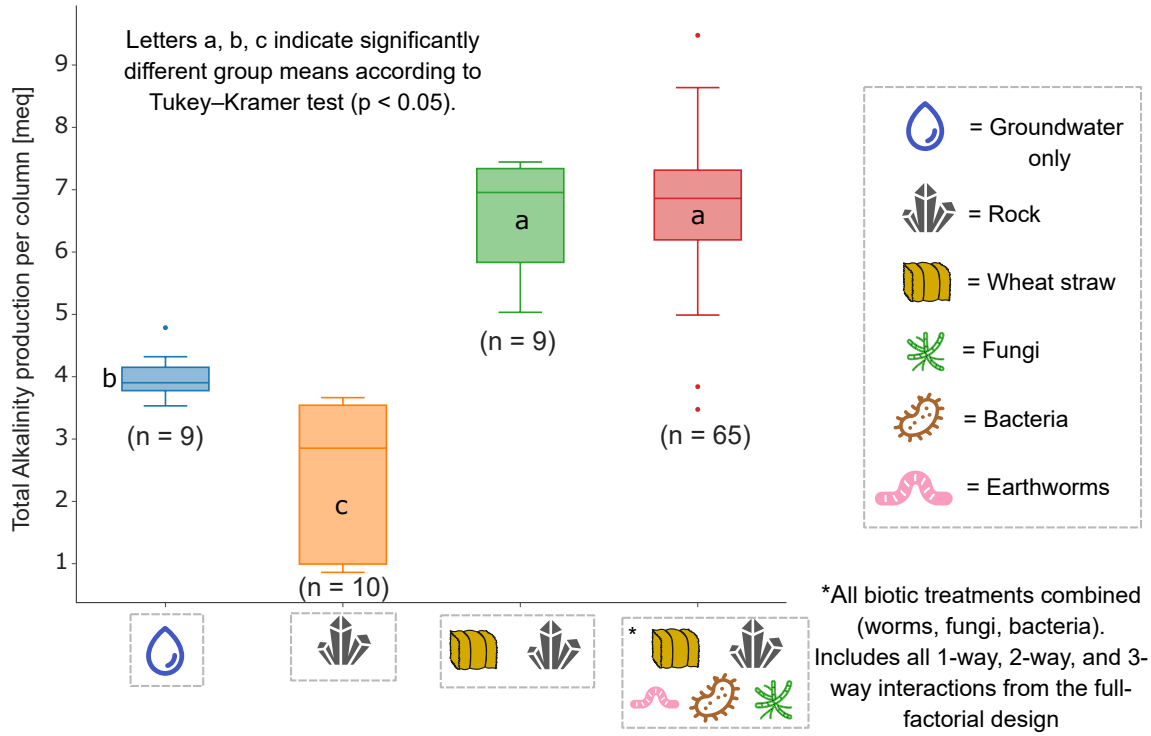


Figure 4.1: Conceptual overview of the rock weathering experiments and associated alkalinity generation

4.1. Introduction

An increase in global surface temperature is one of the most pressing environmental issues of the 21st century. To limit human-caused global warming to a specific temperature, the worldwide cumulative carbon dioxide (CO_2) emissions and other greenhouse gas emissions, such as methane (CH_4) and nitrous oxide (N_2O), must be significantly and urgently reduced. However, to limit global surface temperature rise to 2 °C or lower by 2100, mitigation efforts must combine emission reductions with carbon dioxide removal (CDR). This requirement is reflected in the IPCC's modelled Shared Socioeconomic Pathways (SSPs) that are consistent with climate targets of 2 °C or lower (IPCC, 2022b; IPCC, 2022a; Steve Smith et al., 2024).

Enhanced weathering (EW) is a promising CDR technology that aims to accelerate rock dissolution and increase alkalinity fluxes to the oceans (Beerling et al., 2020; Goll et al., 2021; Hartmann et al., 2013; Schuiling and Krijgsman, 2006; Seifritz, 1990). The key mechanism for CO_2 capture is the chemical weathering or dissolution of minerals, particularly silicates (Lasaga et al., 1994). Silicate weathering is a natural process that has regulated the Earth's carbon cycle over geological timescales. In contrast, the weathering of carbonate minerals

provides a CO_2 sink on shorter timescales, primarily through the later carbonate formation in the ocean and subsequent CO_2 degassing (Berner, 2003; Lasaga et al., 1994; Walker, Hays, and Kasting, 1981).

Due to their global abundance and high weathering rates, mafic and ultramafic silicate-rich rocks are the main focus of EW application studies (Hartmann et al., 2013). Mafic and ultramafic rocks are mainly composed of low-silica silicate minerals, including olivine, pyroxene, and plagioclase. Dissolution rates vary between minerals by several orders of magnitude for constant environmental conditions. For example, at pH = 5 and $T = 25\,^{\circ}\mathrm{C}$, the rates range from $10^{-8}\,\mathrm{mol\,m^{-2}\,s^{-1}}$ (wollastonite) down to $10^{-13}\,\mathrm{mol\,m^{-2}\,s^{-1}}$ (kaolinite) (Lasaga et al., 1994). Compared to terrestrial weathering of carbonate minerals like calcite, which dissolve at faster rates of $\approx 10^{-6}\,\mathrm{mol\,m^{-2}\,s^{-1}}$ under the same environmental conditions (Fan et al., 2022; Morse and Arvidson, 2002), silicate weathering and transfer of bound CO_2 in the form of alkalinity into the ocean are assumed to represent a more stable CO_2 removal mechanism. This is due to the fact that reprecipitation of dissolved carbonate species (HCO_3^-, CO_3^{2-}) into carbonate minerals (in the ocean or in soils) leads to CO_2 release (see Equation 4.2 to Equation 4.3) at natural pH levels. Below the reaction equations for wollastonite ($CaSiO_3$) and calcite ($CaCO_3$) are shown. In the examples the acid responsible for dissolution is H_2CO_3, thus the dissolution process will bind CO_2. Other acids are not directly connected to the inorganic carbon pool (Rieder et al., 2026).

$$\text{Silicate dissolution} \quad CaSiO_{3(s)} + 2\,CO_{2(g)} + 3\,H_2O \longrightarrow Ca^{2+} + 2\,HCO_3^- + H_4SiO_{4(aq)} \tag{4.1}$$

$$\text{Carbonate dissolution} \quad CaCO_{3(s)} + CO_{2(g)} + H_2O \longrightarrow Ca^{2+} + 2\,HCO_3^- \tag{4.2}$$

$$\text{Mineral carbonation} \quad Ca^{2+} + 2\,HCO_3^- \longrightarrow CaCO_{3(s)} + CO_{2(g)} + H_2O \tag{4.3}$$

After the dissolution reaction, the previously gaseous CO_2 is bound as aqueous carbonate species (HCO_3^-, CO_3^{2-}), which at a pH of around 7–8 are mostly HCO_3^- ions.

So far, strategies to enhance mineral weathering have largely focused on abiotic factors, such as mineralogical composition of rocks, grain size of applied rock substrates, soil pH, and precipitation amount (Beerling et al., 2025; Deng et al., 2023; Hartmann et al., 2013; Renforth, Pogge Von Strandmann, and Henderson, 2015; Romero-Mujalli et al., 2019; Te Pas, Hagens, and Comans, 2023). Although studies indicate that biota can enhance weathering, the potential role of biotic factors is often overlooked (Vicca et al., 2022). In this study we are going to test the impact of selected earthworms, fungi and bacteria on rock weathering.

Earthworms can promote mineral dissolution through several interconnected processes, including organic matter decomposition, increased CO_2 production, and the mechanical grinding of mineral particles in their gizzard (Du, 2018; Lubbers et al., 2013; Suzuki, Matsubara, and Hoshino, 2003). Among the main ecological groups (epigeic, anecic, and endogeic; (Bouché, 1977; Bouché, 1971)), endogeic species are particularly relevant because they ingest more mineral soil and less organic litter, thus directly interacting with the mineral substrate (Edwards and Arancon, 2022). For this reason, the endogeic earthworm *Apporectodea caliginosa*

[Savigny] was selected for the experiment, as it is a common temperate soil species in the Netherlands that feeds primarily within the mineral horizon (Calogiuri, Janssens, et al., 2025).

Bacteria and fungi can further contribute to biogenic weathering by acidifying their surroundings and releasing organic compounds that complex metal ions, thereby promoting mineral dissolution (Hoffland et al., 2004; Rensink et al., 2024; Uroz et al., 2009). In addition to these chemical effects, fungi can also physically degrade rocks by penetrating mineral surfaces with their hyphae, widening pores, and enhancing access to reactive mineral phases (Lybrand et al., 2022).

For the present experiment, the fungus *Aureobasidium pullulans* was selected due to its ecological ubiquity, metabolic versatility, and ability to colonize diverse substrates (Rensink et al., 2024; Schoeman and Dickinson, 1996). The bacterium *Bacillus subtilis* was chosen because of its well-documented effects on enhancing mineral dissolution and its frequent use as a model organism in biogenic weathering studies (J.-U. Lee and Fein, 2000; H. Liu et al., 2021; Niron et al., 2024; W. Song et al., 2007).

For bacterial inoculation, *Bacillus subtilis* was selected due to its well-documented influence on rock weathering. Several studies have demonstrated its ability to enhance mineral dissolution. For instance, the addition of *Bacillus subtilis* to gibbsite ($Al(OH)_3$) increased aluminum release by a factor of 30 (J.-U. Lee and Fein, 2000). In another study, application of basalt powder to soil together with *Bacillus subtilis* showed higher CDR potential than basalt-only application (Niron et al., 2024). Similarly, its application to serpentine increased magnesium release (H. Liu et al., 2021). Beyond chemical effects, *Bacillus subtilis* has also been shown to promote physical weathering processes, such as pit formation and widening of micropores on granite surfaces (W. Song et al., 2007).

Despite separate extensive research, the dominant mechanisms by which biota accelerate mineral weathering remain unclear. Here, we investigate whether the addition of soil microorganisms and endogeic earthworms to an organo-mineral substrate can enhance the weathering. Thus, increase cation amounts and alkalinity equivalents. To answer those questions, we conducted a flow-through microcosm experiment comparing biologically amended treatments of an organo-mineral substrate control. This organo-mineral substrate is composed of tephrite rock and wheat straw.

4.2. Materials and methods

4.2.1. Experimental setup

The experimental setup was designed to investigate the impact of selected microorganisms and endogenic earthworms on rock dissolution. The goal was to enhance rock dissolution rates through the interaction of different biotic and abiotic factors. The setup included Tephrite rock filled in small cylinders that were irrigated with groundwater, to which microorganisms (*Aureobasidium pullulans* and *Bacillus subtilis*), endogenic earthworms (*Apporrectodea caliginosa* [Savigny]), and wheat straw were added. Details on the materials and biota can be found in section subsection 4.2.2 and subsection 4.2.3, respectively.

The microcosm system used in this study is described in detail by Calogiuri et al. (2023). Each microcosm consisted of a 15 cm-long polyvinyl chloride (PVC) tube fitted with a double filter mesh at the base (Figure 4.2). The microcosms were placed in a climate chamber maintained at a constant temperature of 25 °C and irrigated daily from the top using automated sprinklers with groundwater (Table 4.4). Water percolated through the columns and drained through the bottom mesh, where it was collected and stored in high-density polyethylene (HDPE) jerrycans at 4 °C in a refrigerated unit located beneath the setup.

The experiment lasted for 56 d, during which the irrigation rate was maintained at 50 mL per day, equivalent to an annual precipitation rate of 1 200 mm, based on the column geometry. At the end of the experiment, leachate samples were collected from the jerrycans for the analysis of dissolved constituents.

The experimental design included 10 different treatments, each with 10 replicates (totaling 100 columns), arranged in a randomized block design. The columns were randomly distributed across the climate chamber to minimize potential spatial biases caused by ventilation, temperature gradients, or the watering system, ensuring that any such effects would influence all treatments equally. However, due to occasional malfunctions in the irrigation system affecting a few columns across different treatments, the final number of samples was reduced to 93. The random distribution of columns ensured that each treatment still had at least 9 replicates.

To prevent desiccation stress during the initial phase, the organo-mineral substrate was pre-saturated to 80 % of its water-holding capacity (WHC) prior to the start of the experiment, ensuring the survival of the inoculated microorganisms and earthworms. The WHC was determined as described in (Calogiuri et al., 2023).

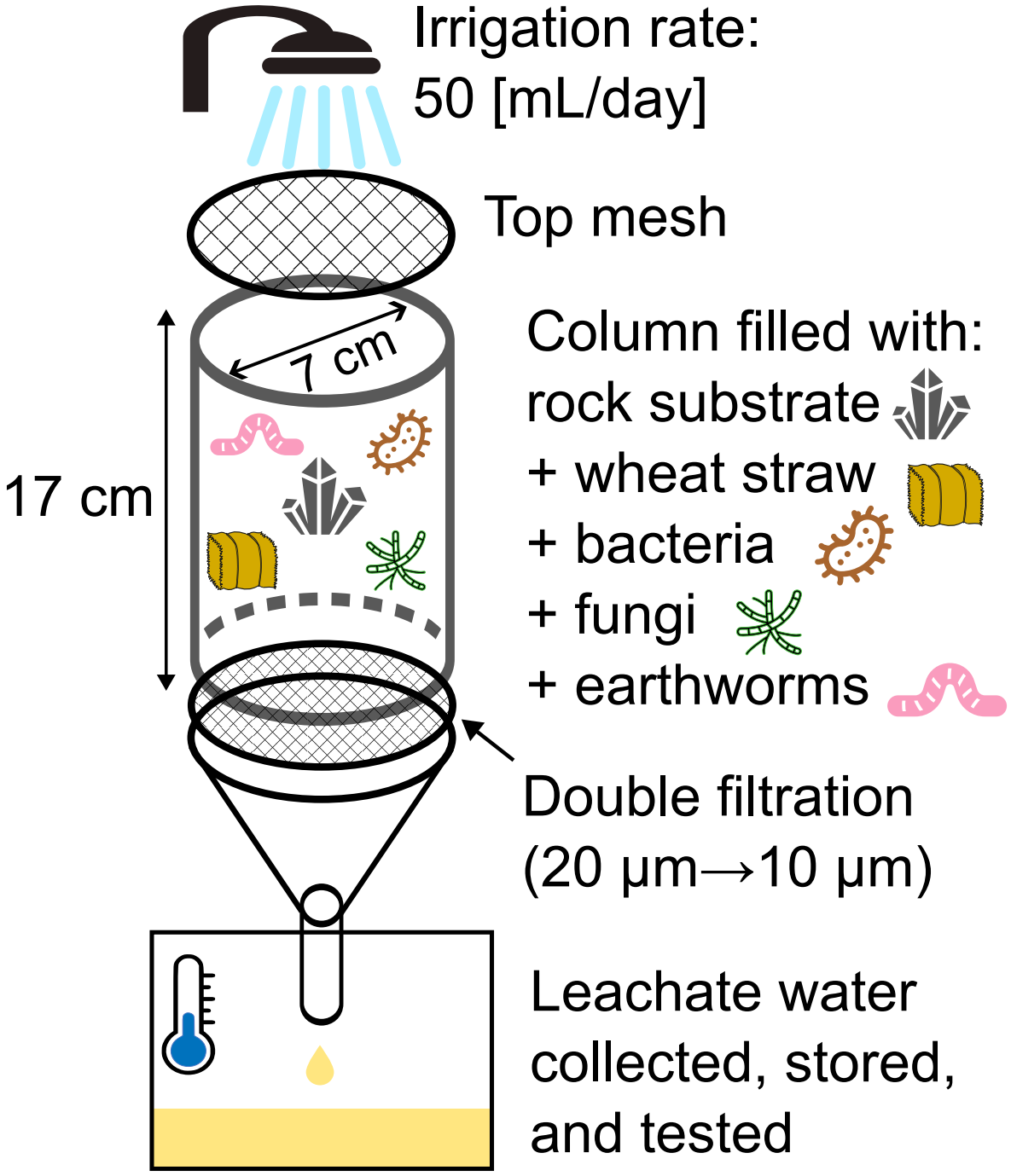


Figure 4.2: Illustration of the flow-through columns (microcosms).

As we use groundwater for irrigation, it is crucial to know its initial composition. Therefore, one group of treatments consisted only of empty columns serving as blanks. The next group consisted of columns with each containing 4 000 g of crushed rock only. To assess not only the individual effects of earthworms, fungi, and bacteria but also their interactions, the microcosm treatments were established in a full factorial design with three binary factors (2^3 design). For

this purpose, all biotic treatment columns were filled with 400 g of crushed rock mixed with 10 g of wheat straw. The factorial design resulted in eight combinations covering all possible single and combined biotic treatments, including the rock–straw mixture without any added organisms. Together with the blank and pure rock columns, this resulted in a total of ten treatments. All columns were irrigated daily with 50 mL of groundwater applied from the top (Figure 4.2). Details of the individual treatments are provided in the Supplement Section 2.

Bacterial (*B. subtilis*) and fungal (*A. pullulans*) inoculum were added at densities of approximately 10^{10} and 10^{8} cells per column, respectively, using a pipette. For groups containing earthworms, four endogenic earthworms (*A. caliginosa*) were placed on top of the substrate after filling. A mesh cover prevented earthworms from escaping and was installed on all columns to ensure consistency across treatments (Figure 4.2).

4.2.2. Materials

Rock substrate
The crushed rock (0 to 2 mm) is sourced from a volcanic rock in the Eifel region of Germany. It was supplied by *RPBL Basalt & Lava aus der Eifel* and is commercially referred to as *Lavagestein*. The rock was mined near the *Laacher See* volcanic crater lake in the East Eifel volcanic field, close to Nickenich, Germany (50.424 6° N, 7.325 7° E).

The rock particles are porous (up to 50 % porosity), reddish-brown in color, and have a heterogeneous particle size distribution (PSD) determined through laser diffraction (particle-sizer Sympathec HELOS/KF Magic) (see Appendix Figure C.1). Its elemental composition was measured by X-ray fluorescence (XRF) analysis using a Panalytical Magix Pro system. The XRF results are shown in Table 4.1. The mineralogical composition was analyzed by bulk X-ray diffraction (XRD) using a Bruker D8 Advance diffractometer equipped with an XE-T detector and using Cu-K4α radiation. The rock samples were finely ground in a wet milling device using alcohol and subsequently dried in a manner that minimized preferred orientation. The XRD results are shown in Table 4.2.

The rock was classified based on XRF and XRD analysis. According to the TAS (Total Alkali-Silica) classification, it falls within the U1 Basanite/Tephrite field. Given its olivine content of less than 10 %, the rock is further classified as Tephrite (Bas et al., 1986).

Table 4.1: Elemental composition of the rock was measured using X-ray fluorescence (XRF) measurements. (nd = below detection limit, LOI = loss of ignition, i.e., heating the sample to 1 000 °C to gas out all carbon) (n = 3).

Elements (as oxides)	**mass percent (%)**
SiO_2	43.44 ± 0.27
TiO_2	2.58 ± 0.33
Al_2O_3	13.79 ± 0.25
Fe_2O_3	11.19 ± 0.26
MnO	0.17 ± 0.01
MgO	8.68 ± 0.12
CaO	12.6 ± 0.1
Na_2O	2.99 ± 0.08
K_2O	3.29 ± 0.09
P_2O_5	0.53 ± 0.07
SO_3	0.03 ± 0.01
LOI	0.62 ± 0.08
Sum	99.91 ± 0.44

Table 4.2: Bulk mineralogical composition of the rock as tested with bulk X-ray diffraction (XRD).

Group	Mineral	Mineral Formula	Mass %
Silicates	Quartz	SiO_2	
	K-feldspar	$KAlSi_3O_8$	
	Plagioclase	$(Na,Ca)(Si,Al)_4O_6$	9.65
	Clinopyroxene	$(Ca,Na)(Mg,Fe,Al,Ti)(Si,Al)_2O_6$	49.15
	Amphibole	$Ca_2(Mg,Fe)_5Si_8O_{22}(OH)_2$	0.2
	Forsterite	$(Mg,Fe)_2SiO_4$	6.75
	Nepheline	$(Na,K)AlSiO_6$	11.75
	Leucite	$KAlSi_2O_6$	11.95
	Hauyne	$(Na,Ca)_{4–8}Al_6Si_6(O,S)_{24}(SO_4,Cl)_{1–2}$	0.2
	2:1 layer silicates	$(K,H_3O)(Al,Mg,Fe)_2(Si,Al)_4O_{10}[(OH)_2,H_{20}]$	3.15
	Chlorite	$(Mg,Fe)_5Al(Si_3Al)O_{10}(OH)_8$	
	Kaolinite	$Al_2Si_2O_5(OH)_4$	
Carbonates	Dolomite/Ankerite	$Ca(Fe_2^{+x},Mg_{1–x})(CO_3)_2$	
Phophates	Apatite	$Ca_5(PO_4)_3(OH,F,Cl)$	0.95
Oxides/Hydroxides	Rutile	TiO_2	
	Anatase	TiO_2	
	Goethite	$Fe^{3+}O(OH)$	
	Hematite	Fe_2O_3	4.75
	Spinel-type minerals	$Fe^{2+}Fe_2^{3+}O_4$	1.1
	Ilmenite	$Fe^{2+}TiO_3$	0.2
	Armalcolite	$(Mg,Fe^{2+})Ti_2O_5$	0.35
Other/Amorphous	Opal-CT	$SiO_2 \cdot n(H_2O)$	
Sum			100.15

This particular rock type was selected for the experiment due to its very low initial inorganic carbon content to avoid interference from fast dissolving carbonate minerals as explained in the introduction. Total carbon (C) and nitrogen (N) was measured using a CN analyzer, revealing a total carbon content (including both organic and inorganic forms) of just 0.012 ± 0.001 % ($n = 5$).

Additionally, previous studies using the same rock powder have shown that it supports higher earthworm activity and survival compared to other rock types (Calogiuri, Hagens, Van Groenigen, et al., 2025). In previous and related studies the same rock powder was referred to as the commercial manufacturer name *Lavagestein* or basanite (Calogiuri, Janssens, et al., 2025; Calogiuri, Hagens, Van Groenigen, et al., 2025; Janssens et al., 2025).

Wheat straw

Wheat straw was used as an organic feedstock for the added biota. As a widely available and inexpensive agricultural by-product, it offers a practical and scalable option for experimental setups. In addition to its use in agriculture, wheat straw is commonly employed as bedding material for animals. The wheat straw was obtained from Pets Place, Netherlands.

To also account for the elements released by the wheat straw, the elemental composition of it was tested. Therefore, it was analyzed by ICP-MS after digestion with nitric and hydrochloric acid and heating in a microwave, adapted from the method described by Novozamsky et al. (1996). Total C and N levels were measured using an elemental analyzer (FlashSmart, Thermo Fisher Scientific, USA). It has a C:N ratio of 86 (see Table 4.3) and is thus more stable for microbial decomposition due to the N limitation.

Table 4.3: Elemental composition of the wheat straw used in the microcosms, presented as mean ± s.d. (n = 4).

Element	Unit	Value
K	$mg\,g^{-1}$	8.00 ± 0.08
Na		0.019 ± 0.002
Ca		2.92 ± 0.07
Mg		0.46 ± 0.01
P		0.47 ± 0.01
Zn		0.004 ± 0.001
Fe		0.112 ± 0.016
Mn		0.051 ± 0.001
C		443.64 ± 9.83
N		5.16 ± 0.97
C:N ratio	$g\,g^{-1}$	85.98 ± 16.27

Groundwater

To enhance the applicability and scalability of the mineral dissolution experiments, locally sourced groundwater was used to irrigate the microcosms. The water was pumped from a borewell on the Wageningen University campus and underwent only a single filtration step without further treatment. The composition of the input irrigation water can be found in Table 4.4. Given the high initial pH and load of dissolved compounds, using groundwater will not lead to the strongest dissolution. Consequently, the resulting amounts are not directly comparable to mineral dissolution rates obtained from experiments using pure water or acidic solutions.

Table 4.4: Composition of the natural groundwater used for irrigation of the microcosms (mean ± s.d., n = 10). For the values below the detection limit (bdl), the detection limit is added between brackets.

Parameter	unit	Mean ± standard dev
pH		7.99 ± 0.10
Water Temperature	°C	14.87 ± 1.56
Electrical Conductivity (normalized to 25 °C)	$\mu S\,cm^{-1}$	194.30 ± 6.60
Measured total alkalinity (TA)	$eq\,kgw^{-1}$	1 551.01 ± 65.32
Charge balance error (CBE)	%	−1.09 ± 0.79
Saturation index (SI) calcite	-	0.993
Total Carbon		1 460.11 ± 0.08
Dissolved inorganic carbon (DIC)		1 409.54 ± 8.03
Dissolved organic carbon (DOC)		44.69 ± 6.57
dissolved silica		220.58 ± 9.08
Ca^{2+}		714.72 ± 14.60
K^{+}		23.59 ± 9.02
Mg^{2+}		105.42 ± 17.68
P (total P)	$\mu mol\,L^{-1}$	0.29 ± 0.25
Na^{+}		283.22 ± 11.60
F^{-}		6.19 ± 3.38
Cl^{-}		237.89 ± 23.65
NO_2^{-}		bdl (0.01)
SO_4^{2-}		98.09 ± 11.32
PO_4^{3-}		bdl (0.01)
Br^{-}		bdl (0.005)

4.2.3. Biota Preparations

The microbial cultures were received freeze dried and were subsequently rehydrated and propagated following the supplier instructions. A 100 mL volume of growth media solution was transferred into 500 mL Erlenmeyer flasks, which were stoppered and sealed with aluminum foil prior to autoclaving at 121 °C for 20 min, and then allowed to cool prior to inoculation. New cultures were prepared by transferring a hundredth volume of the culture to fresh media. All reagents were purchased from Merck (Sweden).

Fungi strain incubation
Aureobasidium pullulans (from Westerdijk Institute, The Netherlands) was grown in a malt extract broth (MEB), containing 2 % (w/v) malt extract, 0.1 %(w/v) casein-digested peptone, and 2 %(w/v) D-(+)-glucose, in MilliQ (18.2 mΩ) water. At the beginning of the experiment, the cells were added together with the broth on top of the organo-mineral mixture at a cell density of 10^8 cells per column.

Bacterial strain incubation
Bacillus subtilis (from Leibniz Institute, Germany) was grown on nutrient broth (DSMZ media 1). The nutrient broth was prepared by dissolving 5.0 g peptone, 3.0 g NaCl, and 3.0 g meat

extract in MilliQ (1 000 mL). The pH was adjusted to 7.0 using 1 mol L^{-1} NaOH or HCl. Both bacteria were grown at 30 °C, in the dark, on an orbital shaker at 30 rpm. At the beginning of the experiment, the cells were added together with the broth on top of the organo-mineral mixture at a cell density of 10^10 cells per column.

Earthworm collection and preparation
The earthworms used in this study are abundant in the Netherlands and were collected at the beginning of the experiment from the nearby park De Blauwe Bergen in Wageningen (51.981 1° N, 5.660 6° E). To ensure accurate identification of the earthworm species *Apporrectodea caliginosa* [Savigny], a picking location was chosen where it co-occurs only with the epigeic species *Lumbricus rubellus*. These two species were distinguished based on pigmentation differences. At the start of the experiments, the earthworms were placed on the surface of the organo-mineral substrate after being starved for two days, and their weight was recorded, following the method of (Dalby, G. Baker, and S.E. Smith, 1996).

4.2.4. Measurements

Leachate water collection and subsampling
At the end of the experiment, all leachate jerrycans were removed from the refrigerators, weighed, and subsequently sampled. First, the jerrycans were weighed using an electronic hook scale, and then they were shaken to homogenize the leachate water. Next, the representative subsamples were taken and first filtered through 0.45 µm polyether sulfone syringe filters prior to any measurements.

Physicochemical analyses
In the collected leachate samples, we measured pH, electrical conductivity (EC), total alkalinity (TA), major cations and anions, trace elements, dissolved inorganic and organic carbon (DIC and DOC), and dissolved silica (DSi).

pH was measured with a WTW Multimeter 3430 IDS and a SenTix 940 probe. EC was measured using the same unit with a TetraCon® 925 probe with non-linear temperature compensation referenced to 25 °C, in accordance with *DIN EN 27888* (1993).

TA was quantified by automated Gran potentiometric titration using four pH endpoints (4.5, 4.3, 4.0, 3.7), following the method described by Koenig (2005). This titration was performed using a Metrohm 888Titrando, equipped with a 10/20 mL cylinder and an Aquatrode Plus pH electrode.

Total elemental concentrations—including Ca, Mg, K, P, Fe, Ni, Cr, Sr, Cu, Al, Li, Mn, and Zn—were determined using either ICP-MS or ICP-OES, depending on the expected concentration levels. The ICP-OES was used for the higher concentrations of Ca, Mg, K, Al, and Fe, while the other elements were analyzed by ICP-MS. The elements ICP-MS measurements were conducted with a Thermo Scientific™ Element2™, while ICP-OES analyses were performed using a Thermo Scientific™ iCAP 6500 duo.

Anions such as fluoride (F^-), chloride (Cl^-), nitrite (NO_2^-), nitrate (NO_3^-), and sulfate (SO_4^{2-}) were analyzed by ion chromatography using a Metrohm 881 Compact IC Pro system equipped with a Metrosep A Supp 17–150/4.0 column.

DSi concentrations were determined photometrically at a wavelength of 810 nm via the molybdate-blue method, as described by Hansen and Koroleff (1999), using a Hach Lange spectrophotometer DR3800 (Type: LPG 424.99.00001).

DIC and DOC were quantified using a catalytic combustion-based TOC analyzer (FormacsHT, Skalar, NLD), where DIC was measured after acidification with 4 % H_3PO_4.

Earthworm survival and activity
After the experiment, solid samples were collected, and the number and activity of earthworms were determined following the method described by Garamszegi et al. (2024). Based on these counts, the survival and activity rates of the earthworms were calculated. The survival rate was defined as the ratio of the final number of earthworms to the initial number introduced. The activity rate was calculated by dividing the number of active earthworms by the total number of surviving individuals.

Microbial sample preparation and sequencing
After the experiment, when the columns were discharged, a solid sample of 50 g was taken from each treatment group with a sterilized spoon and transferred to a falcon tube for microbial the analysis. The substrate samples were prepared by shaking approximately 50 g of unwashed mineral in approximately 20 to 30 mL of 0.9 % NaCl for 3 to 4 h. Similarly, for comparison pure straw samples were prepared by shaking ≈1 g straw. The liquid fraction was collected and centrifuged for 10 min at 4 000 rpm followed by retrieval of cell pellet and DNA extraction according to the protocol by (Singh, 2025).

The DNA metabarcoding for prokaryotic (16S rRNA gene) and eukaryotic (18S rRNA gene) microbial communities was done at Novogene (UK) Co. Ltd. The demultiplexed fastq reads were used for the primer trimming and quality control using Cutadapt (v3.5) (Martin, 2011). The paired end reads were merged using Vsearch (v2.27) followed by removal of chimera sequences, generation amplicon sequence variants and taxonomic assignments using package dada2 (v1.22.0) in RStudio running R (v4.1.3). Taxonomic annotations of the prokaryotic and eukaryotic datasets were done using GTDB (v207) formatted for use with DADA2 (Alishum, 2021) and PR2 database (v5.0.0) (Vaulot et al., 2023) formatted for DADA2, respectively. The visualisation of microbial community was done using package phyloseq and ggplot2.

4.2.5. Data analysis

The main focus of this study lies on the dissolved constituents in the leachate water captured in the jerrycans. Observed concentrations were converted to total amounts for comparison between treatments (total=concentration [mol L^{-1}]$\cdot m_{water}/\rho$). The primary focus was placed on leached TA and major cations. To ensure temperature-independent consistency, we used water-mass-based amounts. For conversion purposes, water mass was translated into volume

by assuming a water density of $\rho = 1\,\mathrm{kg\,L^{-1}}$. Only for the TA, the conversion was not necessary as it is always mass-based.

Factorial linear model (factorial ANOVA)
To assess the effects of biotic species on TA production in a substrate consistently composed of rock and straw, we employed a factorial linear model using ordinary least squares (OLS) regression (Kutner et al., 2005; Montgomery, 2013). Multiple indicators can be used to assess substrate dissolution, including cation and anion amounts, TA equivalents, and pH. For our factorial model, we selected TA as the response variable.

Given that wheat straw was always present when biota was added, it was treated as a co-variable, not included in the model, to prevent confounding effects. Additionally, the blank water columns were removed from the dataset for this model. The resulting model included the following predictors/factors:

- **Main effects**: addition of earthworms, addition of fungi cells, addition of bacteria cells
- **Two-way interactions**: earthworms × fungi, earthworms × bacteria, fungi × bacteria
- **Three-way interaction**: earthworms × fungi × earthworms

The key assumptions of factorial ANOVA are homogeneity of variance (all groups have the same standard deviation), normality of the residuals, and independence of the observations. The homogeneity of variance of the residuals is tested with the Levene test for homogeneity of variance (Levene, 1960) implemented. The normality of residuals was tested with the Shapiro-Wilk test (Shapiro and Wilk, 1965). Both tests were implemented with SciPy version 1.14.1 (Virtanen et al., 2020).

Boxplots (ANOVA + Tukey-Kramer test)
To interpret the full dataset, including also the pure crushed rock and blank, we have used boxplots. Including these treatment groups helps interpret the overall response magnitude and shows how tephrite, both alone and in combination with wheat straw, interacts with water.

All those results are presented as boxplots, created using the interactive plotting library Plotly in Python. The different treatment groups were statistically compared. Statistical significance was assessed using ANOVA followed by a post hoc Tukey-Kramer test (Kramer, 1956; Tukey, 1949).A significance level of $\alpha = 0.05$ was applied. The method and its potential pitfalls of applying this test are further elaborated in Appendix section C.3.

4.3. Results

4.3.1. Biota effect on TA

One outlier sample was removed from the dataset because its inclusion caused a violation of model assumptions for factorial ANOVA (non-normal residuals, as indicated by the Shapiro–Wilk test). Excluding this single point restored normality of residuals without affecting the overall interpretation of the results.

The overall performance of the factorial linear model was extremely poor. With an overall coefficient of determination being 0.083 (see model results in Appendix section C.4). The ANOVA results show that none of the factors and factor interactions have a significant effect on TA equivalents (Table 4.5). There is no significant effect of biota on the TA observable in the given dataset, see also Figure 4.3.

Table 4.5: Factorial analysis of variance (ANOVA) results for the effects of earthworms, fungi, and bacteria on total alkalinity equivalents (TA [meq]). Shown are sums of squares (SS), degrees of freedom (df), F-values, and associated p-values.

Factor	**SS**	**df**	**F**	**p-value**
Earthworms	0.196	1	0.174	0.678
Fungi	0.05	1	0.045	0.833
Bacteria	1.651	1	1.469	0.23
Earthworms × Fungi	0.144	1	0.128	0.721
Earthworms × Bacteria	3.472	1	3.089	0.083
Fungi × Bacteria	0.283	1	0.251	0.618
Earthworms × Fungi × Bacteria	0.927	1	0.824	0.367
Residual	74.195	66		

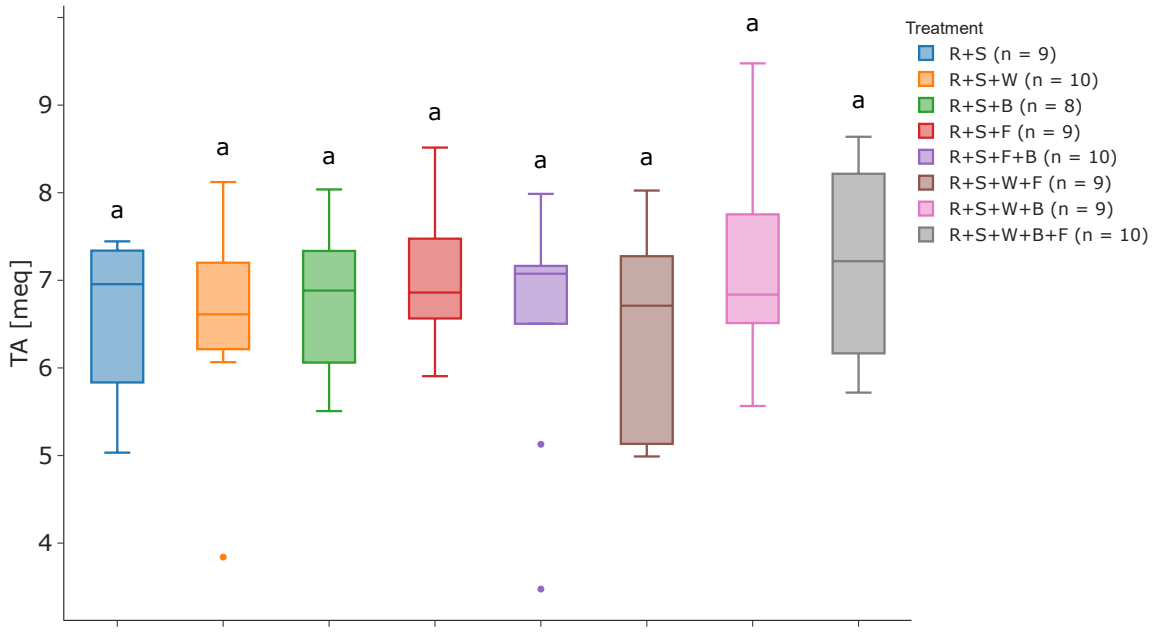


Figure 4.3: Total alkalinity (TA) observed in the leachate water. Abbreviations used in the legend: R = rock, S = straw, W = worms, B = bacteria, F = fungi. Different letters indicate statistically distinct groups (ANOVA with Tukey post-hoc).

4.3.2. Overall leachate water analysis

Water and carbonate system variables

First, we will compare the collected leachate water volume in the experimental setup to get an idea of the water retention time and evaporation occurring in the system. As the setup uses groundwater, the evaporation and co-occurring precipitation can also lead to a net loss of elements when the dissolved compounds are transferred to the solid phase.

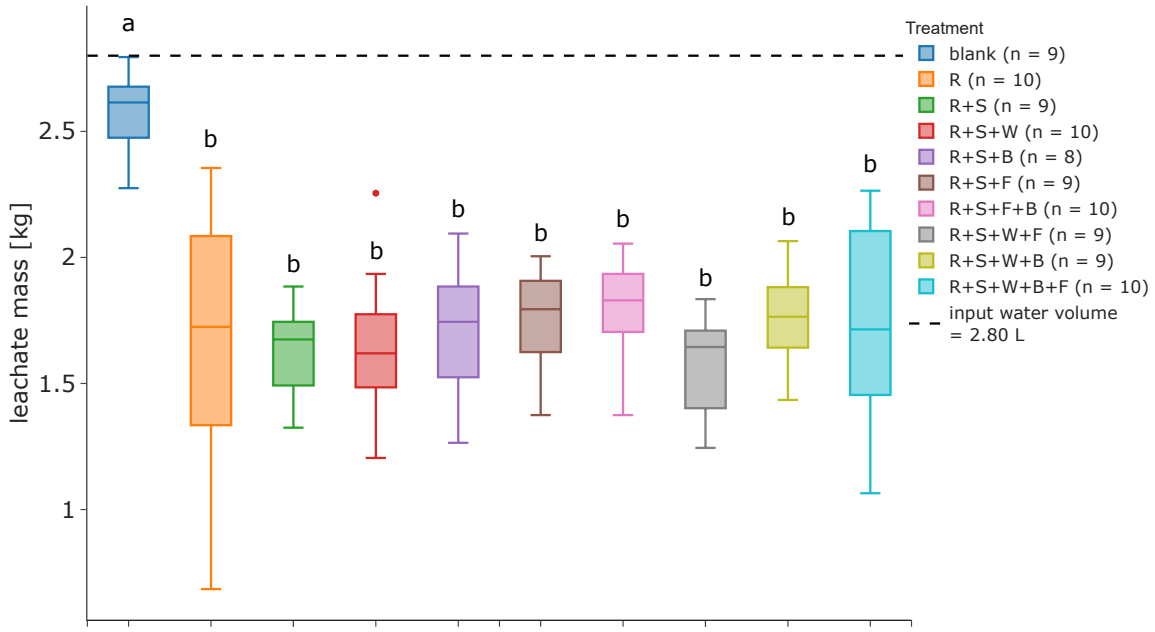


Figure 4.4: Leachate water mass that has been collected in the refrigerated containers over the experimental phase of 56 days. Abbreviations used in the legend: R = rock, S = straw, W = worms, B = bacteria, F = fungi. Different letters indicate statistically distinct groups (ANOVA with Tukey post-hoc).

For the observed leachate water mass, all treatments can be grouped into two categories (Figure 4.4). The blank columns (controls without substrate) produced a leachate water mass of approximately 2.6 kg, whereas all other treatments yielded leachate masses ranging from 1.5 kg to 2.0 kg.

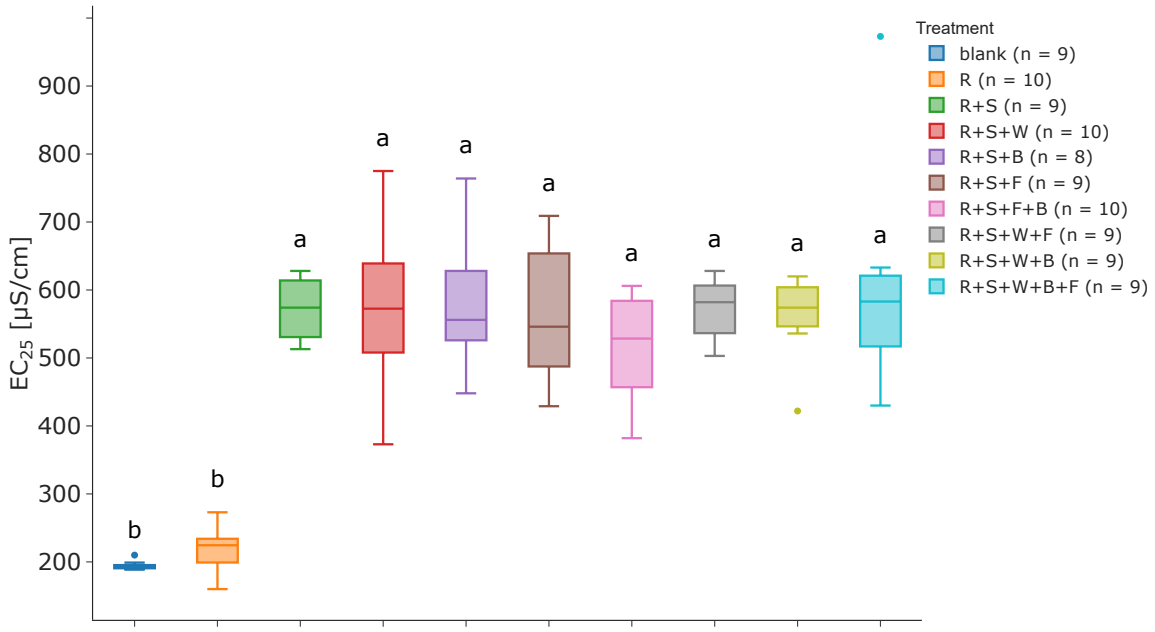


Figure 4.5: Electrical conductivity (EC) measured in the leachate water at the end of the experiment, normalized to 25 °C. Abbreviations used in the legend: R = rock, S = straw, W = worms, B = bacteria, F = fungi. Different letters indicate statistically distinct groups (ANOVA with Tukey post-hoc).

EC increased significantly for all treatments with straw (Figure 4.5). The EC of blank and rock-only treatments does not differ significantly. For the biotic treatments, the variability in EC is higher than for other treatment categories.

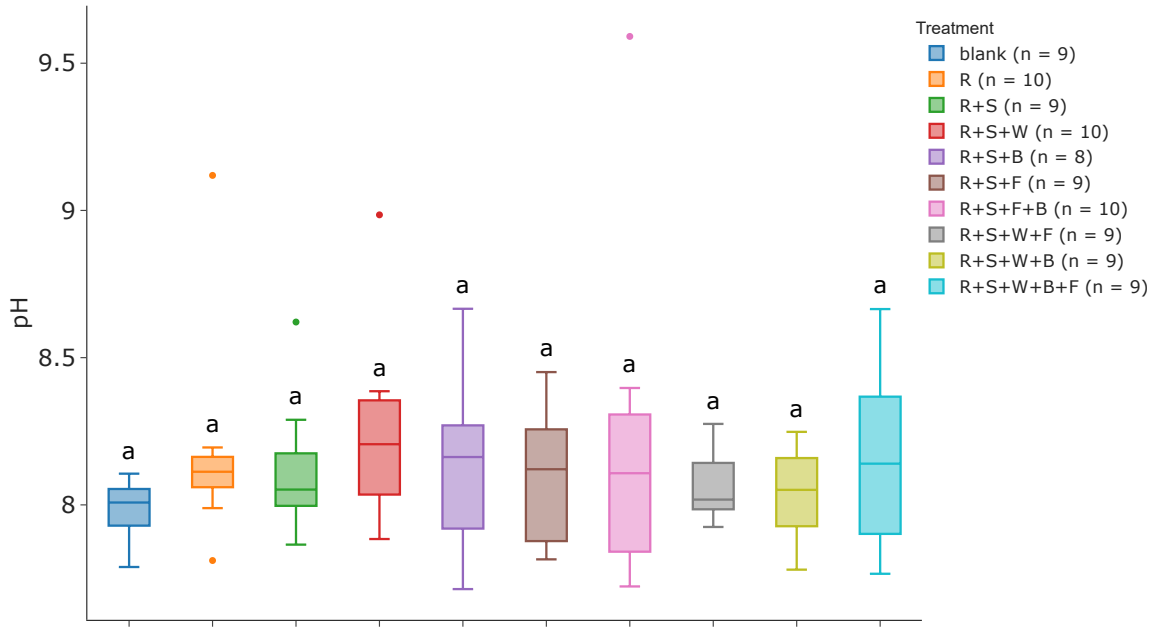


Figure 4.6: pH observed in the leachate water. Abbreviations used in the legend: R = rock, S = straw, W = worms, B = bacteria, F = fungi. Different letters indicate statistically distinct groups (ANOVA with Tukey post-hoc).

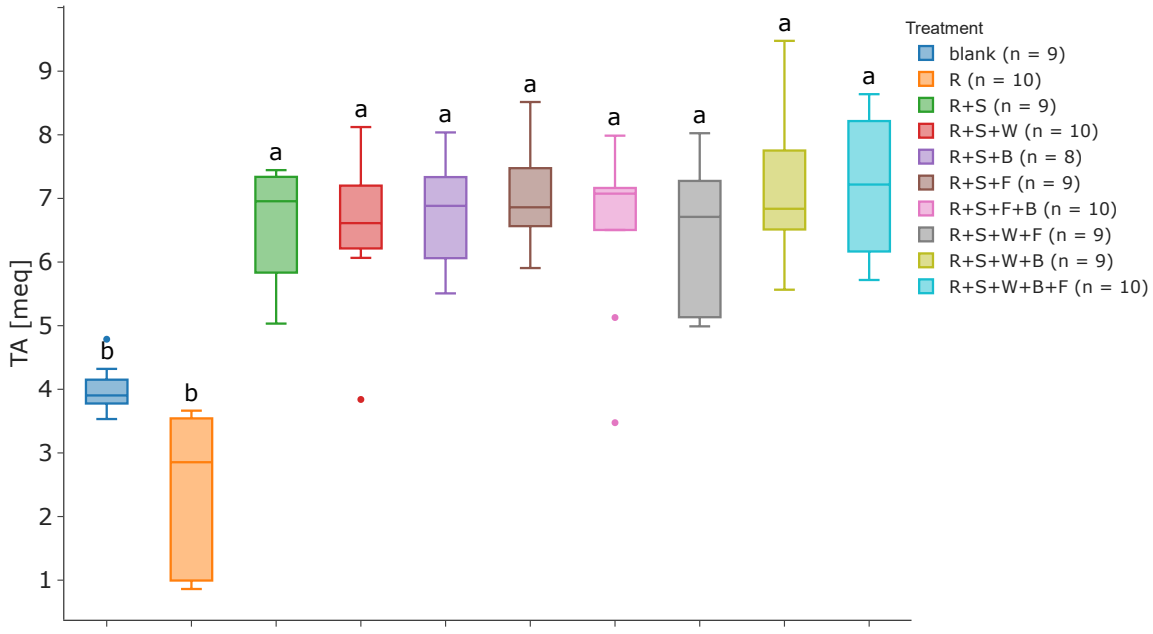


Figure 4.7: Total alkalinity (TA) observed in the leachate water. Abbreviations used in the legend: R = rock, S = straw, W = worms, B = bacteria, F = fungi. Different letters indicate statistically distinct groups (ANOVA with Tukey post-hoc).

However, for TA, there are significant changes among the treatments. Wheat straw addition

increased TA equivalents. But when comparing the biotic treatments to pure straw and rock mix, no significant increase in TA equivalents could be observed. The blank and pure rock fall into the same category, not being statistically different in the given setup. Although the TA equivalents for rock seem to be lower than the blank.

Data quality was assessed by calculating the charge balance error (CBE). The overall mean CBE of the water analyses was 0.07 %, indicating good analytical consistency. CBE values for the individual experimental groups are shown in Appendix Figure C.4.

The dissolved inorganic carbon (DIC) and dissolved organic carbon (DOC) data are not presented, as the measurements were found to be unreliable and could not be repeated due to temporal constraints. In particular, the DIC concentrations were inconsistent with the measured total alkalinity (TA), making the results implausible, especially for samples with very low DOC.

Major cations

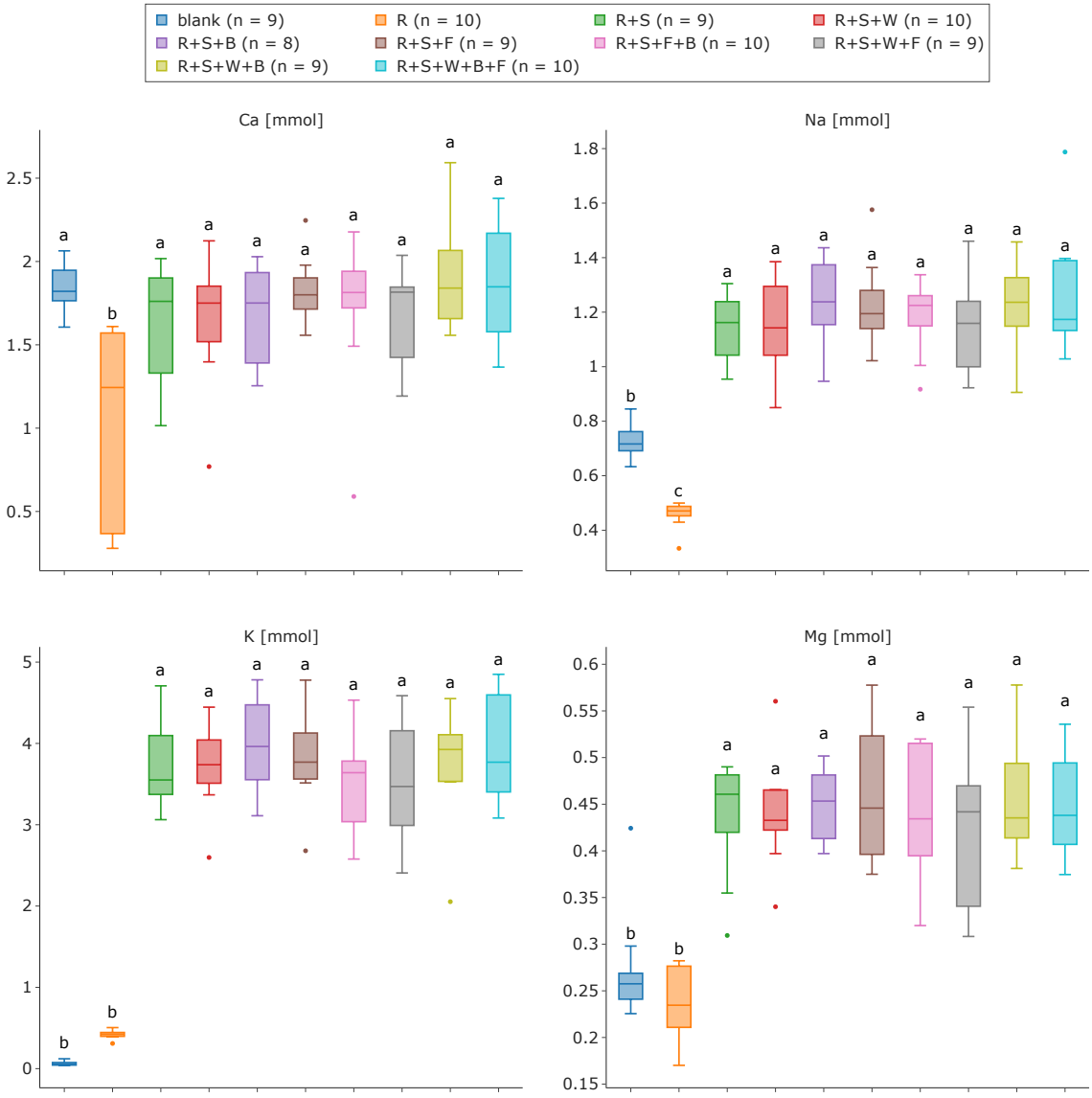


Figure 4.8: Calcium (Ca), Sodium (Na), Potassium (K), and Magnesium (Mg) observed in the leachate water. Abbreviations used in the legend: R = rock, S = straw, W = worms, B = bacteria, F = fungi. Different letters indicate statistically distinct groups (ANOVA with Tukey post-hoc).

Similar to TA or EC, cation concentrations also responded to straw addition, but not to the different biotic treatments (Figure 4.8). For calcium, all treatments containing straw showed a similar amount, while the pure rock treatment exhibited lower values. Sodium showed three statistically distinct groups: the blank, the pure rock, and the treatments with straw addition. Potassium displayed two groups, with all straw-containing treatments forming one, and the blank and pure rock treatments forming the other. Magnesium followed a similar pattern, although the effect was less pronounced.

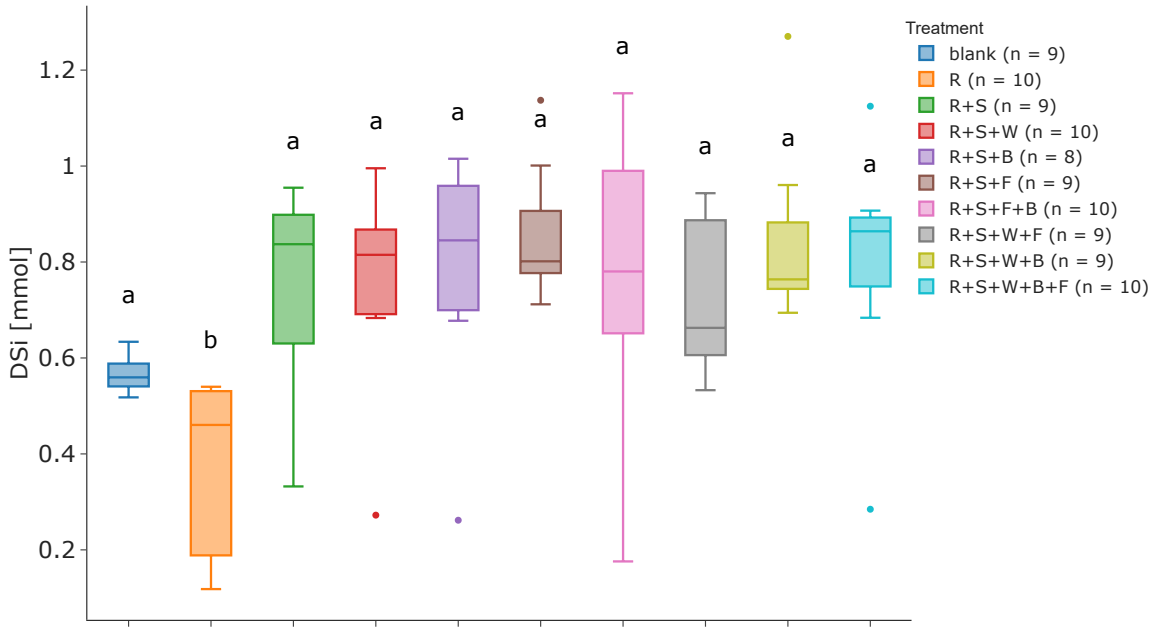


Figure 4.9: Dissolved silica (DSi) observed in the leachate water. Abbreviations used in the legend: R = rock, S = straw, W = worms, B = bacteria, F = fungi. Different letters indicate statistically distinct groups (ANOVA with Tukey post-hoc).

Dissolved silica (DSi) showed no clear response to the different biotic treatments (Figure 4.9). Owing to the large variability within some groups, the treatments with straw addition were not statistically distinct from the blank. However, the pure rock treatment exhibited a lower DSi amount compared to all other treatments.

Major anions

Among the analyzed anions, fluoride (F^-), chloride (Cl^-), nitrite (NO_2^-), nitrate (NO_3^-), and sulfate (SO_4^{2-}), only Cl^- and SO_4^{2-} were detected.

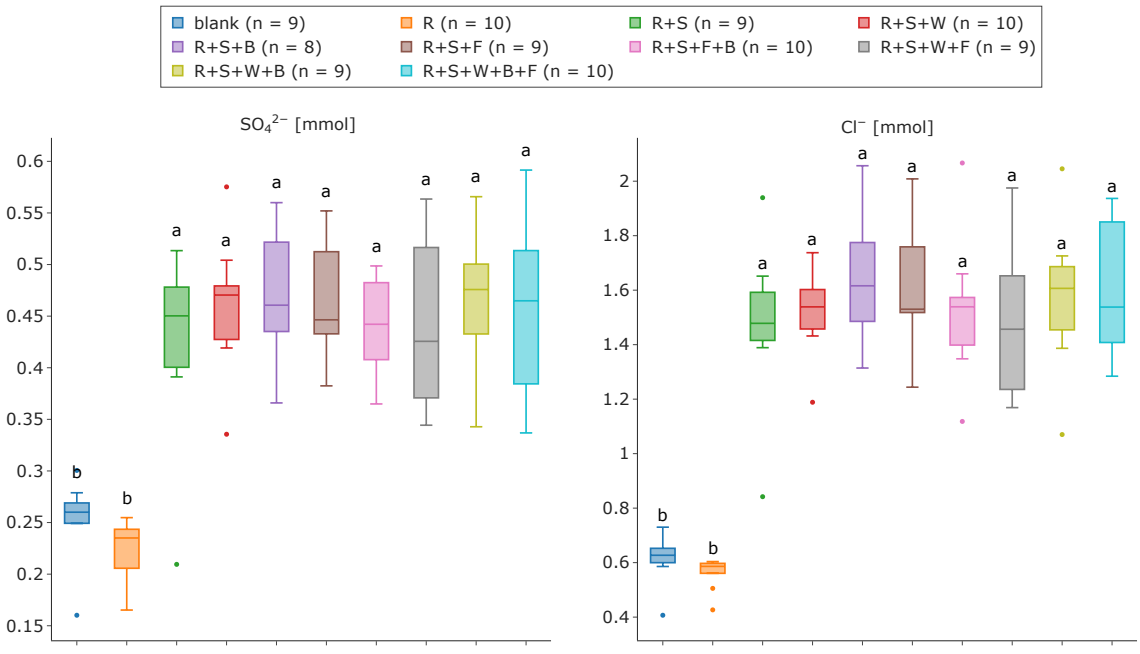


Figure 4.10: Sulfate (SO_4^{2-}) and chloride (Cl^-) observed in the leachate water. Abbreviations used in the legend: R = rock, S = straw, W = worms, B = bacteria, F = fungi. Different letters indicate statistically distinct groups (ANOVA with Tukey post-hoc).

Both sulfate and chloride amounts (Figure 4.10) followed the same trend, showing elevated values in treatments with straw addition, while remaining unaffected by the biotic factors.

4.3.3. Biological Indications

Earthworm survival and activity

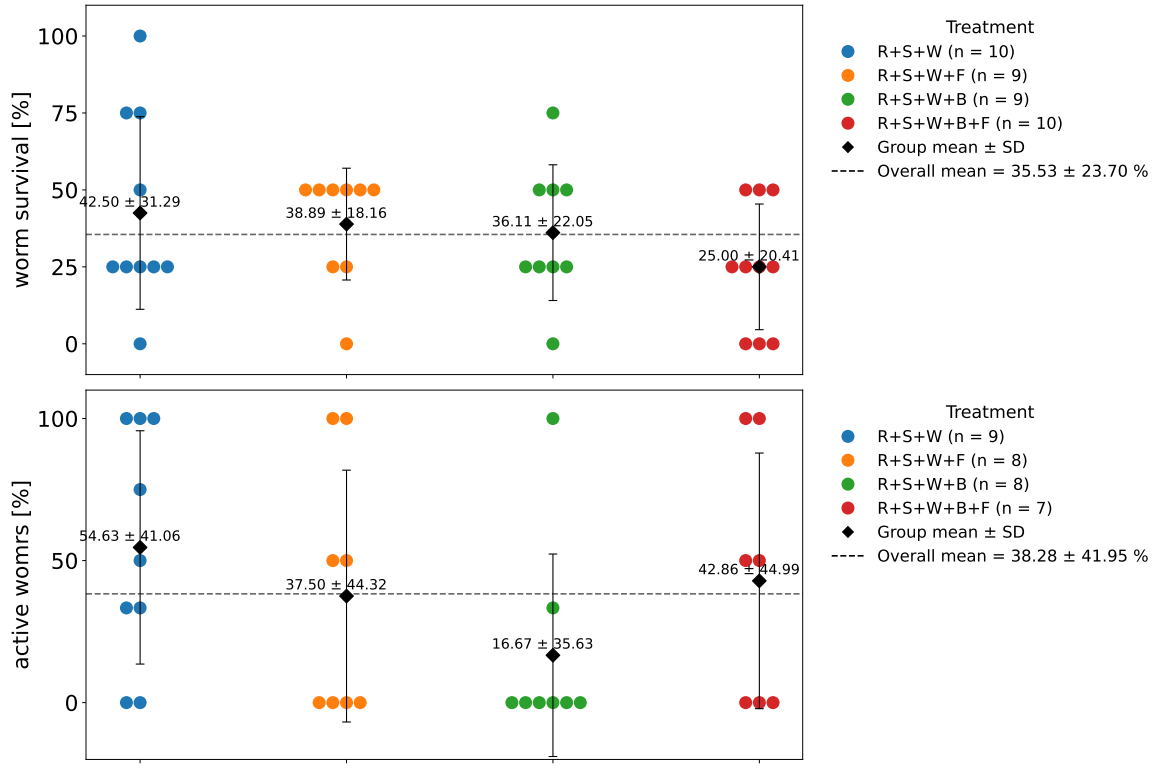


Figure 4.11: Survival and activity rate of the earthworms collected from the substrate after the experiment. Abbreviations used in the legend: R = rock, S = straw, W = worms, B = bacteria, F = fungi. Different letters indicate statistically distinct groups (ANOVA with Tukey post-hoc).

Each of the treatment groups contained four earthworms at the beginning of the experiment. The group mean values for earthworm survival range from 42.50 ± 31.29 % to 25.00 ± 20.41 % with an overall mean value of 35.53 ± 23.70 % (Figure 4.11). The earthworm activity ranges from 54.63 ± 41.06 % to 16.67 ± 35.63 % with an overall mean of 38.28 ± 41.95 %.

Microbial analysis

After the experimental run, the solid samples were also analyzed for their microbial community. The inoculated microbial species *A. pullulans* and *B. subtilis*, were either not detected or were below 0.5 % relative abundance. This is why no plots are shown with these. However, a great abundance of microbial species was found in the pure wheat straw. The eukaryotic and prokaryotic community present in the used straw is shown in Appendix Figure C.6 and Figure C.7, respectively.

4.4. Discussion

Overall, the experiment revealed three overarching treatment groups that were relevant across most variables: (1) the blank water treatment, (2) the crushed rock treatment, and (3)

the crushed rock combined with straw (with or without biota).

First, to understand the experimental outcome, it is worthwhile to examine the collected leachate water mass in the jerrycans. The automated irrigation system was programmed to dispense 50 mL of water daily over a period of 56 d, resulting in a theoretical maximum of 2.8 L. Part of this water (around 25 mL per column) can be retained by the substrate due to its remaining water-holding capacity. All experimental treatments remained below this threshold (Figure 4.4). Median water volumes for the pure rock and rock–straw mixture treatments ranged between 1.5 to 2.0 L (Figure 4.4). Although minor inaccuracies in the irrigation system cannot be ruled out, the relatively narrow distribution observed in the control columns (see blue box in Figure 4.4) suggests that technical variation alone does not account for the observed differences. The blank water flows faster through the columns because there are no rocks or straw holding it back. The substrate, on the other hand, increases retention time and extends the groundwater's exposure to the circulating warm air in the climate chamber (25 °C). At the same time, the larger surface area introduced by columns filled with substrate can lead to stronger evaporation. Both factors will lead to a loss of water from the setup, as shown in the leachate water mass (Figure 4.4).

The reduction in water mass due to evaporation results in higher concentrations of conservative compounds in groundwater. This increases the mineral saturation state, thereby increasing the likelihood of precipitation. For example, calcite is already supersaturated in groundwater, with a saturation index of ≈1. We observed slight decreases in Na, Mg, Ca, TA, DSi, Cl^-, and SO_4^{2-} for the treatment group with only crushed rocks (Figure 4.7–Figure 4.10) compared to the blank. However, only the decrease in Ca and Na was statistically significant. The concurrent decline in Ca (Figure 4.8) and TA (Figure 4.7), combined with the initially high pH and saturation index, strongly suggests that calcite precipitation occurred within the system. The decline in TA was 1.05 meq, while the decline in Ca was 0.58 mmol (1.16 eq); both changes are stoichiometrically consistent with each other. Likely, other salts also precipitated, incorporating sodium to some extent. However, this is not typically expected, as Na salts are generally highly soluble in water. A part of it might have been impurities in the carbonates.

With the straw addition to the crushed rock, the leached elements increased, but the added biota couldn't show any significant effects, which is further elaborated in the two following sections.

4.4.1. (Additional) biotic weathering effect

None of the biotic additions or their interactions increased TA significantly (Figure 4.3 and Table 4.5). The biotic effect on leached cations (Figure 4.8) was also not significant.

DNA extraction from the substrate after the experiment could reveal that the inoculated microorganisms were undetectable in the substrate. Both microorganisms, *A. pullulans* and *B. subtilis*, were either not detected or had relative abundances of less than 0.5 %. Thus, we can conclude that the added fungi and bacteria species were unable to colonize the organo-mineral mix. This can be due to multiple reasons. Either the initial present microbial species were too dominant, the setup design was not suitable for the selected microorganisms, the

wrong microbial species were selected, or the daily watering just flushed out the inoculated microorganisms. Likely, the latter was the main cause. Using ultrapure water, sterilizing the straw and rock substrate, and working with water recirculation are recommended to study their actual effects on rock weathering.

The earthworms (*A. caliginosa*) did not show a significant effect either, but their survival was extremely poor. Across all treatment groups containing earthworms, the average survival rate was 35.53 ± 23.70 %. The activity rate of the earthworms that survived was 38.28 ± 41.95 %. Both parameters indicate that the experimental setup is unsuitable for earthworms to survive and thrive. Bart et al. (2018) reported a life cycle of *A. caliginosa* of 5 months and a lifespan of more than 2 yr. Therefore, it is highly unlikely that the observed mortality resulted from natural senescence within the 56 d experimental period. Additionally, the temperature of the climate chamber in which the experiment took place (25 °C) may not have been favorable for this species. Lowe and Butt (2005) report that adults prefer temperatures between 10 to 15 °C. Furthermore, the groundwater used, with a pH of 8, might not have been optimal. G. H. Baker and Whitby (2003) found a slight aversion of another endogeic earthworm species, *Aporrectodea longa*, to soils above a pH of 7. The beneficial effects of earthworms on rock weathering should therefore be studied in a more soil-like substrate and over substantially longer durations under suitable temperature conditions.

4.4.2. Wheat straw effect

The addition of straw to the tephrite substrate increased the leached amount of K, Mg, and Na, as well as leached TA equivalents. In contrast, introducing biota did not further K, Mg, Na, and TA release. When all biotic treatments are pooled into a single group for comparison (see red boxplots in Figure 4.12), no significant increase in cation amount or TA was observed relative to the rock + straw treatment alone. Thus, the added wheat straw is considered the key driver for the observed amounts of substance and TA equivalents.

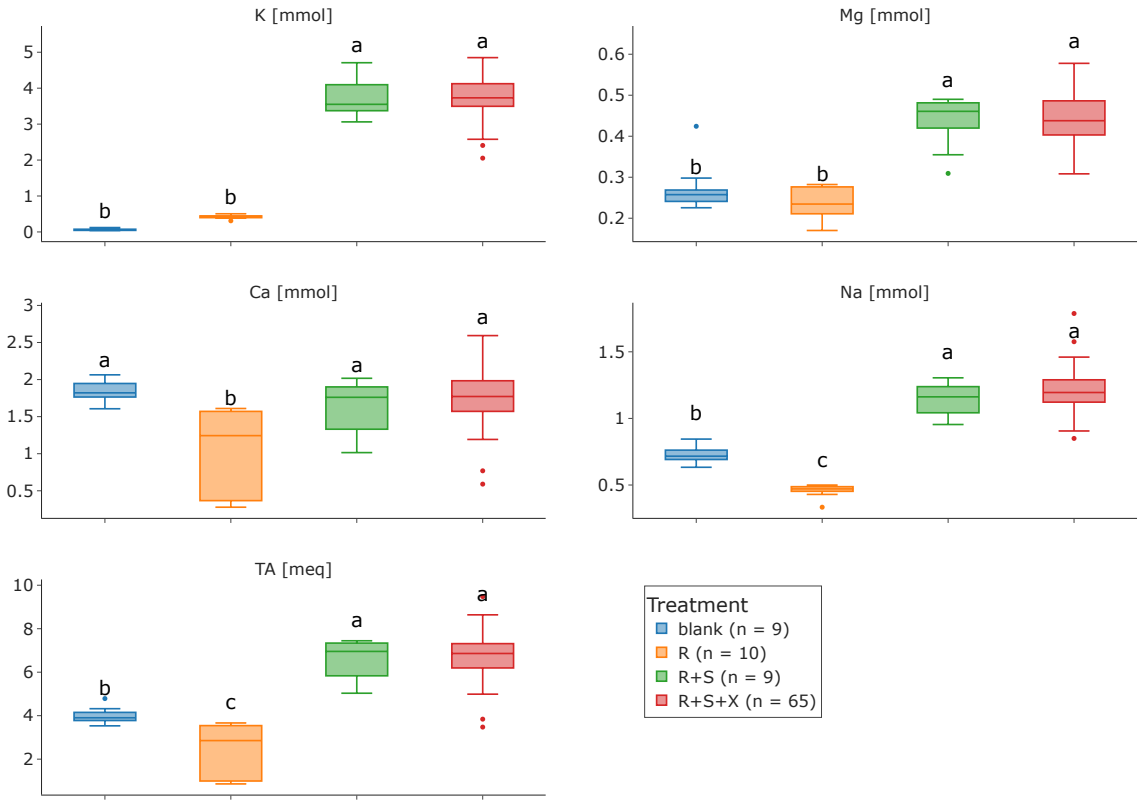


Figure 4.12: Major cations and total alkalinity (TA) observed in the leachate water. Abbreviations used in the legend: R = rock, S = straw. The group R+S+X is all biotic treatments pooled into a single group. Different letters indicate statistically distinct groups (ANOVA with Tukey post-hoc).

The straw is mainly composed of 11 to 26 % lignin, 32 to 45 % cellulose, 20 to 45 % hemicellulose, 0 to 3 % starch, 2 to 6 % protein, and 0 to 2 % ash (L. Zhang et al., 2022). Except for ash, all these components contain solely C, H, and O, and additionally N in the case of proteins. The ash content is the most interesting aspect of the weathering experiments, as it interferes with the weathering signal. Cations originating from the wheat straw therefore need to be removed from the rock weathering assessment. This separation is crucial to disentangle the signals and assess whether an additional effect on rock weathering arises from the straw. To analyze the potential additional effect, the straws' elemental composition was used (Table 4.3).

The elemental composition of pure wheat straw (Table 4.3) was analyzed to estimate the maximum amounts of Na, K, Ca, and Mg that could potentially leach from the straw alone. In each straw + rock treatment, 10 g of straw was added. This serves as a baseline to differentiate the influence of the straw from the combined effects of straw and rock. If the elemental concentrations in the straw-rock mixtures exceed both the rock-only controls and the maximum values expected from the elemental composition of straw alone, it suggests that additional processes beyond simple straw dissolution may be contributing.

The amount of monovalent cations K and Na seems to be increased above the level of

the rock only with added elemental content from the straw (Figure 4.13). The divalent cations Ca and Mg seem to be unaffected by the straw addition, as they are statistically not different. However, the release of Ca and Na amounts for rock only was even lower than in the blank, indicating precipitation of minerals. The straw was able to stop the loss. For Ca, we hypothesize that the elevated partial CO_2 pressure in the columns, resulting from straw decomposition, stopped the formation of $CaCO_3$. The biggest release was found for K, and it is in line with the leached TA equivalents.

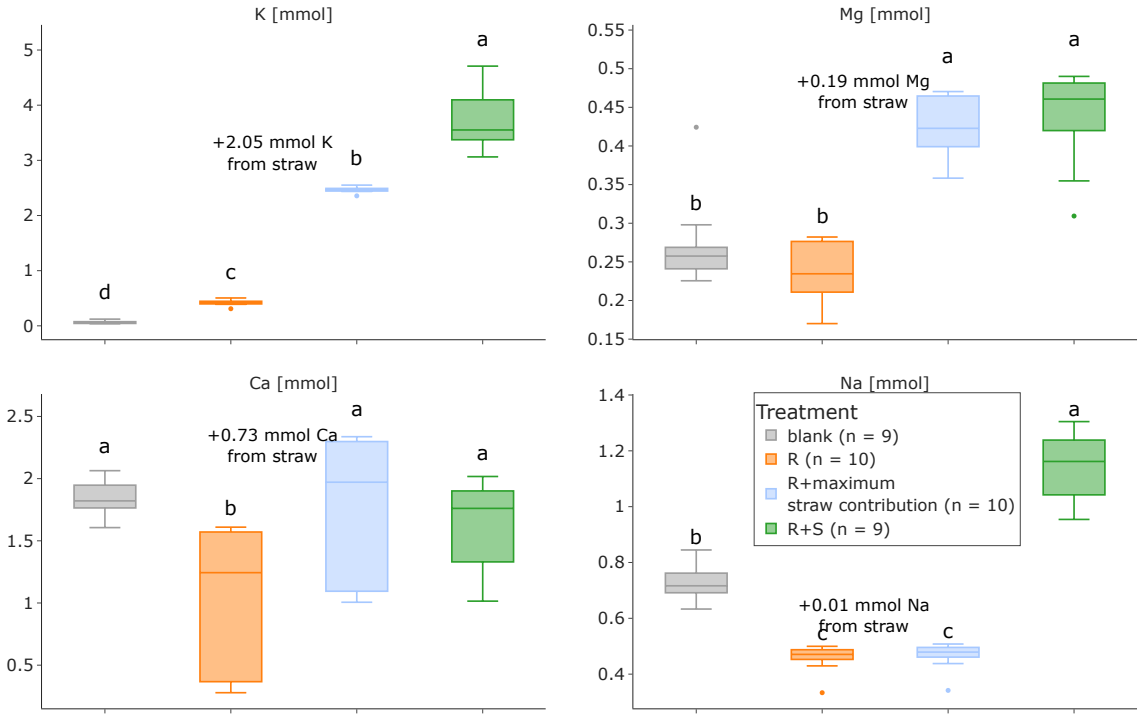


Figure 4.13: Calcium (Ca), sodium (Na), potassium (K), and magnesium (Mg) in the leachate. Abbreviations used in the legend: R = rock, S = straw. The R + maximum straw contribution group represents rock-only values adjusted by adding the theoretical elemental contribution from the wheat straw. Letters indicate statistically distinct groups (ANOVA with Tukey post-hoc test). Values in parentheses refer to the number of replicates per treatment.

Overall, the experiment was not designed to isolate the effect of straw, as the factorial setup did not include straw as an independent factor. Including straw as a separate treatment would not be meaningful, since straw serves as a food source for earthworms and microorganisms and is therefore intrinsically linked to the presence of biota. As such, straw was co-applied in all biotic treatments.

It is recommended to study the straw effect in another separate experimental design without all the biota additions. Therefore, some straw blank would be required. Only filling the used columns with wheat straw might not be sufficient for that case, as it will affect the water flow through the column, which can control the chemical reactions. Clear separation of straw derived cations (Na, K, Ca, Mg) and alkalinity from rock-derived solutes is essential to

evaluate whether straw provides a beneficial enhancement to tephrite rock weathering and alkalinity release. If a positive effect is observed, it will be important to discern whether it results from the direct biotic activity of the non-sterilized straw or from straw decomposition, which produces elevated CO_2 partial pressure, lower pH, and consequently higher dissolution rates. Furthermore, future work in microbially enhanced weathering (MEW) aimed at CO_2 removal rather than just element release should always quantify the carbonate contribution to total alkalinity by using DIC, pH, and temperature to distinguish true carbonate alkalinity from non-carbonate alkalinity sources.

4.5. Conclusion

In the conducted weathering experiment, which lasted 56 days, the added biota did not show a significant effect on the weathering process. None of the treatments, including microorganisms (*Aureobasidium pullulans* and *Bacillus subtilis*), and endogenic earthworms (*Apporrectodea caliginosa* [Savigny]), increased the release of Na, K, Ca, Mg, or TA. The added fungi and bacteria were unable to colonize the substrate, as evidenced by the microbial community analysis. Similarly, earthworms did not thrive under the experimental conditions, with a mean survival rate of 35.53 ± 23.70 % and a mean activity level of 38.28 ± 41.95 % among the surviving individuals.

However, the addition of wheat straw might have enhanced the dissolution of the tephrite rock substrate, evidenced by the elevated leached K amount and TA equivalents. The native microbial community introduced together with the straw likely produced CO_2 and organic acids, thereby enhancing rock weathering beyond what atmospheric CO_2 alone would generate. To clearly isolate and quantify the role of straw, its presence should be included as an explicit factor in a full factorial experimental design. This would allow for the disentangling of the leached elements and total alkalinity derived from the straw itself from any symbiotic effects with the rock substrate.

5

Using Electrical Conductivity as a predictor for Total Alkalinity in controlled ERW systems

Abstract

Total alkalinity (TA) is widely used to infer carbon dioxide (CO_2) removal in enhanced rock weathering (ERW) systems. Its determination relies on destructive titration methods that require substantial sample volumes and are time-consuming. Moreover, achieving high temporal resolution is challenging, as TA measurements require discrete sampling, acidification, and offline analysis. In contrast, electrical conductivity (EC) can be measured directly in flowing water streams without sample preparation, enabling continuous, non-destructive, high-frequency monitoring. However, the applicability of EC as a proxy for TA depends on solution chemistry and rock or feedstock composition.

Here, we investigate the relationship between EC and TA in a controlled rock-weathering reactor experiment conducted under constant CO_2 partial pressure and temperature using a peridotite feedstock rich in olivine/forsterite. Measurements of EC, TA, and major dissolved cations were combined with aqueous speciation modeling to evaluate the conditions under which EC can reliably predict TA and the associated CO_2 uptake.

For homogeneous materials, alkalinity and dissolved cations are released in a constant stoichiometric ratio, resulting in a stable and predictable EC–TA relationship. Under these conditions, temperature-corrected EC serves as a robust proxy for TA. In contrast, heterogeneous rocks composed of multiple mineral phases exhibit time-dependent EC–TA relationships driven by the sequential dissolution of minerals with differing dissolution rates, requiring periodic recalibration of EC-based TA estimates. In more complex systems such as soils, agricultural practices including fertilization, organic amendments, or tillage can introduce dissolved ions that are not derived from the ERW rock feedstock. Such external ion inputs alter solution composition and destabilize the EC–TA relationship, thereby limiting the reliability of EC as a proxy for TA.

5.1. Introduction

Total alkalinity (TA) is a widely used proxy for quantifying CO_2 uptake in enhanced rock weathering (ERW) applications ((Amann and Hartmann, 2022; Dupla et al., 2025; Hasemer, Borevitz, and Buss, 2024; Larkin et al., 2022; Maxbauer et al., 2026; Te Pas et al., 2025; Vienne et al., 2022). However, TA determination by potentiometric titration is inherently destructive, as the sample must be acidified to the equivalence point. Typical titration volumes are on the order of 25 mL (APHA, AWWA & WEF, 2017), although the required volume ultimately depends on the titration setup, expected alkalinity range, and electrode configuration. The aqueous sample must be sufficiently large to ensure proper immersion of the pH electrode, adequate mixing, and reliable acid delivery.

Because each measurement consumes a discrete sample aliquot, direct TA determination becomes labor-intensive and sample-consuming when applied at high temporal resolution. Consequently, continuous or in-line monitoring of TA is analytically challenging compared to non-destructive parameters such as electrical conductivity.

For water samples, it has been shown that EC can be a robust proxy for bulk solution chemistry. It is a collective measure of dissolved ions (Hem, 1982). It has long been used as a reliable estimator of total dissolved solids in waters (J. D. Rhoades, 1996; Thirumalini and Joseph, 2009; Walton, 1989). A closely related example is the laboratory assessment of soil salinity using EC measurements of aqueous soil extracts (D. L. Corwin and Yemoto, 2020)). Another prominent example is in ocean science, where EC is a standard parameter measured routinely using conductivity–temperature–depth (CTD) sensors (S. Xiao et al., 2023). In this context, EC is used to derive practical salinity (Lewis, 1980), which reflects the concentration and composition of dissolved ionic constituents in seawater.

TA and EC are mechanistically linked. In weathering systems composed of a homogeneous feedstock, mineral dissolution releases cations and associated alkalinity-generating species in constant stoichiometric proportions. For example, the dissolution of forsterite by carbonic acid (Equation 5.1) produces two Mg^{2+}, four HCO_3^-, and dissolved silica (H_4SiO_4) per mole of mineral dissolved.

As a consequence, the relative ionic composition of the solution remains stable over time, and EC increases proportionally with the concentration of dissolved ions. Under such conditions, a stable EC–TA relationship emerges, allowing EC to serve as a proxy for both total dissolved ion concentrations and total alkalinity.

$$Mg_2SiO_4(s) + 4\,CO_2(g) + 2\,H_2O \longrightarrow 2\,Mg^{2+} + 4\,HCO_3^- + H_4SiO_4(aq). \tag{5.1}$$

The EC of an aqueous solution can be calculated by taking the molar conductivities (Λ_i) of each ion present in the solution and multiplying it by the molality of the species (m_i (Equation 5.2).

$$EC = \sum_i \Lambda_i(T, I) \times m_i \tag{5.2}$$

The molar ionic conductivity (Λ_i) of the dissolved species depends on the specific ion, temperature, and the ionic strength of the solution (McCleskey, Nordstrom, and Ryan, 2012). Consequently, each ion contributes individually to the overall EC according to its charge and mobility (see Table 5.1).

Table 5.1: Molar conductivities (Λ) for selected ions at infinite dilution (Vanysek, 1993)

Ion	Λ at 25 °C ($S\,cm^2\,mol^{-1}$)
HCO_3^-	44.5
Na^+	50.08
K^+	73.48
Mg^{2+}	106
Ca^{2+}	118.94
CO_3^{2-}	138.6
OH^-	198
H^+	349.65

Because different aqueous species exhibit distinct molar conductivities, changes in ionic composition or speciation can alter EC even at constant total solute concentration. This implies that EC not only reflects total dissolved ion content but may also provide indirect information on shifts in aqueous speciation.

EC measurements are typically temperature-compensated and reported at a reference temperature of 25 °C to facilitate comparison among measurements made at different temperatures (McCleskey et al., 2012). Different methods can be used to correct to the reference temperature of 25 °C (*DIN EN 27888* 1993).

The relationship between EC and TA has been investigated in a range of aquatic and geochemical studies (Amann and Hartmann, 2022; Bouillon et al., 2014; Proulx et al., 2018; Sechriest, 1960). In the context of enhanced rock weathering, Amann and Hartmann (2022) applied this approach to leachate samples from column experiments filled with crushed rock substrate, where solute release was largely controlled by mineral dissolution.

In contrast, soil systems are considerably more complex. Soil porewater contains dissolved species originating not only from the applied rock feedstock but also from organic matter turnover, fertilizer inputs, atmospheric deposition, and microbial processes. These additional ion sources alter the ionic composition independently of silicate weathering and decouple EC from alkalinity production, thereby limiting the robustness of EC as a proxy for TA in soil environments (Rieder, Amann, and Hartmann, 2024).

Unlike soil-based systems, this experiment was conducted in a purely inorganic reactor using only crushed olivine-rich rock and demineralized water. No soil, organic amendments, biota, or fertilizers were present. This highly controlled setup isolates rock weathering as the sole source of dissolved ions, allowing us to directly test whether EC can serve as a robust predictor of TA and associated CO_2 uptake.

5.2. Materials and Methods

5.2.1. Experimental setup

We conducted experiments in a closed, continuously mixed, flow-through-recirculating reactor (working water mass around 25 kg of water) operated at ambient temperature and pressure (Figure 5.1). The headspace was continuously flushed with CO_2 at 1 atm with 0.1 NL/min, while the granular rock substrate was mixed at 0.1 rpm, to avoid the development of preferential pathways through the substrate. The leachate water was recirculated in the system at 1 200 L h^{-1}. At the top of the reactor, the recirculated leachate water was distributed via drippers to ensure uniform wetting and mixing across the substrate.

At the start of the experiment, the reactor's solid basin was filled with 42 kg of granular peridotite rock substrate (section subsection 5.2.2). Then the reactor was sealed to make it airtight. The liquid basin was filled with 25 kg of demineralized water. Then, the reactor headspace was purged with CO_2 to displace the ambient air, thereby establishing a CO_2 partial pressure of 1 atm.

Under these conditions, the flow-through reactor was operated continuously for 31 days. Reactor leachate was discharged 3 times per week (Monday, Wednesday, Friday) at around $\approx$ 2-day intervals; when a weekend intervened, the interval was extended to 3 days. This produced a recurring discharge schedule of 2, 2, and 3 days (repeating). Due to residual dead volume in the leachate collection basin, remaining pore water within the rock substrate, and water retained in the tubing (approximately 3 L in total), the system cannot be completely drained during emptying. As a result, the solute concentrations in the reactor do not decrease to the low levels expected after refilling with demineralized water, because residual leachate is present in the subsequent cycle. The discharged leachate mass was quantified gravimetrically using a weighing scale.

During the study period, the reactor was flushed 14 times. These flushing events are critical for carbon accounting because they define the moments at which TA and associated carbon species are exported from the reactor. The total CO_2 removed is quantified at these time points based on the discharged water mass and the corresponding TA concentration.

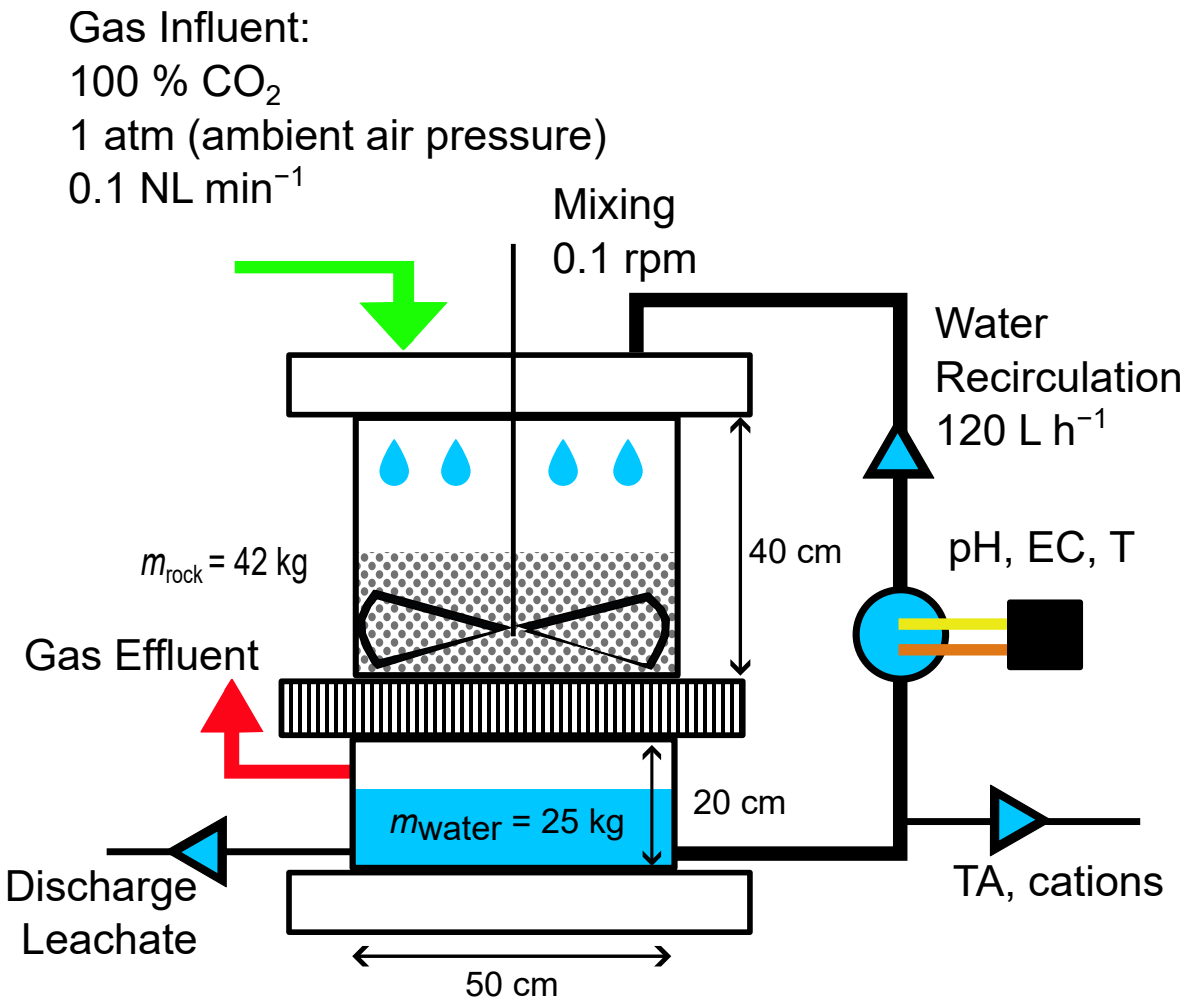


Figure 5.1: Flow-through reactor setup that was used for the experiment.

5.2.2. Rock type

The granular rock substrate used was provided by Sibelco and is marketed under the commercial name *Olivine*. It was mined near Åheim, Norway, from an open-pit mine (62.003 6° N, 5.580 3° E). It has a grey-green color (Supplementary Figure D.1), consistent with its high olivine content. Petrographically, it is a plutonic ultramafic igneous rock and is classified as peridotite. By the IUGS classification dunite is defined as peridotite with 90 to 100 vol % of olivine (Le Maitre et al., 2002; Streckeisen, 1973). Our rock sample contains 86.85 % (by mass) olivine (forsterite) and is therefore very close to the compositional boundary of the dunite field (see Table 5.2). Although formal ultramafic rock classification is based on modal volume percentages, conversion from weight to volume percent would only slightly reduce the olivine proportion and would not substantially alter the petrographic interpretation. Given natural small-scale heterogeneity within the deposit, adjacent material could plausibly meet the ≥ 90 % (by volume) criterion. Accordingly, the sample can be described as an olivine-dominated peridotite, approaching dunite composition.

The high content of forsterite makes this rock substrate an interesting material for carbon dioxide removal applications, as it dissolves comparably fast with a rate $logR = -8.603\,\mathrm{mol\,m^{-2}\,s^{-1}}$ at pH = 5 and $T = 25\,^{\circ}\mathrm{C}$ (Rimstidt, Brantley, and Olsen, 2012). The dissolution of forsterite releases magnesium (Mg) which is beneficial as it generally will not form solid carbonates at ambient temperature. Anhydrous magnesite ($MgCO_3$) needs elevated temperatures and pressure to form (Giammar, Bruant, and Peters, 2005; O'Connor et al., 2002; Pokharel et al., 2019; Rimstidt, Brantley, and Olsen, 2012; Sanna et al., 2014), typically requiring temperatures above 100 °C and CO_2 pressures more than 100 bar (Entezari Zarandi et al., 2017; Scott et al., 2021). Under atmospheric or near-atmospheric conditions, hydrated Mg carbonates such as nesquehonite may form (Entezari Zarandi et al., 2017; Scott et al., 2021).

However, the present study focuses exclusively on the generation and export of TA in the aqueous phase. Carbonate precipitation removes TA from solution and therefore represents unrealized TA in our TA-based carbon accounting. Accordingly, the system is conceptually simplified to the reaction of carbonic acid with forsterite (Equation 5.3), considering only the dissolved products.

$$Mg_2SiO_4(s) + 4\,CO_2(g) + 2\,H_2O \longrightarrow 2\,\mathbf{Mg^{2+}} + 4\,\mathbf{HCO_3^-} + H_4SiO_4(aq). \tag{5.3}$$

Table 5.2: The bulk mineralogical composition was determined by X-ray diffraction (XRD) using a Bruker D8 Advance diffractometer equipped with an XE-T detector and Cu-Kα radiation. Prior to analysis, rock samples were finely ground in a wet milling device using alcohol, followed by controlled drying to minimize preferred orientation effects ($n = 2$).

Group	Mineral	Formula	mass %
	Quartz	SiO_2	
	K-feldspar	$KAlSi_3O_8$	
	Plagioclase	$(Na,Ca)(Si,Al)_4O_6$	
	Clinopyroxene	$(Ca,Na)(Mg,Fe,Al,Ti)(Si,Al)_2O_6$	1.2
	Orthopyroxene	$(Ca,Na)(Mg,Fe,Al,Ti)(Si,Al)_2O_7$	4.65
Silicates	Amphibole	$Ca_2(Mg,Fe)_5Si_8O_{22}(OH)_2$	
	Forsterite	$(Mg,Fe)_2SiO_4$	86.85
	2:1 layer silicates	$(K,H_3O)(Al,Mg,Fe)_2(Si,Al)_4O_{10}[(OH)_2,H_{20}]$	2.5
	Chlorite	$(Mg,Fe)_5Al(Si_3Al)O_{10}(OH)_8$	2.25
	Serpentine	$(Mg,Fe,Ni,Mn,Al,Zn)_3[Si_2O_5](OH)_4$	2.05
	Talc	$Mg_3Si_4O_{10}(OH)_2$	0.5
Carbonates	Dolomite/Ankerite	$Ca(Fe_x^{2+},Mg_{1-x})(CO_3)_2$	
Sum			100

Table 5.3: Elemental composition of the rock was measured using X-ray fluorescence (XRF) measurements. (nd = below detection limit, LOI = loss of ignition, i.e., heating the sample to 1 000 °C to gas out all carbon) (n = 3).

Elements	mass %
SiO_2	41.55 ± 0.23
TiO_2	0.02 ± 0.01
Al_2O_3	0.78 ± 0.01
Fe_2O_3	7.26
MnO	0.09
MgO	47.87 ± 0.24
CaO	0.35 ± 0.19
Na_2O	0.03
K_2O	0.03 ± 0.01
P_2O_5	0.01
SO_3	nd
LOI	1.80 ± 0.13
Sum	99.78 ± 0.12

5.2.3. Measurements

In the reactor leachate, pH, electrical conductivity (EC), temperature (T), total alkalinity (TA), and the major cations Na^+, K^+, Ca^{2+}, and Mg^{2+} were measured. EC was monitored inline using a JUMO BlackLine CR-GT probe (Series 202922), pH with a JUMO tecLine electrode (Series 201020), and temperature with a JUMO compensation thermometer (Series 201085). All probes were installed in a single flow-through chamber (Figure 5.1) and recorded at 15 s intervals.

TA was determined by automated Gran titration using four endpoints (pH 4.5, 4.3, 4.0, and 3.7) with a Metrohm 2035 Process Analyzer. As TA analysis is destructive and time-intensive, measurements were performed every 3 h, beginning with the discharge event preceding each flushing cycle. The TA is measured in line in a processing line together with the cations.

Base cations (Na^+, K^+, Ca^{2+}, and Mg^{2+}) were quantified by ion chromatography (930 Compact IC Flex, Metrohm) using a Metrosep C6–150/4.0 column. Cation concentrations were measured every 1.5 h between successive discharge events.

Major anions were not quantified, as the feedstock contains negligible amounts of sulfur, phosphorus, and organic constituents (Table 5.3). The analytical dataset exhibits a mean charge balance error (CBE) of 1.34 % (Appendix Figure D.2) when anion concentrations are assumed to be zero in Equation 5.4. This low CBE indicates that unmeasured anionic species are minor. Substantial concentrations of unaccounted anions would have resulted in a pronounced positive charge balance error.

$$\mathrm{CBE} = \frac{\sum \text{cations} - (\sum \text{anions} + TA)}{\sum \text{cations} + (\sum \text{anions} + TA)} \cdot 100 \tag{5.4}$$

5.2.4. Data treatment

Before analyzing the dataset, the data needed to be homogenized, given the different sampling frequencies of the parameters.

First, the data were resampled on a 30 min temporal resolution using Python with the pandas library (version 2.2.3) (McKinney, 2010). Median values were used to obtain representative measurements on a common time grid across all sensors, as this approach is more robust to short-term fluctuations and rapid transitions compared to a mean approach. Second, for the calibration between EC and TA, data points within 1 h before and after discharge events were excluded. These transition periods are non-representative due to the water replacement and a temporal mismatch between EC and TA measurements. After the discharge, fresh demineralized water is pumped into the system, diluting the residual leachate water within the reactor system. In addition, time is required for the new solution to equilibrate with the elevated pCO_2 conditions. Because EC, temperature, and pH are measured inline within a dedicated chamber, the recirculation pump must first replace the residual water in this chamber before the recorded EC corresponds to the TA of the newly equilibrated leachate (Figure 5.1). Only after this flushing and equilibration phase do EC and TA reflect the same water composition.

The excluded data points are indicated in the EC–TA calibration diagram. Based on the derived EC–TA calibration function, TA was predicted for the entire time series. This enabled a direct visual comparison with the measured data and allowed missing TA values to be reconstructed from the EC–TA relationship.

Prior to filtering, a total of 157 TA data points were available. After exclusion of non-representative samples, 133 data points remained for the EC–TA calibration. With the relationship, TA could then be recovered and calculated on 30 min timesteps like EC, leading to a time series of 1491 datapoints.

In a subsequent step, the whole predicted TA time series was analyzed to identify local maxima using the SciPy library in Python (Virtanen et al., 2020). These peaks in concentrations were then used together with the discharged water mass to calculate the total TA fluxes and CO_2 removal.

5.2.5. Calculation of CO_2 removal

Because the setup includes only demineralized water and a forsterite-dominated rock, we can assume that acid-base systems other than the carbonate system are irrelevant. Therefore, we. take the TA as a proxy for the sequestered CO_2 in the water.

The reactor operates at elevated pCO_2, resulting in a relatively low pH of the leachate water. Under these conditions, most TA will be held by HCO_3^- and the contribution of

CO_3^{2-} to TA will be minor. Importantly, the CO_2 quantified via TA does not represent the total dissolved inorganic carbon (DIC) of the closed carbonate system. Rather, it reflects only the alkalinity-derived carbon generated by mineral dissolution, i.e., the fraction of DIC that is charge-balanced by weathering-derived base cations. Within the closed, pressurized reactor system, the carbonate system can therefore be simplified by assuming a 1:1 stoichiometric relationship between TA and stored CO_2 (i.e., 1 eq TA corresponds to 1 mol CO_2).

Upon discharge, however, the leachate comes into contact with atmospheric pCO_2. The resulting degassing increases the pH and shifts carbonate speciation toward a higher fraction of $CO3^{2-}$. Because $CO3^{2-}$ contributes two equivalents of alkalinity per mole of carbon, the effective stoichiometric CO_2–TA conversion factor ($\gamma(CO_2/TA)$) decreases toward 0.5 (i.e., 1 eq TA corresponds to 0.5 mol CO_2). Depending on the discharge pH and the extent of dilution, γ therefore ranges between 1 and 0.5. In general, the lower the TA concentration and the more diluted the solution (low pH), the closer this ratio approaches 1, as alkalinity is then predominantly present as HCO_3^-.

In addition, dissolved inorganic carbon (DIC) not associated with TA will degas upon lower pCO_2. If dilution is limited, elevated carbonate ion concentrations may further promote secondary carbonate precipitation, which can also constrain the net CO_2 storage.

For the CO_2 removal assessment, the peak TA measured immediately prior to each discharge event was used. This value represents the maximum alkalinity generated while the water remained in contact with the rock and thus reflects the cumulative TA production within the quantification interval. Therefore, the pre-discharge TA peak provides the most representative measure of TA generation and associated CO_2 uptake for each cycle.

This peak TA concentration at discharge was multiplied by the corresponding discharged water mass to obtain the total amount of alkalinity exported from the system (in eq). This value was then converted to captured CO_2 using the stoichiometric conversion factor γ, assumed to be 1 molCO_2 per eq TA. Finally, the resulting molar amount of CO_2 was converted to mass using the molar mass of CO_2 (Equation 5.5).

$$m_{CO_2,i}\,[g] \;=\; TA_i \;\cdot m_{\text{water},i} \cdot \gamma \cdot M_{CO_2} \tag{5.5}$$

The mass-specific CO_2 capture was calculated as the ratio of captured CO_2 mass to applied rock mass. For reporting, results are expressed in kg CO_2 per ton of rock.

$$C_{CO_2,\ rock} = \frac{m_{CO_2}}{m_{\text{rock}}} \tag{5.6}$$

5.3. Results

5.3.1. Time series of chemical parameters

TA, EC, and pH showed a repeating sawtooth-like pattern over time, characterized by abrupt decreases during discharge events followed by a gradual recovery in between flushes

(Figure 5.2). The three variables evolved in parallel, indicating that they are not independent but chemically coupled.

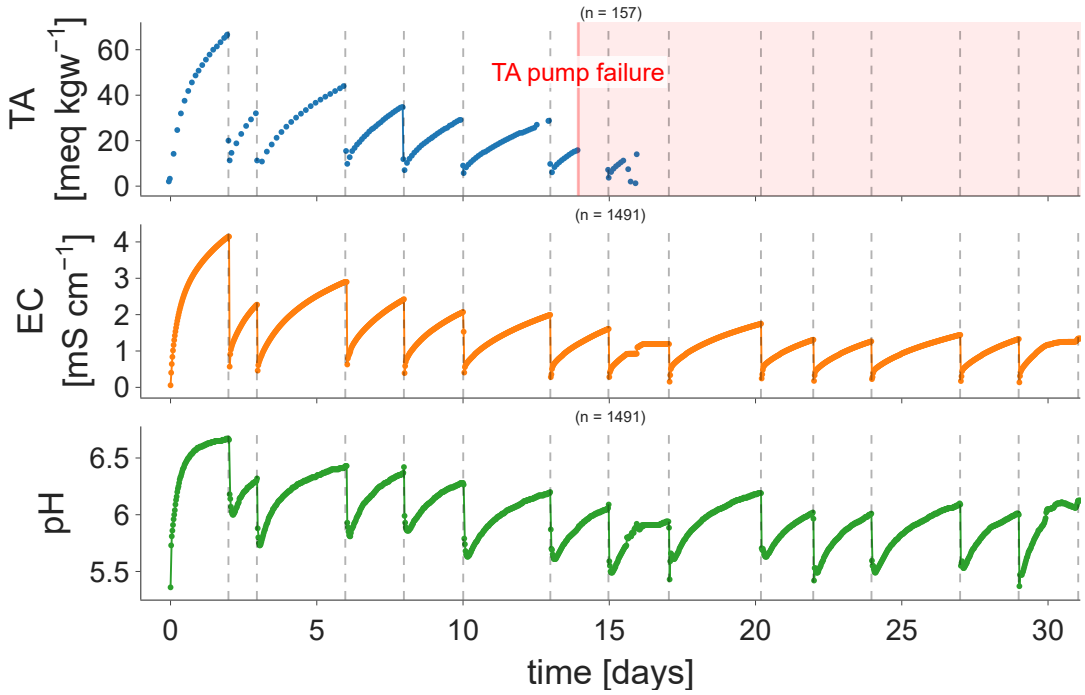


Figure 5.2: Total alkalinity (TA), electrical conductivity (EC), and pH measured in the leachate water in the liquid basin. The dashed gray lines indicate the leachate discharge times. The red shaded area indicates the time period where TA data are unavailable or not representative.

The base cations exhibited the same repeating sawtooth-like pattern over time as pH, TA and EC, but interestingly, their relative contributions changed over time. Magnesium (Mg^{2+}) was consistently the dominant released cation and remained at the highest concentrations across all discharge cycles, followed by potassium (K^+) and then calcium (Ca^{2+}) (Figure 5.3). In contrast, sodium (Na^+) exhibited rapid washout: concentrations were initially higher than those of K^+ during the first cycle but declined across successive cycles, reaching the lowest levels among all cations by the end of the experiment. Similarly, K^+ concentrations decreased over time; although K^+ initially exceeded Ca^{2+} concentrations in the first cycle, it subsequently fell to concentrations comparable to those of Ca^{2+} in later cycles.

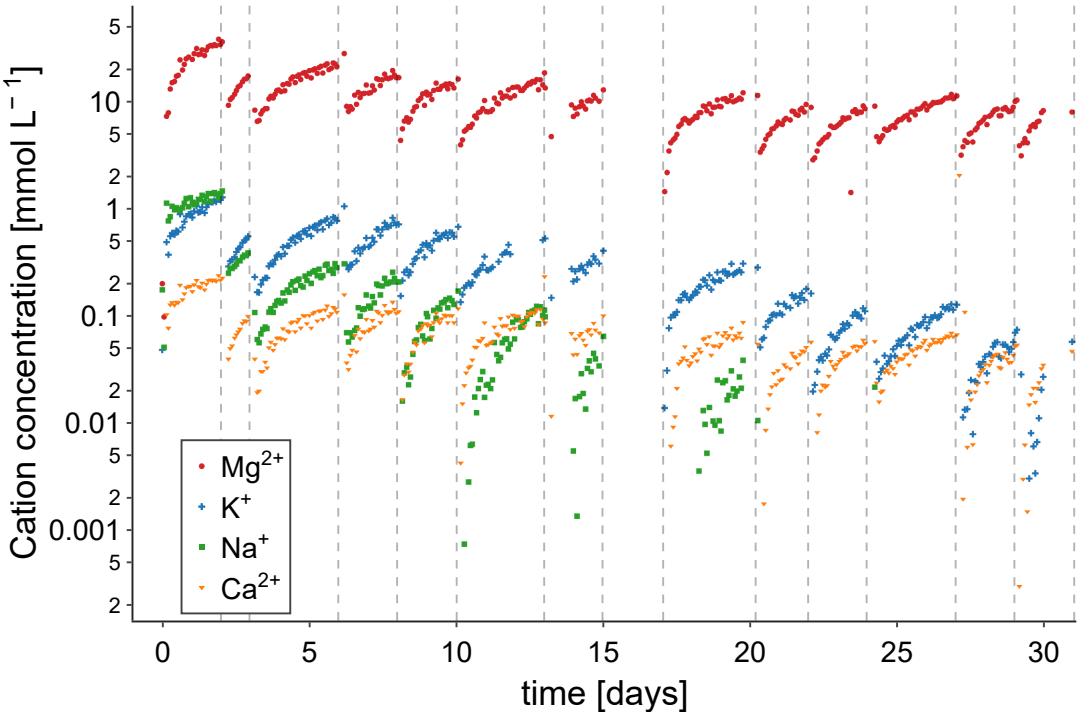


Figure 5.3: Base cation concentrations (Na^+, K^+, Ca^{2+}, and Mg^{2+}) measured in the leachate water during the experiment.

5.3.2. EC-TA calibration

For the EC–TA calibration, both linear and quadratic regression models were evaluated. The quadratic fit yielded a lower residual sum of squares and a higher coefficient of determination (R^2) compared to the linear model, indicating an improved representation of the observed relationship. The datapoints excluded from the calibration (i.e., those associated with transition periods around discharge events) clearly deviate from the main trend and fall outside the fitted curve, supporting their classification as non-representative (grey points in Figure 5.4). Overall, EC and TA exhibit a strong and consistent correlation within the representative dataset, confirming the suitability of EC as a predictor for TA under stable reactor conditions.

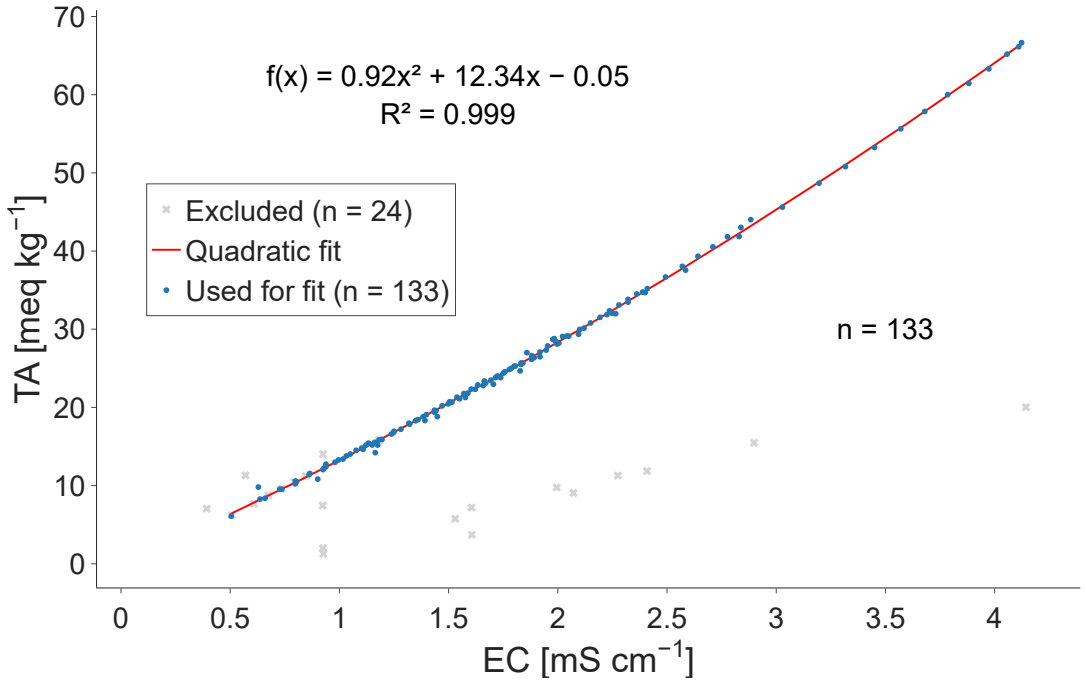


Figure 5.4: Electrical conductivity (EC) and total alkalinity (TA) calibration for 1 atm CO_2 and $T = 25\,°C$.

The model performance was evaluated using the coefficient of determination (R^2), root mean square error (RMSE), mean absolute error (MAE), mean error (bias), and median absolute percent error (MdAPE).

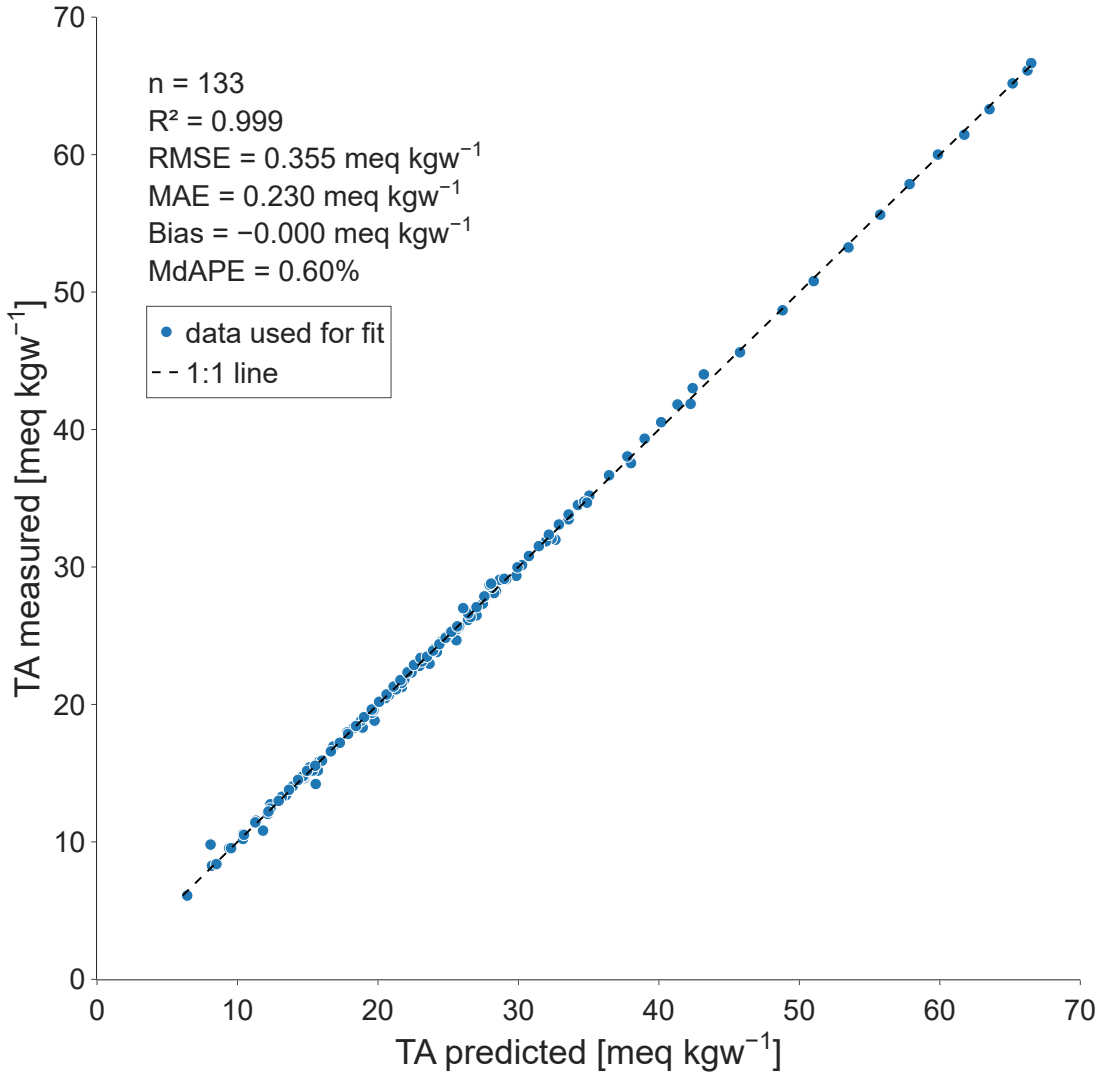


Figure 5.5: Comparison of measured and EC-predicted total alkalinity (TA) using a quadratic calibration model. Performance metrics (R^2, RMSE, MAE, bias, and MdAPE) are shown in the panel. The dashed line indicates the 1:1 agreement between prediction and observation.

The calibration enabled to predict the TA data that were lacking due to malfunctioning of the pump. One can see that the prediction is following the observations to a good extent (Figure 5.6).

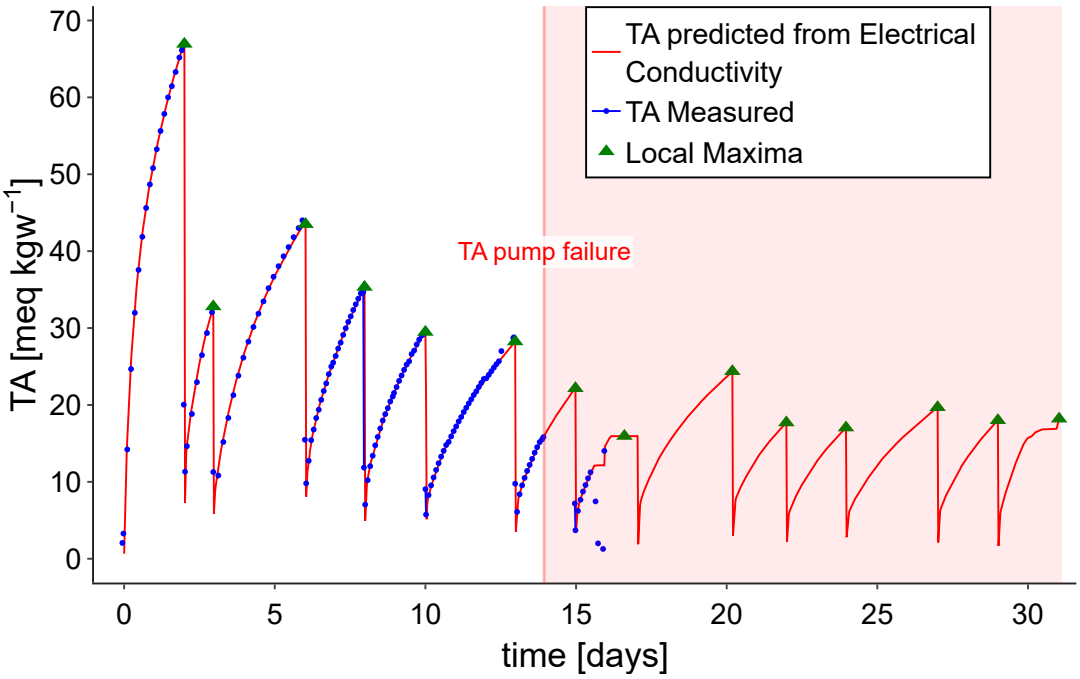


Figure 5.6: Time series of predicted total alkalinity (TA) with measured TA. The green triangles indicate the maximum TA reached before a discharge event. The red shaded area indicates periods where TA data are unavailable or not representative.

The identified TA peaks (local maxima) are indicated in the TA prediction time series as green triangles (see Figure 5.6). These peaks were used together with the extracted water mass to calculate the CO_2 removal in Figure 5.7.

5.3.3. CO_2 removal

The carbon dioxide removal (CDR) assessment of the experiment is shown in Figure 5.7. It is based on the peak TA concentrations and water mass. With 41 904 g of rock used in the setup in the 31 d a cumulative amount of 6.284 eq of TA were produced equating to 277 gCO_2 (assuming 1:1 ratio). For that 230 kg of water were used/discharged that carry the TA making it 831 $kgH_2O/kgCO_2$. Normalized for the used rock mass 6.6 $kgCO_2$ were captured. Also normalizing by the time of the experiment leads to 0.213 $kgCO_2/trock/d$.

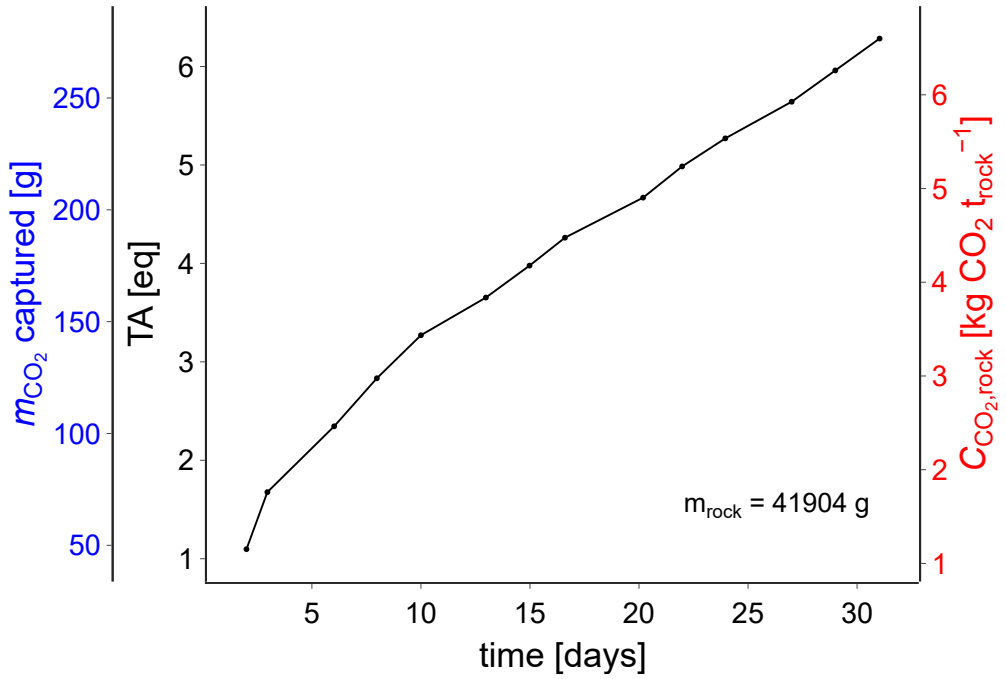


Figure 5.7: Cumulative total alkalinity equivalents leached over time. For the CDR assessment, we simplified TA = sequestered CO_2.

5.4. Discussion

5.4.1. TA prediction from EC

The observed EC and TA data from the reactor experiment cover a broad range. This broad concentration range enabled a robust calibration of the EC–TA relationship in the range of 6 to 67 meq kgw^{-1}.

Figure 5.3 shows a quadratic relationship between electrical conductivity (EC) and total alkalinity (TA), described by following regression result:

$$TA = 0.92EC^2 + 12.34EC - 0.05. \tag{5.7}$$

In many environmental studies, EC–TA relationships are approximated as linear (Amann and Hartmann, 2022; Kney and Brandes, 2007; Paessler et al., 2026; Shrestha and Basnet, 2018; Xue et al., 2017). This is often justified because the observed EC and TA values span only a relatively narrow range, within which a linear approximation is sufficient at the analytical resolution of the measurements. In addition, limited sample numbers may not support statistically robust higher-order regressions.

However, from a chemical perspective, the relationship between EC and TA is inherently

non-linear. As TA increases, carbonate speciation shifts and additional aqueous complexes form. A linear model implicitly assumes that increases in TA are associated solely with proportional increases in free ions such as Mg^{2+} and HCO_3^-. In reality, interactions between magnesium and carbonate species lead to the formation of additional aqueous complexes, which have individual molar conductivities contributing to EC. Consequently, a quadratic formulation can more accurately capture the evolving EC–TA relationship.

In general, the degree of nonlinearity (curvature) depends on the sample's ionic composition, because the major cations (Na^+, K^+, Ca^{2+}, Mg^{2+}) contribute differently to EC as they form different complexes in water. For example, for K^+ and carbonate alkalinity there is little interaction making the relationship linear (see Figure 5.8). The bivalent cations Mg^{2+} and Ca^{2+} however do show strong interaction with carbonate species leading to a less linear relationship (see Figure 5.8).

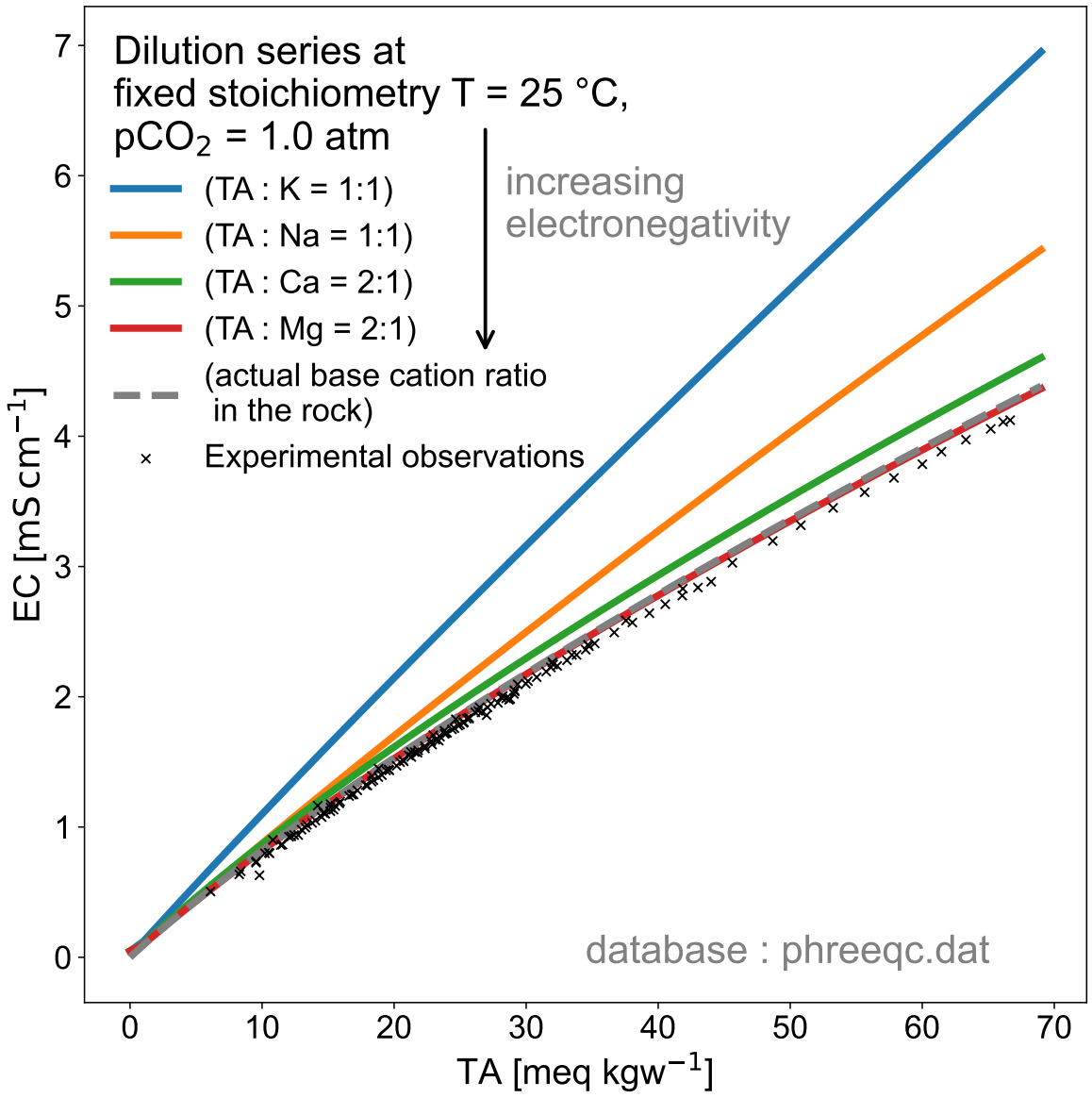


Figure 5.8: Electrical conductivity (EC) as a function of total alkalinity (TA) modeled with PhreeqPython using the *phreeqc.dat* database. The colored curves represent scenarios with constant stoichiometric ratios between base cations and TA. The grey dashed line illustrates EC calculated from TA based on the mean base-cation ratios of the rock feedstock. Experimental TA–EC observations are shown as crosses.

At elevated TA and thereby higher pH, aqueous complexation becomes more important, effectively reducing the activities of free Mg^{2+}, HCO_3^-, and CO_3^{2-}. These complexes are worse conductors than the free ions (David L. Parkhurst and C. a. J. Appelo, 2013; Stumm and Morgan, 1996). To show this pattern, it was modelled with phreeqpython, a Python interface to PHREEQC (David L. Parkhurst and C. a. J. Appelo, 2013), using the four different base cations and TA in fixed stoichiometric ratios (Figure 5.8).

The increase in electrical conductivity with TA ($\Delta EC/\Delta TA$) progressively flattens at higher

TA as aqueous speciation changes (Figure 5.8). At low pH, magnesium occurs predominantly as free Mg^{2+}, and carbonate species are scarce. With increasing pH and TA, more carbonate species form and promote the complexation of Mg^{2+}, reducing the activities of free CO_3^{2-}, HCO_3^-, and Mg^{2+} in solution.

Within the pH range of the experimental setup, the relevant aqueous complex that will form is $MgHCO_3^+$, as predicted by PHREEQC using the *phreeqc.dat* thermodynamic database (David L. Parkhurst and C. a. J. Appelo, 2013) (see Figure 5.9). This complex has a substantially molar conductivity than the corresponding free ions (Mg^{2+} and HCO_3^-) (David L. Parkhurst and C. a. J. Appelo, 2013) and therefore contributes less to electrical conductivity.

This can be shown by the molar limiting conductivities $\Lambda^0_{m,i}$. Those can be calculated by the Nernst Einstein equation (Atkins, de Paula, and Keeler, 2023) with diffusion factors taken from PHREEQC (D L Parkhurst and C. A. J. Appelo, 2013). The molar limiting conductivities were taken from the aqion database (aqion, 2020).

$\Lambda^0_{Mg^{2+}} = 105.1\,\mathrm{S\,cm^2\,mol^{-1}}$

$\Lambda^0_{HCO_3^-} = 44.3\,\mathrm{S\,cm^2\,mol^{-1}}$

$\Lambda^0_{MgHCO_3^+} = 18.0\,\mathrm{S\,cm^2\,mol^{-1}}$

The molar limiting conductivity of the ion pair is substantially smaller than the sum of its free ions:

$$\Lambda^0_{MgHCO_3^+} < \Lambda^0_{Mg^{2+}} + \Lambda^0_{HCO_3^-} \tag{5.8}$$

Consequently, the formation of the aqueous complex $MgHCO_3^+$ reduces the incremental increase in electrical conductivity (EC) per unit TA produced. With increasing pH, enhanced ion pairing therefore leads to the observed flattening of the EC–TA relationship.

In contrast to the tested rock which was relatively rich in only olivine (see Table 5.2), rocks/substrates composed of multiple mineral phases may exhibit a stronger time-dependent EC–TA relationship, reflecting the sequential dissolution of minerals with differing reaction kinetics. In such systems, the initial EC–TA relationship is governed by the fastest-dissolving phase and may shift as slower-reacting minerals begin to dominate solute release. Consequently, periodic recalibration is likely required when applying EC-based TA estimates to heterogeneous materials, because the different base cations contribute in unique ways to EC (see Figure 5.8).

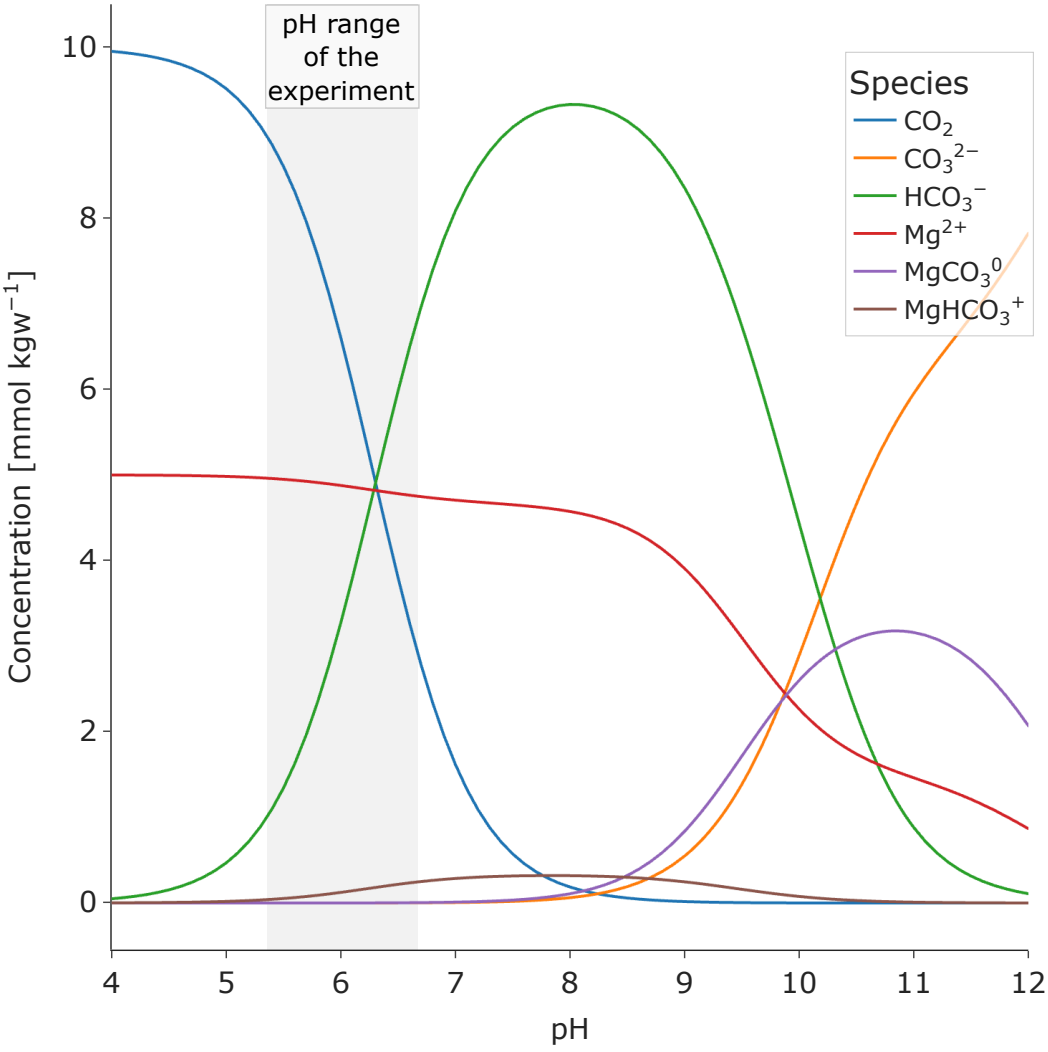


Figure 5.9: Magnesium and carbonate speciation as a function of pH in a closed system. Calculations were performed at fixed DIC = 10 mmol kg^{-1} and Mg = 5 mmol kg^{-1} using PHREEQC with the *phreeqc.dat* database.

5.4.2. CO_2 removal assessment

The system employs a shower-like water application and does not maintain continuous contact between mineral grains and a solution at constant pH, conditions that are commonly used to maximize dissolution rates in laboratory experiments. Consequently, the setup is not optimized for enhancing rock dissolution. Nevertheless, dissolution is sufficiently high to generate TA and Mg concentrations spanning a wide range.

The currency of carbon dioxide removal is measured in tons of CO_2. When extrapolated

to a target of one metric ton of CO_2, our results imply either an operational timescale of 4 702 d (≈ 13 yr) or use of 4 702 trock of rock at the same time. Independent of the operational timescale and rock throughput, the current experimental alkalinity-based setup would require approximately 831 t of demineralized water to achieve the removal of one metric ton of CO_2. Under these conditions, the current reactor configuration is not a practically viable approach for large-scale CO_2 removal.

Further optimization of the experimental setup is required to improve both reaction efficiency and resource use. While less frequent water discharge would reduce overall water consumption, it would simultaneously increase solution pH and thereby suppress dissolution rates. A more promising and technically straightforward modification is the implementation of a slurry-based reactor configuration (Poetra et al., 2025), ensuring continuous rock–water contact, in combination with elevated CO_2 partial pressures and/or increased temperatures.

In the broader context of CDR, the alkalinity-based approach investigated in this study differs from the dominant pathway described in the literature. Most studies focus on direct carbonation of forsterite to form magnesite (Felmy et al., 2012; Giammar, Bruant, and Peters, 2005; Raza et al., 2018; Sanna et al., 2014; Scott et al., 2021). This pathway dramatically reduces water requirements, as CO_2 is sequestered in solid carbonate minerals rather than being temporarily stored in the aqueous phase as carbonate alkalinity.

Overall, the results demonstrate that water demand must be carefully considered when implementing an alkalinity-based CO_2 removal strategy. Because as CO_2 is stored in the aqueous phase as dissolved carbonate alkalinity, sufficient water availability is a critical boundary condition for the scalability and practical feasibility of such approaches.

5.5. Conclusion

Under controlled experimental conditions with constant CO_2 partial pressure and solutions maintained in equilibrium with the gas phase, temperature-corrected electrical conductivity (EC) can serve as a robust proxy for total alkalinity (TA). For homogeneous materials, alkalinity and dissolved cations are released in a constant stoichiometric ratio, resulting in a consistent and predictable relationship between EC and TA. This enables the use of EC as a rapid, indirect estimator of total alkalinity.

In contrast, rocks/substrates composed of multiple mineral phases may exhibit a time-dependent EC–TA relationship, reflecting the sequential dissolution of minerals with differing reaction kinetics. In such systems, the initial EC–TA relationship is governed by the fastest-dissolving phase and may shift as slower-reacting minerals begin to dominate solute release. Consequently, periodic recalibration is likely required when applying EC-based TA estimates to heterogeneous materials.

The direct application of the EC–TA relationship for MRV approaches in soil-based ERW systems requires careful evaluation. Although a robust coupling between EC and TA was observed in the pure olivine-rich rock system investigated here, natural soil environments are

substantially more complex. The presence of additional dissolved ions, particularly non-TA anions, will increase electrical conductivity without contributing to TA. Such inputs decouple EC from TA and thereby reduce the reliability of EC-based alkalinity predictions in soil pore waters.

In principle, this EC–TA decoupling could be addressed by correcting EC for the contribution of non-alkalinity-bearing ions. However, this would require comprehensive chemical characterization of the solution, ultimately diminishing the practical advantage of using EC as a simple proxy compared to directly measuring TA.

6

Synthesis

This thesis examines the implications of using total alkalinity (TA) and electrical conductivity (EC) to quantify carbon dioxide (CO_2) removal in the context of enhanced rock weathering (ERW). The analysis is based on chemical data derived from water samples collected in three experimental systems: (i) soil water from a soil reaction experiment (chapter 2), (ii) leachate water from a crushed rock substrate column experiment with organic matter and biota additions (chapter 3 and chapter 4), and (iii) leachate water from a purely inorganic rock-weathering reactor experiment (chapter 5).

Chapter 2: Soil reaction experiment

In the soil experiment, bulk soil electrical conductivity (EC_b) and volumetric water content (θ) were measured in a soil column. The response of EC_b and θ to alkaline solution additions was tested. The aim was to infer changes in soil solution composition from bulk soil measurements. Four concentrations of $NaHCO_3$ were applied to simulate increasing total alkalinity inputs (0 to 50 mmol L^{-1}). In the two soils tested, a detectable increase in EC_b appeared only at the highest solution concentrations. The quartz sand substrate, in contrast, showed a clear EC_b signal across the tested range.

Subsequent extraction of the soil solution revealed that the soils buffered the alkaline water input by releasing H^+. For the tested brown earth soil, the input alkalinity was reduced by approximately 50 %. The magnitude of this buffering effect can be predicted. It depends on the initial soil pH, and the organic carbon and clay content (Curtin, Campbell, and Messer, 1996). These results demonstrate that initial non-carbonic acid soil acidity must be considered in ERW experiments.

For an initial TA addition of 2 to 10 meq L^{-1}, the TA measured in the soil extract was reduced. However, electrical conductivity increased. This decoupling shows that alkalinity can be neutralized while electrical conductivity continues to rise. The contribution of additional anions, such as nitrate (NO_3^-), nitrite (NO_2^-), chloride (Cl^-), and sulfate (SO_4^{2-}), beyond alkalinity therefore complicates the use of EC as a proxy for TA and associated CO_2 removal in soil systems.

Chapter 3 and Chapter 4: Crushed-rock column experiment

The crushed-rock column experiment with organic matter and biota amendments demonstrated that adding wheat straw to crushed rock resulted in substantial release of dissolved organic carbon (DOC), which in turn affected the observed TA. Based on observed dissolved inorganic carbon (DIC), pH, and temperature (T), the carbonate alkalinity A_C was modeled with phreeqpython (Heinsbroek, 2021). This allowed us to calculate the non-carbonate alkalinity (A_{NC}) as the difference between TA and A_C. In the given dataset, a clear correlation between DOC and A_{NC} was observed, with an approximate ratio of 3.5 mol DOC per equivalent of A_{NC} within the tested system. This relationship suggests the formation of organic alkalinity within the crushed-rock substrate, which was predominantly amended with wheat straw. This highlights the need to measure DIC, pH, and temperature in addition to TA when analyzing, especially organic-rich water samples.

In principle, the carbonate system could also be reconstructed from DIC, pH, and temperature alone, provided a reasonable estimate of ionic strength is available. But for soil pore water samples, it might be hard to measure DIC and pH. The same A_C model was also applied to water samples from mesocosms and estuaries to quantify the relative contribution of A_{NC} to TA. In the crushed rock experiment amended with organic matter, the median contribution of A_{NC} was approximately 5.5 %, with a positively skewed distribution extending toward higher values. In contrast, A_{NC} accounted for only about 1 % of TA in samples from the Elbe River estuary. The relative importance of A_{NC} thus decreases at larger spatial scales, consistent with declining DOC concentrations. In basin-scale assessments of CO_2 removal, the influence of organic alkalinity becomes progressively less significant due to dilution effects and the microbial conversion of organic alkalinity to carbonate alkalinity during downstream transport.

Within the same experimental setup, to further explore the drivers of TA generation, a complementary experiment was conducted to isolate the effects of selected fungi, bacteria, and earthworms on rock dissolution rates. The addition of these biotic components alone did not result in a statistically significant increase in total alkalinity (TA) production or cation release compared to the abiotic control.
In contrast, the amendment of the crushed rock substrate with wheat straw resulted in a significant increase in TA and cation concentrations. This finding indicates that the presence of organic matter had a stronger influence on solute release than the inoculation with selected biota.

The combination of rock feedstock and wheat straw complicates the interpretation of alkalinity generation. Wheat straw can contain soluble organic salts that release cations upon dissolution and contribute to non-carbonate (organic) alkalinity. The observed TA increase may have come from (i) enhanced biological weathering mediated by microorganisms associated with the straw, or (ii) direct dissolution of organic salts and other substances in the wheat straw. Because the original experimental design focused on specific biota rather than the geochem-

ical effects of the organic amendment, these mechanisms could not be accurately disentangled.

Thus, part of the TA increase may reflect mobilization of organic alkalinity rather than inorganic mineral weathering. The dissolution of organic salts also affects both EC and TA, but not in the same stoichiometric way as the rock dissolution. This decoupling complicates how we interpret the EC–TA relationship and, by extension, the assessment of CO_2 removal.

Chapter 5: Abiotic reactor ERW experiment

Because the biotic treatments did not produce a clear or consistent signal in the preliminary experiments and further complicated quantifying CO_2 removal, we designed a follow-up experiment under strictly controlled abiotic conditions. In this setup, only pure crushed peridotite rock substrate was used, and physical boundary conditions were carefully controlled.

The experiment was done in a closed reactor, maintained at $pCO_2 = 1$ atm and $T = 25\,^{\circ}C$, with continuous water recirculation. Under these conditions, and with no organic amendments or biological additions, a clear and reproducible relationship between total alkalinity (TA) and electrical conductivity (EC) was observed. The relationship was best described by a quadratic calibration function with a coefficient of determination of $R^2 = 0.999$.
Feedstock-specific calibrations can also be made for other rock types. However, each system needs an initial calibration phase, since the EC–TA relationship is controlled by both the pCO_2 and the mineralogical composition of the feedstock.

For mineralogically heterogeneous materials, the EC–TA relationship may exhibit pronounced temporal dependence. This behavior arises because individual minerals dissolve at different rates (Lasaga et al., 1994), resulting not only in changing solute concentrations but also in changes in the qualitative ionic composition of the leachate over time. Released base cations differ in their molar ionic conductivities (Vanysek, 1993). So, changes in the ratio of, for example, Mg^{2+}, Ca^{2+}, Na^{+}, or K^{+} alter the electrical conductivity response per unit alkalinity. Consequently, the EC–TA relationship can change over time.

Despite these complexities, once an appropriate calibration has been established, EC can be used as a robust predictor of TA. This approach can be applied to systems in which no additional ions unrelated to feedstock dissolution are released after calibration, as the calibration captures the specific relationship between EC and TA generated by the feedstock. Electrical conductivity measurements are highly precise, do not require sample acidification, and can be performed continuously without disturbing the system. Consequently, EC monitoring provides a cost-effective and non-invasive method for tracking TA production at high temporal resolution.

Concluding Remarks

This thesis advances the methodological framework for improving the assessment of CO_2 removal in enhanced rock weathering (ERW) systems.
In soil-based ERW applications, using leachate electrical conductivity (EC) as a proxy for total alkalinity (TA) is generally not recommended. Additional ions can increase EC without contributing to TA, thereby introducing substantial uncertainty. In agricultural soils, crop growth and associated plant–soil interactions can further alter solute release and uptake. This further complicates the EC–TA relationship in soil leachate.

Moreover, the inorganic CO_2 removal can only be reliably inferred from changes in TA if these changes correspond to equal changes in carbonate alkalinity (A_C). Relying solely on TA can be insufficient in organic-rich systems, where non-carbonate alkalinity (A_{NC}) may significantly contribute to the measured TA signal. In such systems, a robust assessment of aquatic CO_2 removal would require the simultaneous measurement of TA, dissolved inorganic carbon (DIC), pH, and temperature (T) within the leachate water sample. This combined approach fully determines the carbonate system and enables the quantification of A_C, TA, and contributions from A_{NC} sources and is therefore suggested to quantify the CO_2 removal precisely.

In contrast to cropland ERW deployments, in controlled reactor-based ERW applications, EC can serve as a reliable proxy for TA after thorough feedstock characterization and an initial calibration phase. In such systems, EC offers a non-invasive, cost-effective method for continuously tracking alkalinity production at high temporal resolution.

Overall, this thesis strengthens the scientific basis for quantifying CO_2 removal in ERW deployments by identifying methodological limitations and providing guidance on key factors to consider for reliable monitoring, reporting, and verification (MRV).

A

Appendix for Chapter 2

A.1. Used reagent $NaHCO_3$

Certificate of Analysis

Item number: 0965

Sodium hydrogen carbonate

≥99 %

batch: 081306657

CAS No.:	144-55-8	print date:	23.02.2021
formula:	$NaHCO_3$	recommended retest date:	17.02.2025
density:		release date:	19.02.2021
molecular weight:	84,01 g/mol		

	Type analysis	batch results
Assay	≥99 %	100.2 %
Loss on drying	≤0,25 %	< 0.25 %
Arsenic (As)	≤0,0002 %	< 0.0001 %
Calcium (Ca)	≤0,01 %	0.008 %
Iron (Fe)	≤0,0005 %	0.00002 %

Our products are tested for laboratory use only.
The stated information refers to the current status of product quality.
We reserve the right to implement necessary changes.

D. Pados
Quality Control

D. Mijic
Quality Assurance

This document is computer printout and has therefore not been signed by hand.

Carl Roth GmbH + Co. KG
Schoemperlenstraße 3-5
76185 Karlsruhe

Telefon 0721/5606-0
Telefax 0721/5606-149
E-Mail: info@carlroth.de

Die Firma ist eine Kommanditgesellschaft mit Sitz in Karlsruhe, Reg. Gericht Mannheim HRA 100055. Persönlich haftende Gesellschafterin ist die Firma Roth Chemie GmbH mit Sitz in Karlsruhe, Reg. Gericht Mannheim HRB 100428. Vorsitzender des Aufsichtsrats: Eberhard Gaul Geschäftsführer: André Houdelet

B

Appendix for Chapter 3

B.1. Total alkalinity determination

The total alkalinity/titrated alkalinity (TA) was measured via a potentiometric titration with 4 endpoints pH = [4.5, 4.3, 4.0, 3.7]. The equivalence point was calculated using a linear regression, including those four points (x = acid volume, y = Gran value). The automated titration was done with the Tiamo 3.0 software following (Koenig, 2005). The basic underlying equations are explained below. In this text, it is called TA measured, because there are different procedures to do so, and so different results when dealing with a lot of non-carbonate species in water samples that also buffer the added acid.

The Gran value (G) is calculated with the following equation:

$$G_i = \mathrm{H}_i^+ = 10^{-\mathrm{pH}_i} \cdot (V_0 + V_i) \tag{B.1}$$

V_0 = sample volume
V_i = added acid volume to a given endpoint
$\mathrm{pH_i}$ = pH endpoints $\in \{4.5; 4.3; 4.0; 3.7\}$

To get the equivalence point, a linear regression of the ($x = V_i$) and ($y = G_i$) data is performed. The regression line G(x) has slope m and intercept b.

$$\mathrm{TA_{measured}} = \frac{b}{m} \cdot c_a \cdot n_{\mathrm{H^+}} \tag{B.2}$$

c_a = concentration/molality of the used acid
$n_{\mathrm{H^+}}$ = deprotonation number of the strong acid used for the titration (for HCl: $n_{\mathrm{H^+}} = 1$)

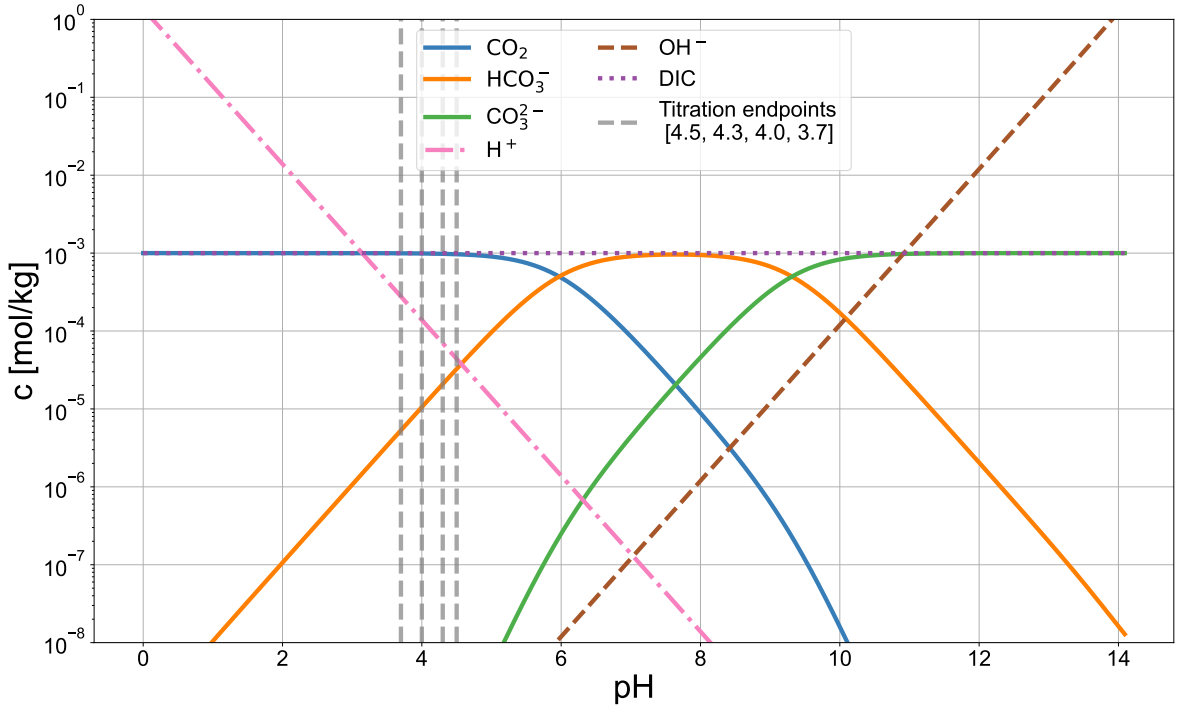


Figure B.1: Bjerrum plot showing the contribution of carbonate species to total DIC (closed system DIC = 0.001 mol kg^{-1}) for freshwater. NaOH is added to the solution to raise the pH, and HCl is added to lower it. The vertical lines indicate the endpoints used for the alkalinity titration [4.5; 4.3, 4.0; 3.7] after(Koenig, 2005).

B.2. Dissolved organic and inorganic carbon determination

The DIC and DOC are measured with the FORMACS™ HT TOC analyzer extended with the PRIMACS™ MCS module which consists of two integrated reactors for both TC and TIC analysis without any sample preparation. The Total carbon content (TC) is determined by catalytic oxidation of the sample at 1 100 °C, which converts all carbon to CO_2. The DIC is determined by acidification of the sample in a separate reactor, which converts inorganic carbon (IC) to CO_2. The PRIMACS™ MCS uses the NDIR detector of the FORMACS™series for the detection of CO_2. The PRIMACS™ MCS analyses TC, TIC and TOC. The software calculates the DOC concentration of the samples by subtraction (DOC = TC − DIC).

B.3. Carbonate alkalinity models comparison

The simple model uses (T, pH, DIC) to calculate the carbonate alkalinity A_C. Whereas the comprehensive model uses (cations, anions, T, pH, DIC) to calculate the carbonate alkalinity A_C.

$$A_C = [HCO_3^-] + 2 \cdot [CO_3^{2-}] \tag{B.3}$$

We have calculated the following error metrics to assess the performance of the simplified model (y) over the comprehensive model (x): Root Mean Squared Error (RMSE), Mean Absolute Error (MAE), Mean Absolute Percentage Error (MAPE), and R^2 (Rsquared) the

coefficient of determination. The error metrics have been calculated with sklearn.metrics — scikit-learn 1.6.1 documentation.

In the lower end of A_C from 0 to 6 meq kgw^{-1} the models do match very well. Just in the upper end, there is more deviation.

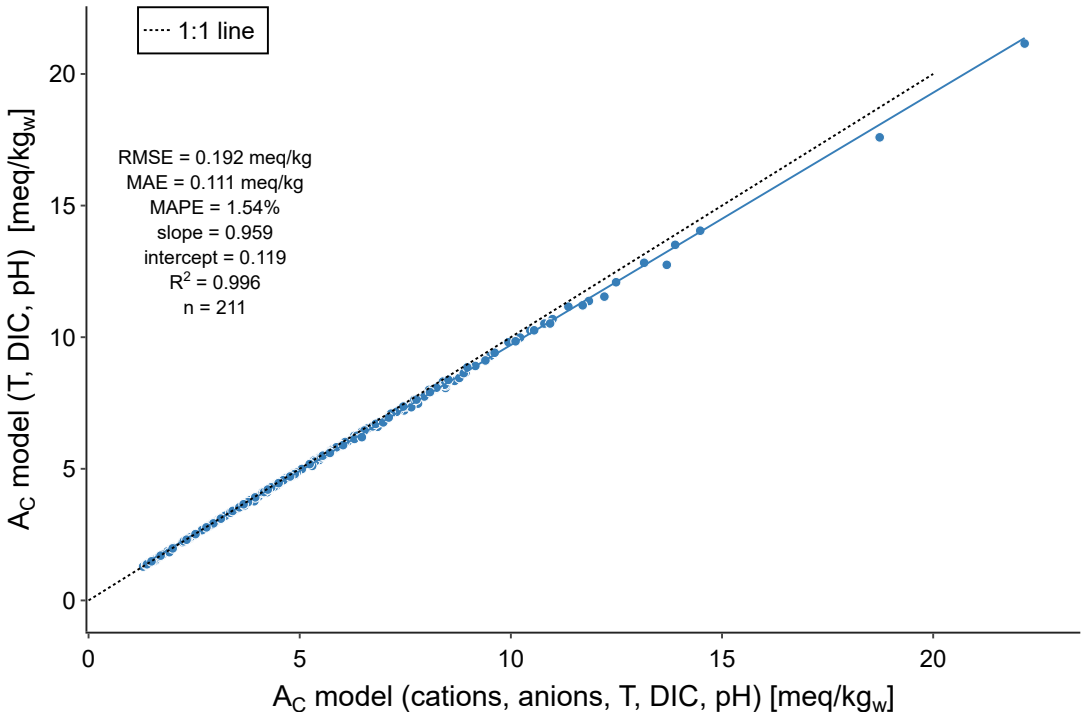


Figure B.2: Carbonate alkalinity model (A_C) comparison. On the x-axis the comprehensive model with cations and anions is shown and, on the y-axis, the simplified model just using dissolved inorganic carbon (DIC), pH and Temperature.

B.4. Charge balance determination

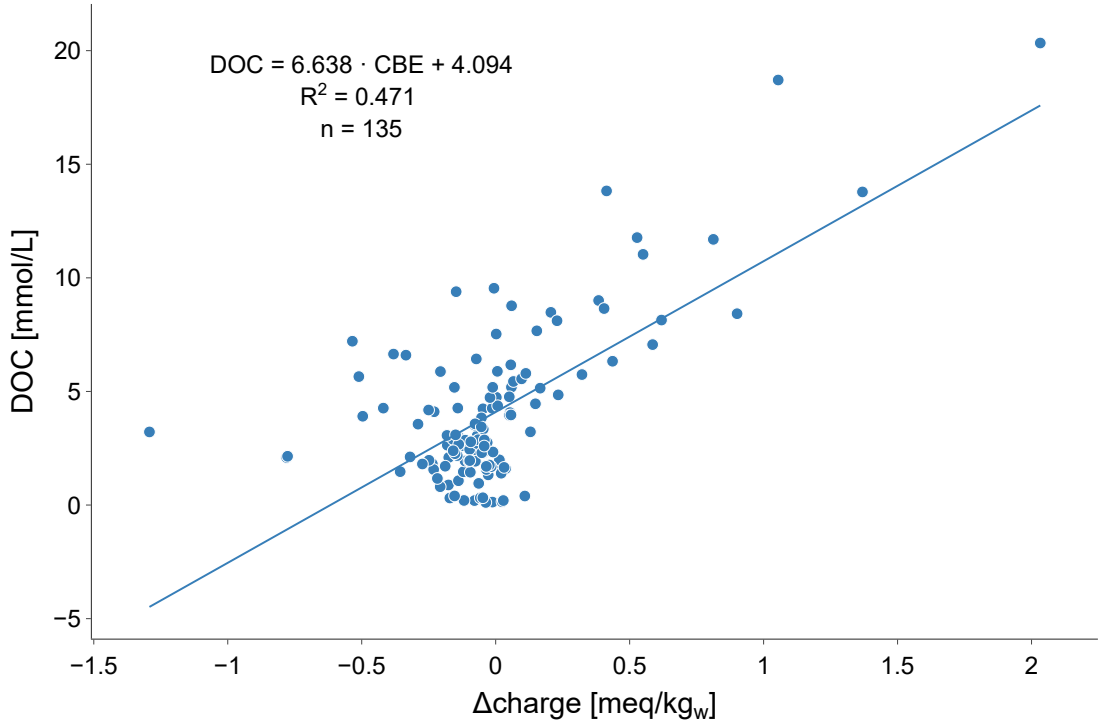


Figure B.3: The dissolved organic carbon (DOC) concentration against the absolute charge balance (positive–negative charge).

B.5. Irrigation rate impact

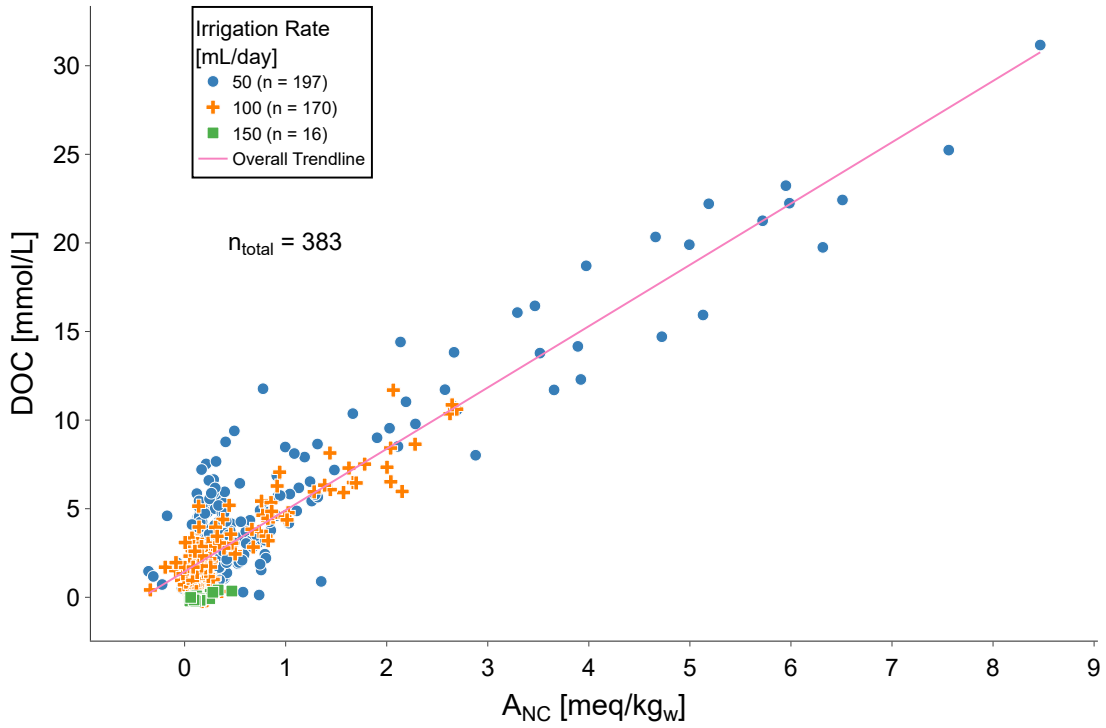


Figure B.4: The relationship between dissolved organic carbon (DOC) concentration and non-carbonate alkalinity (ΔTA) in the leachate water. The color represents the different irrigation rates used to water the microcosms.

Analyzing the total dissolved organic carbon amount, calculated as the product of volume and concentration, instead of focusing solely on the DOC concentration, can rule out the influence of dilution. Figure B.5 illustrates the relationship between the total leached DOC amount and the mass of the leachate for the different irrigation categories.

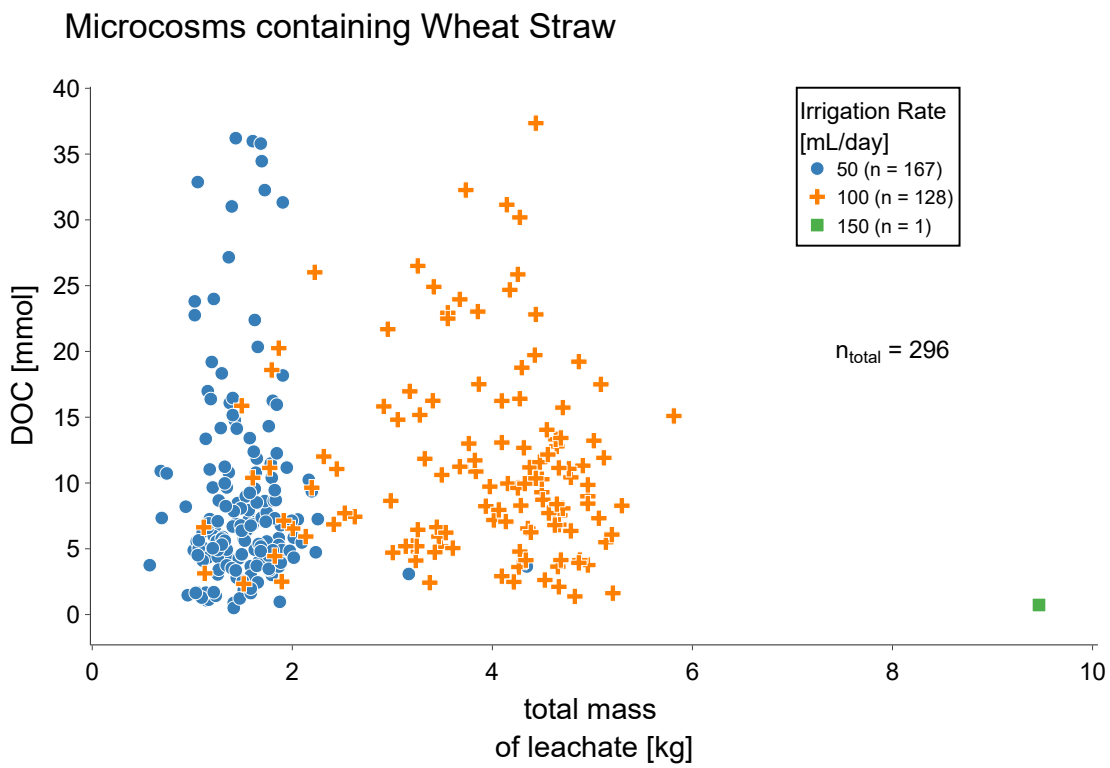


Figure B.5: Relationship between dissolved organic carbon (DOC) amount and the total mass of leachate in microcosms containing wheat straw. The color represents different irrigation rates used in the microcosms.

B.6. Organic-rich soil

The soil used in this experiment was collected from an agricultural plot in Bramstedt, northern Germany (53.353 3° N, 8.694 8° E). It is abundant in organic matter and is classified as a Dystric Histosol according to the WRB system, with a total organic carbon (TOC) content of 7.2 %. The rock amendment used in this experiment was a product called *Eifelgold*, manufactured by Lava Union GmbH (`https://www.rpbl.de`). The chemical composition of the soil and basanite is shown in Table B.1.

Table B.1: The XRF (X-ray fluorescence) results for soil and basanite used in this study, in wt%. (a) The soil originates from an agricultural plot in Northern Germany, an organic-rich soil. (b) The rock material is classified as basanite and was mined in Eifel, Germany

Element	Initial Bramstedt Soil (a) mass percent (%)	Initial Basanite (b) mass percent (%)
SiO_2	81.79	43.49
Al_2O_3	2.8	14.32
Fe_2O_3	0.68	11.1
MnO	0.02	0.18
MgO	0.12	9.05
CaO	0.36	11.52
Na_2O	0.35	2.98
K_2O	0.92	3.37
TiO_2	0.33	2.69
P_2O_5	0.17	0.51
SO_3	0.02	
LOI	12.12	
Sum	99.68	99.21

B.7. Brown earth soil

The soil used in the experiments was obtained from Fürth, Bavaria, Germany (53.353 3° N, 8.694 8° E). It is a clay-rich soil, containing 7.5 % 2:1 layer silicates, 0.8 % chlorite as determined by XRD, and a total organic carbon (TOC) content of 1.4 %. SiO_2 is the most abundant component, accounting for 82.16 % of the total. Most of its cations were lost. Na_2O, K_2O, CaO, and MgO account for only 0.43 %, 3.8 %, 0.44 %, and 0.44 % of the total, respectively. The elemental ratios are Mg/Ti = 3.6, Na/Ti = 4.6, Ca/Ti = 2.6, and K/Ti = 26.9. Furthermore, the average grain size of this soil is 42 µm, with a d_{90} of 128.4 µm.

Table B.2: The XRF (X-ray fluorescence) results for soil, basanite, and gabbro and basanite used in this study, in wt%. (a) The XRF results. (a) Fürth soil, in Bayern, Germany. (b) Basanite, from Eifelgold. (c) Gabbro, from DACCUS project.

Element	Initial soil mass percent (%)	Basanite mass percent (%)	Gabbro mass percent (%)
SiO_2	82.16	44.02	52.63
Al_2O_3	7.34	14.07	7.64
Fe_2O_3	1.38	11.32	12.38
MnO	0.11	0.18	0.19
MgO	0.44	8.33	11.3
CaO	0.44	11.7	11.17
Na_2O	0.43	3.29	1.38
K_2O	3.8	3.3	0.87
TiO_2	0.24	2.77	0.94
P_2O_5	0.19	0.62	0.06
SO_3	0.01	bdl	0.03
LOI	3.98	0.47	0.58
Sum	100.52	100.07	99.17

B.8. Experimental setup for both soils

The column experiment at ambient pCO_2 (Figure B.6) started in September 2021 and ran for 294 d. Acrylic cylinders were used, with an inner diameter of 5.5 cm and a length of 25 cm. A nylon cloth with a mesh size of 20 µm was attached at the bottom of the columns to prevent solid particles from entering the sample bottles. The columns were filled to a height of approximately 20 cm with a mixture of soil and 9.5 g, 23.8 g, and 95.0 g of basanite powder, corresponding to application doses of 40, 100, and 400 t ha^{-1}, respectively. The total mass of each column was approximately 595 g. Room temperature was maintained at around 23 °C. Milli-Q water was added to the columns using a 5 mL pipette (Eppendorf) on weekdays at rates of 3.64, 7.28, 10.92, and 14.56 mL d^{-1}, representing four precipitation regimes of 400, 800, 1200, and 1 600 mm yr^{-1}. Each setup comprised two replicates. Leachate samples were collected every two weeks.

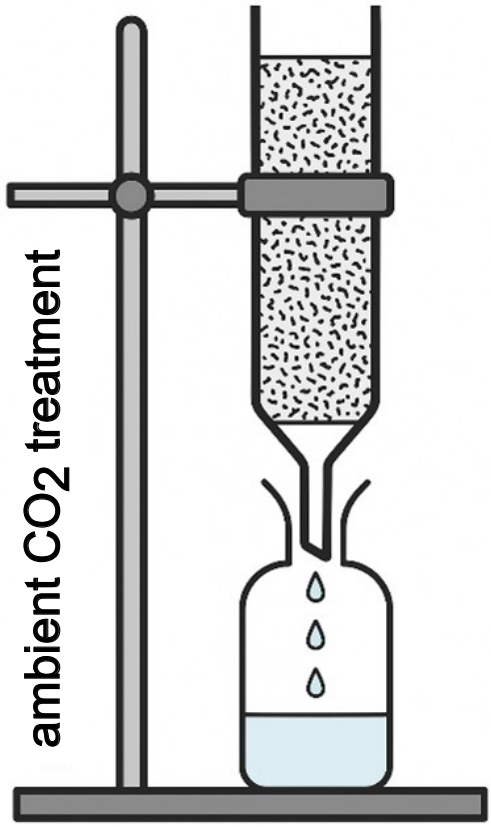


Figure B.6: Schematic of a column under ambient conditions, edited from (Amann and Hartmann, 2022).

B.9. Rock powder pictures



Figure B.7: Basalt (referred to as *Basaltgestein* by the supplier Rheinische Provinzial-Basalt- und Lavawerke (RPBL), Germany). The coarse grain size 1 to 2 mm is shown here.



Figure B.8: Basanite/Tephrite (referred to as *Lavagestein* by the supplier Rheinische Provinzial-Basalt- und Lavawerke (RPBL), Germany)

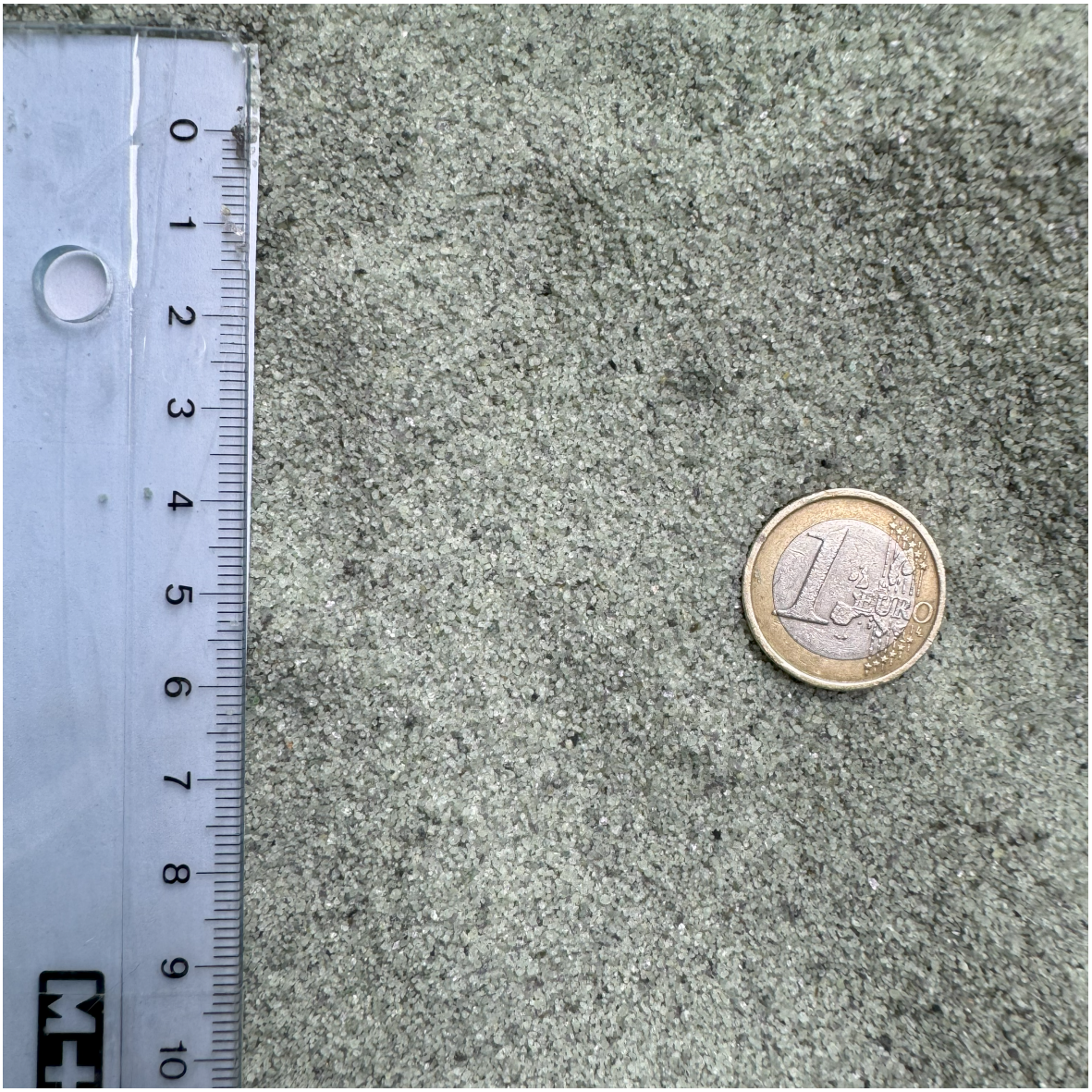


Figure B.9: Dunite (called *Olivine* by the supplier Sibelco, Norway)

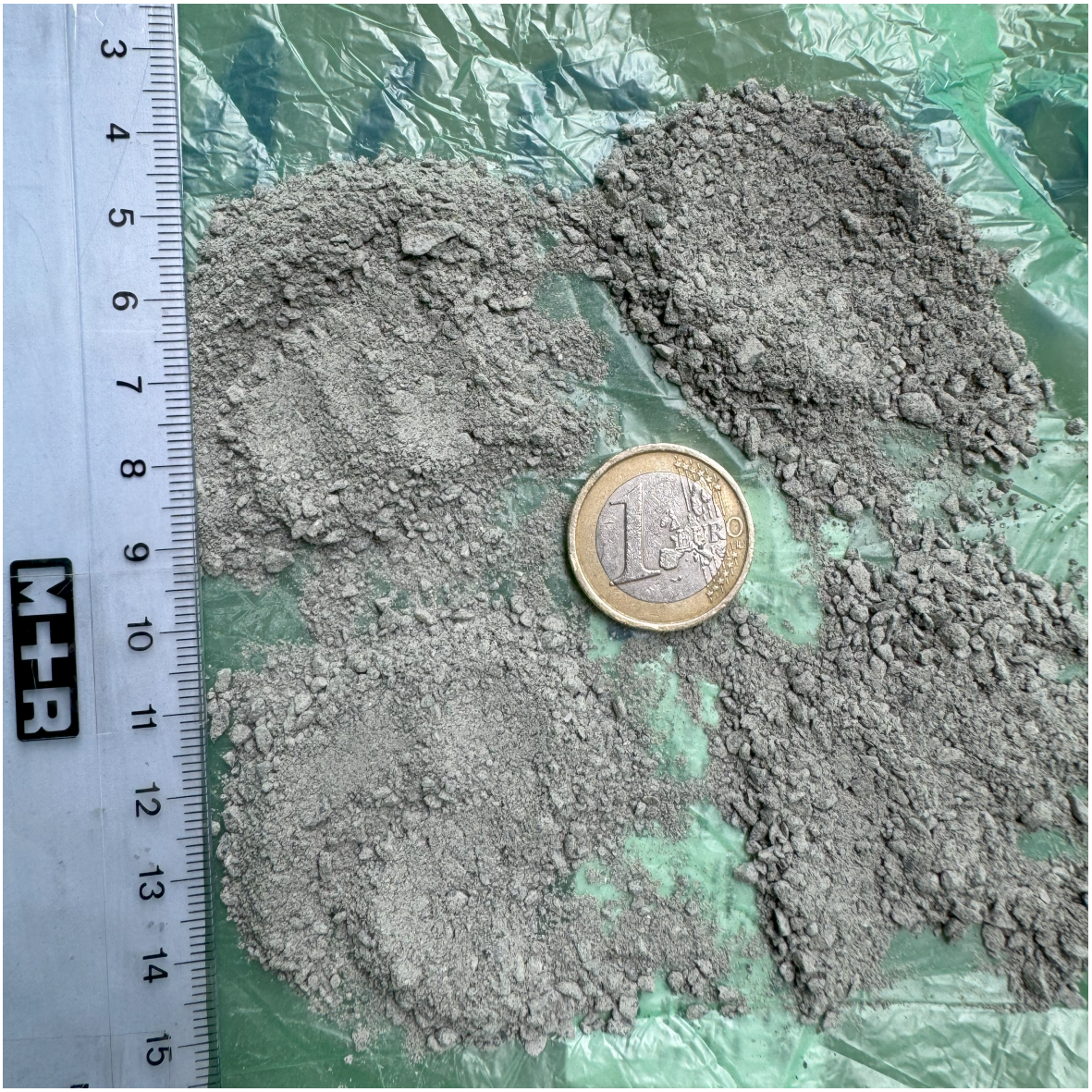


Figure B.10: Diabase (reffered to as *Diabas Urgesteinsmehl* by the supplier Schicker Mineral, Germany).

B.10. Rock Classification

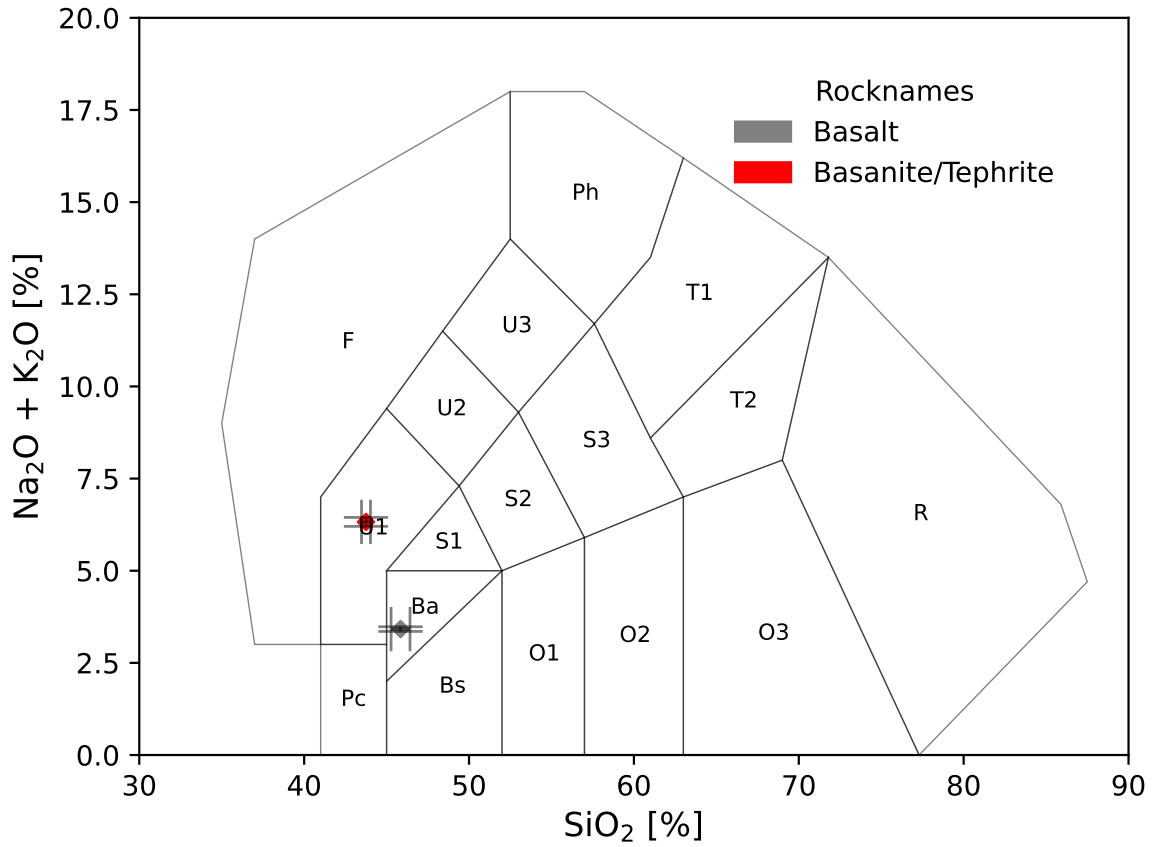


Figure B.11: The Total alkali-silica (TAS) diagram with the two used volcanic rocks. The standard deviation in SiO_2 and Na_2O+K_2O is indicated by the error bars. The XRF data were first normalized with the loss of ignition (LOI) and then plotted. This plot was generated with pyrolite (Williams et al., 2020). For the names of all types, see Figure B.12.

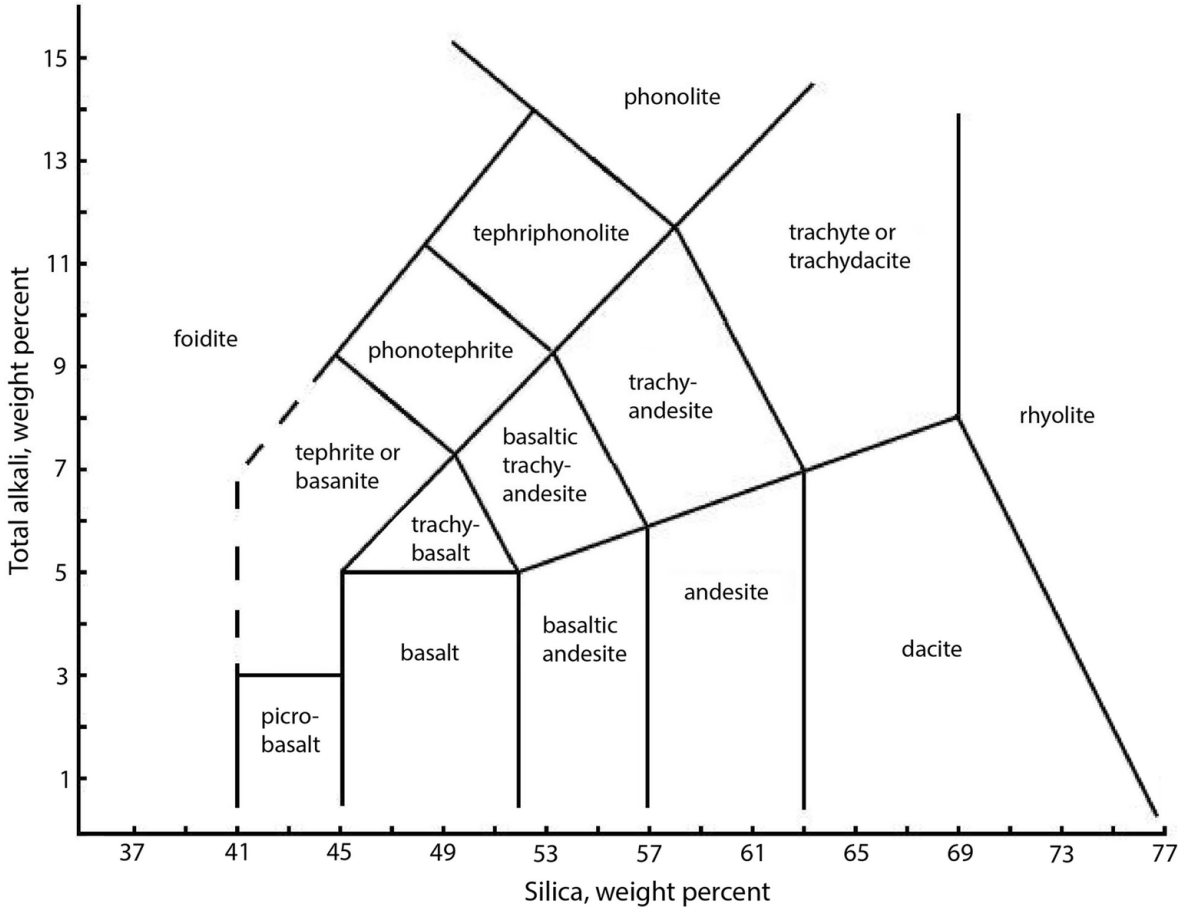


Figure B.12: TAS diagram defining the names of 15 different types of volcanic rocks. The names tephrite or basanite are two alternative names for the same type of rock (Olea, 2022).

C

Appendix for Chapter 4

C.1. Tephrite rock substrate



Figure C.1: Tephrite crushed rock substrate (0 to 2 mm) composed of mixed grain sizes, including both coarse grains and fine material.

The grain size is very heterogeneous (see Figure C.1). A lot of rock particles bigger than 2 mm are visible. Those can't be detected by the grain size analysis, which has the cutoff at 3.5 mm.

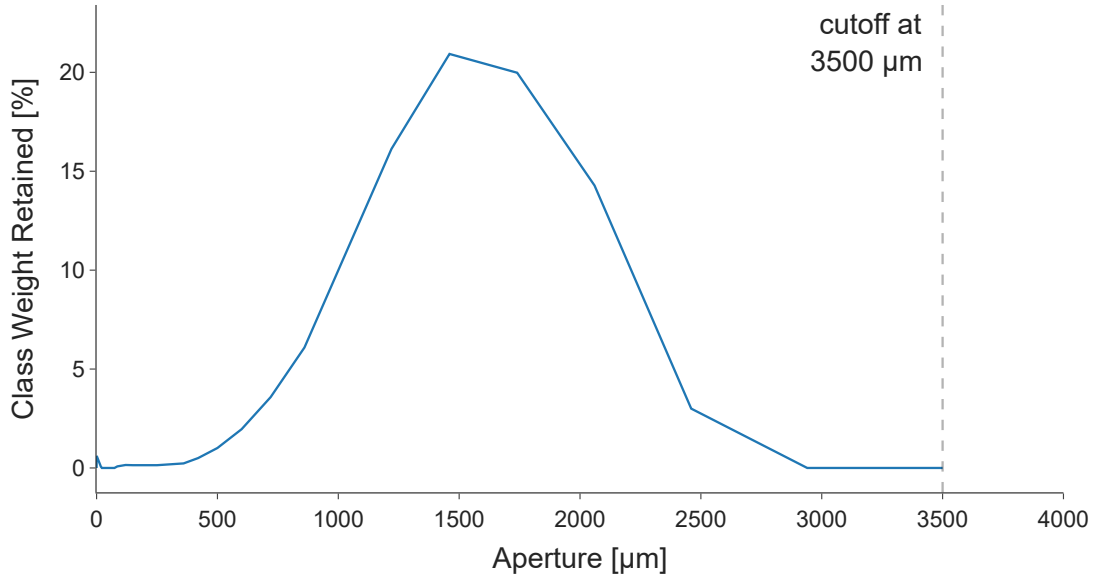


Figure C.2: Grain size distribution (GSD) for the used rock substrate.

C.2. Experimental setup

Table C.1: Experimental combinations of increasing complexity, ranging from a groundwater-only control to treatments including rock, wheat straw, and biotic additions (earthworms, fungi, and bacteria).

Combination	**Groundwater irrigation** [mL d^{-1}]	**Crushed Rock** [g]	**Wheat straw** [g]	**Earthworm** [number]	**Fungi** [cells]	**Bacteria** [cells]
1 (empty/blank)	50					
2	50	400				
3	50	400	10			
4	50	400	10	4		
5	50	400	10		10^8	
6	50	400	10			10^{10}
7	50	400	10	4	10^8	
8	50	400	10	4		10^{10}
9	50	400	10		10^8	10^{10}
10	50	400	10	4	10^8	10^{10}

C.3. Tukey-Kramer test

There are important considerations when using the Tukey-Kramer test, including the fact that the threshold for statistical significance becomes more stringent as the number of group comparisons increases. This is explained in greater detail here. The H_0 hypothesis is that both group means are equal. By definition, it is a two-sided test.

$$H_0 : \bar{x}_i = \bar{x}_j$$
$$H_1 : \bar{x}_i \neq \bar{x}_j$$

This test is a multiple-comparison procedure for comparing the means of all pairs of groups. It makes pairwise comparisons between all groups of observations. The equations are taken from with some variable names being renamed (Montgomery, 2013).

$$f = \sum_{i=1}^{k} n_i - k \tag{C.1}$$

In our case, often the groups mostly have unequal sample sizes. This leads to the Honestly Significant Difference (HSD) being calculated in the following way:

$$HSD = \frac{q_\alpha(k, f)}{\sqrt{2}} \cdot \sqrt{MS_E \cdot \left(\frac{1}{n_i} + \frac{1}{n_j}\right)}. \tag{C.2}$$

With the mean squares MS_E being calculated in the following way:

$$MS_E = \frac{1}{N-k} \sum_{i=1}^{k} \sum_{j=1}^{n_i} \left(x_{ij} - \overline{x}_i\right)^2. \tag{C.3}$$

It is important to note that the threshold for rejecting the null hypothesis becomes more stringent as the number of groups being compared increases. This means that a result deemed significant in a smaller comparison may no longer be considered significant when more groups are included. The critical value, q, from the studentized range distribution, depends on the total number of groups (k) and the degrees of freedom (f), which are influenced by the number of observations per group (see Figure C.3).

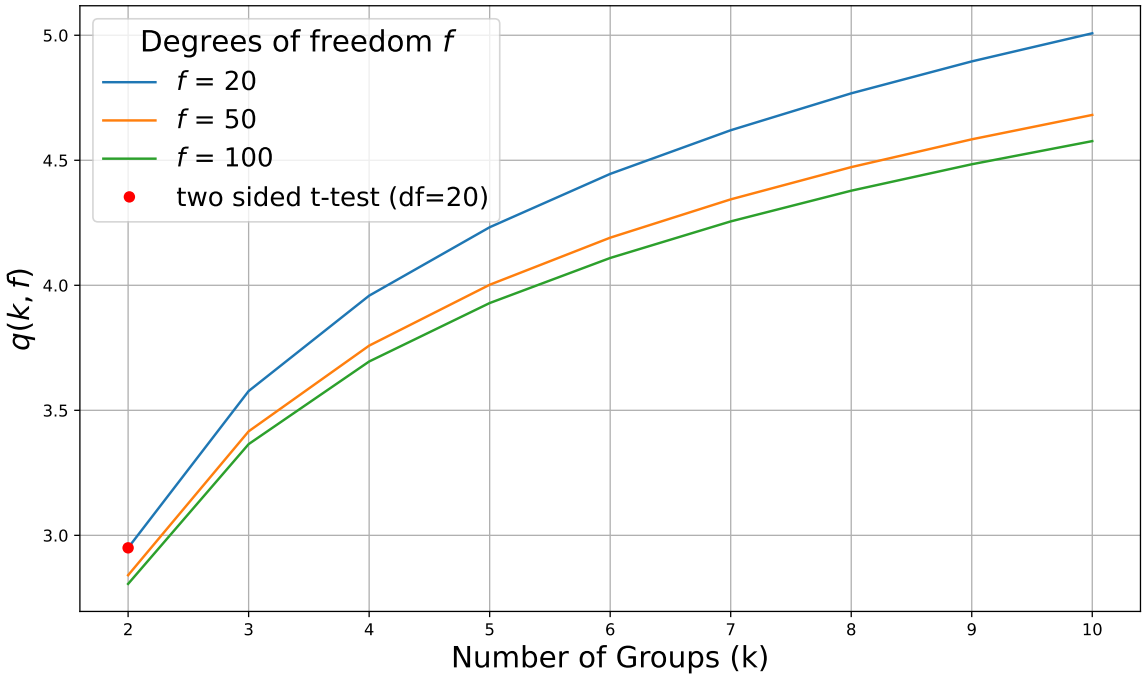


Figure C.3: Effect of Number of Groups (k) and Degrees of Freedom (f) on the critical value q for $\alpha = 0.05$.

A difference between two groups is considered significant if the absolute value of the difference of their means exceeds the HSD:

$$|\bar{x}_i - \bar{x}_j| > \text{HSD}$$

Another important point to note is that the boxplots display median values and mark specific data points as outliers. In contrast, the Tukey-Kramer test is based on comparing group means, calculated from all observations within each group.

C.4. Factorial linear model results

Table C.2: Coefficients of the ordinary least squares (OLS) regression model with total alkalinity equivalents (TA meq) as the dependent variable. The model includes the main effects and interaction terms of earthworms, fungi, and bacteria.

	Coef.	**Std.Err.**	**t**	**P> |t|**	**[0.025**	**0.975]**
Intercept	6.539	0.353	18.501	10^{-27}	5.833	7.244
Earthworms	−0.022	0.487	−0.045	0.964	−0.995	0.951
Fungi	0.496	0.5	0.993	0.324	−0.502	1.494
Bacteria	0.224	0.515	0.435	0.665	−0.804	1.253
Earthworms × Fungi	−0.625	0.698	−0.895	0.374	−2.018	0.769
Earthworms × Bacteria	0.407	0.709	0.574	0.568	−1.009	1.822
Fungi × Bacteria	−0.709	0.709	−1.001	0.321	−2.125	0.706
Earthworms × Fungi × Bacteria	0.898	0.989	0.908	0.367	−1.076	2.871

C.5. Leachate water analysis

The following section includes additional plots that were not shown in the main text but provide further context and may be informative to interested readers.

C.5.1. Charge balance error (CBE)

The charge balance error shows the measurement precision. Almost all samples are far below the typically accepted ±5 %. The calculation of the charge balance error is given in Equation C.4. The cations included were Na^+, K^+, Ca^{2+}, and Mg^{2+}, while the anions considered were Cl^- and SO_4^{2-}.

$$\text{CBE}\,[\%] = \frac{\sum \text{cations} - (\sum \text{anions} + TA_{\text{measured}})}{\sum \text{cations} + (\sum \text{anions} + TA_{\text{measured}})} \cdot 100 \tag{C.4}$$

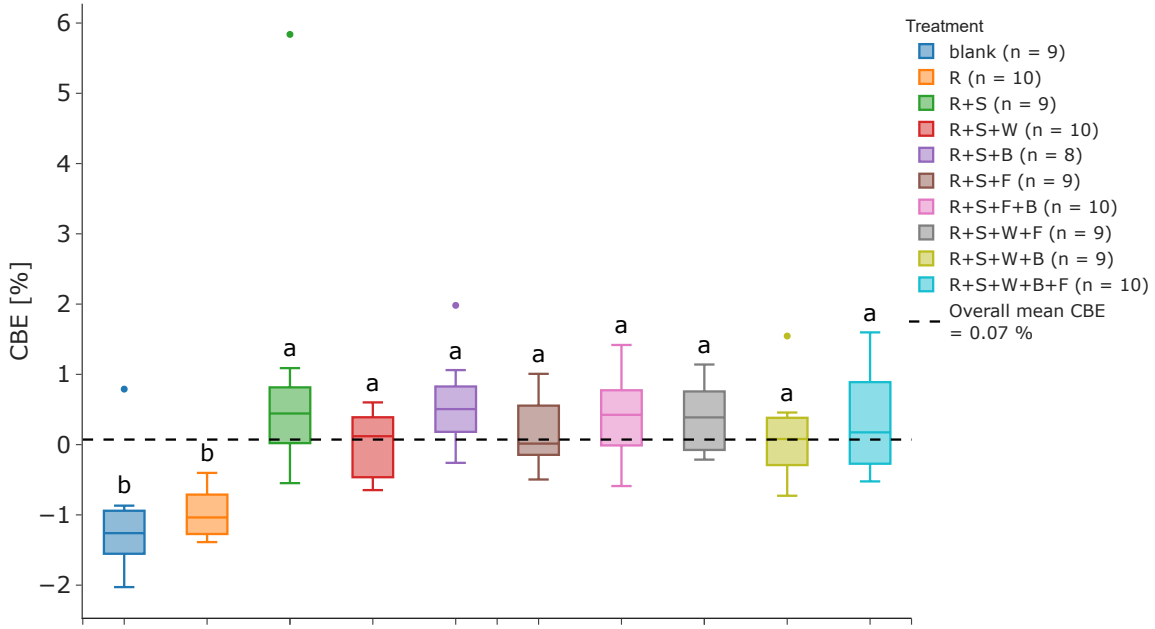


Figure C.4: Charge balance error (CBE) calculated for the leachate water samples. Abbreviations used in the legend: R = rock, S = straw, W = worms, B = bacteria, F = fungi. Different letters indicate statistically distinct groups (ANOVA with Tukey post-hoc).

C.5.2. Molar ratio

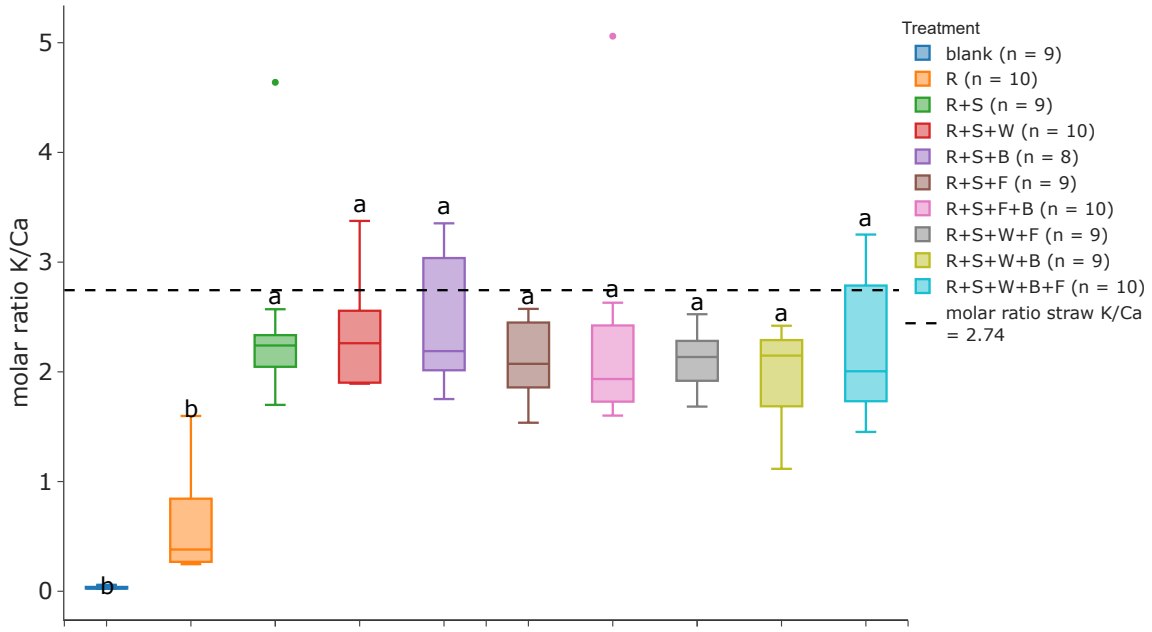


Figure C.5: Molar ratio of K and Ca observed in the leachate water. Abbreviations used in the legend: R = rock, S = straw, W = worms, B = bacteria, F = fungi. Different letters indicate statistically distinct groups (ANOVA with Tukey post-hoc).

C.6. Microbial community in wheat straw

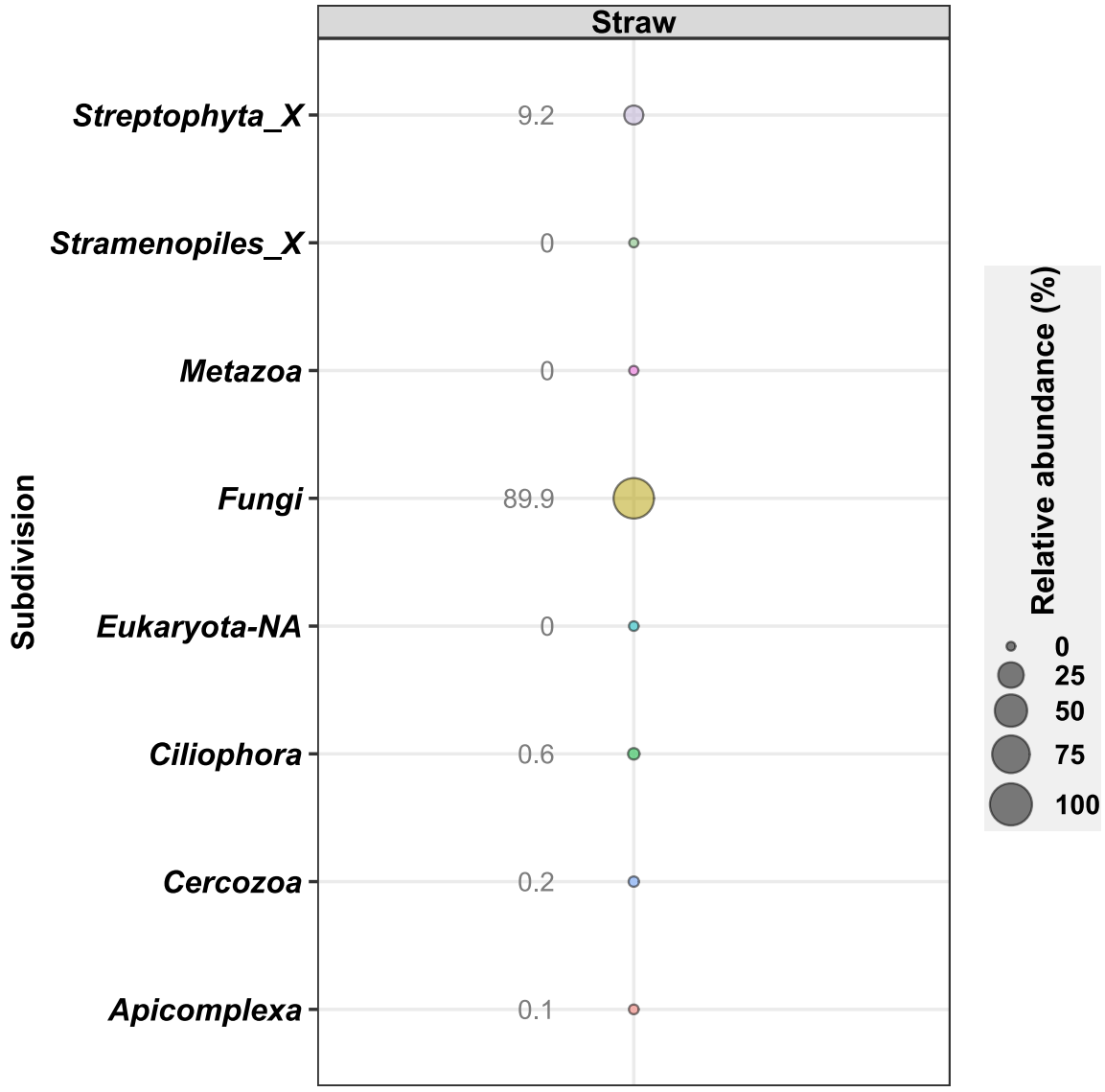


Figure C.6: Relative abundance of eukaryotes in the wheat straw.

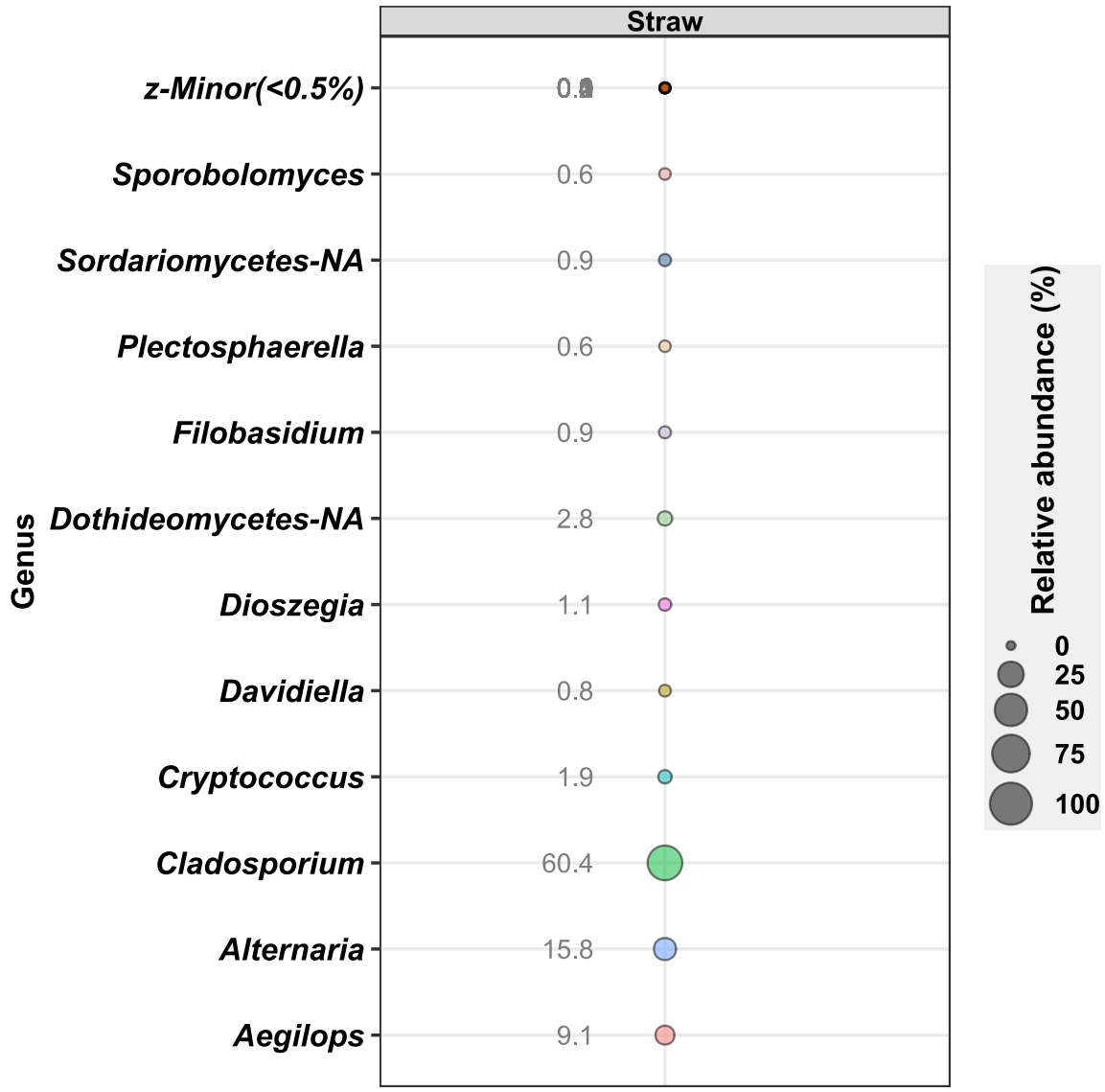


Figure C.7: Relative abundance of prokaryotes in the wheat straw.

D

Appendix for Chapter 5

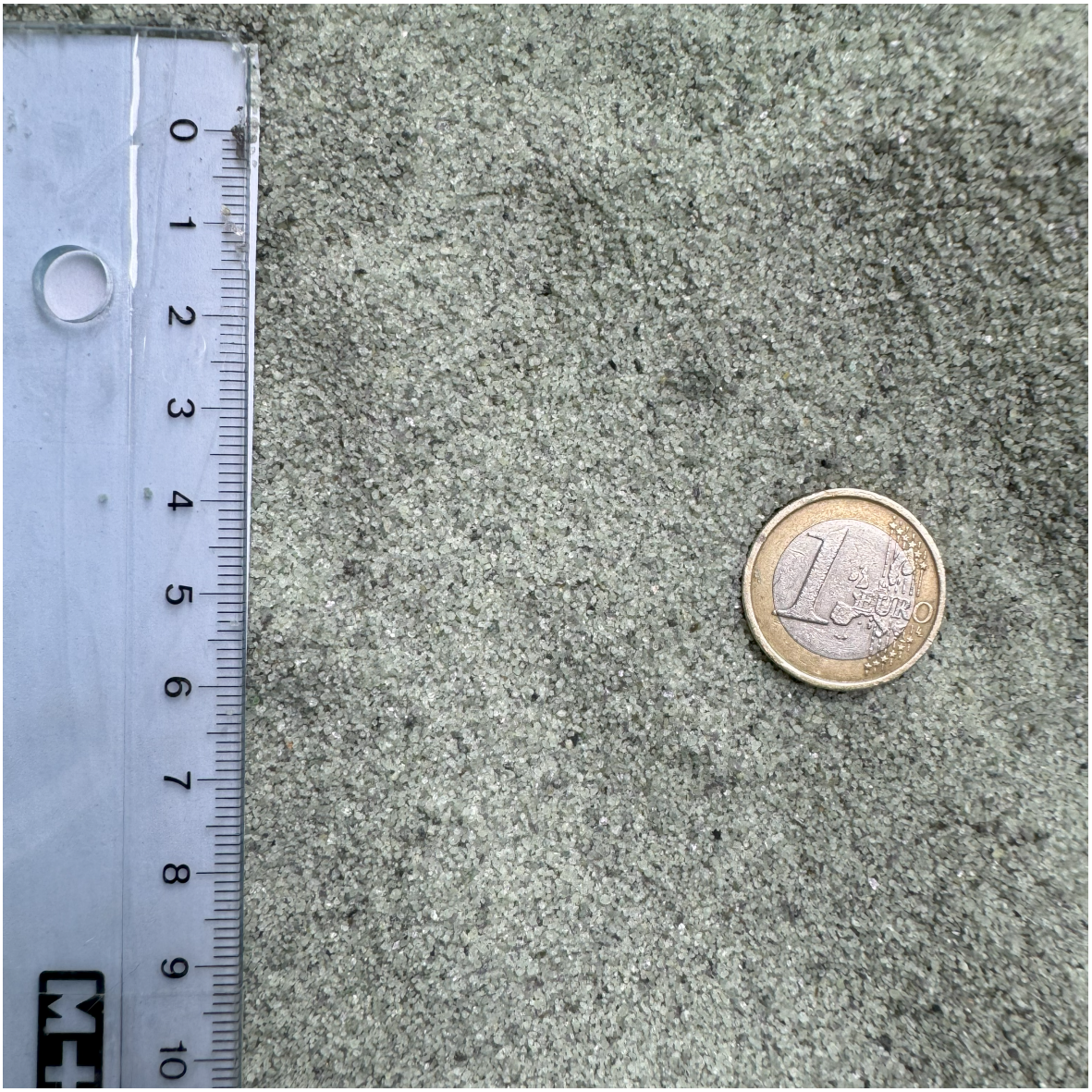


Figure D.1: Peridotite rock powder used in the experiment, with grain sizes of approximately 1 mm.

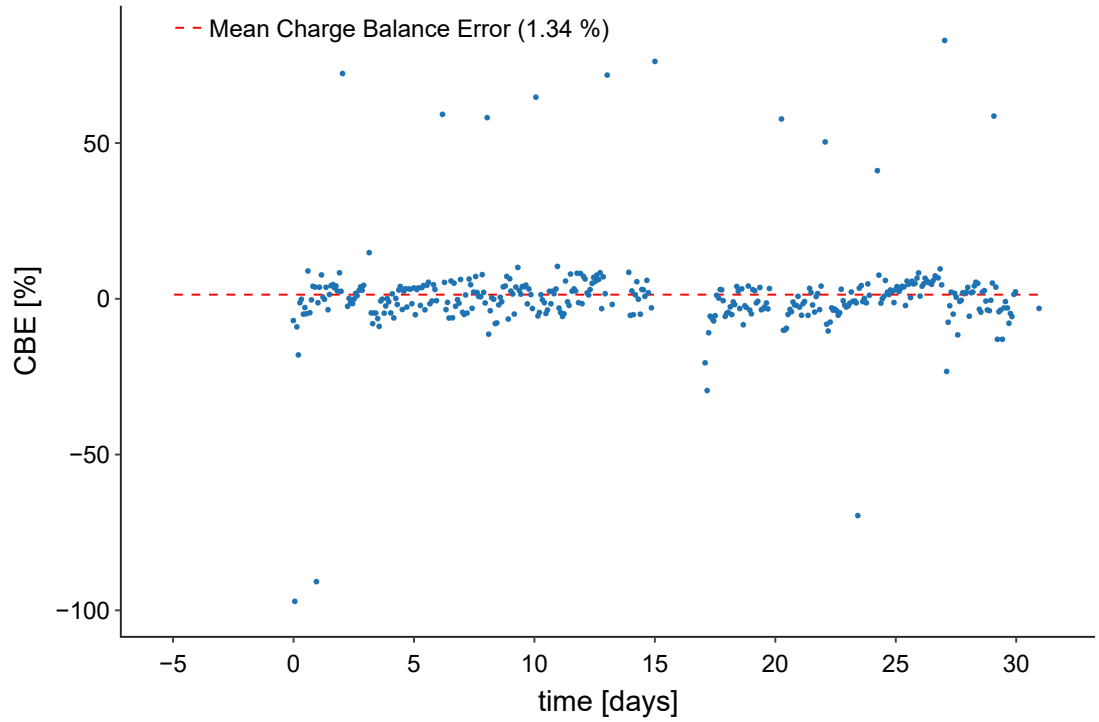


Figure D.2: Charge balance error (CBE) of the data calculated with Equation 5.4.

D.1. Calibration for Mg

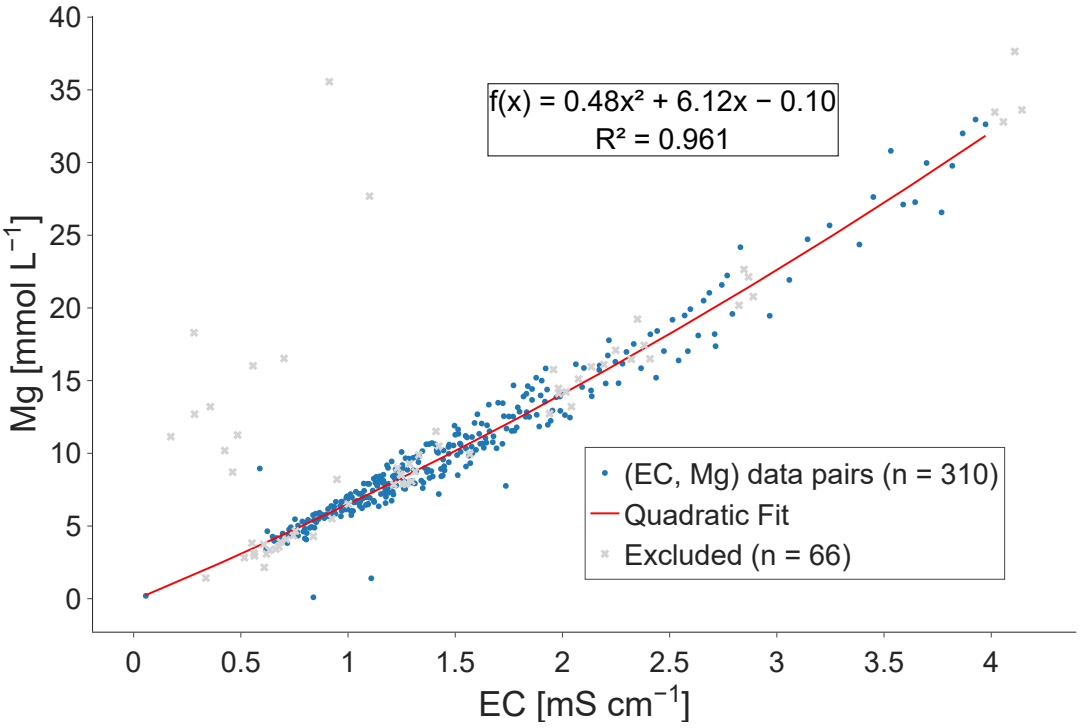


Figure D.3: Mg–EC calibration

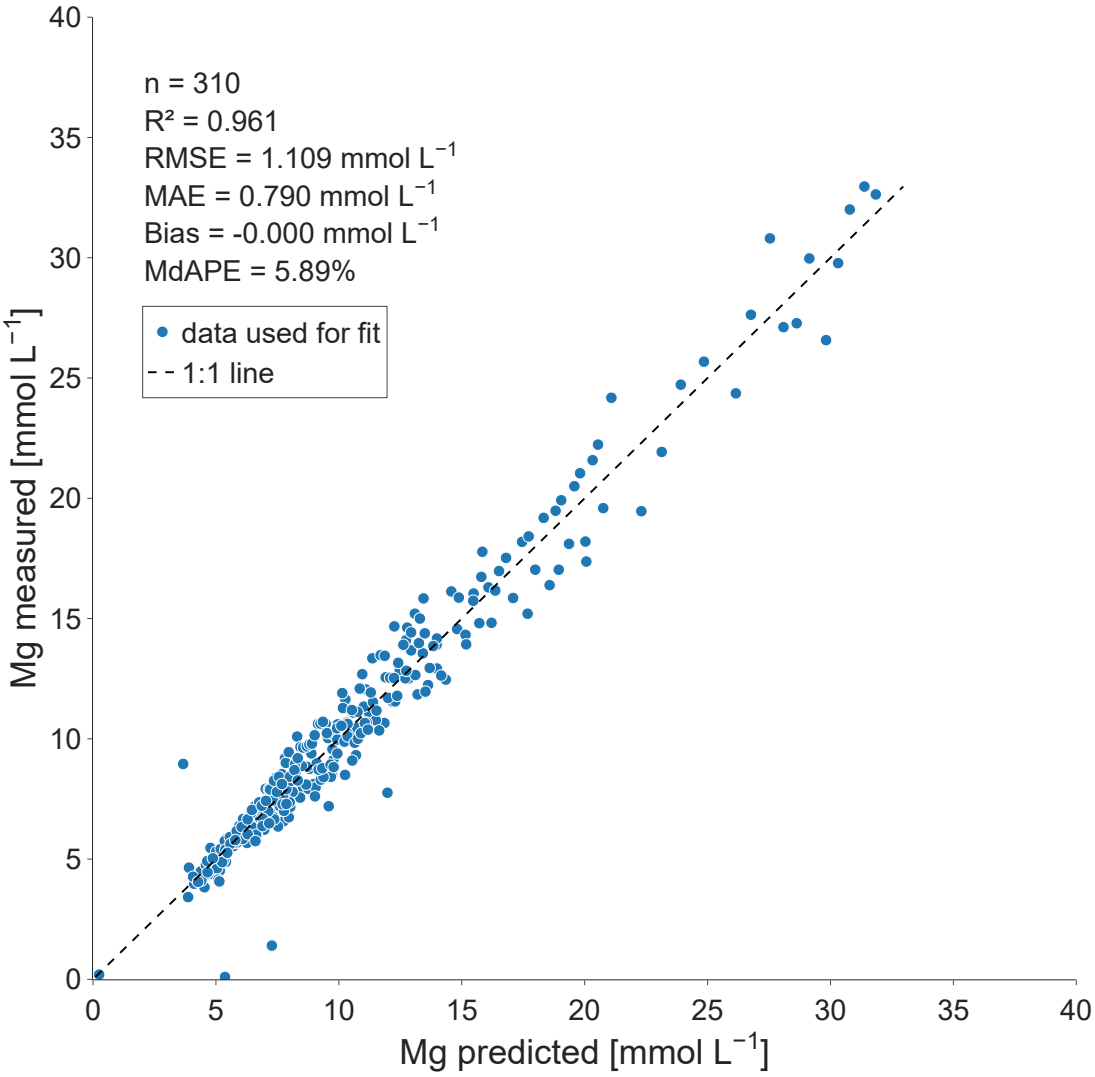


Figure D.4: Mg–EC calibration

D.2. Apparent dissolution rate

To compare the experimentally derived weathering rates with literature values for the same mineral phase, we additionally calculated a dissolution rate for the applied rock material. Because the substrate represents a heterogeneous mixture of different minerals, no single stoichiometric reaction can strictly describe its bulk dissolution. Consequently, a unique compound-specific dissolution rate cannot be derived for the entire rock matrix.

To ensure comparability with published kinetic data, we therefore express the dissolution rate with respect to the most abundant mineral phase in the substrate. As mineralogical analyses indicate that the material is predominantly composed of forsterite, the dissolution

rate is calculated using the stoichiometric coefficients of forsterite dissolution (Equation 5.3). Dissolution of one mol of Mg_2SiO_4 releases two mol of Mg^{2+} and produces four equivalents of TA.

Alternatively, the dissolution rate can be expressed only as TA or base cation release rate. But these are not common in geochemical literature.

$$Mg_2SiO_4(s) + 4\,CO_2(g) + 2\,H_2O \longrightarrow 2\,Mg^{2+} + 4\,HCO_3^- + H_4SiO_4(aq). \tag{D.1}$$

$$r_i = \frac{\mathrm{TA}_i \cdot m_{\mathrm{water},i}}{4 \cdot m_{\mathrm{rock}} \cdot A_{\mathrm{BET},i} \cdot (t_i - t_{i-1})} \tag{D.2}$$

$$r_i = \frac{{\mathrm{Mg}^{2+}}_i \cdot m_{\mathrm{water},i}}{2 \cdot m_{\mathrm{rock}} \cdot A_{\mathrm{BET},i} \cdot (t_i - t_{i-1})} \tag{D.3}$$

The surface area of the rock ($A_{BET,i}$) was tested with Brunauer–Emmett–Teller (BET) method (Naderi, 2015). BET samples were taken five times during the experiment, with each 3 replicates from the substrate.

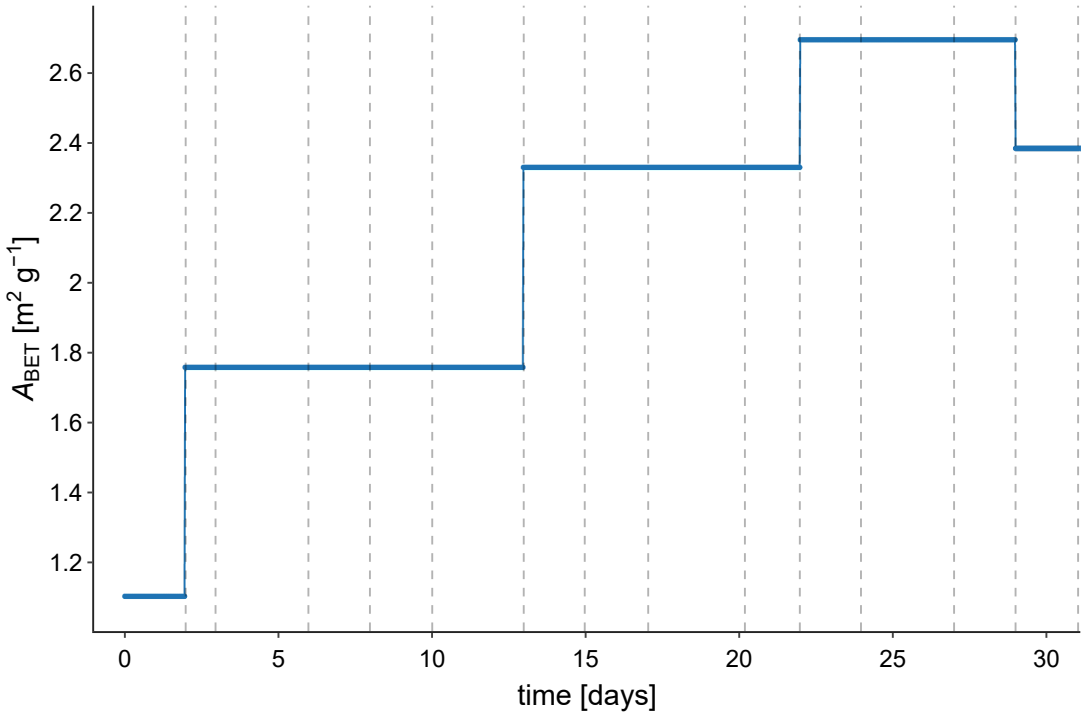


Figure D.5: The specific surface area of the rock was determined using the Brunauer–Emmett–Teller (BET) method . Each BET analysis was performed in triplicate. For the dissolution rate calculations, the BET surface area was treated as a stepwise time-dependent parameter. Upon each new BET measurement, the updated surface area value was applied to all subsequent time steps.

Based on Equation D.2 and Equation D.3, the dissolution rate was calculated using EC-predicted TA and Mg concentrations.

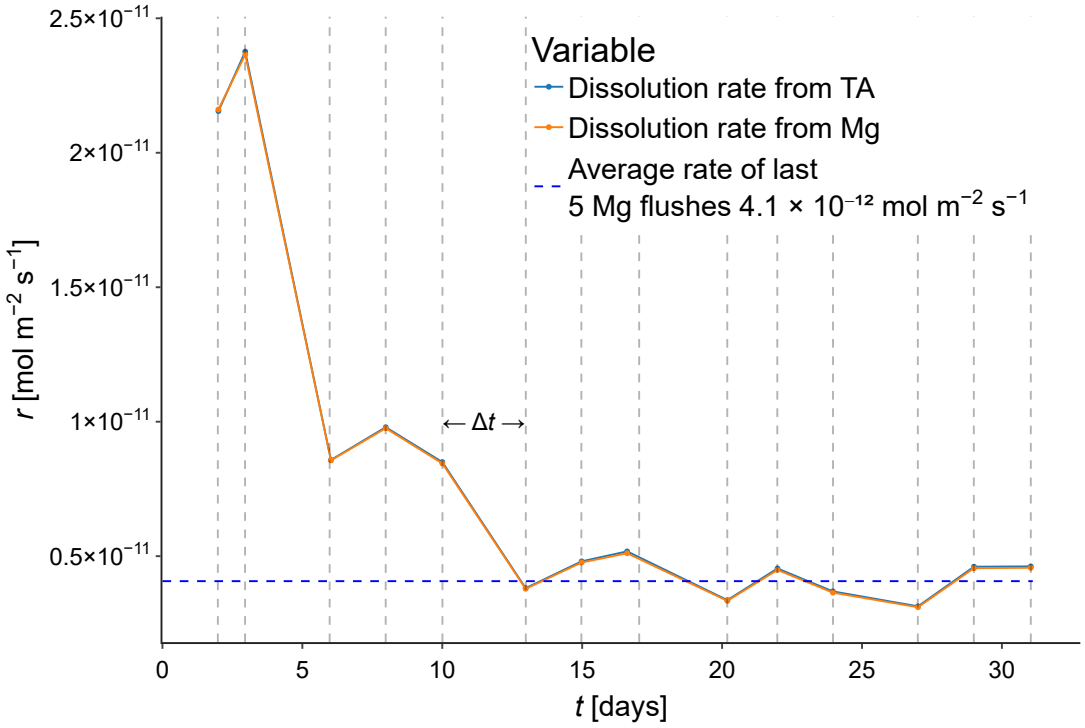


Figure D.6: Dissolution rate for forsterite (Mg_2SiO_4) calculated based on the released total alkalinity (TA) and Mg. The surface arrea for the rock was tested with Brunauer–Emmett–Teller (BET) method .

The pH of the reactor leachate ranged from 5.36 to 6.67, with an average value of 6.00 (see Figure 5.2). The dissolution of forsterite dependent on pH and T was described by Rimstidt, Brantley, and Olsen (2012). See the equation Equation D.4.

$$\log_{10} r_{\text{geo}} = 4.07 - 0.256\,\text{pH} - \frac{3465}{T} \tag{D.4}$$

Using the dissolution rate expression Equation D.4 and the average reactor water temperature (25 °C) and pH (6.00) conditions of our experiment, a dissolution rate of $8.17 \cdot 10^{-10}$ mol m^{-2} s^{-1} is predicted. In contrast, based on the final five flushes and calculated from Mg^{2+} (or TA) release, the experimentally derived dissolution rate in our setup was $4.1 \cdot 10^{-12}$ mol m^{-2} s^{-1}. This corresponds to a difference of slightly more than two orders.

The discrepancy likely arises from differences in reactor configuration. In our system, water is not in continuous contact with the rock substrate but is applied intermittently in a shower-like manner. Such limited fluid–rock interaction reduces effective reaction time and therefore lowers apparent weathering rates. To enhance dissolution kinetics, operation under slurry-like conditions, where the rock material remains in constant contact with the aqueous phase, would be preferable.

Acknowledgements

First, I would like to thank my first supervisor, Jens Hartmann, for giving me the freedom to work independently and develop my own scientific perspective. I also appreciate your remarkable ability to secure funding.

I am also very grateful to my second supervisor, Mathilde Hagens, for the exceptionally fast and comprehensive feedback on my manuscripts throughout my PhD. While writing these lines, I am still impressed by how quickly you always responded to my drafts and helped improve them.

Another person who significantly influenced my PhD journey is Thorben Amann, who previously served as my second supervisor. Thank you for the close collaboration, for your valuable feedback on my first manuscript, and for encouraging me to start working with Jupyter Notebook.

I would also like to thank my project and office mate, Reinaldy Poetra. Without you, the PhD would have been much less enjoyable. I cannot imagine the many work-related trips to Wageningen and Antwerp without you. In Hamburg, you also regularly challenged me with PHREEQC-related questions, which often led to fruitful discussions from which we both learned a lot.

Many thanks go to our lab team, Peggy Bartsch and Tom Jäppinen, for their support in analyzing the large number of samples generated during our experiments.

I would also like to thank Dirk Paessler, Ralf Steffens, and Jens Steffen Hammes for the financial support of my PhD and for the collaboration. I closely followed the Carbdown LinkedIn posts during my PhD, and the transparency of your greenhouse experiment has provided valuable insights for the enhanced rock weathering community.

Thanks as well to all members of SICSS for their patience with my many questions in the PhD WhatsApp group. I also greatly appreciated the retreats organized by the graduate school. For future PhD students reading these lines, I can only recommend participating in such a program, as it helps to structure the PhD journey and maintain a realistic timeline.

I am grateful for the support provided through the BAM project, which funded a major part of my PhD and served as an important source of data. Many people have contributed to the manuscripts presented in this dissertation, and I am grateful for the valuable discussions, feedback, and collaboration. Working in such a large interdisciplinary collaboration with many institutes and contributors taught me a lot about the challenges and opportunities of collaborative research.

I would also like to thank all my other colleagues in Hamburg, who often listened patiently to my many PhD-related concerns during lunch breaks. Your support, discussions, and shared experiences made the challenges of the PhD much easier to handle.

Finally, and most importantly, I would like to thank my family for their continuous support and encouragement, which helped me stay grounded during the challenging and stressful phases of the PhD.

References

Adeleke, R., Nwangburuka, C., and Oboirien, B. (Jan. 2017). "Origins, Roles and Fate of Organic Acids in Soils: A Review". In: *South African Journal of Botany* 108, pp. 393–406. ISSN: 02546299. DOI: 10.1016/j.sajb.2016.09.002. (Visited on 11/06/2025).

Alishum, Ali (Apr. 2021). *DADA2 Formatted 16S rRNA Gene Sequences for Both Bacteria & Archaea*. DOI: 10.5281/ZENODO.4735821. (Visited on 11/03/2025).

Amann, Thorben (June 2013). "Spatiotemporal Variability of Carbon and Silica Fluxes through the Inner Elbe Estuary, Germany". PhD thesis. Hamburg: University of Hamburg.

Amann, Thorben and Hartmann, Jens (May 2022). "Carbon Accounting for Enhanced Weathering". In: *Frontiers in Climate* 4, p. 849948. ISSN: 2624-9553. DOI: 10.3389/fclim.2022.849948. (Visited on 02/28/2023).

Amann, Thorben, Weiss, Andreas, and Hartmann, Jens (Jan. 2015). "Inorganic Carbon Fluxes in the Inner Elbe Estuary, Germany". In: *Estuaries and Coasts* 38.1, pp. 192–210. ISSN: 1559-2723, 1559-2731. DOI: 10.1007/s12237-014-9785-6. (Visited on 05/09/2025).

Amelung, Wulf et al. (2018). "Chemische Eigenschaften Und Prozesse". In: *Scheffer/Schachtschabel Lehrbuch Der Bodenkunde* -. Berlin Heidelberg New York: Springer-Verlag, pp. 173–177. ISBN: 978-3-662-55871-3.

aqion (2020). *Table of Diffusion Coefficients*. https://www.aqion.de/site/diffusion-coefficients. (Visited on 02/25/2026).

Atkins, Peter W., de Paula, Julio, and Keeler, James J. (2023). *Atkins' Physical Chemistry*. Twelfth edition. Oxford: Oxford University Press. ISBN: 978-0-19-884781-6.

Babiker, Mustafa et al. (Apr. 2022). "Cross-Sectoral Perspectives". In: 220 pp. DOI: 10.1017/9781009157926.005.

Baker, Geoff H. and Whitby, Wendy A. (Jan. 2003). "Soil pH Preferences and the Influences of Soil Type and Temperature on the Survival and Growth of Aporrectodea Longa (Lumbricidae)". In: *Pedobiologia* 47.5-6, pp. 745–753. ISSN: 00314056. DOI: 10.1078/0031-4056-00254. (Visited on 10/30/2025).

Baldock, Jeffrey A. and Broos, Kris (2011). "Soil Organic Matter". In: *Handbook of Soil Sciences: Properties and Processes*. CRC Press.

Barnard, Romain L., Blazewicz, Steven J., and Firestone, Mary K. (Aug. 2020). "Rewetting of Soil: Revisiting the Origin of Soil CO2 Emissions". In: *Soil Biology and Biochemistry* 147, p. 107819. ISSN: 00380717. DOI: 10.1016/j.soilbio.2020.107819. (Visited on 10/17/2023).

Bart, Sylvain et al. (Dec. 2018). "Aporrectodea Caliginosa, a Relevant Earthworm Species for a Posteriori Pesticide Risk Assessment: Current Knowledge and Recommendations for Culture and Experimental Design". In: *Environmental Science and Pollution Research* 25.34,

pp. 33867–33881. ISSN: 0944-1344, 1614-7499. DOI: 10.1007/s11356-018-2579-9. (Visited on 10/30/2025).

Bas, M. J. L. et al. (June 1986). "A Chemical Classification of Volcanic Rocks Based on the Total Alkali-Silica Diagram". In: *Journal of Petrology* 27.3, pp. 745–750. ISSN: 0022-3530, 1460-2415. DOI: 10.1093/petrology/27.3.745. (Visited on 07/18/2025).

Baumhardt, R. L., Jones, O. R., and Schwartz, R. C. (May 2008). "Long-Term Effects of Profile-Modifying Deep Plowing on Soil Properties and Crop Yield". In: *Soil Science Society of America Journal* 72.3, pp. 677–682. DOI: 10.2136/sssaj2007.0122.

Beerling, David J. et al. (July 2020). "Potential for Large-Scale CO2 Removal via Enhanced Rock Weathering with Croplands". In: *Nature* 583.7815, pp. 242–248. ISSN: 0028-0836, 1476-4687. DOI: 10.1038/s41586-020-2448-9. (Visited on 08/16/2023).

Beerling, David J. et al. (Sept. 2025). "Challenges and Opportunities in Scaling Enhanced Weathering for Carbon Dioxide Removal". In: *Nature Reviews Earth & Environment* 6.10, pp. 672–686. ISSN: 2662-138X. DOI: 10.1038/s43017-025-00713-7. (Visited on 10/14/2025).

Berner, Robert A. (Nov. 2003). "The Long-Term Carbon Cycle, Fossil Fuels and Atmospheric Composition". In: *Nature* 426.6964, pp. 323–326. ISSN: 0028-0836, 1476-4687. DOI: 10.1038/nature02131. (Visited on 04/25/2023).

Bijma, Jelle et al. (Jan. 2026). "Reviews and Syntheses: Carbon vs. Cation Based MRV of Enhanced Rock Weathering and the Issue of Soil Organic Carbon". In: *Biogeosciences* 23.1, pp. 53–75. ISSN: 1726-4189. DOI: 10.5194/bg-23-53-2026. (Visited on 03/03/2026).

Birch, H. F. (Sept. 1958). "The Effect of Soil Drying on Humus Decomposition and Nitrogen Availability". In: *Plant and Soil* 10.1, pp. 9–31. ISSN: 0032-079X, 1573-5036. DOI: 10.1007/BF01343734. (Visited on 10/17/2023).

Bloom, Paul R. and Skyllberg, Ulf (2011). "Soil pH and pH Buffering". In: *Handbook of Soil Sciences: Properties and Processes*. Ed. by Pan Ming Huang, Yuncong Li, and Malcolm E Sumner. 2nd ed. Vol. 2. CRC Press. Chap. 12.

Bouché, MB (1971). "Relations Entre Les Structures Spatiales et Fonctionelles Des Écosystemes, Illustrées Par Le Rôle Pédobiologique Des Vers de Terre". In: *La vie dans les sols.–Gauthier-Villars, Paris*, pp. 187–209.

— (1977). "Strategies Lombriciennes". In: *Ecological Bulletins*, pp. 122–132. ISSN: 0346-6868.

Bouillon, Steven et al. (June 2014). "Contrasting Biogeochemical Characteristics of the Oubangui River and Tributaries (Congo River Basin)". In: *Scientific Reports* 4.1, p. 5402. ISSN: 2045-2322. DOI: 10.1038/srep05402. (Visited on 01/19/2026).

Bourg, Ian C. and Sposito, Garrison (2011). "Ion Exchange Phenomena". In: *Handbook of Soil Sciences: Properties and Processes*. Ed. by Pan Ming Huang, Yuncong Li, and Malcolm E Sumner. 2nd ed. Vol. 2. CRC Press. Chap. 16.

Boyer, Treavor H., Singer, Philip C., and Aiken, George R. (Oct. 2008). "Removal of Dissolved Organic Matter by Anion Exchange: Effect of Dissolved Organic Matter Properties". In:

Environmental Science & Technology 42.19, pp. 7431–7437. ISSN: 0013-936X. DOI: 10.1021/es800714d.

Brander, Matthew et al. (2021). "Carbon Accounting for Negative Emissions Technologies". In: *Climate Policy* 21.5, pp. 699–717. DOI: 10.1080/14693062.2021.1878009.

Breitenbach, Romy et al. (May 2022). "The Role of Extracellular Polymeric Substances of Fungal Biofilms in Mineral Attachment and Weathering". In: *npj Materials Degradation* 6.1, p. 42. ISSN: 2397-2106. DOI: 10.1038/s41529-022-00253-1. (Visited on 03/14/2025).

Brook, George A., Folkoff, Michael E., and Box, Elgene O. (Jan. 1983). "A World Model of Soil Carbon Dioxide". In: *Earth Surface Processes and Landforms* 8.1, pp. 79–88. ISSN: 01979337, 10969837. DOI: 10.1002/esp.3290080108. (Visited on 06/28/2023).

Bryce, Casey C. et al. (Apr. 2016). "Rock Geochemistry Induces Stress and Starvation Responses in the Bacterial Proteome". In: *Environmental Microbiology* 18.4, pp. 1110–1121. ISSN: 1462-2912, 1462-2920. DOI: 10.1111/1462-2920.13093. (Visited on 03/14/2025).

Byloos, Bo et al. (May 2018). "The Ability of Basalt to Leach Nutrients and Support Growth of *Cupriavidus Metallidurans* CH34 Depends on Basalt Composition and Element Release". In: *Geomicrobiology Journal* 35.5, pp. 438–446. ISSN: 0149-0451, 1521-0529. DOI: 10.1080/01490451.2017.1392650. (Visited on 03/14/2025).

Cai, Wei-Jun, Wang, Yongchen, and Hodson, Robert E. (Feb. 1998). "Acid-Base Properties of Dissolved Organic Matter in the Estuarine Waters of Georgia, USA". In: *Geochimica et Cosmochimica Acta* 62.3, pp. 473–483. ISSN: 00167037. DOI: 10.1016/S0016-7037(97)00363-3. (Visited on 11/15/2024).

Calogiuri, Tullia, Hagens, Mathilde, Van Groenigen, Jan Willem, et al. (Nov. 2025). "Alive and Dead Earthworms Capture Carbon during Mineral Weathering through Different Pathways". In: *Communications Earth & Environment* 6.1, p. 851. ISSN: 2662-4435. DOI: 10.1038/s43247-025-02766-4. (Visited on 11/11/2025).

Calogiuri, Tullia, Janssens, Iris, et al. (Feb. 2025). "How Earthworms Thrive and Drive Silicate Rock Weathering in an Artificial Organo-Mineral System". In: *Applied Geochemistry* 180, p. 106271. ISSN: 08832927. DOI: 10.1016/j.apgeochem.2024.106271. (Visited on 03/24/2025).

Calogiuri, Tullia et al. (Nov. 2023). "Design and Construction of an Experimental Setup to Enhance Mineral Weathering through the Activity of Soil Organisms". In: *Journal of Visualized Experiments* 201, p. 65563. ISSN: 1940-087X. DOI: 10.3791/65563. (Visited on 03/27/2024).

Calogiuri, Tullia et al. (2024). "Earthworms Foster Carbon Capture during Mineral Weathering Both Alive and after Dying through Contrasting Pathways". In: *Submitted to Applied Geochemistry*.

Carbdown (2022). *Carbon Drawdown Initiative (Home)*. https://www.carbon-drawdown.de/home-en. (Visited on 10/09/2023).

Churchman, G. Jock (Feb. 2018). "Game Changer in Soil Science. Functional Role of Clay Minerals in Soil". In: *Journal of Plant Nutrition and Soil Science* 181.1, pp. 99–103. ISSN: 1436-8730, 1522-2624. DOI: 10.1002/jpln.201700605. (Visited on 08/17/2023).

Ciesielski, H. et al. (1997). "Determination of Cation Exchange Capacity and Exchangeable Cations in Soils by Means of Cobalt Hexamine Trichloride. Effects of Experimental Conditions". In: *Agronomie* 17.1, pp. 1–7. ISSN: 0249-5627. DOI: 10.1051/agro:19970101. (Visited on 09/25/2023).

Clarkson, Matthew O. et al. (June 2024). "A Review of Measurement for Quantification of Carbon Dioxide Removal by Enhanced Weathering in Soil". In: *Frontiers in Climate* 6, p. 1345224. ISSN: 2624-9553. DOI: 10.3389/fclim.2024.1345224. (Visited on 07/16/2024).

Corwin, Dennis and Lesch, Scott (Mar. 2005). "Application of Soil Electrical Conductivity Measurements in Agriculture". In: *Computers and Electronics in Agriculture* 46, pp. 11–43. DOI: 10.1016/j.compag.2004.10.005.

Corwin, Dennis L and Yemoto, Kevin (2020). "Salinity: Electrical Conductivity and Total Dissolved Solids". In: *Soil science society of America journal* 84.5, pp. 1442–1461.

Curtin, Denis, Campbell, CA, and Messer, Duaine (1996). *Prediction of Titratable Acidity and Soil Sensitivity to pH Change*. Tech. rep. Wiley Online Library.

Dalby, P.R., Baker, G.H., and Smith, S.E. (Apr. 1996). ""Filter Paper Method" to Remove Soil from Earthworm Intestines and to Standardise the Water Content of Earthworm Tissue". In: *Soil Biology and Biochemistry* 28.4-5, pp. 685–687. ISSN: 0038-0717. DOI: 10.1016/0038-0717(95)00157-3. (Visited on 07/24/2025).

"PHYSICAL CONSTANTS OF INORGANIC COMPOUNDS (CONTINUED)" (2005). In: *CRC Handbook of Chemistry and Physics*. Ed. by David R. Lide. Vol. Internet Version 2005. Boca Raton, FL: CRC Press, Taylor & Francis Group.

de los Ríos, Asunción and Souza-Egipsy, Virginia (2021). "1.1 The Interface of Rocks and Microorganisms". In: *Life at rock surface*, pp. 3–38.

De Villiers, J. M. and Jackson, M. L. (July 1967). "Cation Exchange Capacity Variations with pH in Soil Clays". In: *Soil Science Society of America Journal* 31.4, pp. 473–476. ISSN: 0361-5995, 1435-0661. DOI: 10.2136/sssaj1967.03615995003100040017x. (Visited on 11/11/2023).

Deng, Hang et al. (June 2023). "The Environmental Controls on Efficiency of Enhanced Rock Weathering in Soils". In: *Scientific Reports* 13.1, p. 9765. ISSN: 2045-2322. DOI: 10.1038/s41598-023-36113-4. (Visited on 10/14/2025).

Dickson, Andrew Gilmore et al., eds. (2007). *Guide to Best Practices for Ocean CO2 Measurements*. PICES Special Publication no. 3. Sidney, BC: North Pacific Marine Science Organization. ISBN: 978-1-897176-07-8.

Dietzen, Christiana and Rosing, Minik T. (May 2023). "Quantification of CO2 Uptake by Enhanced Weathering of Silicate Minerals Applied to Acidic Soils". In: *International Journal of Greenhouse Gas Control* 125, p. 103872. ISSN: 17505836. DOI: 10.1016/j.ijggc.2023.103872. (Visited on 06/15/2023).

DIN 19682-2 (2023). *DIN 19682-2:2014-07, Bodenbeschaffenheit_- Felduntersuchungen_- Teil_2: Bestimmung Der Bodenart*. Tech. rep. Beuth Verlag GmbH. DOI: 10.31030/2147102. (Visited on 09/25/2023).

DIN EN 27888 (1993). *DIN EN 27888:1993-11, Wasserbeschaffenheit; Bestimmung Der Elektrischen Leitfähigkeit (ISO_7888:1985); Deutsche Fassung EN_27888:1993*. Tech. rep. Beuth Verlag GmbH. DOI: 10.31030/2569904. (Visited on 03/25/2024).

Dragino (2022). *Dragino LSE01 LoRaWAN Soil Moisture & EC Sensor UserManual*. Dragino.

Drever, James I. (1997). *The Geochemistry of Natural Waters: Surface and Groundwater Environments*. 3rd ed. Upper Saddle River: Prentice-Hall. ISBN: 978-0-13-272790-7.

Du, J H (Mar. 2018). "The Earthworm Gastrointestinal Effect on the Release of Organic Bound Residues in Soils". In: *IOP Conference Series: Earth and Environmental Science* 128, p. 012039. ISSN: 1755-1307, 1755-1315. DOI: 10.1088/1755-1315/128/1/012039. (Visited on 07/21/2025).

Dupla, Xavier et al. (Jan. 2025). "Geochemical Drivers of Enhanced Rock Weathering in Soils". In: *Geoengineering and Climate Change*. Ed. by Martin Beech. 1st ed. Wiley, pp. 207–230. ISBN: 978-1-394-20438-0. DOI: 10.1002/9781394204847.ch13. (Visited on 05/09/2025).

Edwards, Clive A. and Arancon, Norman Q. (2022). *Biology and Ecology of Earthworms*. New York, NY: Springer US. ISBN: 978-0-387-74942-6. DOI: 10.1007/978-0-387-74943-3. (Visited on 07/21/2025).

Entezari Zarandi, Ali et al. (Apr. 2017). "Nesquehonite as a Carbon Sink in Ambient Mineral Carbonation of Ultramafic Mining Wastes". In: *Chemical Engineering Journal* 314, pp. 160–168. ISSN: 13858947. DOI: 10.1016/j.cej.2017.01.003. (Visited on 01/22/2026).

Evans, C.D., Monteith, D.T., and Cooper, D.M. (Sept. 2005). "Long-Term Increases in Surface Water Dissolved Organic Carbon: Observations, Possible Causes and Environmental Impacts". In: *Environmental Pollution* 137.1, pp. 55–71. ISSN: 02697491. DOI: 10.1016/j.envpol.2004.12.031. (Visited on 11/29/2024).

Fan, Xinmeng et al. (Oct. 2022). "Single Calcite Particle Dissolution Kinetics: Revealing the Influence of Mass Transport". In: *ACS Measurement Science Au* 2.5, pp. 422–429. ISSN: 2694-250X, 2694-250X. DOI: 10.1021/acsmeasuresciau.2c00025. (Visited on 07/15/2024).

Felmy, Andrew R. et al. (Aug. 2012). "Reaction of Water-Saturated Supercritical CO2 with Forsterite: Evidence for Magnesite Formation at Low Temperatures". In: *Geochimica et Cosmochimica Acta* 91, pp. 271–282. ISSN: 00167037. DOI: 10.1016/j.gca.2012.05.026. (Visited on 02/02/2026).

Fuss, Sabine et al. (June 2018). "Negative Emissions—Part 2: Costs, Potentials and Side Effects". In: *Environmental Research Letters* 13.6, p. 063002. ISSN: 1748-9326. DOI: 10.1088/1748-9326/aabf9f. (Visited on 02/28/2023).

Garamszegi, Péter et al. (Dec. 2024). "A Density-Based Method to Objectively Quantify Earthworm Activity". In: *Applied Soil Ecology* 206, p. 105771. ISSN: 09291393. DOI: 10.1016/j.apsoil.2024.105771. (Visited on 10/23/2025).

García-Gil, J.C et al. (July 2004). "Long-Term Effects of Amendment with Municipal Solid Waste Compost on the Elemental and Acidic Functional Group Composition and pH-buffer Capacity of Soil Humic Acids". In: *Geoderma* 121.1-2, pp. 135–142. ISSN: 00167061. DOI: 10.1016/j.geoderma.2003.11.004. (Visited on 06/14/2023).

Geden, Oliver, Smith, Steve, and Cowie, Annette (2024). "Chapter 1: Introduction, The State of Carbon Dioxide Removal - 2nd Edition". In: DOI: 10.17605/OSF.IO/E5M86. (Visited on 03/02/2026).

Georgiadis, Anna et al. (July 2019). "Do Earthworms Affect the Fractionation of Silicon in Soil?" In: *Pedobiologia* 75, pp. 1–7. ISSN: 00314056. DOI: 10.1016/j.pedobi.2019.05.001. (Visited on 04/10/2025).

Gerrits, R. et al. (Aug. 2020). "How the Rock-Inhabiting Fungus K. Petricola A95 Enhances Olivine Dissolution through Attachment". In: *Geochimica et Cosmochimica Acta* 282, pp. 76–97. ISSN: 00167037. DOI: 10.1016/j.gca.2020.05.010. (Visited on 03/14/2025).

Giammar, Daniel E., Bruant, Robert G., and Peters, Catherine A. (Apr. 2005). "Forsterite Dissolution and Magnesite Precipitation at Conditions Relevant for Deep Saline Aquifer Storage and Sequestration of Carbon Dioxide". In: *Chemical Geology* 217.3-4, pp. 257–276. ISSN: 00092541. DOI: 10.1016/j.chemgeo.2004.12.013. (Visited on 01/22/2026).

Goll, Daniel et al. (July 2021). "Potential CO2 Removal from Enhanced Weathering by Ecosystem Responses to Powdered Rock". In: *Nature Geoscience* 14, pp. 1–5. DOI: 10.1038/s41561-021-00798-x.

Hammer, Karoline et al. (Sept. 2017). "Acid-Base Properties of Baltic Sea Dissolved Organic Matter". In: *Journal of Marine Systems* 173, pp. 114–121. ISSN: 09247963. DOI: 10.1016/j.jmarsys.2017.04.007. (Visited on 04/08/2025).

Hansen, H. P. and Koroleff, F. (Jan. 1999). "Determination of Nutrients". In: *Methods of Seawater Analysis*. Ed. by Klaus Grasshoff, Klaus Kremling, and Manfred Ehrhardt. 1st ed. Wiley, pp. 159–228. ISBN: 978-3-527-29589-0. DOI: 10.1002/9783527613984.ch10. (Visited on 04/11/2024).

Haque, Fatima, Santos, Rafael M., and Chiang, Yi Wai (June 2020). "CO2 Sequestration by Wollastonite-Amended Agricultural Soils – An Ontario Field Study". In: *International Journal of Greenhouse Gas Control* 97, p. 103017. ISSN: 17505836. DOI: 10.1016/j.ijggc.2020.103017. (Visited on 04/26/2023).

Harned, Herbert S and Davis Jr, Raymond (1943). "The Ionization Constant of Carbonic Acid in Water and the Solubility of Carbon Dioxide in Water and Aqueous Salt Solutions from 0 to 50". In: *Journal of the American Chemical Society* 65.10, pp. 2030–2037. ISSN: 0002-7863.

Hartmann, Jens et al. (Apr. 2013). "Enhanced Chemical Weathering as a Geoengineering Strategy to Reduce Atmospheric Carbon Dioxide, Supply Nutrients, and Mitigate Ocean Acidification". In: *Reviews of Geophysics* 51.2, pp. 113–149. ISSN: 87551209. DOI: 10.1002/rog.20004. (Visited on 02/28/2023).

Hasemer, Heath, Borevitz, Justin, and Buss, Wolfram (Sept. 2024). "Measuring Enhanced Weathering: Inorganic Carbon-Based Approaches May Be Required to Complement

Cation-Based Approaches". In: *Frontiers in Climate* 6, p. 1352825. ISSN: 2624-9553. DOI: 10.3389/fclim.2024.1352825. (Visited on 02/16/2026).

Hastings, A Baird and Sendroy Jr, Julius (1925). "The Effect of Variation in Ionic Strength on the Apparent First and Second Dissociation Constants of Carbonic Acid". In: *Journal of Biological Chemistry* 65.2, pp. 445–455. ISSN: 0021-9258.

Havlin, J. L. (2005). "FERTILITY". In: *Encyclopedia of Soils in the Environment*. Ed. by Daniel Hillel. Oxford: Elsevier, pp. 10–19. ISBN: 978-0-12-348530-4. DOI: 10.1016/B0-12-348530-4/00228-9.

Haynes, William M. (2015). "CRC Handbook of Chemistry and Physics, 96th Edition -". In: Boca Raton, Fla: CRC Press, p. 194. ISBN: 978-1-4822-6097-7.

Heinsbroek, Abel (2021). *Phreeqpython: Vitens Viphreeqc Wrapper and Utilities*. Vitens. (Visited on 04/08/2024).

Helling, Charles S., Chesters, G., and Corey, R. B. (July 1964). "Contribution of Organic Matter and Clay to Soil Cation-Exchange Capacity as Affected by the pH of the Saturating Solution". In: *Soil Science Society of America Journal* 28.4, pp. 517–520. ISSN: 03615995. DOI: 10.2136/sssaj1964.03615995002800040020x. (Visited on 03/08/2023).

Hendrickx, Jan M. H. et al. (Jan. 2002). "6.1 Solute Content and Concentration". In: *Methods of Soil Analysis: Part 4 Physical Methods*. Soil Science Society of America, pp. 1253–1321. DOI: 10.2136/sssabookser5.4.c54.

Herdtweck, Eberhardt et al. (May 2011). "Crystal Structure, Synthesis, and Properties of *Tri* -Calcium *Di* -Citrate *Tetra* -Hydrate [Ca_3 (C_6 H_5 O_7)$_2$ (H_2 O)$_2$]·2H_2 O". In: *Zeitschrift für anorganische und allgemeine Chemie* 637.6, pp. 655–659. ISSN: 0044-2313, 1521-3749. DOI: 10.1002/zaac.201100088. (Visited on 04/16/2025).

Hoffland, Ellis et al. (2004). "The Role of Fungi in Weathering". In: *Frontiers in Ecology and the Environment* 2.5, pp. 258–264. ISSN: 1540-9309.

Hu, Xinping (June 2020). "Effect of Organic Alkalinity on Seawater Buffer Capacity: A Numerical Exploration". In: *Aquatic Geochemistry* 26.2, pp. 161–178. ISSN: 1380-6165, 1573-1421. DOI: 10.1007/s10498-020-09375-x. (Visited on 04/09/2025).

Hunt, C. W., Salisbury, J. E., and Vandemark, D. (Oct. 2011). "Contribution of Non-Carbonate Anions to Total Alkalinity and Overestimation of p CO_2 in New England and New Brunswick Rivers". In: *Biogeosciences* 8.10, pp. 3069–3076. ISSN: 1726-4189. DOI: 10.5194/bg-8-3069-2011. (Visited on 05/12/2025).

IPCC (2022a). *Climate Change 2022 - Mitigation of Climate Change: Working Group III Contribution to the Sixth Assessment Report of the Intergovernmental Panel on Climate Change*. 1st ed. Cambridge University Press. ISBN: 978-1-009-15792-6. DOI: 10.1017/9781009157926. (Visited on 07/12/2024).

— (2022b). *IPCC AR6 WGIII: CDR Factsheet*. URL: https://www.ipcc.ch/report/ar6/wg3/downloads/outreach/IPCC_AR6_WGIII_Factsheet_CDR.pdf (visited on 07/12/2024).

IPCC (Mar. 2023). "Climate Change 2023: Synthesis Report. Contribution of Working Groups I, II and III to the Sixth Assessment Report of the Intergovernmental Panel on Climate Change [Core Writing Team, H. Lee and J. Romero (Eds.)]. IPCC, Geneva, Switzerland". In: pp. 35–115. DOI: 10.59327/IPCC/AR6-9789291691647.

— (Oct. 2025). *Sixty-Third Session of the IPCC (IPCC-63)*. Tech. rep. 63. Lima, Peru. (Visited on 03/02/2026).

IUSS Working Group WRB (2022). *World Reference Base for Soil Resources. International Soil Classification System for Naming Soils and Creating Legends for Soil Maps*. 4th. Vienna, Austria: International Union of Soil Sciences (IUSS). ISBN: 979-8-9862451-1-9.

Janssens, Iris et al. (Sept. 2025). "Machine Learning-Based Identification of Key Biotic and Abiotic Drivers of Mineral Weathering Rate in a Complex Enhanced Weathering Experiment". In: *Open Research Europe* 5, p. 71. ISSN: 2732-5121. DOI: 10.12688/openreseurope.19252.3. (Visited on 10/14/2025).

Kalbitz, K. et al. (Apr. 2000). "CONTROLS ON THE DYNAMICS OF DISSOLVED ORGANIC MATTER IN SOILS: A REVIEW". In: *Soil Science* 165.4, p. 277. ISSN: 0038-075X. (Visited on 11/29/2024).

Karki, Renisha et al. (June 2021). "Anaerobic Co-Digestion: Current Status and Perspectives". In: *Bioresource Technology* 330, p. 125001. ISSN: 09608524. DOI: 10.1016/j.biortech.2021.125001. (Visited on 04/17/2025).

Kerr, Daniel E. et al. (Dec. 2021). "The Influence of Organic Alkalinity on the Carbonate System in Coastal Waters". In: *Marine Chemistry* 237, p. 104050. ISSN: 03044203. DOI: 10.1016/j.marchem.2021.104050. (Visited on 06/21/2023).

Kim, Hyun-Cheol and Lee, Kitack (Oct. 2009). "Significant Contribution of Dissolved Organic Matter to Seawater Alkalinity". In: *Geophysical Research Letters* 36.20, 2009GL040271. ISSN: 0094-8276, 1944-8007. DOI: 10.1029/2009GL040271. (Visited on 04/10/2025).

Kney, Arthur D. and Brandes, David (Mar. 2007). "A Graphical Screening Method for Assessing Stream Water Quality Using Specific Conductivity and Alkalinity Data". In: *Journal of Environmental Management* 82.4, pp. 519–528. ISSN: 03014797. DOI: 10.1016/j.jenvman.2006.01.014. (Visited on 02/25/2026).

Ko, Young Ho et al. (July 2016). "Organic Alkalinity Produced by Phytoplankton and Its Effect on the Computation of Ocean Carbon Parameters". In: *Limnology and Oceanography* 61.4, pp. 1462–1471. ISSN: 0024-3590, 1939-5590. DOI: 10.1002/lno.10309. (Visited on 05/12/2025).

Koenig, Nils (Jan. 2005). *Handbuch Forstliche Analytik - Eine Loseblatt-Sammlung Der Analysemethoden Im Forstbereich.*

Kramer, Clyde Young (Sept. 1956). "Extension of Multiple Range Tests to Group Means with Unequal Numbers of Replications". In: *Biometrics* 12.3, p. 307. ISSN: 0006341X. DOI: 10.2307/3001469. JSTOR: 3001469. (Visited on 07/31/2025).

Kuliński, Karol et al. (Apr. 2014). "The Influence of Dissolved Organic Matter on the Acid–Base System of the Baltic Sea". In: *Journal of Marine Systems* 132, pp. 106–115. ISSN: 09247963. DOI: 10.1016/j.jmarsys.2014.01.011. (Visited on 04/08/2025).

Küsel, Kirsten and Drake, Harold L (Jan. 1998). "Microbial Turnover of Low Molecular Weight Organic Acids during Leaf Litter Decomposition". In: *Soil Biology and Biochemistry* 31.1, pp. 107–118. ISSN: 00380717. DOI: 10.1016/S0038-0717(98)00111-4. (Visited on 11/19/2025).

Kutner, Michael H. et al. (2005). *Applied Linear Statistical Models*. Fifth edition. Boston: McGraw-Hill Irwin. ISBN: 978-0-07-238688-2.

Kutus, Bence et al. (Aug. 2020). "Recent Advances in the Aqueous Chemistry of the Calcium(II)-Gluconate System – Equilibria, Structure and Composition of the Complexes Forming in Neutral and in Alkaline Solutions". In: *Coordination Chemistry Reviews* 417, p. 213337. ISSN: 00108545. DOI: 10.1016/j.ccr.2020.213337. (Visited on 04/17/2025).

Lan, Xin et al. (2023). *Trends in Globally-Averaged CO2 Determined from NOAA Global Monitoring Laboratory Measurements.* DOI: 10.15138/9N0H-ZH07. (Visited on 05/04/2023).

Larkin, Christina S. et al. (Aug. 2022). "Quantification of CO2 Removal in a Large-Scale Enhanced Weathering Field Trial on an Oil Palm Plantation in Sabah, Malaysia". In: *Frontiers in Climate* 4, p. 959229. ISSN: 2624-9553. DOI: 10.3389/fclim.2022.959229. (Visited on 04/25/2023).

Lasaga, Antonio C. et al. (May 1994). "Chemical Weathering Rate Laws and Global Geochemical Cycles". In: *Geochimica et Cosmochimica Acta* 58.10, pp. 2361–2386. ISSN: 00167037. DOI: 10.1016/0016-7037(94)90016-7. (Visited on 07/15/2024).

Lazo, Daniel Eduardo, Dyer, Laurence G., and Alorro, Richard Diaz (Jan. 2017). "Silicate, Phosphate and Carbonate Mineral Dissolution Behaviour in the Presence of Organic Acids: A Review". In: *Minerals Engineering* 100, pp. 115–123. ISSN: 08926875. DOI: 10.1016/j.mineng.2016.10.013. (Visited on 04/17/2025).

Le Maitre, R. W. et al., eds. (2002). *Igneous Rocks: A Classification and Glossary of Terms*. 2nd ed. Cambridge: Cambridge University Press. ISBN: 978-0-511-53558-1. DOI: 10.1017/CBO9780511535581. (Visited on 11/18/2025).

Lee, Chang-Ho et al. (Dec. 2024). "Persistent Organic Alkalinity in the Ocean". In: *Geochimica et Cosmochimica Acta* 387, pp. 53–62. ISSN: 00167037. DOI: 10.1016/j.gca.2024.06.010. (Visited on 04/10/2025).

Lee, Jong-Un and Fein, Jeremy B. (May 2000). "Experimental Study of the Effects of Bacillus Subtilis on Gibbsite Dissolution Rates under Near-Neutral pH and Nutrient-Poor Conditions". In: *Chemical Geology* 166.3-4, pp. 193–202. ISSN: 00092541. DOI: 10.1016/S0009-2541(99)00191-6. (Visited on 03/14/2025).

Levene, Howard (1960). "Robust Tests for Equality of Variances". In: *Contributions to probability and statistics*, pp. 278–292.

Lewis, E. (Jan. 1980). "The Practical Salinity Scale 1978 and Its Antecedents". In: *IEEE Journal of Oceanic Engineering* 5.1, pp. 3–8. ISSN: 0364-9059. DOI: 10.1109/JOE.1980.1145448. (Visited on 01/07/2026).

Liu, Hailong et al. (Mar. 2021). "The Molecular Regulatory Mechanisms of the Bacteria Involved in Serpentine Weathering Coupled with Carbonation". In: *Chemical Geology* 565, p. 120069. ISSN: 00092541. DOI: 10.1016/j.chemgeo.2021.120069. (Visited on 03/14/2025).

Liu, Shaoda, Butman, David E., and Raymond, Peter A. (2020). "Evaluating CO2 Calculation Error from Organic Alkalinity and pH Measurement Error in Low Ionic Strength Freshwaters". In: *Limnology and Oceanography: Methods* 18.10, pp. 606–622. DOI: 10.1002/lom3.10388.

Lozovik, P. A. (Nov. 2005). "Contribution of Organic Acid Anions to the Alkalinity of Natural Humic Water". In: *Journal of Analytical Chemistry* 60.11, pp. 1000–1004. ISSN: 1061-9348, 1608-3199. DOI: 10.1007/s10809-005-0226-3. (Visited on 04/04/2025).

Lubbers, Ingrid M. et al. (Mar. 2013). "Greenhouse-Gas Emissions from Soils Increased by Earthworms". In: *Nature Climate Change* 3.3, pp. 187–194. ISSN: 1758-678X, 1758-6798. DOI: 10.1038/nclimate1692. (Visited on 04/10/2025).

Lukawska-Matuszewska, Katarzyna (Nov. 2016). "Contribution of Non-Carbonate Inorganic and Organic Alkalinity to Total Measured Alkalinity in Pore Waters in Marine Sediments (Gulf of Gdansk, S-E Baltic Sea)". In: *Marine Chemistry* 186, pp. 211–220. ISSN: 03044203. DOI: 10.1016/j.marchem.2016.10.002. (Visited on 04/23/2024).

Lukawska-Matuszewska, Katarzyna et al. (Mar. 2018). "Constituents of Organic Alkalinity in Pore Water of Marine Sediments". In: *Marine Chemistry* 200, pp. 22–32. ISSN: 03044203. DOI: 10.1016/j.marchem.2018.01.012. (Visited on 04/08/2025).

Lv, Xiaofei et al. (Jan. 2023). "Seasonal Variations of Low-Molecular-Weight Organic Acids in Three Evergreen Broadleaf Rhododendron Forests". In: *Metabolites* 13.1, p. 119. ISSN: 2218-1989. DOI: 10.3390/metabo13010119. (Visited on 11/19/2025).

Lybrand, Rebecca A. et al. (Mar. 2022). "Fungal Hyphae Develop Where Titanomagnetite Inclusions Reach the Surface of Basalt Grains". In: *Scientific Reports* 12.1, p. 3407. ISSN: 2045-2322. DOI: 10.1038/s41598-021-04157-z. (Visited on 10/14/2025).

Martin, Marcel (May 2011). "Cutadapt Removes Adapter Sequences from High-Throughput Sequencing Reads". In: *EMBnet.journal* 17.1, p. 10. ISSN: 2226-6089. DOI: 10.14806/ej.17.1.200. (Visited on 10/30/2025).

Maxbauer, Daniel P. et al. (Jan. 2026). "Evidence for Carbon Dioxide Removal via Enhanced Rock Weathering with Steel Slag, Though Not Basalt, in a Midwestern U.S. Field Trial". In: *Frontiers in Climate* 7, p. 1657058. ISSN: 2624-9553. DOI: 10.3389/fclim.2025.1657058. (Visited on 02/16/2026).

McCauley, A., Jones, C., and Jacobsen, J. (Jan. 2005). "Basic Soil Properties". In: *Soil & water management module 1*, pp. 1–12.

McCleskey, Richard, Nordstrom, D. Kirk, and Ryan, Joseph N. (Nov. 2012). "Comparison of Electrical Conductivity Calculation Methods for Natural Waters". In: *Limnology and*

Oceanography: Methods 10.11, pp. 952–967. ISSN: 1541-5856, 1541-5856. DOI: 10.4319/lom.2012.10.952. (Visited on 02/17/2026).

McCleskey, Richard et al. (Jan. 2012). "A New Method of Calculating Electrical Conductivity with Applications to Natural Waters". In: *Geochimica et Cosmochimica Acta* 77, pp. 369–382. DOI: 10.1016/j.gca.2011.10.031.

McKinney, Wes (2010). "Data Structures for Statistical Computing in Python". In: *Python in Science Conference*. Austin, Texas, pp. 56–61. DOI: 10.25080/Majora-92bf1922-00a. (Visited on 01/27/2026).

Mclean, E.O. (Oct. 2015). "Soil pH and Lime Requirement". In: *Agronomy Monographs*. Ed. by A.L. Page. Madison, WI, USA: American Society of Agronomy, Soil Science Society of America, pp. 199–224. ISBN: 978-0-89118-072-2. DOI: 10.2134/agronmonogr9.2.2ed.c12. (Visited on 06/22/2023).

Merkel, Broder J. and Planer-Friedrich, Britta (2008). *Groundwater Geochemistry - A Practical Guide to Modeling of Natural and Contaminated Aquatic Systems*. 2nd ed. Berlin Heidelberg: Springer Science and Business Media. Chap. 1.1. ISBN: 978-3-540-74668-3. DOI: 10.1007/b138774.

Middelburg, Jack J., Soetaert, Karline, and Hagens, Mathilde (Sept. 2020). "Ocean Alkalinity, Buffering and Biogeochemical Processes". In: *Reviews of Geophysics* 58.3, e2019RG000681. ISSN: 8755-1209, 1944-9208. DOI: 10.1029/2019RG000681. (Visited on 04/08/2025).

Miessler, Gary L., Fischer, Paul J., and Tarr, Donald A. (2014). *Inorganic Chemistry*. Fifth edition. Boston: Pearson. ISBN: 978-0-321-81105-9.

Montgomery, Douglas C., ed. (2013). *Design and Analysis of Experiments*. Eighth edition. Hoboken, NJ: John Wiley & Sons, Inc. ISBN: 978-1-118-14692-7.

Morse, John W and Arvidson, Rolf S (July 2002). "The Dissolution Kinetics of Major Sedimentary Carbonate Minerals". In: *Earth-Science Reviews* 58.1-2, pp. 51–84. ISSN: 00128252. DOI: 10.1016/S0012-8252(01)00083-6. (Visited on 07/15/2024).

Mostofa, Khan M. G. et al. (2013). "Dissolved Organic Matter in Natural Waters". In: *Photobiogeochemistry of Organic Matter*. Ed. by Khan M.G. Mostofa et al. Berlin, Heidelberg: Springer Berlin Heidelberg, pp. 1–137. ISBN: 978-3-642-32222-8. DOI: 10.1007/978-3-642-32223-5_1. (Visited on 04/15/2025).

Muller, François L.L. and Bleie, Bjørn (July 2008). "Estimating the Organic Acid Contribution to Coastal Seawater Alkalinity by Potentiometric Titrations in a Closed Cell". In: *Analytica Chimica Acta* 619.2, pp. 183–191. ISSN: 00032670. DOI: 10.1016/j.aca.2008.05.018. (Visited on 03/07/2024).

Müller, Harald, Bourcet, Léa, and Hanfland, Michael (Jan. 2021). "Iron(II)Oxalate Dihydrate—Humboldtine: Synthesis, Spectroscopic and Structural Properties of a Versatile Precursor for High Pressure Research". In: *Minerals* 11.2, p. 113. ISSN: 2075-163X. DOI: 10.3390/min11020113. (Visited on 11/26/2024).

Naderi, Majid (2015). "Surface Area". In: *Progress in Filtration and Separation*. Elsevier, pp. 585–608. ISBN: 978-0-12-384746-1. DOI: 10.1016/B978-0-12-384746-1.00014-8. (Visited on 02/28/2026).

NASEM National Academies of Sciences, Engineering, and Medicine (Mar. 2019). *Negative Emissions Technologies and Reliable Sequestration: A Research Agenda*. Washington, D.C.: National Academies Press, p. 25259. ISBN: 978-0-309-48452-7. DOI: 10.17226/25259. (Visited on 03/09/2023).

Neaman, A. (Feb. 2005). "Implications of the Evolution of Organic Acid Moieties for Basalt Weathering over Geological Time". In: *American Journal of Science* 305.2, pp. 147–185. ISSN: 0002-9599. DOI: 10.2475/ajs.305.2.147. (Visited on 04/17/2025).

Niron, Harun et al. (Sept. 2024). "Exploring the Synergy of Enhanced Weathering and *Bacillus Subtilis* : A Promising Strategy for Sustainable Agriculture". In: *Global Change Biology* 30.9, e17511. ISSN: 1354-1013, 1365-2486. DOI: 10.1111/gcb.17511. (Visited on 08/21/2025).

NIST46 (Jan. 2013). *Critically Selected Stability Constants of Metal Complexes: Version 8.0*. DOI: 10.18434/M32154. (Visited on 04/08/2024).

Novozamsky, I. et al. (Feb. 1996). "Solubilization of Plant Tissue with Nitric Acid-hydrofluoric Acid-hydrogen Peroxide in a Closed-system Microwave Digestor". In: *Communications in Soil Science and Plant Analysis* 27.3-4, pp. 867–875. ISSN: 0010-3624, 1532-2416. DOI: 10.1080/00103629609369603. (Visited on 11/01/2024).

O'Connor, W. K. et al. (May 2002). "Carbon Dioxide Sequestration by Direct Mineral Carbonation: Process Mineralogy of Feed and Products". In: *Mining, Metallurgy & Exploration* 19.2, pp. 95–101. ISSN: 2524-3462, 2524-3470. DOI: 10.1007/BF03403262. (Visited on 01/22/2026).

Olea, Ricardo A. (2022). "Total Alkali-Silica Diagram". In: *Encyclopedia of Mathematical Geosciences*. Ed. by B.S. Daya Sagar et al. Cham: Springer International Publishing, pp. 1–2. ISBN: 978-3-030-26050-7. DOI: 10.1007/978-3-030-26050-7_330-1. (Visited on 06/10/2025).

Orsini, L and Remy, JC (1976). "Utilisation Du Chlorure de Cobaltihexamine Pour La Détermination Simultanée de La Capacité d'échange et Des Bases Échangeables Des Sols". In: *Sci. Sol* 4, pp. 269–275.

Paessler, Dirk et al. (2024). "Insights from Monitoring Leachate Alkalinity, pCO_2 and CO_2 Efflux of 400 Weathering Experiments over One Year Working Paper -V1.0 -April 11th 2024". In: DOI: 10.13140/RG.2.2.14022.28485. (Visited on 03/28/2025).

Paessler, Dirk et al. (2026). "Total Alkalinity, Electrical Conductivity and pH as Potential MRV Proxies for Enhanced Weathering A Guided Tour Through Our Data From A Two-Year Greenhouse Experiment". In: DOI: 10.13140/RG.2.2.23232.39688. (Visited on 02/25/2026).

Parkhurst, D L and Appelo, C A J (2013). *Description of Input and Examples for PHREEQC Version 3–A Computer Program for Speciation, Batch-Reaction, One-Dimensional Transport, and Inverse Geochemical Calculations*.

Parkhurst, David L. and Appelo, C. a. J. (2013). "PHREEQC (Version 3)—A Computer Program for Speciation, Batch-Reaction, One-Dimensional Transport, and Inverse Geochemical Calculations". In: *Model. Tech. B* 6, p. 497.

Pehamberger, AK and Gerzabek, MH (2009). "Die Braunerde Als Häufigster Bodentyp Österreichs". In: *Die Bodenkultur* 53.60, p. 2.

Perminova, Irina V. et al. (June 2003). "Molecular Weight Characteristics of Humic Substances from Different Environments As Determined by Size Exclusion Chromatography and Their Statistical Evaluation". In: *Environmental Science & Technology* 37.11, pp. 2477–2485. ISSN: 0013-936X, 1520-5851. DOI: 10.1021/es0258069. (Visited on 11/06/2025).

Pittman, Edward D. and Lewan, Michael D. (1994). *Organic Acids in Geological Processes*. Berlin, Heidelberg: Springer Berlin Heidelberg. ISBN: 978-3-642-78356-2.

Po, Henry N. and Senozan, N. M. (Nov. 2001). "The Henderson-Hasselbalch Equation: Its History and Limitations". In: *Journal of Chemical Education* 78.11, p. 1499. ISSN: 0021-9584, 1938-1328. DOI: 10.1021/ed078p1499. (Visited on 11/29/2024).

Poetra, Reinaldy et al. (Nov. 2025). *Aqueous Matrix and Limiting Factors in Steel Slag Carbonation under Elevated CO2 at Ambient Conditions*. DOI: 10.21203/rs.3.rs-7992829/v1. (Visited on 02/25/2026).

Pokharel, Rasesh et al. (Oct. 2019). "Mechanisms of Olivine Dissolution by Rock-Inhabiting Fungi Explored Using Magnesium Stable Isotopes". In: *Chemical Geology* 525, pp. 18–27. ISSN: 00092541. DOI: 10.1016/j.chemgeo.2019.07.001. (Visited on 04/08/2024).

Pongratz, Julia et al. (2024). "Chapter 7: Current Levels of CDR, The State of Carbon Dioxide Removal - 2nd Edition." In: DOI: 10.17605/OSF.IO/ZXSKB. (Visited on 03/02/2026).

Power, Ian M. et al. (Jan. 2025). "Are Enhanced Rock Weathering Rates Overestimated? A Few Geochemical and Mineralogical Pitfalls". In: *Frontiers in Climate* 6, p. 1510747. ISSN: 2624-9553. DOI: 10.3389/fclim.2024.1510747. (Visited on 02/16/2026).

Proulx, C. L. et al. (Nov. 2018). "Using a Conductivity–Alkalinity Relationship as a Tool to Identify Surface Waters in Reference Condition across Canada". In: *Water Quality Research Journal* 53.4, pp. 231–240. ISSN: 1201-3080, 2408-9443. DOI: 10.2166/wqrj.2018.030. (Visited on 03/01/2023).

Raza, Waseem et al. (July 2018). "Multistep Sequestration and Storage of CO2 to Form Valuable Products Using Forsterite". In: *Energy* 155, pp. 865–873. ISSN: 03605442. DOI: 10.1016/j.energy.2018.05.077. (Visited on 02/02/2026).

Reershemius, Tom et al. (Dec. 2023). "Initial Validation of a Soil-Based Mass-Balance Approach for Empirical Monitoring of Enhanced Rock Weathering Rates". In: *Environmental Science & Technology* 57.48, pp. 19497–19507. ISSN: 0013-936X, 1520-5851. DOI: 10.1021/acs.est.3c03609. (Visited on 03/03/2026).

Renforth, P. (Sept. 2012). "The Potential of Enhanced Weathering in the UK". In: *International Journal of Greenhouse Gas Control* 10, pp. 229–243. ISSN: 17505836. DOI: 10.1016/j.ijggc.2012.06.011. (Visited on 04/25/2023).

Renforth, P., Pogge Von Strandmann, P.A.E., and Henderson, G.M. (Oct. 2015). "The Dissolution of Olivine Added to Soil: Implications for Enhanced Weathering". In: *Applied Geochemistry* 61, pp. 109–118. ISSN: 08832927. DOI: 10.1016/j.apgeochem.2015.05.016. (Visited on 10/14/2025).

Rensink, Stephanie et al. (Dec. 2024). "Use of Aureobasidium in a Sustainable Economy". In: *Applied Microbiology and Biotechnology* 108.1, p. 202. ISSN: 0175-7598, 1432-0614. DOI: 10.1007/s00253-024-13025-5. (Visited on 03/14/2025).

Rhoades, J., Raats, P.A.C., and Prather, R. (Sept. 1976). "Effects of Liquid-phase Electrical Conductivity, Water Content, and Surface Conductivity on Bulk Soil Electrical Conductivity1". In: *Soil Science Society of America Journal* 40, pp. 651–655. DOI: 10.2136/sssaj1976.03615995004000050017x.

Rhoades, J. D. (Jan. 1996). "Salinity: Electrical Conductivity and Total Dissolved Solids". In: *SSSA Book Series*. Ed. by D.L. Sparks et al. 1st ed. Vol. 5. Wiley, pp. 417–435. ISBN: 978-0-89118-825-4. DOI: 10.2136/sssabookser5.3.c14. (Visited on 01/19/2026).

Rhoades, J. D. et al. (Mar. 1989). "Soil Electrical Conductivity and Soil Salinity: New Formulations and Calibrations". In: *Soil Science Society of America Journal* 53.2, pp. 433–439. ISSN: 03615995. DOI: 10.2136/sssaj1989.03615995005300020020x. (Visited on 04/24/2023).

Rieder, Lukas, Amann, Thorben, and Hartmann, Jens (Jan. 2024). "Soil Electrical Conductivity as a Proxy for Enhanced Weathering in Soils". In: *Frontiers in Climate* 5, p. 1283107. ISSN: 2624-9553. DOI: 10.3389/fclim.2023.1283107. (Visited on 11/17/2025).

Rieder, Lukas et al. (Feb. 2026). "Contribution of Dissolved Organic Carbon to Total Alkalinity in Enhanced Weathering Experiments". In: *Applied Geochemistry* 198, p. 106685. ISSN: 08832927. DOI: 10.1016/j.apgeochem.2026.106685. (Visited on 01/23/2026).

Rimstidt, J. Donald, Brantley, Susan L., and Olsen, Amanda A. (Dec. 2012). "Systematic Review of Forsterite Dissolution Rate Data". In: *Geochimica et Cosmochimica Acta* 99, pp. 159–178. ISSN: 00167037. DOI: 10.1016/j.gca.2012.09.019. (Visited on 08/07/2025).

Robinson, Robert Anthony and Stokes, Robert Harold (2002). *Electrolyte Solutions*. Courier Corporation. ISBN: 0-486-42225-9.

Romero-Mujalli, G. et al. (Nov. 2019). "Ecosystem Controlled Soil-Rock pCO2 and Carbonate Weathering – Constraints by Temperature and Soil Water Content". In: *Chemical Geology* 527, p. 118634. ISSN: 00092541. DOI: 10.1016/j.chemgeo.2018.01.030. (Visited on 04/25/2023).

Rosenstock, Nicholas P. et al. (Sept. 2019). "Biological Enhancement of Mineral Weathering by *Pinus Sylvestris* Seedlings – Effects of Plants, Ectomycorrhizal Fungi, and Elevated CO_2". In: *Biogeosciences* 16.18, pp. 3637–3649. ISSN: 1726-4189. DOI: 10.5194/bg-16-3637-2019. (Visited on 03/18/2025).

Sanna, A. et al. (2014). "A Review of Mineral Carbonation Technologies to Sequester CO_2". In: *Chem. Soc. Rev.* 43.23, pp. 8049–8080. ISSN: 0306-0012, 1460-4744. DOI: 10.1039/C4CS00035H. (Visited on 04/05/2024).

Schiedung, Marcus et al. (Feb. 2026). "Uncertainties of Enhanced Rock Weathering for Climate-Change Mitigation". In: *Nature Reviews Earth & Environment*. ISSN: 2662-138X. DOI: 10.1038/s43017-026-00761-7. (Visited on 03/03/2026).

Schoeman, M.W. and Dickinson, D.J. (Feb. 1996). "Aureobasidium Pullulans Can Utilize Simple Aromatic Compounds as a Sole Source of Carbon in Liquid Culture". In: *Letters in Applied Microbiology* 22.2, pp. 129–131. ISSN: 0266-8254, 1472-765X. DOI: 10.1111/j.1472-765X.1996.tb01125.x. (Visited on 03/14/2025).

Schuiling, R. D. and Krijgsman, P. (Jan. 2006). "Enhanced Weathering: An Effective and Cheap Tool to Sequester Co2". In: *Climatic Change* 74.1-3, pp. 349–354. ISSN: 0165-0009, 1573-1480. DOI: 10.1007/s10584-005-3485-y. (Visited on 08/16/2023).

Schwartzman, David (2015). *The Geobiology of Weathering: A 13th Hypothesis*. DOI: 10.48550/ARXIV.1509.04234. (Visited on 04/10/2025).

Schwarzenbach, René P., Imboden, Dieter M., and Gschwend, Philip M. (2003). *Environmental Organic Chemistry*. 2nd ed. Hoboken, N.J: Wiley. ISBN: 978-0-471-64964-9. DOI: 10.1002/0471649643.

Scott, Allan et al. (Feb. 2021). "Transformation of Abundant Magnesium Silicate Minerals for Enhanced CO2 Sequestration". In: *Communications Earth & Environment* 2.1, p. 25. ISSN: 2662-4435. DOI: 10.1038/s43247-021-00099-6. (Visited on 01/22/2026).

Sechriest, Ralph E (1960). "Relationship between Total Alkalinity, Conductivity, Original pH, and Buffer Action of Natural Water". In: ISSN: 0030-0950.

Seifritz, W. (June 1990). "CO2 Disposal by Means of Silicates". In: *Nature* 345.6275, pp. 486–486. ISSN: 0028-0836, 1476-4687. DOI: 10.1038/345486b0. (Visited on 07/12/2024).

Shapiro, S. S. and Wilk, M. B. (Dec. 1965). "An Analysis of Variance Test for Normality (Complete Samples)". In: *Biometrika* 52.3-4, pp. 591–611. ISSN: 0006-3444, 1464-3510. DOI: 10.1093/biomet/52.3-4.591. (Visited on 10/15/2025).

Sharp, Jonathan D. and Byrne, Robert H. (Nov. 2020). "Interpreting Measurements of Total Alkalinity in Marine and Estuarine Waters in the Presence of Proton-Binding Organic Matter". In: *Deep Sea Research Part I: Oceanographic Research Papers* 165, p. 103338. ISSN: 09670637. DOI: 10.1016/j.dsr.2020.103338. (Visited on 05/05/2025).

Shrestha, Arun Kumar and Basnet, Nabin (July 2018). "The Correlation and Regression Analysis of Physicochemical Parameters of River Water for the Evaluation of Percentage Contribution to Electrical Conductivity". In: *Journal of Chemistry* 2018, pp. 1–9. ISSN: 2090-9063, 2090-9071. DOI: 10.1155/2018/8369613. (Visited on 02/25/2026).

Sims, J. Thomas (Sept. 2018). "Lime Requirement". In: *SSSA Book Series*. Ed. by D.L. Sparks et al. Madison, WI, USA: Soil Science Society of America, American Society of Agronomy, pp. 491–515. ISBN: 978-0-89118-825-4. DOI: 10.2136/sssabookser5.3.c17. (Visited on 03/08/2023).

Singh, Abhijeet (Feb. 2025). "Genomic DNA Extraction from Environmental Samples Having Low Microbial Biomass and Different Characteristics". In: DOI: 10.5281/ZENODO.14918860. (Visited on 11/03/2025).

Smith, Steve et al. (2024). "The State of Carbon Dioxide Removal". In.

Solomon, Theodros (Dec. 2001). "The Definition and Unit of Ionic Strength". In: *Journal of Chemical Education* 78.12, p. 1691. ISSN: 0021-9584, 1938-1328. DOI: 10.1021/ed078p1691. (Visited on 04/11/2025).

Song, Shuzhen et al. (Apr. 2020). "An Important Biogeochemical Link between Organic and Inorganic Carbon Cycling: Effects of Organic Alkalinity on Carbonate Chemistry in Coastal Waters Influenced by Intertidal Salt Marshes". In: *Geochimica et Cosmochimica Acta* 275, pp. 123–139. ISSN: 00167037. DOI: 10.1016/j.gca.2020.02.013. (Visited on 04/08/2025).

Song, W. et al. (Aug. 2007). "Effect of Bacillus Subtilis on Granite Weathering: A Laboratory Experiment". In: *CATENA* 70.3, pp. 275–281. ISSN: 03418162. DOI: 10.1016/j.catena.2006.09.003. (Visited on 03/13/2025).

Sposito, Garrison (2008). *The Chemistry of Soils*. 2nd. Oxford university press. ISBN: 0-19-531369-0.

Streckeisen, Albert (1973). "Plutonic Rocks. Clasification and Nomenclature Recommended by the IUGS Subcommission on the Systematics of Igneous Rocks". In: *Geotimes* 18, p. 26.

Stumm, Werner and Morgan, James J. (1996). *Aquatic Chemistry - Chemical Equilibria and Rates in Natural Waters*. 3rd ed. New York: John Wiley and Sons. ISBN: 978-0-471-51185-4.

Suhrhoff, Tim Jesper et al. (Apr. 2024). "A Tool for Assessing the Sensitivity of Soil-Based Approaches for Quantifying Enhanced Weathering: A US Case Study". In: *Frontiers in Climate* 6, p. 1346117. ISSN: 2624-9553. DOI: 10.3389/fclim.2024.1346117. (Visited on 03/03/2026).

Suhrhoff, Tim Jesper et al. (Dec. 2025). "An Updated Framework and Signal-to-Noise Analysis of Soil Mass Balance Approaches for Quantifying Enhanced Weathering on Managed Lands". In: *Environmental Science & Technology* 59.49, pp. 26440–26453. ISSN: 0013-936X, 1520-5851. DOI: 10.1021/acs.est.5c08303. (Visited on 03/03/2026).

Suzuki, Yoshiaki, Matsubara, Teruo, and Hoshino, Mitsuo (Mar. 2003). "Breakdown of Mineral Grains by Earthworms and Beetle Larvae". In: *Geoderma* 112.1-2, pp. 131–142. ISSN: 00167061. DOI: 10.1016/S0016-7061(02)00300-2. (Visited on 04/10/2025).

Szubstarska, Joanna, Jarzyńska, Grażyna, and Falandysz, Jerzy (Jan. 2012). "Trace Elements in Variegated Bolete (Suillus Variegatus) Fungi". In: *Chemical Papers* 66.11. ISSN: 1336-9075. DOI: 10.2478/s11696-012-0216-5. (Visited on 03/18/2025).

Tani, Masayuki et al. (June 2001). "Determination of Water-Soluble Low-Molecular-Weight Organic Acids in Soils by Ion Chromatography". In: *Soil Science and Plant Nutrition* 47.2, pp. 387–397. ISSN: 0038-0768, 1747-0765. DOI: 10.1080/00380768.2001.10408401. (Visited on 11/06/2025).

Te Pas, Emily E. E. M., Hagens, Mathilde, and Comans, Rob N. J. (Jan. 2023). "Assessment of the Enhanced Weathering Potential of Different Silicate Minerals to Improve Soil Quality and Sequester CO2". In: *Frontiers in Climate* 4, p. 954064. ISSN: 2624-9553. DOI: 10.3389/fclim.2022.954064. (Visited on 07/10/2023).

Te Pas, Emily E. E. M. et al. (Feb. 2025). "Accounting for Retarded Weathering Products in Comparing Methods for Quantifying Carbon Dioxide Removal in a Short-Term Enhanced Weathering Study". In: *Frontiers in Climate* 6, p. 1524998. ISSN: 2624-9553. DOI: 10.3389/fclim.2024.1524998. (Visited on 02/16/2026).

Thirumalini, S and Joseph, Kurian (2009). "Correlation between Electrical Conductivity and Total Dissolved Solids in Natural Waters". In: *Malaysian Journal of Science* 28.1, pp. 55–61. ISSN: 2600-8688.

Thomas, Grant W. and Hargrove, William L. (Oct. 2015). "The Chemistry of Soil Acidity". In: *Agronomy Monographs*. Ed. by Fred Adams. Madison, WI, USA: American Society of Agronomy, Crop Science Society of America, Soil Science Society of America, pp. 3–56. ISBN: 978-0-89118-080-7. DOI: 10.2134/agronmonogr12.2ed.c1. (Visited on 08/21/2023).

Tukey, John W (1949). "Comparing Individual Means in the Analysis of Variance". In: *Biometrics*, pp. 99–114. ISSN: 0006-341X.

Tutiyasarn, Panunporn (2024). "Effect of Biota on Soil Mineral Dissolution in Salt Marsh Sediment". PhD thesis. Hamburg: University of Hamburg. (Visited on 04/02/2025).

Ukalska-Jaruga, Aleksandra et al. (May 2021). "Characterization of Soil Organic Matter Individual Fractions (Fulvic Acids, Humic Acids, and Humins) by Spectroscopic and Electrochemical Techniques in Agricultural Soils". In: *Agronomy* 11.6, p. 1067. ISSN: 2073-4395. DOI: 10.3390/agronomy11061067. (Visited on 05/09/2025).

Uroz, Stéphane et al. (Aug. 2009). "Mineral Weathering by Bacteria: Ecology, Actors and Mechanisms". In: *Trends in Microbiology* 17.8, pp. 378–387. ISSN: 0966842X. DOI: 10.1016/j.tim.2009.05.004. (Visited on 02/03/2025).

US EPA, ORD (Feb. 2013). *MINTEQA2 Equilibrium Speciation Model*. Data and Tools. URL: https://www.epa.gov/hydrowq/minteqa2-equilibrium-speciation-model (visited on 11/11/2024).

Van Der Sluys, William G. (Jan. 2001). "The Solubility Rules: Why Are All Acetates Soluble?" In: *Journal of Chemical Education* 78.1, p. 111. ISSN: 0021-9584, 1938-1328. DOI: 10.1021/ed078p111. (Visited on 11/25/2024).

Vanysek, Petr (1993). "Ionic Conductivity and Diffusion at Infinite Dilution". In: *CRC hand book of chemistry and physics*, pp. 5–92.

Vaulot, Daniel et al. (Apr. 2023). *Pr2database/Pr2database: PR2 Version 5.0.0*. Zenodo. DOI: 10.5281/ZENODO.7805244. (Visited on 10/30/2025).

Vavrusova, Martina and Skibsted, Leif H. (June 2016). "Aqueous Solubility of Calcium Citrate and Interconversion between the Tetrahydrate and the Hexahydrate as a Balance between Endothermic Dissolution and Exothermic Complex Formation". In: *International Dairy Journal* 57, pp. 20–28. ISSN: 09586946. DOI: 10.1016/j.idairyj.2016.02.033. (Visited on 11/26/2024).

Vicca, Sara et al. (Feb. 2022). "Is the Climate Change Mitigation Effect of Enhanced Silicate Weathering Governed by Biological Processes?" In: *Global Change Biology* 28.3, pp. 711–726. ISSN: 1354-1013, 1365-2486. DOI: 10.1111/gcb.15993. (Visited on 07/17/2024).

Vienne, Arthur et al. (May 2022). "Enhanced Weathering Using Basalt Rock Powder: Carbon Sequestration, Co-benefits and Risks in a Mesocosm Study With Solanum Tuberosum". In: *Frontiers in Climate* 4, p. 869456. ISSN: 2624-9553. DOI: 10.3389/fclim.2022.869456. (Visited on 02/16/2026).

Vienne, Arthur et al. (2025). "Weathering without Inorganic CDR Revealed through Cation Tracing". Preprint, EGUsphere. DOI: 10.5194/egusphere-2025-1667. (Visited on 03/03/2026).

Virtanen, Pauli et al. (Mar. 2020). "SciPy 1.0: Fundamental Algorithms for Scientific Computing in Python". In: *Nature Methods* 17.3, pp. 261–272. ISSN: 1548-7091, 1548-7105. DOI: 10.1038/s41592-019-0686-2. (Visited on 10/15/2025).

Vogt, Rolf D. et al. (June 2024). "Factors Governing Site and Charge Density of Dissolved Natural Organic Matter". In: *Water* 16.12, p. 1716. ISSN: 2073-4441. DOI: 10.3390/w16121716. (Visited on 04/15/2025).

Walker, James CG, Hays, PB, and Kasting, James F (1981). "A Negative Feedback Mechanism for the Long-term Stabilization of Earth's Surface Temperature". In: *Journal of Geophysical Research: Oceans* 86.C10, pp. 9776–9782. ISSN: 0148-0227.

Walton, N.R.G. (Dec. 1989). "Electrical Conductivity and Total Dissolved Solids—What Is Their Precise Relationship?" In: *Desalination* 72.3, pp. 275–292. ISSN: 00119164. DOI: 10.1016/0011-9164(89)80012-8. (Visited on 02/16/2026).

Weiss, Andreas (June 2013). "The Silica and Inorganic Carbon System in Tidal Marshes of the Elbe Estuary, Germany : Fluxes and Spatio-Temporal Patterns". PhD thesis. Hamburg: University of Hamburg.

Welch, S. A., Taunton, A. E., and Banfield, J. F. (May 2002). "Effect of Microorganisms and Microbial Metabolites on Apatite Dissolution". In: *Geomicrobiology Journal* 19.3, pp. 343–367. ISSN: 0149-0451, 1521-0529. DOI: 10.1080/01490450290098414. (Visited on 02/03/2025).

Welch, Susan A and Ullman, William J (June 1993). "The Effect of Organic Acids on Plagioclase Dissolution Rates and Stoichiometry". In: *Geochimica et Cosmochimica Acta* 57.12, pp. 2725–2736. ISSN: 00167037. DOI: 10.1016/0016-7037(93)90386-B. (Visited on 02/03/2025).

Wiesenbauer, Julia et al. (Apr. 2025). "Preferential Use of Organic Acids over Sugars by Soil Microbes in Simulated Root Exudation". In: *Soil Biology and Biochemistry* 203, p. 109738. ISSN: 00380717. DOI: 10.1016/j.soilbio.2025.109738. (Visited on 02/17/2025).

Williams, Morgan et al. (June 2020). "Pyrolite: Python for Geochemistry". In: *Journal of Open Source Software* 5.50, p. 2314. ISSN: 2475-9066. DOI: 10.21105/joss.02314. (Visited on 06/10/2025).

Wolf-Gladrow, Dieter A. et al. (July 2007). "Total Alkalinity: The Explicit Conservative Expression and Its Application to Biogeochemical Processes". In: *Marine Chemistry* 106.1-2, pp. 287–300. ISSN: 03044203. DOI: 10.1016/j.marchem.2007.01.006. (Visited on 04/08/2025).

Xiao, Min and Wu, Fengchang (May 2014). "A Review of Environmental Characteristics and Effects of Low-Molecular Weight Organic Acids in the Surface Ecosystem". In:

Journal of Environmental Sciences 26.5, pp. 935–954. ISSN: 10010742. DOI: 10.1016/S1001-0742(13)60570-7. (Visited on 06/23/2023).

Xiao, Shiyu et al. (Jan. 2023). "CTD Sensors for Ocean Investigation Including State of Art and Commercially Available". In: *Sensors* 23.2, p. 586. ISSN: 1424-8220. DOI: 10.3390/s23020586. (Visited on 01/07/2026).

Xinping Hu (Aug. 2020). *The Curious Role of Organic Alkalinity in Seawater Carbonate Chemistry*. (Visited on 05/09/2025).

Xue, Bai et al. (Jan. 2017). "Online Measurement of Alkalinity in Anaerobic Co-Digestion Using Linear Regression Method". In: *International Journal of Agricultural and Biological Engineering* 10.1, pp. 176–183. (Visited on 02/25/2026).

Yang, Bo, Byrne, Robert H., and Lindemuth, Michael (Nov. 2015). "Contributions of Organic Alkalinity to Total Alkalinity in Coastal Waters: A Spectrophotometric Approach". In: *Marine Chemistry* 176, pp. 199–207. ISSN: 03044203. DOI: 10.1016/j.marchem.2015.09.008. (Visited on 11/15/2024).

Zhang, Bingquan et al. (Sept. 2023). "Techno-Economic and Life Cycle Assessment of Enhanced Rock Weathering: A Case Study from the Midwestern United States". In: *Environmental Science & Technology* 57.37, pp. 13828–13837. ISSN: 0013-936X, 1520-5851. DOI: 10.1021/acs.est.3c01658. (Visited on 09/27/2023).

Zhang, Liming et al. (Nov. 2022). "Comparison of Lignin Distribution, Structure, and Morphology in Wheat Straw and Wood". In: *Industrial Crops and Products* 187, p. 115432. ISSN: 09266690. DOI: 10.1016/j.indcrop.2022.115432. (Visited on 11/03/2025).